CRANFIELD UNIVERSITY

School of Applied Sciences

Sustainable Systems Department

Centre for Water Science

ABDULRAHIM M. AL-ISMAILI

MODELLING OF A HUMIDIFICATION-DEHUMIDIFICATION GREENHOUSE IN OMAN

PhD THESIS

CRANFIELD UNIVERSITY

School of Applied Sciences

Sustainable Systems Department

Centre for Water Science

PhD THESIS

Academic Year 2008/2009

ABDULRAHIM M. AL-ISMAILI

MODELLING OF A HUMIDIFICATION-DEHUMIDIFICATION GREENHOUSE IN OMAN

Supervised by: Dr. E. K. Weatherhead

Dr. O. Badr

May 2009

ABSTRACT

The humidification-dehumidification (HD) greenhouse is a relatively new technology. In addition to the humidification process and cultivation normally present in greenhouses in arid countries, the HD greenhouse also integrates a dehumidification process. In these greenhouses, saline or brackish water is evaporated in the ordinary evaporative cooling pads (i.e. 1st humidifier) before passing through the main crop growing section. The air is further loaded with more moisture by passing it through a 2nd humidifier. This humidification process is then followed by a dehumidification process to condense as much water vapour as possible. The main purpose of the HD greenhouses is to find a cheap means of desalinating saline water for the sake of using the condensate for irrigation.

Most of previous attempts to improve the performance of the HD greenhouses have used a trial-and-error approach. An alternative approach is to use simulation models. Due to the absence of such models, this research study aims at developing a simulation model capable of simulating the significant processes of the HD greenhouses. The developed model is an integration of three sub-models each of which simulates one element of the HD greenhouse. The simulated elements are humidifiers, cultivation area (i.e. microclimate) and dehumidifiers. The integrated model can be used for design and optimisation purposes.

Because it was difficult to find an HD greenhouse where the accuracy of the integrated model can be tested, the three sub-models were tested separately. When the simulation results were confronted against the experimental results, a good accuracy was obtained for the three sub-models. It was found that the HD greenhouse model was able to predict the humidification rate with a good accuracy within the range of conditions used for calibration. The model was, then, used to simulate a hypothetical Quonset-type cucumber-cultivated greenhouse using weather data obtained from the site of the HD greenhouse in Oman. The simulation results were similar to the expected results.

The applications and limitations of the HD greenhouse model are discussed in this study. Future investigations to further study and, if necessary, improve the accuracy of the HD greenhouse are highly recommended.

ACKNOWLEDGEMENTS

Initially, my great gratitude is to the Almighty Allah for the assistance, strength and patience He provided to me throughout my study. I owe a big thank to all of those who assisted and encouraged me during the course of this study. The first two people who deserve the highest gratitude are my two supervisors. I gratefully appreciate their valuable guidance and constructive suggestions as well as their patience. I still remember the useful discussions I had with them.

My wife you are the next. I thank you for your support and patience. My sincere gratitude is also extended to my mother, children, relatives and friends for their direct or indirect support. I also wish to express my thanks to the administration of Sultan Qaboos University for granting me this full-time PhD scholarship.

I would also like to extend my appreciation to all of those who helped me in my practical work of this study. I thank particularly Mr. I. Seymour, Mr. M. Al-Belushi, Mr. M. Jumay'a, Mr. S. Al-Ismaili and the technicians of the Agricultural Experiment Station, Sultan Qaboos University, Oman. Many thanks are also due to Dr. B. Halasz for his helpful correspondences to explain things I did not understand about his mathematical model. I thank him for the useful information he provided to me. I also highly appreciate the assistance provided to me from all of those whose names are not mentioned here.

Finally, this study is dedicated to my country Oman, my mother, wife and children and to everyone who likes to see Oman a leading agricultural country.

TABLE OF CONTENTS

LIST OF TABLES

Chapter 3

Chapter 4

Appendix B

LIST OF FIGURES

Glossary

Chapter 1

Chapter 2

Chapter 3

Chapter 4

Chapter 5

Chapter 6

Appendix A

Appendix C

NOMENCLATURE

Latin Symbols

A	surface area, [m^2]
b	thickness, [m]
b	slope of the real air saturation line
B	slope of the linear air saturation line
C_p	specific heat, [J/kg ^oC]
$\hat{C}_p$	specific heat in Penman-Monteith relation, [MJ/kg ^oC]
D	external diameter of dehumidifier tube unless specified, [m]
E	greenhouse effectiveness as a solar collector, [%]
f_a	arrangement factor
F_P	dehumidifier performance factor, [%]
f_v	shape factor from canopy to sky unless specified
$\hat{G}$	sensible heat flux into the soil in Penman-Monteith relation, [MJ/m^2 day]
h	heat transfer coefficient, [W/m^2 ^oC]
h	specific enthalpy, [kJ/kg (dry air)]
$\hbar$	absolute humidity, [kg (water)/m^3 (air)]
H	height, [m]
I	global solar radiation heat flux, [W/m^2]
k	thermal conductivity, [W/m ^oC]
l	characteristic length, [m]
L	length, [m]
L	net thermal radiation heat transfer rate, [W]
$\dot{L}$	net thermal radiation heat flux, [W/m^2]
LAI	leaf area index
L_e	Lewis number ($L_e = \mathrm{M} C_{p,a}/\mathrm{h}_{cv}$, where M is the mass transfer coefficient, [kg (dry air)/m^2 s)
L_v	latent heat of vaporization of water, [J/kg]

$\hat{L}_v$	latent heat of vaporization of water in Penman-Monteith relation, [MJ/kg]
$\dot{m}$	mass flow rate, [kg/s]
M	rate of moisture addition/removal, [kg/s]
$\dot{M}$	rate of moisture addition/removal per unit floor area, [kg/m^2 s]
$\hat{M}$	rate of moisture addition per unit floor area in Penman-Monteith relation, [kg/m^2 day]
N	number
Nu	Nusselt number
P	total air pressure, [kPa]
P	perimeter of greenhouse cover, [m]
PAR	photosynthetically active radiation, [mmole/s m^2]
Pr	Prandtl number, $\Pr = \nu/\alpha$
P_{ratio}	ratio of plants-occupied area to total ground area
Q	heat transfer rate, [W]
$\dot{Q}$	heat flux, [W/m^2]
r_a	bulk surface aerodynamic resistance of plant leaf, [s/m]
Re	Reynolds number
r_{leaf}	leaf stomatal resistance to moisture transfer, [s/m]
$\hat{R}_n$	net radiation flux in Penman-Monteith relation, [MJ/m^2 day]
r_s	canopy surface resistance to moisture transfer, [s/m]
s	spacing between adjacent tubes of the dehumidifier, [m]
S	net short-wave heat transfer rate, [W]
$\dot{S}$	net short-wave heat flux, [W/m^2]
T	temperature, [^{o}C unless specified]
t	time, [s]
T_{pad}	temperature of air leaving the pads, [^{o}C]
T_{rate}	plant transpiration rate, [kg (water) /m^2 s]
u	air speed, [m/s]

u_2	air speed measured at 2 m height, [m/s]
U	overall heat transfer coefficient, [W/m^2 ^{o}C]
v	specific volume of air, [m^3/kg]
V	volume, [m^3]
$\dot{V}$	volumetric flowrate, [m^3/s]
W	water-to-air heat capacity rate ratio
W	width of the greenhouse unless specified, [m]
x	distance from a reference point, [m]
X_o	number of transfer units (NTU)
z	air-to-water heat capacity rate ratio

Greek Symbols

α	thermal diffusivity, [m^2/s]
β	Bowen ratio
γ	psychrometric constant, [kPa/^{o}C]
$\hat{\Delta}$	slope of vapor pressure curve, [kPa/^{o}C]
δ	slope of the water vapour saturation curve, [kPa/^{o}C]
ε	emissivity
$\Im(T_w)$	real enthalpy of saturated air as a function of T_w, [J ^{o}C/kg]. Its value can be obtained from Table I in Halasz (1999) if a total pressure of 1 bar is assumed
η	overall cooling effectiveness unless specified, [%]
μ	dynamic viscosity, [kg/m s]
ν	kinematic viscosity, [m^2/s]
ξ	proportion of sky with cloud cover
ρ	density, [kg/m^3]
σ	Stephan-Boltzmann constant, [5.67 x 10^{-8} W/m^2 K^4]
τ	light transmittance
φ	relative humidity
ϕ	surface reflectance to shortwave radiation

ψ	partial water vapour pressure, [kPa]
ψ'''	vapour pressure deficit $(\psi''' = \psi'' - \psi)$, [kPa]
Ω	water vapour dehumidification rate, [ml/min]
ω	humidity ratio, [kg (water)/kg (dry air)]
ϖ	specific humidity, [kg (water)/kg (air)]

Subscripts

0	at 0^oC
a	air, at air temperature
ai	air inlet value
ao	air outlet value
avg	average
aw	air-water interface
C	dehumidifier column
c	greenhouse cover
cd	conductive transfer
cv	convective transfer
cs	condensation
D	diagonal
da	dry air
db	dry-bulb value, at dry-bulb temperature
deh	dehumidifier, on dehumidifier
dp	dew-point
eff	effective
ent	greenhouse entrance
equip	greenhouse equipment
es	external surface
ET	evapotranspiration
ev	evaporation (e.g. from soil)
ext	external
ext	greenhouse exit

film	film
furn	furnace (heater)
g	greenhouse soil surface
gh	greenhouse
$g+1$	subsurface soil layers
h	heater
hum	humidifier
in	inside of the greenhouse
inner	inner surface
int	internal
is	internal surface
j	greenhouse component(s)
L	parallel to the direction of flow
lat	latent
leaf	plant leaf
max	maximum
mist	misted water
n	net
obs	observed/measured
out	outside of the greenhouse
outer	outer surface
p	greenhouse plants
photo	plant photosynthesis
pot	potential
pred	predicted/estimated
prev	a reference point in the upstream airflow direction
PVC	polyvinylchloride
R	dehumidifier row
resp	plant respiration
s	surface(s) receiving/emitting radiation
sens	sensible

sky	sky
sup	supplemental
t	time
tube	dehumidifier tube
T	transverse
T	plant transpiration
v	ventilation
w	water, at mean water temperature ($T_w = (T_{wi} + T_{wo})/2$)
wall	greenhouse wall
wb	wet bulb value, at wet bulb temperature
wi	water inlet value
wo	water outlet value
wv	water vapour
ww	water in a deep well
λ	long-wavelength

Superscript

"	at saturation
—	average value

ABBREVIATIONS

AES	agricultural experiment station at SQU
CFD	computational fluid dynamic
ET	evapotranspiration
HD	humidification-dehumidification
PC	personal computer
PE	predictive error
$\overline{PE}$	average predictive error
PVC	polyvinylchloride
RMSE	root mean square error
R^2	coefficient of determination
SD	standard deviation
SE	standard error
SQU	Sultan Qaboos University, Muscat, Oman
SWGH	seawater greenhouse
%PE	percentage predictive error, [%]
$\overline{\%PE}$	average percentage predictive error, [%]

GLOSSARY

Air saturation line:

The real air saturation line is basically the *saturation humidity ratio* ω'' as a function of the *air dry-bulb temperature* T_a (see Fig. G.1). In the non-dimensional model discussed in Chapter 3, it was necessary to assume a linear increase in the ω'' for certain segments of the real saturation line in order to keep the non-dimensional nature of the model. The linearized segments are represented by the points connecting the ω'' at the *inlet air* wet-bulb *temperature* $T_{wb,ai}$ to the ω'' at the *water temperature* T_w. The T_w is located between the *inlet* and *outlet water temperatures* (T_{wi} and T_{wo}, respectively) in the evaporative cooling process. The procedure of estimating the T_w is explained in more details in Halasz (1999). Furthermore, this assumption will not lead to a large error since the linearized segments on the real air saturation line are very small. However, with large water temperature differences, this assumption may lead to large errors.

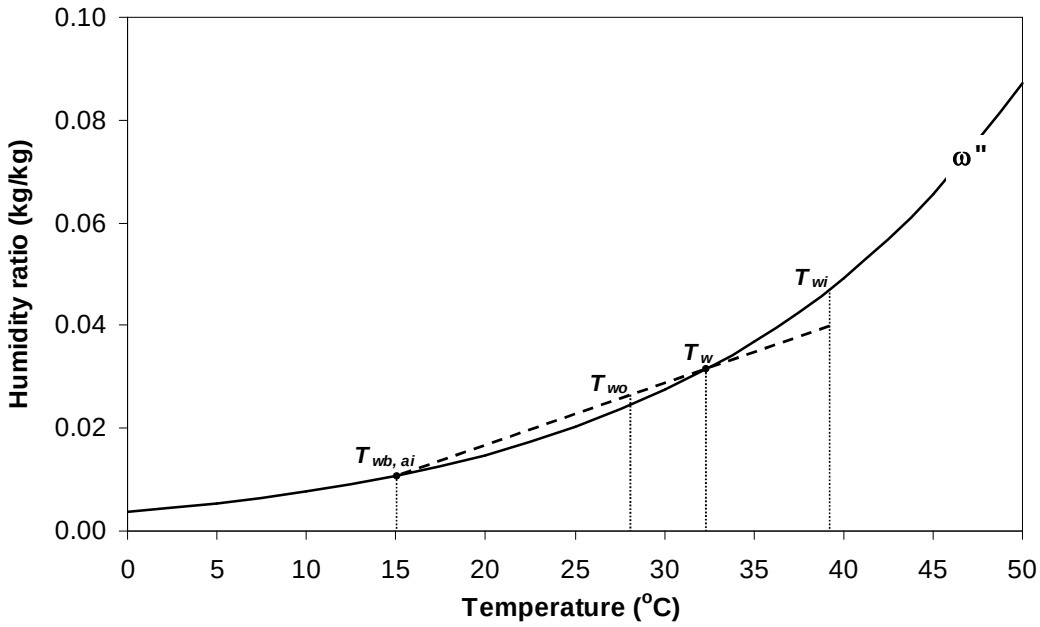

Fig. G.1: The real and straight air saturation lines (ω'' vs. T)

Average percentage predictive error ($\overline{\%PE}$):

The $\overline{\%PE}$ is the arithmetic mean of the normalized predictive error (PE) for all samples within the dataset (see the next two terms). The PE is normalized by dividing it by the measured value. The $\overline{\%PE}$ can be presented as a fraction or as a percentage. In this study, it is presented as a percentage. The $\overline{\%PE}$ is calculated as follows:

$$\overline{\%PE} = 100 \frac{\sum_{i=1}^{n} \left[\frac{\left(x_{pred,i} - x_{obs,i} \right)}{x_{obs,i}} \right]}{n}$$

Average predictive error ($\overline{PE}$):

The $\overline{PE}$ is the arithmetic mean of the PE for all samples within the dataset. It has the same units as of the values for which it is calculated (see the next term). It is calculated using the following relation:

$$\overline{PE} = \frac{\sum_{i=1}^{n} \left(x_{pred,i} - x_{obs,i} \right)}{n}$$

Predictive error (PE):

It is the difference between the value predicted (x_{pred}) by the simulation model and the measured value (x_{obs}). The PE carries a negative sign if the predicted value is lower than the measured one and *vice versa*. It has the same units as of the values for which it is calculated. Let x be any variable, the PE is simply expressed as:

$$PE = x_{pred} - x_{obs}$$

Quonset greenhouse

This type of greenhouse is supported by curved roof bars in the shape of half of a circle. They are also known as around-arched tunnel greenhouses. Figure G.2 shows Quonset greenhouses. The dimensions of this design of greenhouses are as follows: the length varies from 20 to 60 m, the width is 9 m, the height is 3.25 m and the space between the arches is 2 m for arches next to the ending arches and 2.5 m for the intermediate arches. In Oman, this is the most popular type of greenhouses.

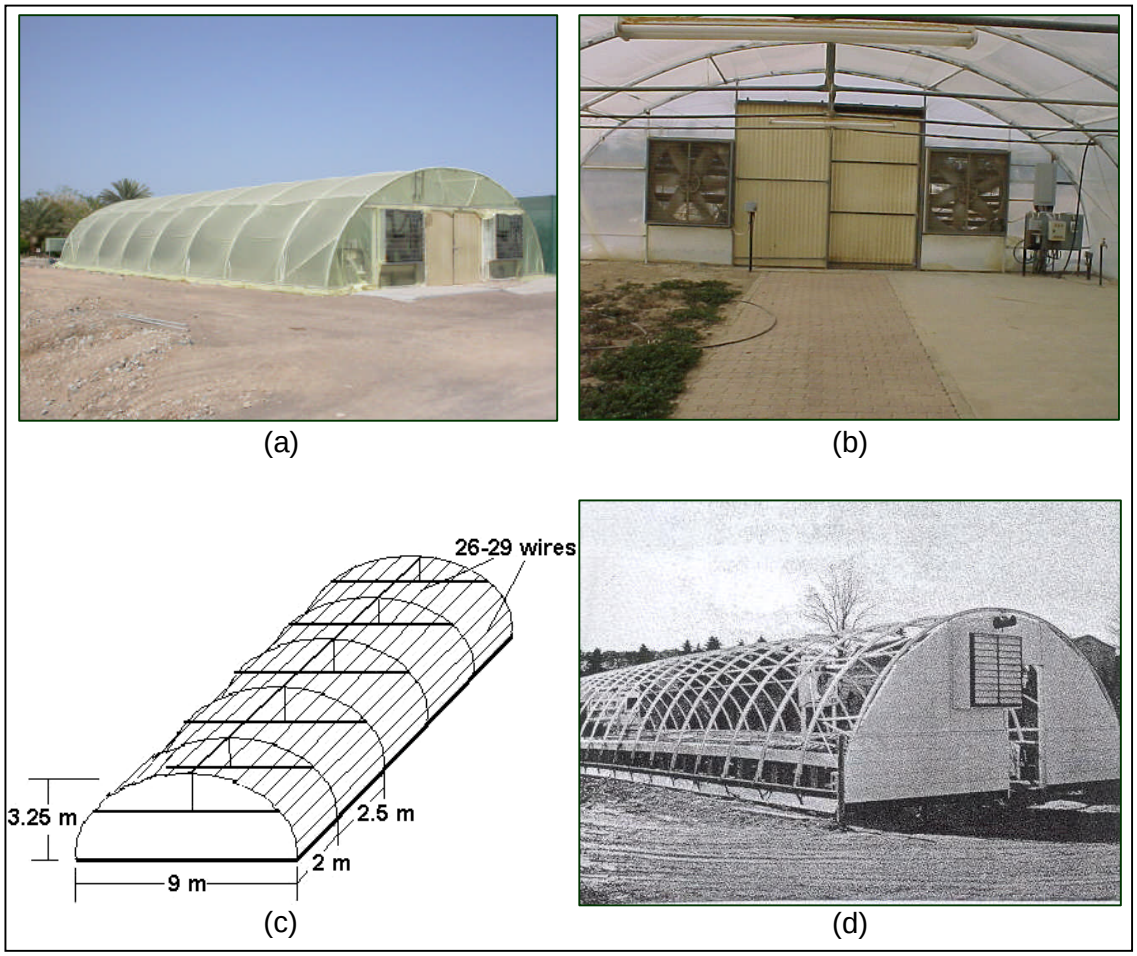

Fig. G. 2: (a) External, (b) internal views of a Quonset greenhouse used at AES, (c) a schematic of a Quonset (round-arched tunnel) greenhouse (von Elsner et al., 2000) and (d) uncovered Quonset greenhouse (Boodley, 1981)

Root mean square error (RMSE)

The RMSE is the square root of the arithmetic mean of the squared PE for all samples within the dataset. The RMSE has the same units as the quantity from which it is calculated. The following formula shows how the RMSE is estimated:

$$\mathrm{RMSE} = \sqrt{\frac{\sum_{i=1}^{n} \left(x_{pred,i} - x_{obs,i} \right)^2}{n}}$$

CHAPTER ONE

1. INTRODUCTION

1.1. BACKGROUND

High temperature and water shortage are two characteristics of the Sultanate of Oman (Fig. 1.1). In Northern coastal areas, the aridity coupled with over-pumping of groundwater have often resulted in seawater intrusion. Irrigating the plants with the intruded groundwater has resulted in contaminating the soil with salts. Consequently, many fertile and cultivated lands in the Batinah region (Fig. 1.2) are being abandoned (Al-Ajmi and Abdel-Rahman, 2001). The Batinah coastal plains produce more than 50 % of the agricultural production of the country (Stanger, 1985; Abdel-Rahman, 1996; and Al-Ajmi and Abdel-Rahman, 2001). Therefore, it is essential to maintain the present productivity of this region. This requires securing enough freshwater for irrigation and can be achieved by building recharge dams to stop and overcome the seawater intrusion into groundwater, finding possible techniques of utilizing the saline groundwater and looking for alternative freshwater sources. The

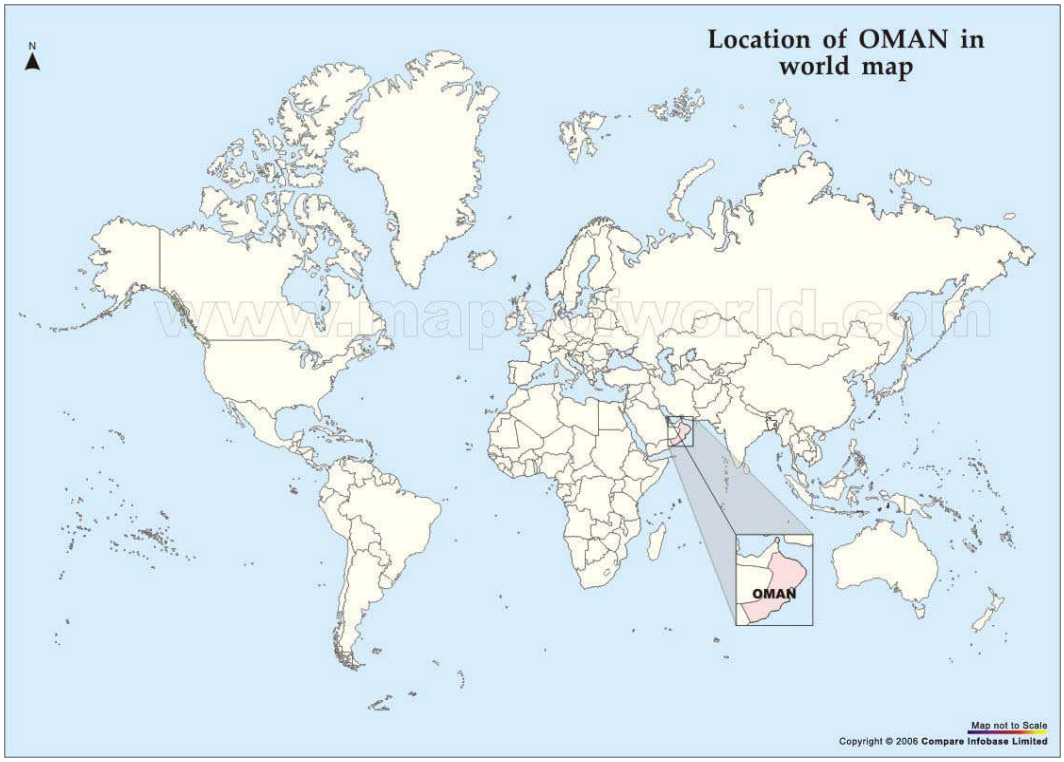

Fig. 1.1: The location of the Sultanate of Oman

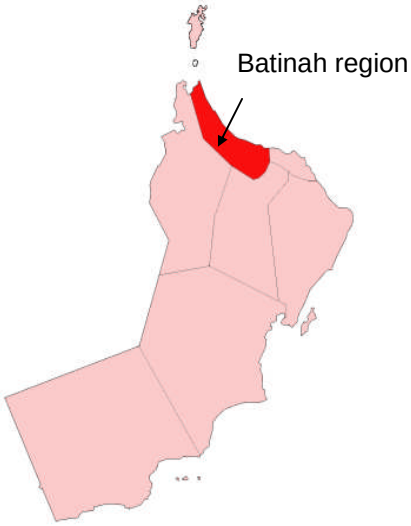

Fig. 1.2: The Batinah coastal area

scarcity and erratic nature of rainfall make the first option only a partial solution. The last two alternatives can be achieved by the use of a new technology called "humidification-dehumidification" greenhouses. This technology can be a promising source of freshwater for irrigation in coastal areas or even inland places where only saline groundwater is accessible.

The HD greenhouse is a greenhouse that has, in addition to the ordinary evaporative cooling system (i.e. 1st humidifier), additional components; namely a 2nd humidifier to further load the air with moisture and a dehumidifier to extract the moisture from the air. The majority of greenhouses in Oman are equipped with pad-and-fan evaporative cooling systems (i.e. humidifiers). Normally, a wall of evaporative cooling pads is placed at one end of the greenhouse (i.e. at the air inlet) and fans are placed at the opposite end (i.e. at the air outlet). In the HD greenhouses, the evaporative pads (i.e. humidifiers) are wetted using saline water.

As a result of the evaporation process taking place in the 1st humidifier, there is always a reduction in the temperature of the air and an increase in the humidity. This evaporation is also associated with a reduction in the temperature of water used to wet the pads. As the air flows through the greenhouse towards the fans, its temperature increases due to the *solar*

radiation input. As a result, the *relative humidity* decreases which implies that the capacity of the air to hold more water vapour increases. This explains why in HD greenhouses a 2nd humidifier is placed at a distance before the fans. Although, the *relative humidity* decreases due to the temperature gradient inside the greenhouse, the *moisture content* of the air inside a cultivated greenhouse increases as a result of the evaporation from the wet soil and the transpiration from the plants (i.e. *evapotranspiration*). The dehumidifier, in the HD greenhouses, is placed just after the 2nd humidifier to remove as much water vapour as possible.

In order for the dehumidification process to take place, the external surface of the dehumidifier tubes must be below the *dew-point temperature* of the air flowing through the dehumidifier. Therefore, for this to happen, a coolant with a temperature below the *dew-point* is required. Al-Ismaili (2003) found that the temperature of the water leaving the humidifier(s) is always lower than the *dew-point temperature of the air*.

Currently, there is one HD greenhouse in Oman. The freshwater produced by this HD greenhouse is less than the irrigation demand of the greenhouse. In their prototype HD greenhouse in Tenerife, Spain, Paton and Davis (1996) reported that the water production could reach twenty times the water requirement inside the greenhouse. Therefore, enhancing freshwater production in the HD greenhouse in Oman is feasible and therefore possible improvements should be studied. Mathematical simulation of heat and moisture processes of the HD greenhouse might be one of the first steps to be undertaken in order to optimize the performance of the HD greenhouse. Therefore, this study will be dedicated to develop a simulation model that takes into account all significant heat and mass transfer processes of the HD greenhouse in Oman.

1.2. AIMS AND OBJECTIVES

The overall aim of the research study is to develop a simulation model accounting for all significant heat and mass transfer processes of the HD greenhouse to assist the optimal design and operation of the HD greenhouse. More specifically, this aim is planned to be achieved by fulfilling the following objectives:

i. Developing a model simulating the moisture and/or temperature changes that air and water undergo as they flow through/over the greenhouse humidifier(s),
ii. Developing a model capable of predicting the temperature and moisture profiles of greenhouse air as it moves through the crop growing section of the greenhouse,
iii. Developing a model that estimates the temperature and humidity variations of the air passing through the dehumidifier and estimates the freshwater production,
iv. Conducting calibration/validation experiments to test the predicting accuracy of the developed models, and
v. Linking all of these models in a working protocol enabling them to work in an integral format

1.3. NOVELTY OF STUDY

The simulation of the greenhouse environment using mathematical modelling has stimulated the interest of many investigators (e.g. Kano and Salder, 1985; Boulard and Baille, 1993; Jolliet, 1994; Khalil, 1995; Kittas et al., 2001 & 2003; Chen, 2003; and Condori and Saravia, 2003). However, this interest was usually focused on the greenhouse microclimate as a single unit. As a result of this broad interest, the literature is enriched with a large number of greenhouse simulation models predicting the average temperature and/or the average moisture levels inside the greenhouse. Other models also include the

prediction of the average temperature of the greenhouse soil, cover and plant leaves. Simulation models integrating the pad-and-fan evaporative cooling systems are rarely found in the literature.

This research study will contribute to the body of knowledge with an integrated simulation mathematical model accounting for all significant processes taking place in the HD greenhouse in Oman. The novelty of the study is based on the nature of the model. Firstly, unlike most greenhouse modellers who considered the greenhouse microclimate as one entity, this model deals with the microclimate as discrete controlled volumes adjacent to each other along the airflow direction. While the approach of most modellers allowed them to find the average *air temperature* and *humidity*, the approach of this study will enable the model to simulate the variations of *air temperature* and *humidity* in the direction of the air stream. Only three studies (Kittas et al., 2001 & 2003; and Chen, 2003) were found to be considering the greenhouse in the same way. This study will be different from those three in terms of the type of greenhouse used (i.e. Quonset) and the type of crop cultivated (i.e. cucumber).

Secondly, although the model of the microclimate is not totally novel, due to the contribution of previous investigators, integrating the humidification process of the evaporative cooler gives it more originality. Only very few studies (e.g. Raoueche, 1997; and Kittas, 2001 & 2003) were found to include the humidification process; however this model improves on the way the humidification process was simulated.

Thirdly, the model will also incorporate the dehumidification process which is an important ingredient of the HD greenhouse. The sub-model dealing with the dehumidification process will be able to predict the change of *air temperature* and *humidity* at both sides of the dehumidifier as well as the change of *coolant temperature* from the inlet to outlet. Furthermore, the sub-model will also be able to estimate the amount of water condensed by the dehumidifier. Only one study (Raoueche, 1997) was found to include the dehumidification process of the HD greenhouses. However, the dehumidifier

simulated in the current study and the number of predict variables are different from those of Raoueche (1997).

The model will be a useful tool to be used by HD greenhouse investigators. Additionally, it can be used by decision makers to decide on the feasibility of introducing HD greenhouse technology based on the weather conditions of the location, the greenhouse structural and operating conditions, and the predicted amount of water production. The model can also be used to foresee the fluctuations in the outputs (e.g. *air temperature* and *humidity* after humidifier(s), within microclimate, after dehumidifier(s), and the amount of expected water production) for any period of time provided that the input data (e.g. weather data and structural and operational variables) is available.

1.4. THESIS ORGANIZATION

This thesis is composed of seven main chapters. Chapter 1, “Introduction”, briefs the reader with an overview of the circumstances from which the idea of this research study came about. It also provides a detailed explanation of the objectives that the researcher is aiming to achieve. The originality of the study, which is a crucial criterion of any study, is elaborately discussed here. Chapter 2, “Critical Review of Literature”, is dedicated to provide, in more details, all necessary information that the reader might need in order to understand the concepts and terminology used in the presentation of the study. Also, it gives a critical assessment on the contributions of previous researchers in the area of study.

The Development of the three sub-models, namely; “The Humidifier Sub-Model”, “The Microclimate Sub-Model” and “The Dehumidifier Sub-Model” are given in Chapters 3, 4 and 5, respectively. These chapters also present details of the experiments carried out to test the accuracy of the developed sub-models. The results obtained from these experiments are presented and discussed in these chapters. Chapter 6, “The Integrated HD Greenhouse

Model", is mainly a description of the final format of the simulation model when all of its sub-models are combined together. The instructions on how to use the model and the applications of the model are presented in this chapter. The conclusions drawn from this study are given in Chapter 7, "Conclusions and Recommendations". It also comprises suggested recommendations for future investigations and optimizations of the HD concept in greenhouses.

CHAPTER TWO

2. CRITICAL REVIEW OF LITERATURE

This chapter comprises two sections. Section 2.1 presents the review of important considerations of the humidification-dehumidification greenhouses. Section 2.2 reviews the most relevant mathematical simulation models of greenhouses.

2.1. HUMIDIFICATION-DEHUMIDIFICATION (HD) GREENHOUSES

In this part of the study, an overview of the recently evolved technology called the “humidification-dehumidification” greenhouse is provided. These greenhouses are also called “seawater” greenhouses. Section 2.1.1 will be dedicated to talk about greenhouses in general. The humidification and dehumidification processes that might occur in some greenhouses are discussed in Sections 2.1.2 and 2.1.3, respectively. Finally, Sec. 2.1.4 will give an explanation of the two processes when they are combined together in a greenhouse.

2.1.1. Greenhouses

Greenhouses are multi-purpose agricultural structures that can be used for various tasks. In cold climates, for instance, they are used to provide a warm environment for the cultivated plants inside them. However, in hot climates, they are used to provide a cool environment. In addition to these two tasks, greenhouses can be used for storage and solar drying of certain types of crops. The predominant purpose of erecting greenhouses is cultivation. Many crops are very sensitive to the harsh external climatic conditions and require a controlled environment that suits their needs. The climatic limitations that can be overcome by the use of greenhouses are high or low temperatures, intensive solar radiation, high precipitation and high wind speed.

In the last two decades, the greenhouse technology has been introduced to the agricultural sector in Oman. Nowadays, greenhouses are widely-spread nationwide for the purpose of cultivating mainly vegetables, such as tomato and sweet pepper, but the most popular vegetable crop cultivated in the country is cucumber. Recently, some fruits, such as strawberry, have been cultivated. The most common greenhouse structure, widely-spread throughout Oman, is the Quonset tunnel-type greenhouse (see Fig. 2.1 and Glossary). In Oman, these greenhouses are normally 20-39 m long, 9 m wide and 3.0-3.25 m high. Most farmers cover their greenhouses with a single layer of *polyethylene* material. This type of covering material makes the greenhouse an airtight structure which is an essential requirement to use pad-and-fan evaporative cooling systems to cool the inner environment of the greenhouse (Luchow and Zabeltitz, 1992; and Fang, 1995).

In Quonset greenhouses, fans are normally placed at one end of the greenhouse and the evaporative cooling pads are placed at the opposite end (see Figs. 2.1 and 2.2). The relatively dry and hot ambient air is drawn by the suction force of the fans through the wall of wet pads, which have a large area for air-water surface contact. This results into a reduction in the *air temperature* which is the intention behind using greenhouses in hot climates. In extremely hot and dry conditions, the *air temperature* might decrease by as much as 11-12^{o}C (Baron's Brae, 1991; and Strobel et al., 1999). Subsequently, an increasing temperature gradient exists as air streams towards the fans as a result of the *solar radiation input*. For long greenhouses (e.g. 39 m), the

Fig. 2.1: The fans of a Quonset greenhouse

Fig. 2.2: Evaporative cooling pads (i.e. humidifier) at one side of a Quonset greenhouse

temperature difference can reach 7.3^{o}C as air approaches the fans (Bucklin et al., 1993).

2.1.2. Humidification

Although greenhouses provide a suitable protected environment for cultivation in hot climates, they become of no use if they are not equipped with some assisting tools such as fans and humidifiers. The fans alone will not be able to lower the *ambient temperature*; the *air temperature* will be slightly higher than the outside temperature in this case (Baille, 1989 as cited by Baroon's Brae, 1991; and Bucklin et al., 1993). Therefore, the use of some cooling means is required. As explained in Sec. 2.1.1, evaporative cooling pads (i.e. humidifier) can be used to lower the temperature of the air entering the greenhouse through the pads.

In the humidifier, the water wetting the pads and the warm dry air passing through them undergo certain changes. These changes take place as a result of the evaporation process which is governed by the "*vapour pressure deficit*" (Wiersma and Short, 1983). The *vapour pressure deficit* indicates the difference between the amount of water vapour that can be held in a saturated air at a given temperature and the actual amount of water vapour that is held in a sample of unsaturated air (Floriculture Factsheet, 1994). This implies that the evaporation increases with low *vapour pressure deficit* between the air passing through the humidifier and the water wetting the humidifier. The evaporation

process causes a decrease in the *air temperature* (Czarick and Lacy, 1996), an increase in the *moisture content* held in the air (McClellan; 1985) and a decrease in the *water temperature* (Cengel and Boles, 1988; Al-Ismaili, 2003; and Perret et al., 2005).

For the evaporation process (i.e. humidification) to take place, the *latent heat of vaporization* L_v needs be supplied to the water to undergo a phase change from liquid to gas. The required heat is obtained from the air passing through the humidifier as well as from the water flowing down the humidifier (Mangold et al., 1983; and Wiersma and Short, 1983). The consequence is a significant decrease in the *air temperature*, as mentioned in Sec. 2.1.1. The degree of achieved cooling depends on many factors including the *inlet air temperature*, *humidity* and *flowrate*, the *inlet water temperature* and *flowrate* and the *cooling effectiveness* of the humidifier.

In addition to the humidification taking place as the warm dry air passes through the humidifier(s), the greenhouse air is also humidified by some other sources. Evaporation from the wet soil and transpiration from the plants are two other sources contributing to the accumulation of the moisture in the microclimate of the greenhouse. Different ways to quantify the *humidity level* of the greenhouse air are discussed in Sec. 2.2.

2.1.3. Dehumidification

High humidity levels might be an undesirable situation at certain instances. In greenhouses, high humidity levels result in the condensation of water vapour on the inner surface of the greenhouse cover. It is unwanted situation by greenhouse cultivars because the condensed water vapour sometimes starts to trickle on plant leaves which might cause the infection of some pathogenic fungi and bacteria (Boulard, et al., 1989; and Jarvis, 1992). Different techniques to dehumidify the air inside greenhouses have been practiced/studied. They included the use of solar (i.e. natural) heating, heat pumps (Brundrett, 1987; Feuilloley and Guillaume, 1990; and Trigui et al., 1999), desiccant materials (Boulard, 1987) and heat exchangers (Paton and Davis, 1996; Goosen et al.,

2000b; Sablani et al., 2003; Goosen et al., 2003; and Davies and Paton, 2005). The first method lowers the *relative humidity* by increasing the *air temperature* (i.e. increasing the *vapour pressure deficit*), the second method reduces it by removing moisture and increasing *air temperature* and the third and fourth methods reduce it by removing moisture from the air. Because the last method of reducing the *relative humidity* in greenhouses is the only relevant technique to this study, it will be explained in more details, below.

The dehumidification process takes place in heat exchangers basically by condensing the water vapour carried in the flowing air. For this to happen, the *surface temperature* of the heat exchanger (i.e. dehumidifier) must be below the *dew-point temperature* of the moist air (Sauer and Howell, 1983; Huang, 1988; Fujii, 1991; and Moran and Shapiro, 1992). The temperature of the dehumidifier can be lowered to that extent by the use of a coolant fluid that has a temperature less than the *dew-point temperature* of the air. Basically, the temperature of the fluid should be less than the *dew-point temperature* of the air owing to the fact that the fluid will not be in direct contact with the air; the cooling fluid will be flowing inside the dehumidifier tubes. Although the thickness of these tubes is relatively small, the *surface temperature* of the tubes will be slightly higher than that of the fluid as a result of gaining some heat (latent and/or sensible) from the moving air. This can be conceived as a loss in the coldness of the fluid which necessitates the fluid to have a cooler temperature in order to overcome this loss.

Once the moist air comes in contact with the dehumidifier surface that has a temperature less than the *dew-point*, the water vapour in the air will undergo a phase change from gas to liquid. This phase change results in the release of the *latent heat of vaporization* L_v. As a result, this heat is expected to slightly raise the surface temperature of the dehumidifier tubes which results, in turn, in an increase in the temperature of the coolant fluid. The dehumidification process will result in a removal of some moisture from the air. Because this dehumidification process has no external heat input/removal except of the two

fluids involved in the process (i.e. the moist air and the coolant), it is considered *adiabatic*.

The dehumidification process is significantly affected by the dehumidifier design. It is not the scope of this study to elaborate on this, however many design criteria should be considered when selecting which dehumidifier design to opt. Examples of these criteria are the flow pattern of the fluids (i.e. *counter*, *parallel* or *cross*), the design material, the size and whether to include fins or not, if finned, what type of fin pattern? Thermodynamic text books can provide a broad understanding of this topic (e.g. Jones and Hawkins, 1986; Brundrett, 1987; Huang, 1988; Haberman and John, 1989; Fujii, 1991; Moran and Shapiro, 1992; Cengel and Boles, 1998; and Kakac et al., 1999).

The dehumidification process is also affected by the conditions of the air. These include the *air temperature*, *humidity* and *flowrate*. As explained above, the whole process depends on the temperatures of the air and coolant fluid. As the *air relative humidity* increases, the *dew-point temperature* approaches the *air temperature* (Esmay and Dixon, 1986). This implies that at high humidity levels, a coolant with a temperature slightly lower than the *air temperature* will be sufficient for the dehumidification to take place. *Air flowrate* is a significant variable that influences the dehumidification. At high flowrates, the air moves with a high speed which reduces the time for surface contact between the air and the dehumidifier. This time is necessary for the release of the L_v which results in the phase change of the water vapour.

The *coolant fluid temperature* and *flowrate* are also factors affecting the dehumidification process. It can also be influenced by some external factors like *solar radiation* if the dehumidifier is not properly shaded. The *solar radiation* impinging on the dehumidifier can increase the *surface temperature* of the dehumidifier tubes and consequently, the temperature of the air and coolant water will increase. Once this (or a similar) heat source is involved in the process, it becomes non-*adiabatic*. Therefore, the contribution of external

factors should be taken into consideration when designing and operating the dehumidifier in order to achieve better performance.

2.1.4. HD greenhouses

The humidification process followed by the dehumidification process can be very often found in industrial applications especially in desalination plants. However, combining these two processes in a greenhouse is a new technology (Goosen et al., 2000a & 2000b; and Delyannis and Belessiotis, 2000). The purpose of the HD greenhouses is not to reduce the humidity inside the greenhouse for the sake of plant growth but mainly to produce fresh water for agricultural purposes by collecting the water vapour inside the greenhouse. In the recent years, studies to combine these two processes together in greenhouses have been conducted. However, the methodology of applying this idea was not always the same, as discussed below.

In some greenhouses, the evaporation and condensation of the water takes place inside the cavity between two layers of the greenhouse glazing material (Selcuk and Tran, 1975; and Chaibi, 2000). These greenhouses use the concept of the so-called “solar still” (see Fig. 2.3).

Other greenhouses use the ordinary evaporative cooling pads to humidify the air. As the air flows inside the greenhouse, its temperature increases mainly due to the *solar heat gain*. The *sensible heat* removed from the plants (Bailey, 1990), soil and cover can be attributable to this temperature increase.

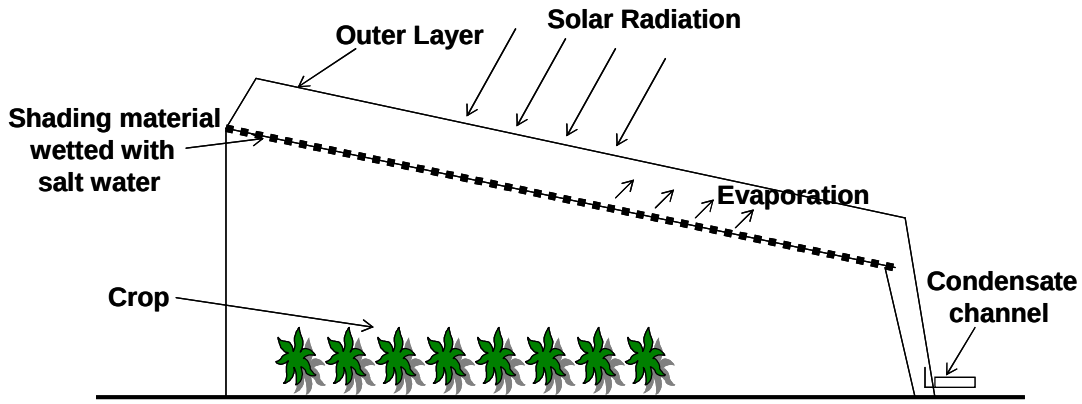

Fig. 2.3: A sketch of a combined solar still and a greenhouse (Chaibi, 2000)

As *air temperature* increases, its *relative humidity* decreases which can be interpreted as an increase in the air capacity to hold more water vapour (Al-Ismaili, 2003; and Perret et al., 2005).

The air is further loaded by moisture through a 2nd humidifier placed before the fans. Then, the moisture is dehumidified at the end of the greenhouse using a dehumidifier located between the 2nd humidifier and the fans (Paton and Davis, 1996; Goosen et al., 2000b; Sablani et al., 2003; Goosen et al., 2003; and Davies and Paton, 2005). Relatively cold water is initially pumped through the dehumidifier as a coolant. This water gains some heat as a result of the release of the L_v from the dehumidification process taking place on the outer surface of the dehumidifier. Then, this preheated water is circulated to the 1st humidifier on which it gets in contact with the warm air passing through the 1st humidifier. Consequently, water evaporation takes place which, in turn, results in a reduction in the *air* and *water temperatures*.

In 1994, a seawater HD greenhouse (Fig. 2.4) working with the same principal, explained above, was erected and investigated in the south of Tenerife (Paton and Davis, 1996; and Davies et al., 2004). The greenhouse was composed of two humidifiers; the 1st humidifier was placed at one side of the greenhouse and the 2nd one was placed at the opposite side before the fans. Moreover, the dehumidifier of this prototype greenhouse was cooled using cold deep seawater. Figure 2.5 illustrates the air and water flows in this

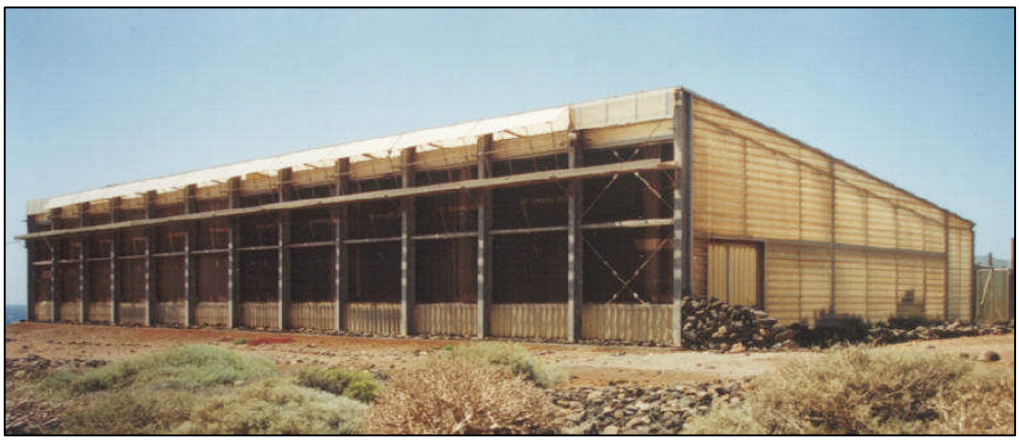

Fig. 2.4: The seawater HD greenhouse in Tenerife (Davies et al., 2004)

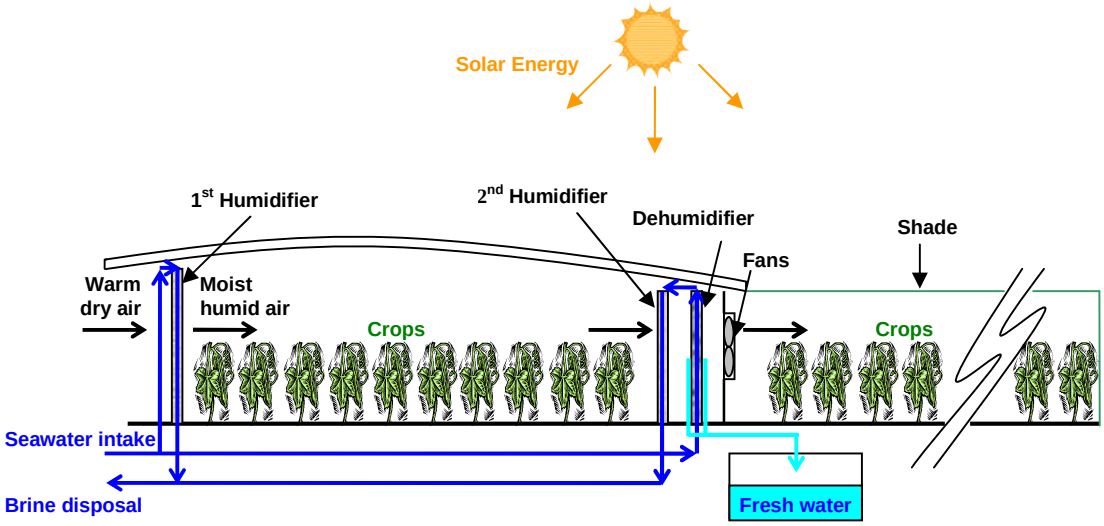

Fig. 2.5: Schematic of the seawater HD Greenhouse (Sablani et al., 2003; and Goosen et al, 2003)

greenhouse. The amount of water produced was more than twice the amount required to irrigate an equivalent ground area of the greenhouse.

In cases where cold feed seawater is not available, the water flowing down the 1st humidifier may be usable as a coolant if its temperature decreased sufficiently as a result of the evaporation (Al-Ismaili, 2003; Perret et al., 2005; and Lovitchit et al., 2007). Al-Ismaili (2003) and Perret et al. (2005) reported that the use of this water as the dehumidifier coolant is feasible owing to its temperature being always below the *saturation temperature* of the moist air passing through the dehumidifier of their experiments (see Fig. 2.6). This

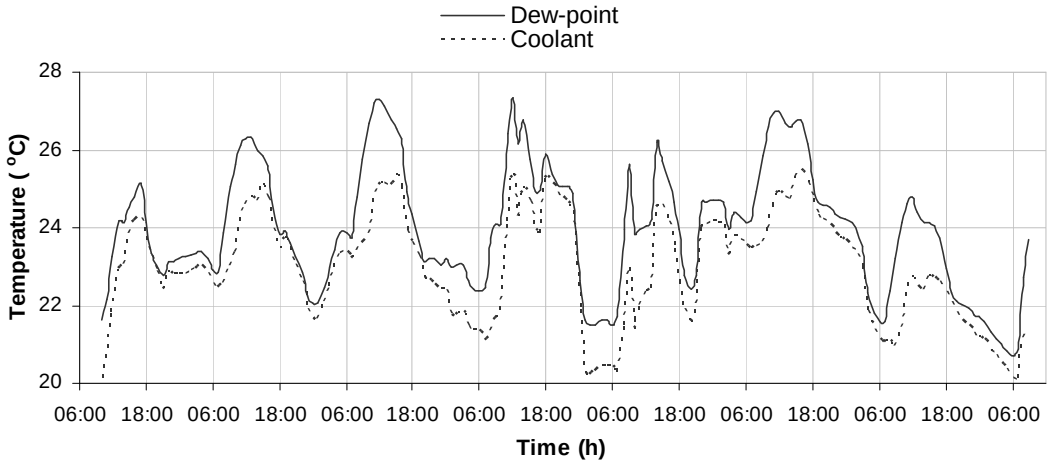

Fig. 2.6: Changes of the dew-point temperature of the air and the coolant temperature with time (Al-Ismaili, 2003; and Perret et al., 2005)

temperature differential was caused by the evaporation in the 1st humidifier even at night due to the dry warm air conditions during their experiments.

A number of modifications to the settings of the Tenerife seawater HD greenhouse was then applied to a second greenhouse constructed in the United Arab Emirates in 2000 (Davies et al., 2004; and Davies and Paton, 2005). The modifications included the use of the water flowing from the 1st humidifier as a coolant in the dehumidifier (Davies et al., 2004). The water production was below expectation. However with a further modification, the greenhouse was able to meet its freshwater requirement. This modification was to preheat the water used to wet the 2nd humidifier by pumping it through a "solar heater" in order to enhance evaporation. The solar heater was basically a tube array made up from black polyethylene hoses lying in the sun.

The third seawater HD greenhouse was constructed in Oman taking into consideration the knowledge gained from the previous two greenhouses. This greenhouse composed of two water circuits. The first circuit was linking the 1st humidifier with the dehumidifier and the 2nd circuit was between the tube array (i.e. the solar heater) and the 2nd humidifier (see Fig. 2.7). The tube array was integrated inside the greenhouse just below the cover. The dehumidifier material was changed from the tube-and-fin dehumidifier made of cupronickel

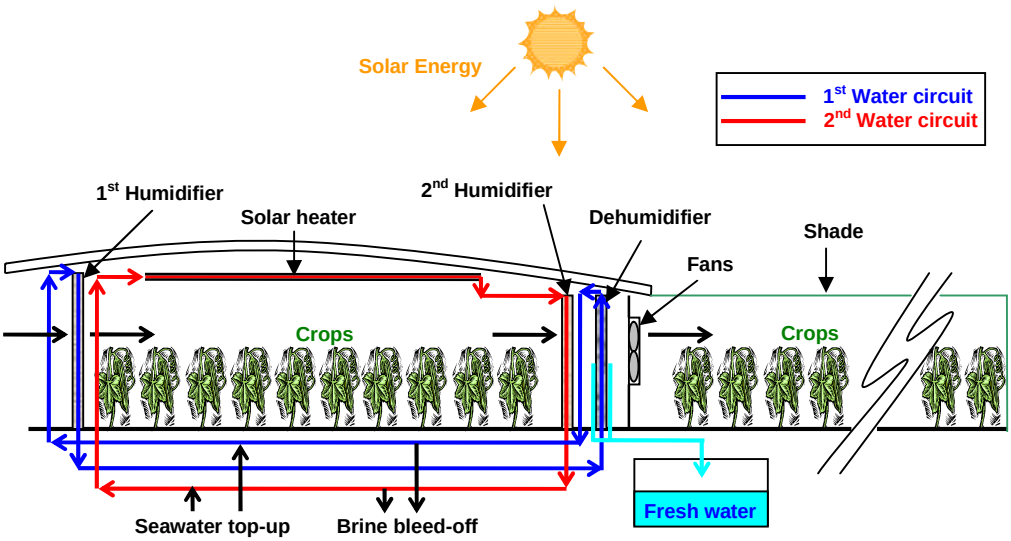

Fig. 2.7: Illustration of the two water circuits of the HD greenhouse in Oman

and aluminium, previously used, to a completely plastic-tube dehumidifier (Davies et al, 2004). No published evidence quantifying the amount of water produced from this greenhouse could be found up to date. However based on visual observations, the greenhouse seemed to be producing reasonable amount of condensate.

Al-Ismaili (2003) studied the HD concept in a Quonset greenhouse in Oman (see Fig. 2.8). He used the nationwide type of greenhouses to investigate the practicality of using such a technique to produce the irrigation water. The findings from that study were valuable; however, water production was not achieved. Since the *coolant temperature* (i.e. water from the cooling pads) was all the time below the *dew-point temperature* (i.e. condensation was theoretically feasible), the absence of significant condensation was attributed to the relatively high *air velocity* (more than 2.4 m/s) through the small cross-sectional area of the dehumidifiers (0.9 m x 0.9 m) (Al-Ismaili, 2003; and Perret et al., 2005).

Mangold et al. (1983) reported that understanding the physical and thermodynamic properties of moist air is a requirement for agricultural engineers when designing environmental control systems for crops and animals. Goosen et al. (2000a) emphasized the importance of understanding the thermodynamics of the greenhouse in order to optimize processes like the

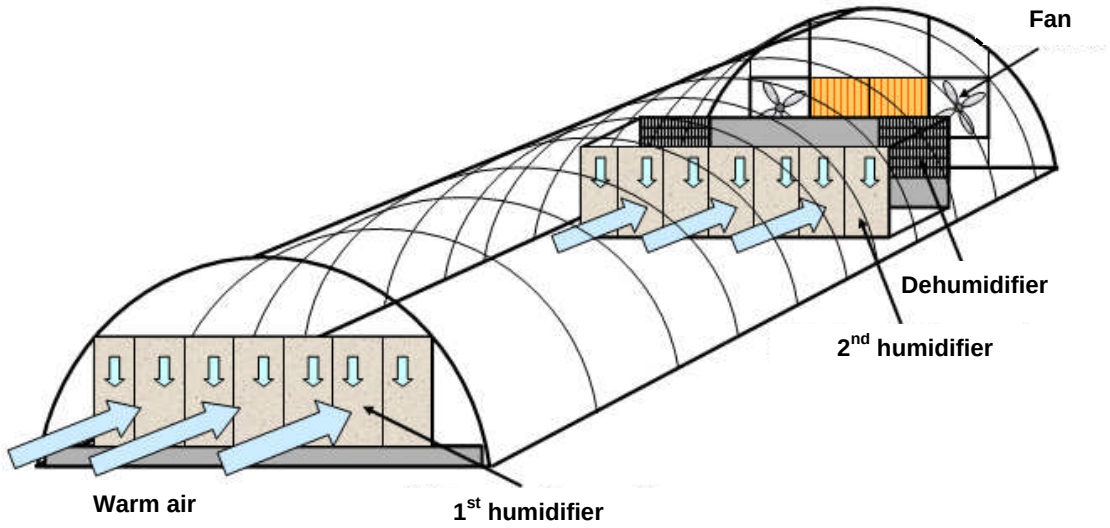

Fig. 2.8: Illustration of the greenhouse used by Al-Ismaili (2003)

humidification and dehumidification. Therefore, with good understanding of the thermodynamic processes taking place in the HD greenhouse, the researcher can save both cost and time before proceeding to real constructions and practical investigations. Mathematical simulation models can be very helpful in quantifying the essential parameters involved in the thermodynamic processes of the HD greenhouse.

2.2. GREENHOUSE SIMULATION MODELS

2.2.1. Introduction

Mathematical simulations of greenhouse processes are helpful tools that enable understanding the influence of various climatic conditions and greenhouse structural and operational variables on the microclimate environment. The simulation models can present the complex interrelationships of the climatic, structural and operational variables in a usable mathematical format. In the literature, numerous simulation models dealing with the greenhouse inner environment (microclimate) can be found. Different considerations have been taken into account when developing these models. The required output(s) and the accuracy of the prediction as well as the nature (i.e. *dynamic* or *steady-state*) and composition of the model are among those considerations. Therefore, one can understand the reason for the large number of the available models focusing only on the microclimate of the greenhouses.

Kano and Salder (1985) provided a descriptive review of most of greenhouse models developed in the period between 1965 and 1983. The models they mentioned can be classified into two main categories; *steady-state* and *dynamic* models. Those models can be used for predicting different variables including; the temperature of the greenhouse air, soil and plants, the *relative humidity*, the heating and cooling requirements (e.g. ventilation rates, shading percentage and evaporating pad area), and the crop growth and production. Other benefits of the greenhouse models are to use them to control

the inner environment of the greenhouse and to improve the design and performance of greenhouses.

The process of developing *heat* and *mass transfer* models, as found in literature, starts with the formulation of *energy* and sometimes *moisture balance* equations. In the case of the *energy balance*, the equation represents an inventory of all heat gain/loss terms of the controlled volume for which the balance is dedicated. Similarly the *moisture balance* equations balance the moisture transfer terms. The controlled volume can be the entire greenhouse or only one component or section within the greenhouse. In order to develop accurate-prediction models, the balance equations should integrate all significant variables. However, a variable might be considered significant by one model developer and the same variable can be neglected by another developer because it is assumed insignificant for the sake of simplicity or for some other reasons.

Once the balance equations are formulated and the simulation model to predict the required unknown(s) is developed, calibration/validation experiments are normally carried out to test the accuracy of the model. The calculated values from the model are compared to the measured results. Thus, if a satisfactory agreement between both results was achieved then it is a good indicator that the model included all significant variables and so, it can be further utilized for prediction purposes. Otherwise, model developers need to revisit the model again and modify it accordingly.

In this section, several greenhouse models are studied and analysed. *Steady-state* and *dynamic* models simulating the inner environment of the greenhouse are discussed in sub-Sections 2.2.2 and 2.2.3, respectively. The process of studying each model will start by looking at the balance equation(s) used to develop that model. Included and discarded moisture and/or heat terms of the balance equations will be discussed. Further, a schematic illustration of these terms will be presented. Then, a final comprehensive format of the model will be presented. Validation tests, if conducted, will be reviewed and the

expected reliability of the model will be indicated. Any further importance of the model will be stated. An overall discussion of the models presented can be found in Sec. 2.2.4. Section 2.2.5 discusses the only HD greenhouse simulation model found in literature. The developed/adapted greenhouse heat and mass transfer simulation models that will be utilized in this study will be discussed in details in the next chapters.

2.2.2. Steady-state greenhouse models

This section deals with the *steady-state* (or time-independent) heat and mass transfer models focusing on the greenhouse microclimate. With *steady-state* models, the time variation of the various inputs on greenhouse components (e.g. air, plants and soil) is not considered. In other words, the *internal energy* (i.e. *energy level*) or *moisture content* of any component/section within the greenhouse at any given time are assumed to be independent of the *energy level* or *moisture content* at some previous time. Therefore, the moisture and/or heat storage of all components/sections within the greenhouse are not considered in these models. Each of the following sub-sections will be addressing one (or more) greenhouse heat and mass transfer model(s).

2.2.2.1. Walker's model to predict average air temperature

When talking about the *steady-state* heat and mass transfer models in greenhouses, the major work done by Walker (1965) cannot be ignored. Kano and Salder (1985) mentioned that Walker's work was the most-often-cited reference in the field of greenhouse modelling. Walker aimed from his study to develop a model capable of predicting the average *air temperature* of the greenhouse. In formulating the balance equation, the entire greenhouse inner environment was considered as the controlled volume. Energy predominant flow directions are shown in Fig. (2.9).

The following *heat balance* equation, introduced by Walker, considers any heat to the greenhouse as a heat gain and any heat out of it as a heat loss. His *heat balance* (Eq. 2.1) was a good attempt to incorporate all possible

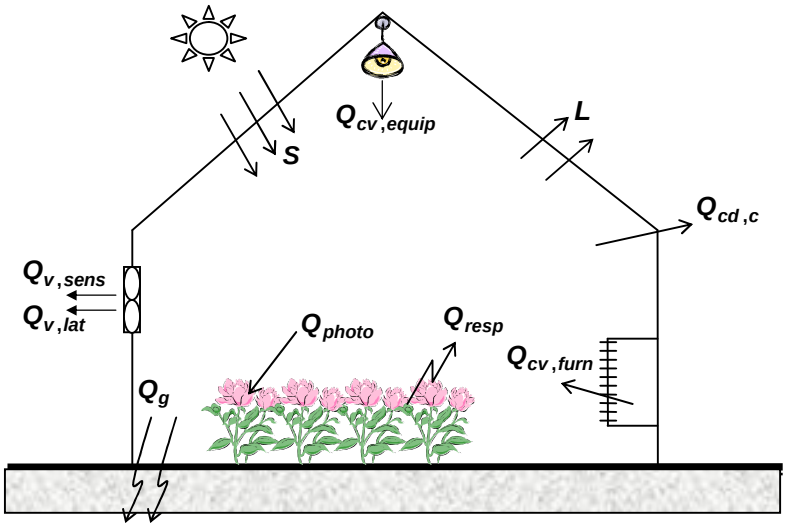

Fig. 2.9: Schematic of energy flows in a greenhouse

influencing heat/moisture terms in one equation. This balance can, then, be used for developing several *steady-state* greenhouse simulation models by considering the relevant terms and discarding the irrelevant ones.

$$S + Q_{cv,furn} + Q_{cv,equip} + Q_{resp} = L + Q_{cd,c} + Q_{photo} + Q_g + Q_{v,sens} + Q_{v,lat} \quad (2.1)$$

Walker used this energy budget to develop his model that predicts the *air temperature* of a greenhouse similar to the one illustrated in Fig. (2.9), but with no plants, furnace or equipments that might contribute in the *heat balance* of the greenhouse. As a result of the absence of any means of supplemental heat, the furnace and equipments heat terms (i.e. $Q_{cv,furn}$ and $Q_{cv,equip}$, respectively) were not included in Walker's model. Besides, the *latent heat* removal by the ventilation, $Q_{v,lat}$, was also neglected from the model since it was solely representing the *latent heat* of transpired water by plants.

Regarding the other terms, Walker studied their order of magnitude and included only the significant ones. Among them, the heat gain from the *solar radiation* S and the *sensible heat* losses due to the ventilation $Q_{v,sens}$, conduction (through the cover) $Q_{cd,c}$ and *thermal* (i.e. long wavelength) *radiation* L were considered. However, the terms for the *photosynthetic heat* loss Q_{photo}, the heat transfer (i.e. convective and conductive) between the

greenhouse environment and the floor (soil) Q_g and the *respiratory heat* gain Q_{resp} were neglected due to their minute value relative to the *solar heat gain* S. Although *conductive heat transfer* of the soil Q_g was considered insignificant, Walker pointed out that at some conditions this source of heat might be significant.

The four terms included in the model were calculated using these formulae;

$$S = \phi_s \, A_s \, \tau_c \, \mathrm{I}_{out} \,,$$

$$Q_{cd,c} = U_c \, A_c (T_{in} - T_{out})$$

$$Q_{v,sens} = C_{p,a} \frac{\dot{V}_a}{\mathrm{v}} (T_{in} - T_{out})$$

$$L = \sigma \, A_s \, \tau_{\lambda,\,c} \left(\varepsilon_s \, T_{s,K}^4 - T_{out,K}^4 \right)$$

Walker's model appeared in the format shown in Eq. (2.2).

$$T_{in} = \frac{\phi_s \, A_s \, \tau_c \, \mathrm{I}_{out} + U_c \, A_c \, T_{out} + C_{p,a} \frac{\dot{V}_a}{\mathrm{v}} T_{out} - \sigma \, A_s \, \tau_{\lambda,\mathrm{c}} \left(\varepsilon_s \, T_s^4 - T_{out}^4 \right)}{U_c \, A_c + C_{p,a} \frac{\dot{V}_a}{\mathrm{v}}} \qquad (2.2)$$

This model was tested in a physical model and a full size greenhouse. For the four experimental days in the physical model, the mean variation of the predicted and measured results of the *air temperature* was approximately 1.4^{o}C and the mean percent error was 17.6 %. Although a quantitative presentation was not provided for the full size greenhouse, it was reported that the predicted values were consistent with the measured data of *air temperature* and winter heat requirements.

Price and Peart (1973) employed Walker's *steady-state* model as an integrated part of a *dynamic* simulation setup that also included in addition to the greenhouse, a steam-electric power plant, a hot-water storage reservoir, an aquaculture reservoir and a cooling/recreational lake. They did not use the final

format of Walker's model (Eq. 2.2) but the balance equation (Eq. 2.1). All the heat terms that were not considered by Walker due to their insignificance or irrelevance were considered by Price and Peart. These heat terms are the *soil heat transfer*, the supplemental heat from greenhouse equipments and the air heater, the *photosynthetic* and *respiratory heat* from the plants and the *latent heat* removed by the ventilation.

The formulae suggested by Walker to calculate the *soil heat exchange*;

$$Q_g = 0.568\, A_g (T_g - T_{ww})$$

and *latent heat of ventilation*;

$$Q_{v,lat} = L_v\, A_g\, \dot{M}_{ET}$$

were used by Price and Peart (1973). Also, it seems that they used Walker's suggested approximations to obtain the heat necessary for the *plant photosynthesis* and the heat given off by the *plant respiration*. The heat released by greenhouse equipments and the air heater could be calculated using conventional methods.

Although Price and Peart did not provide a comparative analysis of the predicted and observed results, they reported that the whole *dynamic* simulation model, in which the greenhouse *steady-state* model was integrated, operated satisfactorily throughout the year for the weather conditions of their study place. From that, it can be deduced that even the *steady-state* model performed satisfactorily during the 12-month simulation period.

2.2.2.2. von Elsner's model to predict average air temperature

In another study that is not distinct from Walker's model, von Elsner (1980) provided the following *heat balance* equation to develop a model that enables the prediction of the average *air temperature* of the greenhouse (see Fig. 2.10):

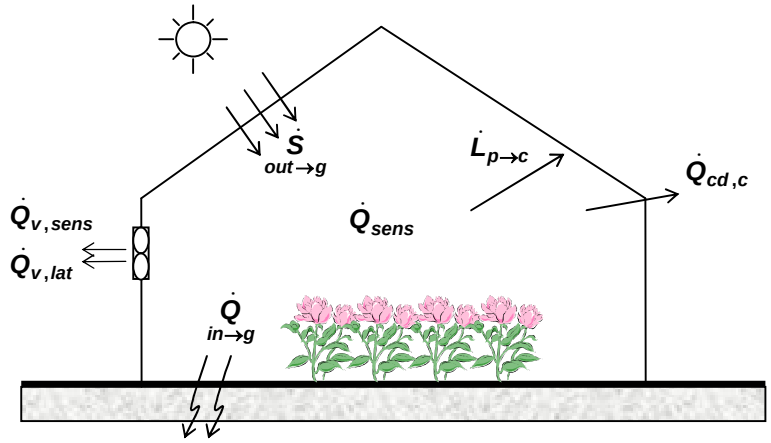

Fig. 2.10: Schematic of energy terms considered in von Elsner's (1980) study

$$\rho_a \, C_{p,a} \frac{V_a}{A_g} \frac{dT}{dt} = \dot{Q}_{sens} - \dot{Q}_{cd,c} - \dot{Q}_{v,sens} - \dot{Q}_{v,lat} \qquad (2.3)$$

In this balance, the amount of heat stored in greenhouse masses (e.g. plants, soil and benches), the heat required for *photosynthesis* and the heat released by *respiration* were neglected because they were considered insignificant. The *long-wave heat exchange* between greenhouse inner surfaces and the outer atmosphere was not included due to the use of a glazing material which is opaque to *long-wave radiations*. However, the *long-wave heat exchange* between the plants and the greenhouse cover was considered in the *sensible heat* term $\dot{Q}_{sens}$. In addition, the heat supplied to the greenhouse by the *solar radiation* was accounted for in the same term. Further, the left hand side of Eq. (2.3) represents the change in the *internal energy* of the greenhouse with time. Assuming a *steady-state* condition, this term vanishes and the equation can be rewritten as:

$$\dot{Q}_{sens} = \dot{Q}_{cd,c} + \dot{Q}_{v,sens} + \dot{Q}_{v,lat} \qquad (2.4)$$

The four terms considered in this equation are; the *sensible heat* $\dot{Q}_{sens}$ of the greenhouse, the heat exchange through the cover $\dot{Q}_{cd,c}$ and the *sensible* and *latent heat of ventilation* ($\dot{Q}_{v,sens}$ and $\dot{Q}_{v,lat}$, respectively). Equation (2.4) reveals that the change in the $\dot{Q}_{sens}$ is equivalent to the heat losses through the

ventilation and the greenhouse structure. The following formulae were provided in von Elsner (1980) to calculate the terms of Eq. (2.4);

$$\dot{Q}_{sens} = \frac{\beta \dot{Q}_n}{\beta + 1}$$

$$\dot{Q}_{cd,c} = U_c \frac{A_c}{A_g}(T_{in} - T_{out})$$

$$\dot{Q}_{v,\text{sens}} = \frac{\dot{V}_a}{A_g} \rho_a \, C_{p,a}(T_{ext} - T_{ent})$$

$$\dot{Q}_{v,lat} = \frac{\dot{V}_a}{A_g} \rho_a \, L_v(\varpi_{ext} - \varpi_{ent})$$

where

$$\dot{Q}_n = (1 - \phi_s)\tau_c \, I_{out} - L_{p \to c}$$

The *Bowen ratio* β involved in the calculation of the $\dot{Q}_{sens}$ is the ratio of the *sensible heat* to the *latent heat*. In the formula used to calculate the $\dot{Q}_{v,lat}$, a variable von Elsner called the *absolute humidity* ϖ, [kg (water) /kg (air)], was integrated. In fact, this parameter is neither *absolute humidity* [kg (water) /m^3 (air)] nor *humidity ratio* [kg (water) /kg (dry air)], but it is "*specific humidity*" [kg (water) /kg (air)] (ASHRAE, 2001; and Huang, 1988). From the balance equation (Eq. 2.4), the following model that enables the prediction of the average *air temperature* of the greenhouse was derived:

$$T_{in} = \frac{\frac{\beta \dot{Q}_n}{\beta + 1} + U_c \frac{A_c}{A_g} T_{out} + 2\frac{\dot{V}_a}{A_g} \rho_a \, C_{p,a} \, T_{ent} + 2\frac{\dot{V}_a}{A_g} \rho_a \, L_v(\varpi_{ent} - \varpi_{avg})}{U_c \frac{A_c}{A_g} + 2\frac{\dot{V}_a}{A_g} \rho_a \, C_{p,a}} \quad (2.5)$$

In this literature, the model was not accompanied with any test results that could show its accuracy to predict the average *air temperature*. Also, it included

the *Bowen ratio* which can be considered as a limitation of the model since its value is difficult to estimate.

2.2.2.3. Model of Maher and O'Flaherty to predict average air temperature, humidity ratio and plant temperature

Maher and O'Flaherty (1973) developed a simulation model that enables the prediction of average *air temperature* and *humidity* of the greenhouse as well as *plant temperature*. In developing their model, they considered three components of the greenhouse; crops, greenhouse structure and inside air. Four balance equations were formulated in order to get to an accurate simulation of the greenhouse processes. It was assumed that all incident solar radiation inside the greenhouse is intercepted by the plants. The soil was assumed not to play an important role in the heat and mass budgets. Figure (2.11) illustrates all heat terms and their flow directions that were considered in the balance equations.

The first equation was the *energy balance* at the surface of crop leaves. It can be expressed as shown in Eq. (2.6):

$$\dot{S}_p - \dot{L}_{p\to c} - \dot{Q}_{cv,p\to in} - \dot{Q}_T = 0 \qquad (2.6)$$

The energy expressions included in this balance are similar to those previously included by Wolpert (1962). The terms of Eq. (2.6) were calculated using;

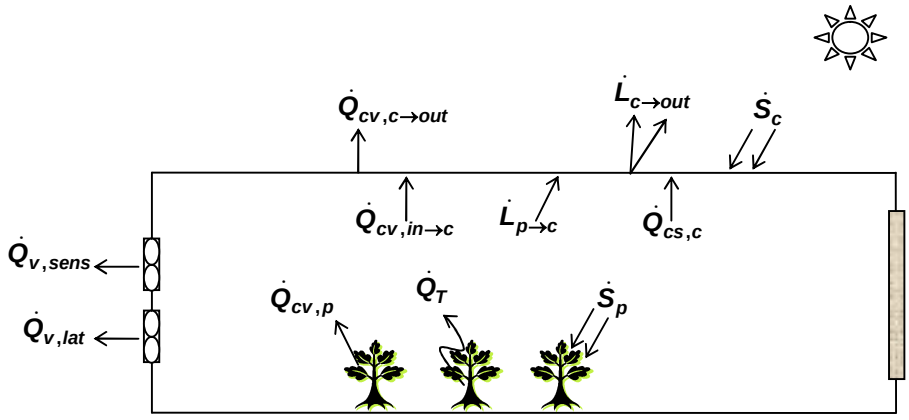

Fig. 2.11: A sketch of energy terms considered by Maher and O'Flaherty (1973)

$$\dot{S}_p = \left(1-\phi_p\right)\tau_c \, \mathrm{I}_{out}$$

$$\dot{L}_{p\to c} = \varepsilon_{p\to c}\,\sigma\left(T_{p,K}^4 - T_{c,K}^4\right)$$

$$\dot{Q}_{cv,p} = \rho_a \, C_{p,a} \, \frac{T_p - T_{in}}{r_a}$$

$$\dot{Q}_T = \rho_a \, L_v \, \frac{\hbar_p - \hbar_{in}}{r_{leaf}}$$

In order to get the correct units for the transpiration term $\dot{Q}_T$, the formula should be modified as follows:

$$\dot{Q}_T = \rho_a \, L_v \, \frac{\varpi_p - \varpi_{in}}{r_{leaf}}$$

Equations (2.7) and (2.8) present, respectively, the *sensible* and *latent heat balances* of the inside air:

$$\dot{Q}_{cv,p} - \dot{Q}_{cv,in\to c} - \dot{Q}_{v,sens} = 0 \qquad (2.7)$$

$$\dot{Q}_T - \dot{Q}_{cs,c} - \dot{Q}_{v,lat} = 0 \qquad (2.8)$$

The following expressions were used to calculate the new terms of the *energy balance* equations of the inside air;

$$\dot{Q}_{cv,in\to c} = 4.36\left(T_{in} - T_c\right)^{5/4}$$

$$\dot{Q}_{v,sens} = \rho_a \, C_{p,a} \, \frac{\dot{V}_a}{A_g}\left(T_{in} - T_{out}\right)$$

$$\dot{Q}_{cs,c} = 1.06\times 10^4 \left(T_{in} - T_c\right)^{1/4}\left(\varpi_{in} - \varpi_c\right)$$

$$\dot{Q}_{v,lat} = \rho_a \, L_v \, \frac{\dot{V}_a}{A_g}\left(\varpi_{in} - \varpi_{out}\right)$$

For the greenhouse structure, the following *heat balance* equation was considered:

$$\dot{S}_c + \dot{L}_{p\to c} + \dot{Q}_{cv,in\to c} + \dot{Q}_{cs,c} - \dot{Q}_{cv,c\to out} - \dot{L}_{c\to out} = 0 \qquad (2.9)$$

The three terms of Eq. (2.9) that were not previously expressed are calculated using the following relations;

$$\dot{S}_c = \phi_p \, \mathrm{I}_{out}$$

$$\dot{Q}_{cv,c\to out} = 1.98\,\mathrm{u}_a^{0.8}\left(T_c - T_{out}\right)$$

$$L_{c\to out} = \left(\varepsilon_c \, \sigma \, T_{c,K}^4 - 5.31\times 10^{-13} \, T_{out,K}^6\right)\left(1.0 - 0.9\,\xi\right)$$

An iterative approach was followed to solve all of the four balance equations to come up with predictions for the *air temperature* and *humidity* of the greenhouse and the *plant temperature*. Maher and O'Flaherty used their model to simulate a hypothetical glasshouse with given structural and vegetation properties. They reported that the predictions of their model were in agreement with the available practical experience.

2.2.2.4. Model of Boulard and Baille to predict average air temperature, partial vapour pressure, plant temperature and transpiration rate

The aim of the study of Boulard and Baille (1993) was to develop a greenhouse simulation model that predicts the average *air temperature* and *humidity* of the greenhouse and *plant temperature* and *transpiration rate*. In developing their model, they dealt with the greenhouse (Fig. 2.12) as a solar collector.

Three balance equations were developed to simulate the thermal environment of the greenhouse. The general *energy balance* equation for the greenhouse air (Eq. 2.10) did not include the amount of heat absorbed or released by greenhouse soil or any masses other than the plants. Further, the evaporation from the soil was not considered in the analysis because soil-less cultivation was practiced. In addition, the *latent heat* released by condensation was neglected since this phenomenon was considered unlikely to occur.

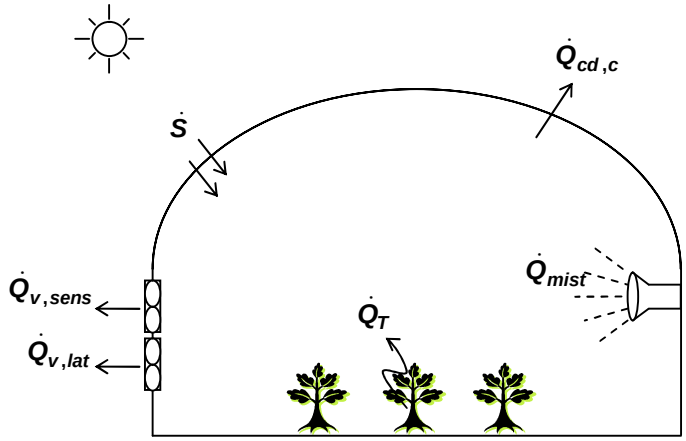

Fig. 2.12: An illustration of the evaporatively cooled greenhouse considered by Boulard and Baille (1993)

$$\dot{S} - \dot{Q}_{cd,c} - \dot{Q}_{v,sens} - \dot{Q}_{v,lat} = 0 \qquad (2.10)$$

Because the analysis considered the greenhouse functioning as a solar collector, the *solar heat gain* $\dot{S}$ was calculated using a similar expression as a solar collector;

$$\dot{S} = E\, \mathrm{I}_{out}$$

where E is the *effectiveness* of the greenhouse as a solar collector. The other three terms of Eq. (2.10) were calculated using;

$$\dot{Q}_{cd,c} = U_c\, \Delta T$$

$$\dot{Q}_{v,sens} = \rho_a\, C_{p,a}\, \frac{\dot{V}_a}{A_g}\, \Delta T$$

$$\dot{Q}_{v,lat} = q\, \rho_a\, L_v\, \frac{\dot{V}_a}{A_g}\, \Delta \psi$$

where

$$\Delta T = \left(T_{in} - T_{out}\right)$$

$$\Delta \psi = \left(\psi_{in} - \psi_{out}\right)$$

and the constant $q = 6.25 \times 10^{-6}$ [kg (water)/kg (air) Pa]

The other equation presented by Boulard and Baille (1993) was the *latent heat balance* of the greenhouse air (Eq. 2.11). This equation integrated three heat terms which are the *latent heats of ventilation* $\dot{Q}_{v,lat}$, *plant transpiration* $\dot{Q}_T$ and *evaporation of the sprayed water* $\dot{Q}_{mist}$. It implies that the *latent heat* gained through the plant transpiration and the misted-water evaporation is equivalent to the *latent heat* lost by ventilation.

$$\dot{Q}_{v,lat} = \dot{Q}_T + \dot{Q}_{mist} \tag{2.11}$$

Boulard and Baille (1993) calculated the $\dot{Q}_T$ using a linearized form of the well known Penman-Monteith formula;

$$\dot{Q}_T = L_v \, \mathrm{T}_{rate} = q_1 \left(1 - \phi_p\right) \tau_c \, \mathrm{I}_{out} + q_2 \, \psi'''_{in}$$

where the coefficients q_1 and q_2 are expressed as functions of the *aerodynamic* and *canopy resistances*, respectively. Because

$$\psi'''_{in} = \psi''_{in} - \psi_{in}$$

is not a linear function of T_{in}, it was decomposed and modified in order to linearize it. As a result of the linearization, it was expressed as;

$$\psi'''_{in} = \delta(T_{out}) \, \Delta T - \Delta\psi + \psi'''_{out}$$

where $\delta(T_{out})$ is the slope of the water vapour saturation curve at $T = T_{out}$. The last term of Eq. (2.11) has two cases; the misted water used for cooling either (a) completely or (b) partially vaporizes. For both cases, the *vaporization heat flux* $\dot{Q}_{mist}$ was suggested to be calculated as follows;

(a) $$\dot{Q}_{mist} = L_v \frac{\dot{M}_{mist}}{A_g}$$

and

(b) $$\dot{Q}_{mist} = \dot{Q}_{mist,\max} = q_3 \, L_v \, \frac{\dot{M}_{mist}}{A_g}$$

where q_3 is the vaporized fraction of the total sprayed water. Empirically, it was found that;

$$\dot{Q}_{mist,\max} = q_4 \, \psi'''_{in}$$

where the coefficient q_4 can be found through experiments.

In order to make the prediction of the *crop leaf temperature* and the *crop transpiration rate* feasible, the following *sensible heat* balance for the greenhouse crop was formulated:

$$T_p - T_{in} = \frac{r_a \left((1-\phi_p) \tau_c \, \mathrm{I}_{out} - L_v \, \mathrm{T}_{rate} \right)}{\rho_a \, C_{p,a} \, LAI} \qquad (2.12)$$

where

$$r_a = \frac{\rho_a \, C_{p,a}}{2 \, \mathrm{h}_a}$$

in which

$$\mathrm{h}_a = 1.95 \frac{\left| T_p - T_{in} \right|^{1/4}}{l_{leaf}}$$

Boulard and Baille (1993) used the first two balance equations (Eqs. 2.10 & 2.11) to obtain the values of the *air temperature* and *humidity*. With the aid of Eq. (2.12), the *plant temperature* and *transpiration rate* were calculated. They reported that a good agreement between computed and observed results was achieved especially for the *air temperature* and *humidity*. As an application of their model, they used it to study the effect of the ventilation and water misting rates on the four output variables; *air temperature* and *humidity* and *plant temperature* and *transpiration rate*. They found that the first two parameters were the most sensitive to the misting rates.

2.2.2.5. Model of Kittas and co-authors to predict air temperature as a function of longitudinal distance

Kittas et al. (2001 & 2003) contributed to the field of greenhouse heat and mass transfer modelling by developing a simple mathematical relation that predicts greenhouse *air temperature* variations along the airflow direction. Initially, four heat energies were considered namely; the *short-wave solar radiation* S, the heat required for the plant transpiration Q_T, the *conductive heat loss* through the greenhouse structure $Q_{cd,c}$ and the *sensible heat* removal by ventilation $Q_{v,sens}$ (see Fig. 2.13). The balance equation used to develop the model was:

$$Q_{v,sens} = (S - Q_T) - Q_{cd,c} \tag{2.13}$$

The following relations were used to obtain the terms of Eq. (2.13);

$$Q_{v,sens} = \dot{V}_a \, \rho_a \, C_{p,a} \, \Delta T_{in}$$

$$S = (W \, dx)(1 - \phi_p) \, \tau_c \, I_{out}$$

$$Q_{cd,c} = U_c \, (P \, dx)(T_{in}(x) - T_{out})$$

The term representing the heat required for the *transpiration* Q_T was then eliminated from Eq. (2.13). Kittas et al. (2003) justified that by assuming that

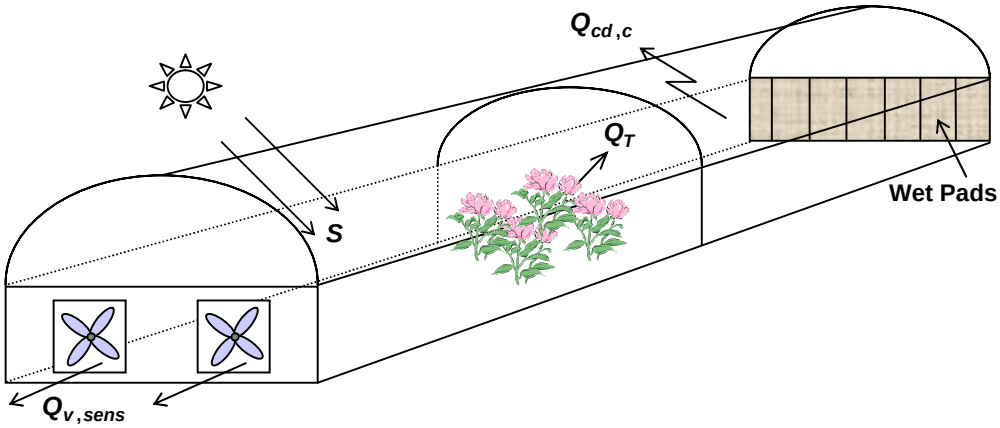

Fig. 2.13: Schematic illustrating the heat terms considered by Kittas et al. (2001 & 2003)

the *absorptivity coefficient* of greenhouse plants, $(1-\phi_p)$, is taking care of the amount of heat required for the *plant transpiration*. Consequently, the coefficient $(1-\phi_p)$ was considered to be representing the fraction of the *solar radiation* incident on the plant canopy and directly converted into *transpiration*. Therefore, the *transpiration* was assumed to be affected mainly by the *solar radiation* in ventilated greenhouses. In reality, the entire amount of the *solar radiation* absorbed by the plants is not consumed entirely by *plant transpiration* but also lost through *long-wave thermal exchange* and *convective heat transfer*.

Equation (2.13) states that the change in the *internal energy* of the greenhouse between any two points, separated by a differential distance *dx* , is equivalent to the difference between the *solar heat gain* on that ground area (i.e. *W dx*) and the *cover heat exchange* of the corresponding area of the structure (i.e. *P dx*). It can be clearly observed that this equation neglects the energy gain by the soil-water evaporation, the heat storage in the soil and the *radiative heat exchange* between the greenhouse radiating surfaces and the sky.

Using Eq. (2.13) and its terms, Kittas and the co-authors derived the following mathematical model:

$$T_{in}(x) = T_{out} + (T_{pad} - T_{out} - A_1)\exp[-A_2\ x] + A_1$$

However, this relation is dimensionally inconsistent and seems that the last parameter to the right needs to be multiplied by the variable x. Therefore, this relation becomes

$$T_{in}(x) = T_{out} + (T_{pad} - T_{out} - A_1)\exp[-A_2\ x] + A_1\ x \qquad (2.14)$$

where

$$A_2 = \frac{U_c\ P}{\dot{V}_a\ \rho_a\ C_{p,a}}$$

It was found that the parameter A_1 in Kittas et al. (2001) and Kittas et al. (2003) was different. After confronting both references, it was found that

$$A_1 = \frac{W\,(1-\phi_p)\,\tau_c\,\mathrm{I}_{out}}{\dot{V}_a\,\rho_a\,C_{p,a}}$$

as in Kittas et al. (2003).

In Eq. (2.14), the temperature of the air leaving the pads T_{pad} was used as a reference datum which somewhat limits the use of the model to predict the temperature for the subsequent points along the airflow direction particularly if some variables of the greenhouse configuration change with distance (e.g. τ_c, ϕ_p and W). Therefore, this model should be modified to accommodate this type of changes and the following is a suggested improvement:

$$T_{in}(x) = T_{out} + \left(T_{prev} - T_{out} - A_1\right)\exp[-A_2\,x] + A_1 \qquad (2.15)$$

This model can be rewritten in another simpler form as follows:

$$T_{in}(x) = \frac{\left(W\,dx\right)(1-\phi_p)\,\tau_c\,\mathrm{I}_{out} + \dot{V}_a\,\rho_a\,C_{p,a}\,T_{prev} + U_c\,\left(P\,dx\right)T_{out}}{\dot{V}_a\,\rho_a\,C_{p,a} + U_c\,\left(P\,dx\right)} \qquad (2.16)$$

Although some heat gain/loss expressions were not considered in this model, Kittas et al. (2001 & 2003) reported that a good agreement was obtained when the results predicted by the model (Eq. 2.14) were tested against experimental data. This conformity might bring some doubt about the importance of some heat terms that have been addressed earlier and neglected here. Albeit the *thermal radiative exchange* was considered a crucial parameter by Walker, Kittas et al. (2003) attained a good conformity without considering it. Therefore, the decision whether to include or neglect the *thermal radiative exchange* in the balance equation is still susceptible to further investigations.

In order to get more benefits of the model, Kittas et al. (2003) used their model to study the relationship between the microclimate temperature, the

ventilation rates and the use of a shading material in the second half of the greenhouse under different outside climatic conditions. They stated that if the ambient climatic conditions and the maximum allowable temperature of the microclimate are known then, the proper ventilation rate and the optional shading can be determined.

2.2.2.6. Model of Condori and Saravia to predict exit air temperature

In the study conducted by Condori and Saravia (2003), a model that enables the prediction of the temperature at the exit of the greenhouse was developed. Condori and Sarvia dealt with the greenhouse as a solar air heater. The greenhouse was divided into two chambers; one for air heating and the other for drying a certain crop product (see Fig 2.14). For the air heating chamber, the following balance equation was developed:

$$S = Q_{v,sens} + Q_{cd,c} \tag{2.17}$$

Equation (2.17) implies that the total amount of heat captured in the greenhouse is the sum-up of the *internal energy* of the greenhouse and the heat lost through the greenhouse cover. As can be clearly seen from this equation, the *radiative heat exchange* and the *latent heat gain* due to *evapotranspiration* have not been considered. Neglecting the latter is justified since the air-heating chamber of the greenhouse was only used to heat up the air as it moves along the greenhouse cavity.

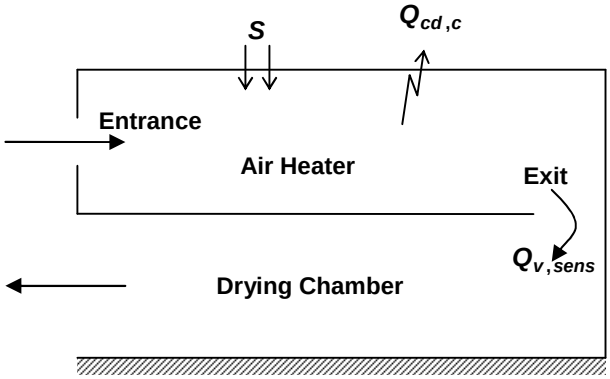

Fig. 2.14: Schematic of a longitudinal view of the greenhouse considered by Condori and Saravia (2003)

The heat terms of the balance equation (Eq. 2.17) were solved using;

$$S = \tau_c \left(1 - \phi_{avg}\right) A_g \, \mathrm{I}_{out}$$

$$Q_{v,sens} = \dot{V}_a \, \rho_a \, C_{p,a} \left(T_{ext} - T_{out}\right)$$

$$Q_{cd,c} = U_c \, A_c \left(T_{ext} - T_{out}\right)$$

Using these expressions, the following model was derived:

$$T_{ext} = T_{out} + \frac{\tau_c \left(1 - \phi_{avg}\right) A_g}{\dot{V}_a \, \rho_a \, C_{p,a} + U_c \, A_c} \mathrm{I}_{out} \tag{2.18}$$

This model considers the temperature at the entrance of the greenhouse equivalent to the *outside temperature* T_{out}. In order to make this model as a temperature predicting tool along the greenhouse airflow direction, T_{out} in the ventilation term should be replaced by T_{prev}. Also, A_g and A_c should be decomposed into their primary variables (i.e. $(W\,dx)$ and $(P\,dx)$, respectively). The model can then be expressed as:

$$T_{in}(x) = \frac{\tau_c \, \phi_{avg} (W\,dx) \mathrm{I}_{out} + \dot{V}_a \, \rho_a \, C_{p,a} \, T_{prev} + U_c (P\,dx) T_{out}}{\dot{V}_a \, \rho_a \, C_{p,a} + U_c (P\,dx)} \tag{2.19}$$

Condori and Saravia (2003) conducted a validation test to verify the accuracy of their model. It was concluded that a temperature deviation of 2^{o}C was experienced between predicted and experimental results. They attributed that variation to the *soil heat storage* being not considered in the balance equation.

2.2.2.7. Chen's model to predict longitudinal air temperature and relative humidity profiles

Along the same path, Chen (2003) developed a model that functions similar to the model addressed in Sec. 2.2.2.5. In a further step, Chen studied the prediction of the *relative humidity* gradient in the longitudinal direction of the

greenhouse. In the formulation of the *heat* and *moisture balance* equations, the greenhouse was divided into small sections along the airflow direction (see Fig. 2.15).

An inventory of all heat and moisture terms was performed in order to originate the balance equations (see Fig. 2.16). For any arbitrary section within the greenhouse, the following *heat* and *moisture balance* equations (Eqs. 2.20 & 2.21, respectively) were formulated:

$$S - L - Q_{cd,c} - Q_T - Q_{v,sens} = 0 \tag{2.20}$$

$$M_v = M_T \tag{2.21}$$

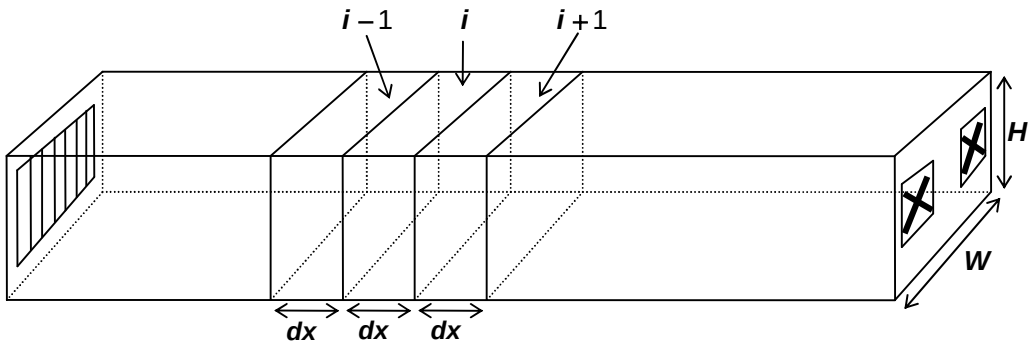

Fig. 2.15: Schematic of three sequential sections along the airflow direction of the greenhouse

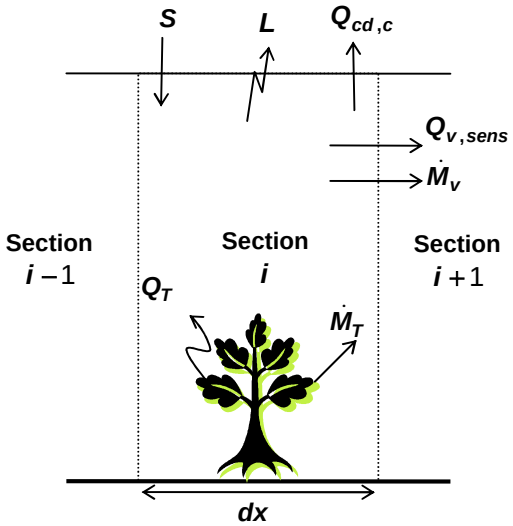

Fig. 2.16: Heat and moisture terms of section *i* inside the greenhouse illustrated in Fig. 2.15

The *latent heat* removed by the ventilation and water-vapour condensation (on the greenhouse cover and/or crop leaves) and the *latent heat* added through soil-water evaporation were not considered in Eq. (2.20). Similarly, the *soil long-wave radiation* was ignored since the crops were assumed to cover most of the floor area. However, the *long-wave heat exchange L* between greenhouse crops and sky was included.

All terms of the balance equations were calculated as follows;

$$S = (W\ dx)\mathrm{I}_{in}$$

$$L = \tau_{\lambda,c}\ \sigma\ (W\ dx) f_v\ \left(T_{i,K}^4 - T_{sky,K}^4\right)$$

$$Q_{cd,c} = \left[2(H_{gh}\ dx)U_{wall} + (W\ dx)U_c\right](T_i - T_{out})$$

$$Q_T = L_v\ P_{ratio}\ (W\ dx)\ \mathrm{T}_{rate}$$

$$Q_{v,sens} = \dot{V}_a\ \rho_a\ C_{p,a}(T_i - T_{i-1})$$

$$M_v = \dot{V}_a\ \rho_a(\omega_i - \omega_{i-1})$$

$$M_T = P_{ratio}\ (W\ dx)\ \mathrm{T}_{rate}$$

The sky temperature was obtained from

$$T_{sky,K} = 0.0552\left(T_{out,K}\right)^{1.5}$$

Chen investigated two models to predict the *transpiration rate* T_{rate} and he found that Jolliet's (1994) model called "HORTITRANS" was giving reliable results. Thus, Chen decided to use this model in his study. In addition, a variable called *absolute humidity* was used in the calculation of the M_v but that variable was associated with the units of the *humidity ratio*. In fact, the *humidity ratio* cannot be used in that expression because it will result in unit-inconsistency. Nevertheless, the correct parameter to be used is the *absolute humidity* but, with its correct units (i.e. kg (water)/m^3 (air)). Thus,

$$M_v = \dot{V}_a(\hbar_i - \hbar_{i-1})$$

Unfortunately, Chen (2003) did not provide the final form of the temperature-predicting model because it was indeed difficult to separate T_i from all terms of Eq. (2.20) and explicitly put it in one side of the equation. In a trial to express the model that can be derived from the *heat balance* equation (Eq. 2.20), the following relation is obtained:

$$T_i = \frac{\mathrm{I}_{in}(W\,dx) + L_v\,\mathrm{T}_{rate}\,P_{ratio}(W\,dx) - \tau_{\lambda,c}\,\sigma(W\,dx)\,f_{v,in\to out}\left(T_{i,K}^4 - T_{sky,K}^4\right) + \left[2(H_{gh}\,dx)U_{wall} + (W\,dx)U_c\right]T_{out} + \dot{V}_a\,\rho_a\,C_p\,T_{i-1}}{2(H_{gh}\,dx)U_{wall} + (W\,dx)U_c + \dot{V}_a\,\rho_a\,C_{p,a}} \quad (2.22)$$

As it is clearly seen from Eq. (2.22), T_i is raised to two different powers (1st and 4th) and thus, it is mathematically not a straightforward process to predict its magnitude. Therefore, an iterative process is required to perform the prediction. Chen used a Q-Basic program (COOLING.BAS) in order to obtain T_i.

Once T_i is obtained, calculating the *relative humidity* is much simpler. Firstly, it requires the prediction of the *absolute humidity* using the *moisture balance* equation (Eq. 2.21) by substituting its terms as follows:

$$\hbar_i = \frac{\mathrm{T}_{rate}\,P_{ratio}(W\,dx) + \dot{V}_a\,\hbar_{i-1}}{\dot{V}_a} \quad (2.23)$$

Then, Chen used the values of the predicted *temperature* and *absolute humidity* of section i to calculate the *relative humidity* using some standard formulae that involve also the calculation of *partial* and *saturation water vapour pressures*. In order to obtain the temperature and humidity gradient along the longitudinal direction of the greenhouse, the outputs from section i were considered as the inputs to the next section (i.e. $i+1$). Then, the same calculation procedure, explained above, was repeated to obtain the temperature and *relative humidity* of the relevant section.

Chen (2003) conducted some validation experiments for the purpose of testing the accuracy of the simulation models. It was found that the performance of the model to predict the *air temperature* was within 2.5^{o}C of the

measured values. The predictive performance of the *relative humidity* was within 8 %. Chen's model can be used to improve the design and performance of the greenhouse components. For instance, Chen studied the influence of the *ventilation rates* and *solar radiation intensity* on the temperature of the greenhouse air. He concluded that higher *ventilation rates* and lower *solar radiation* significantly reduce the inside temperature.

2.2.3. Transient greenhouse models

The *dynamic* models found in the literature range from models very similar to the *steady-state* models to very sophisticated ones. The first type of models deals with most greenhouse components in a *steady-state* mode except one component or two (e.g. greenhouse soil or air). Section 2.2.3.1 presents an example of this type. The other type of *dynamic* models deals with most greenhouse components as being in the *transient-state* which resulted into a very tedious effort to develop and solve them. On top of that, the sophistication increases if the transient variables such as I_{out} and τ_c are calculated using time-dependent techniques. An example of this type of model is discussed in Sec. 2.2.3.2.

2.2.3.1. Model of Duncan and co-authors to predict average air temperature

In a model that combines *steady-state* and *dynamic* features, Duncan et al. (1981) developed a mathematical relation that enables the prediction of the greenhouse *air temperature*. The model deals with the greenhouse in a similar manner to a *steady-state* model; however, it does not ignore the greenhouse energy levels at some previous time. Energy terms considered in this study are shown in Fig. (2.17).

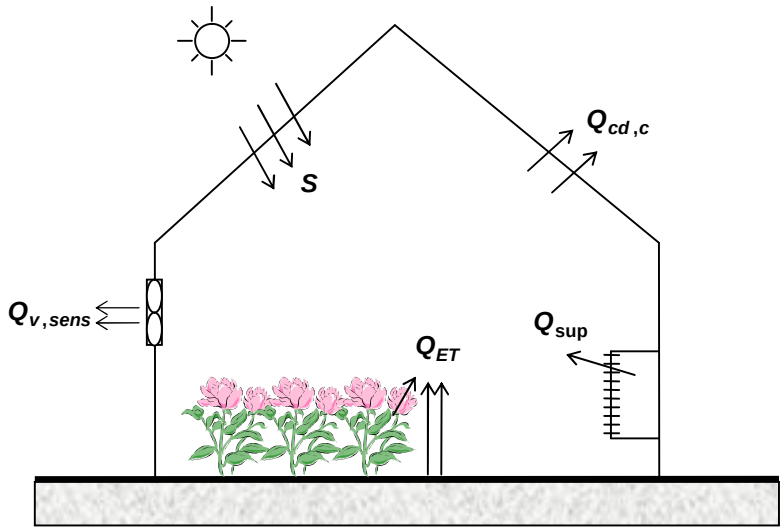

Fig. 2.17: Energy flows of the greenhouse studied by Duncan et al. (1981)

Using the energy terms illustrated in Fig. (2.17), the following balance equation was expressed:

$$\rho_a \, C_{p,a} \, V_a \, \frac{\left(T_{in,t} - T_{in,t-\Delta t}\right)}{\Delta t} = S - Q_{cd,c} - Q_{v,sens} - Q_{ET} + Q_{\text{sup}} \qquad (2.24)$$

In this balance, the *soil heat exchange* and the *net radiative heat loss* were not included. The terms of Eq. (2.24) were calculated using the following expressions;

$$S = A_s \left(1 - \phi_s\right) \tau_c \, \mathrm{I}_{out}$$

$$Q_{cd,c} = U_c \, A_c \left(T_{in} - T_{out}\right)$$

$$Q_{v,sens} = C_{p,a} \, \dot{V}_a \left(\frac{T_{in}}{\mathrm{v}_{in}} - \frac{T_{out}}{\mathrm{v}_{out}} \right)$$

$$Q_{ET} = L_v \sum_{j=plant;wet\ soil} A_j \; \dot{M}_{ET,pot}$$

The last term (i.e. Q_{sup}) of Eq. (2.24) was easily calculated since the heat added by the heater and other equipments was known. The time lags that happen in the energy paths of the components with high energy capacity (e.g. greenhouse

soil) were not neglected in this study. The final format of the model can be expressed as:

$$T_{in,t} = \frac{V_a\ \rho_a\ C_{p,a}\ T_{t-\Delta t} + \Delta t\left(S - Q_{cd,c} - Q_{v,sens} - Q_{ET} + Q_{\sup}\right)}{V_a\ \rho_a\ C_{p,a}} \qquad (2.25)$$

Duncan et al. (1981) tested the accuracy of the model in an actual greenhouse. A FORTRAN based simulation language was used to carry out the calibration and validation experiments. At the end of the tests, it was found that the mean differences between computed and observed results for the calibration and validation tests were 0.74 and 0.85^{o}C, respectively. They reported that such a model can be used to improve the greenhouse design variables and the management practices (e.g. ventilation rates).

2.2.3.2. Model of Takakura and co-authors to predict average temperature of air, plants and floor

In a very detailed analysis, Takakura et al. (1971) provided a comprehensive transient *heat* and *mass transfer* study of each component of the greenhouse. At least one *heat balance* equation was used for each greenhouse component. The components considered in this simulation were the outer and inner surfaces of the glass cover, the greenhouse air, plants, heater and soil surface and the underneath layers (see Fig. 2.18). Also, one *moisture balance* was formulated for the inside air. This resulted in 25 separate differential balance equations simulating the greenhouse microclimate. Takakura et al. (1971) incorporated the heat transferred and stored in the soil which was not considered by many model developers as explained in Sec. 2.2.2. The soil profile under the greenhouse was divided into several horizontal layers and vertical columns. The interception of a layer and a column represented a soil block (see Fig. 2.18). Twenty equations, out of the overall number of *energy balance* equations, were used to study the change in the *internal energy* of these soil blocks.

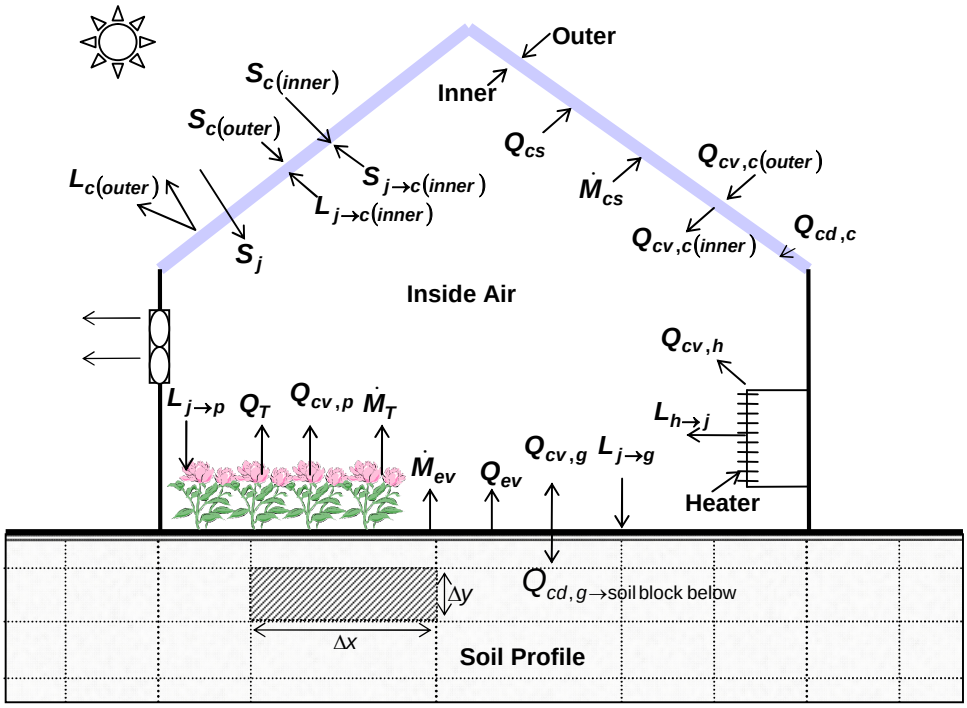

Fig. 2.18: Schematic of the thermal and moisture environment of the greenhouse considered by Takakura et al. (1971)

The *heat balance* equations for the inside and outside surfaces of the glass cover can be written as expressed in Eqs. (2.26) and (2.27), respectively:

$$Q_{c\,(\text{outer})} = Q_{cv,c\,(\text{outer})} + S_{c\,(\text{outer})} - L_{c\,(\text{outer})} - Q_{cd,c} \tag{2.26}$$

$$Q_{c\,(\text{inner})} = S_{c\,(\text{inner})} + \sum_{j=p;h;g}\left(S_{j\to c\,(\text{inner})}\right) + \sum_{j=p;h;g}\left(L_{j\to c\,(\text{inner})}\right) - Q_{cv,c\,(\text{inner})} + Q_{cs} + Q_{cd,c} \tag{2.27}$$

Additionally, the *energy balance* for the air inside the greenhouse was incorporating the following terms:

$$\rho_a\, C_{p,a}\, V_{gh}\, \frac{dT_{in}(t)}{dt} = Q_{cv,c\,(inner)} + Q_{cv,g} + Q_{cv,h} + Q_{cv,p} - Q_{v,sens} \tag{2.28}$$

On the other hand, Eq. (2.29) presents the *moisture balance* of the inside air:

$$\rho_a\, V_{gh}\, \frac{d\omega_{in}(t)}{dt} = M_{ev} + M_T - M_v - M_{cs} \tag{2.29}$$

For the surface of plant leaf, Takakura et al. (1971) developed the following *energy balance*:

$$\rho_p \, C_{p,p} \, V_p \, \frac{dT_p(t)}{dt} = S_p - Q_{cv,p} - Q_T + \sum_{j=c\,(inner);\,h;\,g} \left(L_{j \to p}\right) \qquad (2.30)$$

The *heat balance* equation they developed for the inside soil surface can be written as:

$$\rho_g \, C_{p,g} \, \Delta x \, \Delta y \, \frac{dT_g(t)}{dt} = S_g - Q_{cv,g} - Q_{ev} + \sum_{j=c\,(inner);\,h;\,p} \left(L_{j \to g}\right) - Q_{cd,g \to g+1} \qquad (2.31)$$

A similar equation was also developed for the outside soil surface. Furthermore, the twenty balance equations, dealing with the under-surface soil blocks, analysed the *conductive heat transfer* of the soil blocks with each other. Eq. (2.32) is an example of one heat balance for the shaded soil block of Fig. 2.18:

$$\rho_g \, C_{p,g} \, \mathrm{W} \, \Delta x \, \Delta y \, \frac{dT_g(t)}{dt} = \sum_{\substack{j=soil\ blocks:\ above;\\ below;\ right;\ left}} \left(Q_{cd,\,j \to shaded\ block}\right) \qquad (2.32)$$

In addition to these detailed balance equations, Takakura and the co-investigators suggested even other detailed formulae to solve some variables of the terms of these equations. This methodology followed by Takakura et al. (1971) to study each greenhouse component separately is a systematic way of simulating the entire environment of the greenhouse. However, the complexity of expressions and the interlink between equations made it extremely difficult to find a lineal solving technique in order to estimate any greenhouse environmental or structural variable. Therefore, a FORTRAN simulation program was particularly written to solve the differential equations and to test the validity of the model in a full size greenhouse.

Takakura et al. (1971) used the simulation model to predict the temperatures of the inside air, leaf surface and soil surface as well as the periods of condensation on the inner surface of the cover. At the end of the

validation experiment, they reported that a reasonable agreement between the predicted and observed values of the temperatures of the inside air, leaf surface and soil surface was attained. The predicted *air temperatures* were found to be closer to reality than the other two predicted variables. The difficulty to monitor average *surface temperatures* of the plant leaves caused the scattering of the measured values from the computed ones. Also, it was found that not all energy flows were simultaneously achieving their maximum values because some time delays existed in the energy paths of large heat capacity components such as the soil layers. Another crucial finding was the emphasis on the importance of considering *evapotranspiration* and *radiative heat exchange* inside the greenhouse in the analysis. Their thermal contribution was found to be very large and thus, they should not be neglected according to Takakura et al. (1971).

2.2.4. Comparison of steady-state and dynamic models

Greenhouse models undergo three stages; the balance equation(s) formulation, the development of the simulation model and, finally, the conduction of validation tests. One more stage that should be added to these three is the utilization of the model(s) to improve the performance of the greenhouse. It was observed from the models explained in Sections 2.2.2 and 2.2.3 that the balance equations are used to provide an inventory of all significant terms involved in the *heat* or *moisture balances* of any greenhouse component. Some model developers initially put together all terms (significant and insignificant) in the balance equation(s) and then they study the order of magnitude of each term. Eventually, they only keep the significant terms in the final expression of the model. Other modellers prefer to present, from the beginning, the significant terms only without paying a lot of attention to the terms they excluded. Therefore, the balance equations can be classified into general and specific (i.e. target-oriented) equations. The general equations can be used for any greenhouse but, the target-oriented ones can only be used for greenhouses similar in characteristics to the greenhouse for which they were originally developed.

In the formulation of the *heat* and *mass balances* of the *steady-state* models, a quasi-equilibrium situation for the greenhouse (and all of its components) is assumed. This assumption implies that the instantaneous energy and moisture status of any component is not affected by its preceding status. Therefore, the effect of the heat and moisture build-up/removal between the two time instances is neglected. However, the time effect is taken into consideration in the *dynamic* models. In other words, *dynamic* models do not disregard the prior *heat* or *moisture level* of the greenhouse component.

The *steady-state* models as well as the simple *dynamic* models can be used for online control of the greenhouse microclimate. On the other hand, Boulard and Baille (1993) and Khalil (1995) reported that complex *dynamic* models (e.g. Sec. 2.2.3.2) are difficult to be used for online control due to their sophistication. Although this sophistication in the balance equations of each component was anticipated to significantly increase the accuracy of the prediction, the predicted values using such models were not found to be far better than the predicted values using simple *steady-state* models (see Sec. 2.2.2). Also, the simulation using these models cannot be conducted in direct computational software (e.g. MS-Excel) because they require utilizing programming languages such as FORTRAN to conduct the simulation.

By comparing the models mentioned in Sections 2.2.2 and 2.2.3, one can observe that most of them did not include the influence of the amount of heat stored in the soil. Also, very few models considered the net effect of *long-wave thermal radiation* which was considered by Walker (1965) to be a significant parameter in greenhouses covered with plastic films having high *thermal transmittance* to certain wavelengths (6-40 μm). Neglecting some heat terms might result in a less accuracy of the developed models. Therefore, choosing which term to include is a very sensitive task and requires a lot of vigilance before coming up with a final decision.

In addition to the *steady-state* and *dynamic* models mentioned in the last two sections, the greenhouses can also be simulated using some numerical

techniques such as computational fluid dynamic (CFD) approaches. In the last few years with the development of incredibly fast-processing computers, CFD approaches have recruited the interest of greenhouse modellers to simulate greenhouses. Nowadays, many studies (e.g. Mistriotis et al., 1997a & 1997b; Bartzanas et al., 2002; Boulard and Wang, 2002; Mistriotis and Briassoulis, 2002; Reichrath and Davies, 2002; Campen and Bot, 2003; Davies et al., 2004; Shklyar and Arbel, 2004; Fatnassi et al., 2006; Ould-Khaoua et al., 2006; and Kim et al., 2008) simulating the greenhouse inner environment can be found in literature. Norton et al. (2007) provided a very recent review of the different applications of CFD techniques in the simulation of greenhouses and livestock buildings.

In this study, it was decided to use a *steady-state* model (similar to Sec. 2.2.2) to simulate the inner environment of the greenhouse. This is because *steady-state* models are simple to run and provide a deep understanding of all *heat* and *mass transfer* processes taking place inside the greenhouse.

2.2.5. HD greenhouse simulation model

The first attempt to simulate HD greenhouses was done by Raoueche (1997) (see also, Raoueche et al., 1996; and Bailey and Raoueche, 1998). In his PhD study, Raoueche (1997) aimed to simulate the 1st (seawater) HD greenhouse located in the Tenerife island, Spain. The simulated components/sections of the Tenerife greenhouse were the 1st humidifier, greenhouse microclimate, roof cavity, 2nd humidifier and dehumidifier. This greenhouse is slightly different from the HD greenhouse located in Oman. The dehumidifier of the Tenerife greenhouse was cooled using a coolant having a temperature similar to deep seawater temperature. On the other hand, the dehumidifier of Oman greenhouse is cooled using the water leaving the 1st humidifier as explained in Sec. 2.1.4. Also, the Oman HD greenhouse does not include the roof cavity that served two purposes in the Tenerife greenhouse; heating up the water flowing to the 2nd humidifier and adding more moisture to

the air flowing through the dehumidifier. Figure 2.19 illustrates the main components/sections of the Tenerife HD greenhouse.

In the simulation of the 1st humidifier, Raoueche's (1997) used Eqs. (2.33) and (2.34) to predict the *outlet air temperature* T_{ao} and *absolute humidity* $\hbar_{ao}$, respectively. Equation (2.33) is the *air cooling effectiveness* of the humidifier and Eq. (2.34) is the *evaporative effectiveness* of the humidifier.

$$\eta_a = \frac{T_{ai} - T_{ao}}{T_{ai} - T_{wb}} \tag{2.33}$$

$$\eta_{ev} = \frac{\hbar_{ai} - \hbar_{ao}}{\hbar_{ai} - \hbar''_{wb}} \tag{2.34}$$

In this study, the 1st humidifier is simulated using a more precise technique than these relations used by Raoueche (1997) to predict the *outlet air temperature* and *humidity*. The reason for not using this type of relations is provided in Chapter 3. In addition to the prediction of the *outlet air temperature* and *humidity*, the humidifier simulation sub-model used in this study can predict the *outlet water temperature* which cannot be predicted using Eqs. (2.33) and (2.34).

For the simulation of the greenhouse inner environment, Raoueche (1997) used a *dynamic* model originally developed by Chalabi and Bailey (1989 & 1991). This model was used to predict average values for the *air temperature*

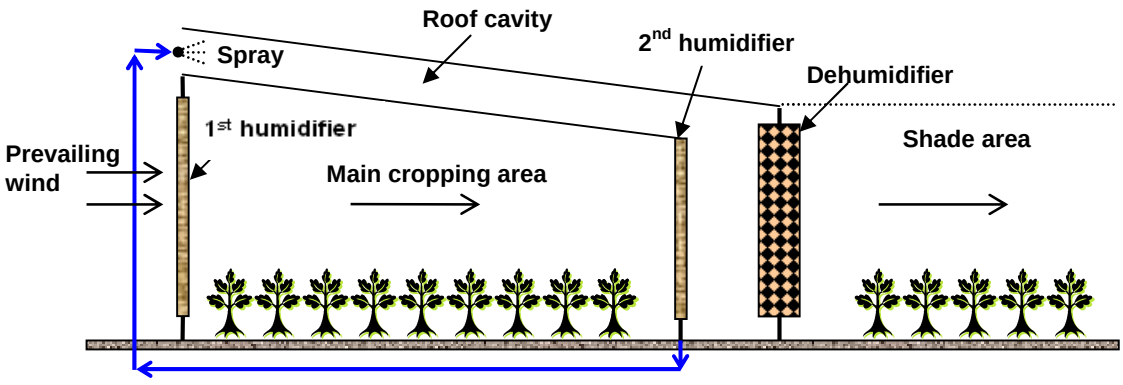

Fig. 2.19: Schematic of the Tenerife HD greenhouse (Raoueche, 1997)

and *humidity*. Also, it was used to predict the average temperatures of plants, soil and inner and outer cladding covers. Taking average values for long fan-ventilated greenhouses is not practical due to the large differences between their inlet and exit temperature and humidity values as will be explained in Chapter 4. The simulation model used in this study can predict the *air temperature* and *humidity* profiles along a fan-ventilated long-tunnel greenhouse which is the case in the HD greenhouse in Oman.

For the simulation of the 2nd humidifier, Raoueche (1997) used a detailed simulation technique. The humidifier sub-model used in this study took into consideration the simulation technique adopted in Raoueche (1997) and provided an accurate, simpler procedure. The reason(s) for using different methods to simulate the 1st and 2nd humidifiers in Raoueche (1997) were not foreseen. However, in this study, the same simulation technique was used to simulate both humidifiers.

For the simulation of the dehumidifier, different procedures were followed in this study and Raoueche's (1997) study owing to the use of different types of dehumidifiers. Raoueche's (1997) model was able to predict the *outlet air humidity* of the dehumidifier and the *volume of condensate*. The model developed in this study can predict the *outlet air temperature* in addition to the *outlet air humidity* and the *volume of condensate*.

In terms of the accuracy of simulation, Raoueche's (1997) model was found to predict the temperature values much better than the *relative humidity* values. It also appeared that the model was poorly predicting the *volume of condensate* as was deduced from the little information provided on the model's predictions of the *volume of condensate*. In this study, the humidifier sub-model is predicting the outlet *air temperature* and *humidity* more accurate than their predictions using Raoueche's (1997) model. Similarly, this is the case for the greenhouse *air temperature*. However, for the greenhouse *air humidity*, both models seem to have a similar accuracy. In the model of this study, the accuracy to predict the *dehumidification rate* was fairly good.

CHAPTER THREE

3. THE HUMIDIFIER SUB-MODEL

In this chapter, a detailed description of the mathematical sub-model that will be used to simulate the heat and moisture transfer processes of the greenhouse humidifier(s) is provided. Section 3.1 gives a brief introduction of the greenhouse evaporative cooling system (i.e. humidifier). The development and working procedure of the sub-model can be found in Sec. 3.2. A description of the experiments conducted to test the accuracy of the sub-model is given in Sec. 3.3. Section 3.4 presents the results obtained from the experimental work and then a critical discussion of these results is given in Sec. 3.5. Finally, the main conclusions that can be drawn about the humidifier sub-model are presented in Sec. 3.6.

3.1. INTRODUCTION

Evaporative cooling is employed in many greenhouses where the *ambient temperatures* are too high for cultivated plants and need to be reduced. Pad-and-fan systems are one means of achieving evaporative cooling of greenhouses (Langhans, 1990; and Nelson, 1998). Various designs and construction materials of evaporative cooling pads are currently available on the market with different costs and *effectiveness*. Evaporative cooling pads made from cellulose material (Fig. 3.1) have recently gained a wide popularity. They provide high *evaporation effectiveness* and low resistance to air flow and are impregnated with insoluble anti-rot salt (USGR, 2007). Dowdy and Karabash (1987) studied this type of evaporative cooling media and provided empirical relations to calculate the *heat* and *mass transfer* coefficients.

Many studies (e.g. Bernier, 1994; Liao et al., 1998; Liao and Chiu, 2002; Camargo et al., 2003 & 2005; and Beshkani and Hosseini, 2006) focused on the simulation of the thermal performance of evaporative cooling media. One major

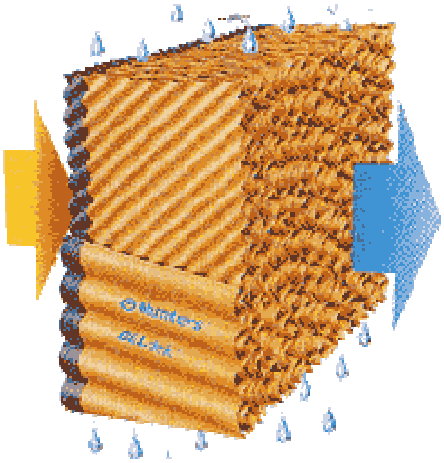

Fig. 3.1: Cross-fluted design of impregnated cellulose pads (USGR, 2003)

aim of some of these studies was to predict the temperature and moisture changes of the air and water as they flow through/down the evaporative media. A simple relation that is widely used to calculate the *air cooling effectiveness* η_a through evaporative cooling media (Abdellatif, 1993; Kittas et al., 2001 & 2003; and ASHRAE, 2004) is;

$$\eta_a = 100 \frac{T_{ai} - T_{ao}}{T_{ai} - T_{wb,ai}}$$

where η_a represents the ratio of the achieved cooling of air in the system, $(T_{ai} - T_{ao})$, to the maximum achievable cooling, $(T_{ai} - T_{wb,ai})$. This relation can be used to estimate the *outlet air temperature* T_{ao} once the other three parameters of this relation are known. However, the *air cooling effectiveness* η_a is not constant during the day (Abdellatif, 1993; and Kittas et al., 2001) and is affected significantly by the variations in the *air flowrate* (Camargo et al., 2005) and the *outside relative humidity* (Abdellatif, 1993). Thus, assuming a single value for the η_a would lead to inaccurate predictions.

Halasz (1998) introduced a simple non-dimensional mathematical model suitable for all evaporative cooling devices. This model enables the prediction of the T_{ao} and *humidity ratio* ω_{ao} as well as the *outlet water temperature* T_{wo}. In this study, Halasz's model will be used to predict the outlet conditions of the air

and water leaving the impregnated cellulose evaporative cooling pads (i.e. humidifier) used in greenhouses.

3.2. THE NON-DIMENSIONAL MODEL

A detailed description of the general non-dimensional mathematical model (i.e. set of equations) developed to simulate evaporative cooling devices can be found in Halasz (1998, 1999 & 2000). The intention of Halasz (1998) was to develop a mathematical model capable of simulating all types of evaporative coolers (e.g. cooling towers, air washers, evaporative condensers and fluid coolers) with any flow pattern (i.e. *parallel-*, *counter-* or *cross-flow*). A good accuracy was obtained when the model predictions to simulate cooling towers were compared to published data (Halasz, 1999). Halasz's model was then used by Kairouani et al. (2004) who also reported that the accuracy of the model to simulate their cooling tower was acceptable.

This model was based on *heat* and *mass balance* equations. Four partial differential equations were developed for *moisture balance* of the air passing through the evaporative cooler and *heat balances* of the main fluids involved in the cooling process. These fluids are the air passing through the cooler, the water flowing down and the cooling fluid that exists in some types of evaporative coolers. Although Halasz's model takes into consideration *adiabatic* and non-*adiabatic* processes, the focus in this study will be only on *adiabatic* processes since the humidifiers used in greenhouses fall in this category.

3.2.1. Assumptions

In the process of developing the model, the following assumptions were considered:

i. Air is homogeneous in its thermal and moisture properties across the inlet section of the humidifier
ii. Inlet water is thermally homogeneous and is evenly sprayed on the top of the cooling device
iii. No dry spots are present in the evaporative cooling media
iv. Heat exchange occurs only between the fluids involved in the evaporative cooling process (i.e. *adiabatic* evaporative cooling device)
v. The *water-air interface area* A_{aw} is considered to be the surface area of all layers of the evaporative cooler assuming that water is only wetting the evaporative cooling media with a layer of negligible thickness
vi. *Water-air interface temperature* T_{aw} is the same as *water temperature* T_w (i.e. $T_{aw} = T_w$)
vii. *Saturation humidity ratio* ω'' as a function of temperature is linear (see Glossary for more details on the air saturation line)
viii. *Water-cooling range* ($T_{wi} - T_{wo}$) is $\leq 20^{o}$C because large cooling ranges have a negative impact on the linearization of the air saturation line
ix. *Lewis number* equals unity ($L_e = 1$)
x. The change in *water mass flowrate* due to evaporation is negligible (i.e. $\dot{m}_w = \text{constant}$)
xi. Air is never *over-saturated*
xii. *Latent heat of vaporisation* L_v is the same at T_w and T_{wb}

3.2.2. Non-dimensional format of the model

Halasz (1998) transformed all dimensional balance equations to the non-dimensional form. Halasz (1999) demonstrated, in detail, how the non-dimensional model can be used for a particular device such as the “cooling tower”. After solving the non-dimensional relations of the model, Halasz (1999) provided two equations (see Sec. 3.2.3) that can be used to find the *air outlet temperature* and *humidity ratio* for *counter-* and *parallel-flow* towers. For *cross-flow* towers, a numerical solution is required. However, once the model is used

to obtain the mean values of the *outlet air temperature* T_{ao} *and humidity ratio* ω_{ao} and *the water temperature* T_{wo}, the same solution can be used even for *cross-flow* cooling towers. Because both equations require the *outlet water temperature* T_{wo} to be known beforehand, an iterative approach to obtain it was also explained in Halasz (1999) (see Sec. 3.2.4).

Recently, the application of this model to *counter-* and *parallel-flow* air washers was explained in Halasz (2007). Its application for *cross-flow* air washers, similar to the greenhouse humidifiers, was not highlighted in that paper. However, Halasz (personal contact) asserted that the procedure used for *cross-flow* cooling towers is exactly the same for *cross-flow* air washers when the respective $\eta_w - X_o$ diagram is used (see Fig. 3.2). For this reason, Halasz's model will be used in this study to simulate the *cross-flow* air washers (i.e. humidifiers) used in greenhouses in Oman.

3.2.3. Mathematical relations of non-dimensional model

The two equations that were provided by Halasz (1999) to obtain the T_{ao} and ω_{ao} are:

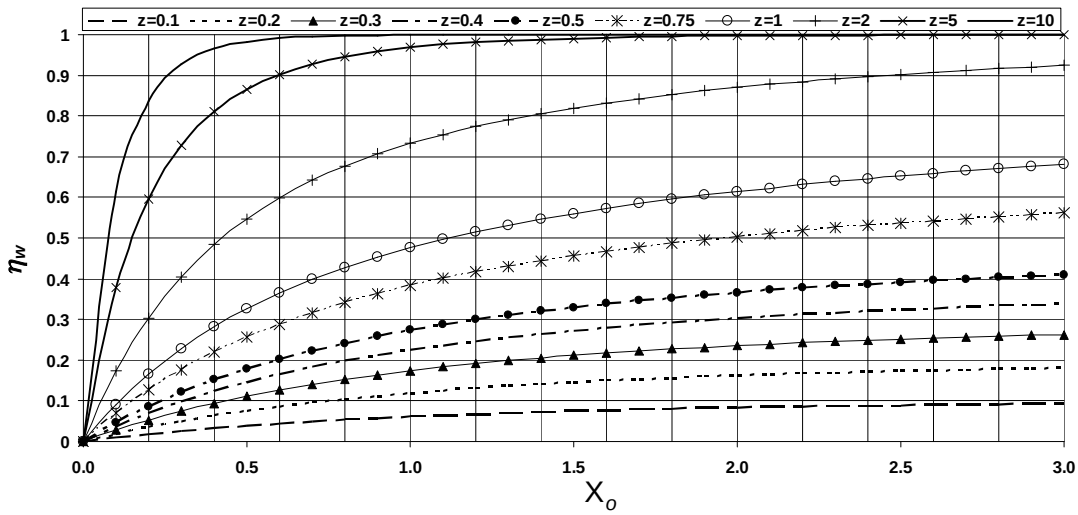

Fig. 3.2: The $\eta_w - X_o$ diagram of a *cross-flow* cooling tower (Halasz, 1999)

$$T_{ao} = T_{wb} + \left[\frac{1}{\mathrm{z}}\left(T_{wi} - T_{wo}\right) + \left(T_{ai} - T_{wb}\right)\exp\left(-\mathrm{X}_o\right)\right] \tag{3.1}$$

$$\omega_{ao} = \omega_{wb} + \left(\omega_{wb} - \omega_{ai}\right)\left[\frac{\mathrm{B}}{\mathrm{z}}\frac{\left(T_{wi} - T_{wo}\right)}{\left(T_{ai} - T_{wb}\right)} - \exp\left(-\mathrm{X}_o\right)\right] \tag{3.2}$$

There are three dimensionless parameters appearing in these two equations, z, X_o and B:

- z: is the *air-to-water heat capacity rate ratio* which can be calculated using;

$$\mathrm{z} = \frac{1+\mathrm{B}}{\mathrm{W}} \tag{3.3}$$

where W is the dimensionless *water-to-air heat capacity rate ratio* that can be obtained using;

$$\mathrm{W} = \frac{\dot{m}_w\, C_{p,w}}{\dot{m}_a\, C_{p,a}} \tag{3.4}$$

in which $C_{p,a}$ is calculated as follows:

$$C_{p,a} = C_{p,\mathrm{da}} + \omega_{wb}\, C_{p,\mathrm{wv}}$$

- X_o: is the number of transfer units;

$$\mathrm{X}_o = \frac{\mathrm{h}_{cv}\, A_{aw}}{\dot{m}_a\, C_{p,a}} \tag{3.5}$$

where h_{cv} is the *convective heat transfer coefficient* of the evaporative cooler which must be known in order to proceed further with the calculation using this model. Fortunately, Dowdy and Karabash (1987) empirically determined this coefficient for the type of evaporative cooler used in this study (i.e. a rigid cellulose evaporative media). Their relation to calculate the h_{cv} is

$$h_{cv} = \frac{k_{da}}{l_{hum}} \left(0.10 \left(\frac{l_{hum}}{b_{hum}} \right)^{0.12} Re_a^{0.8} \, Pr^{1/3} \right) \tag{3.6}$$

in which

$$l_{hum} = \frac{V_{hum}}{A_{aw}} \tag{3.7}$$

and

$$Re_a = \frac{u_a \, l_{hum}}{\nu_{da}} \tag{3.8}$$

The mathematical relations used to evaluate the $C_{p,da}$, k_{da}, ν_{da}, $C_{p,wv}$ and $C_{p,w}$ are given in Sec. C.1 of Appendix C. An understanding of the different terms of Eq. (3.6) is gained from Liao and Chiu (2002).

- B: is the *non-dimensional slope* of the linear air saturation line which can be obtained from;

$$B = \frac{b \, L_{v,wb}}{C_{p,a}} \tag{3.9}$$

where b is the *slope* of the real air saturation line. Halasz (1999) provided the following equation to calculate b:

$$b = \frac{\dfrac{\Im(T_{wi}) - \Im(T_{wo})}{T_{wi} - T_{wo}} - \left(\omega_{wb} \, L_{v,0} + C_{p,a} \, T_w \right)}{C_{p,wv} \left(\dfrac{4T_w^2 - T_{wi} \, T_{wo}}{3} - T_{wb} \, T_w \right) + L_{v,0} \left(T_w - T_{wb} \right)} \tag{3.10}$$

or using the following simpler expression

$$b = \frac{\omega''_w - \omega''_{wb}}{T_w - T_{wb}} \tag{3.11}$$

The $L_{v,wb}$ in Eq. (3.9) is calculated using the relation developed by Henderson-Sellers (1984);

$$L_{v,wb} = 1.91846 \times 10^6 \left(\frac{T_{wb} + 273.15}{T_{wb} + 239.24} \right)^2 \tag{3.12}$$

where the T_{wb} is obtained through the iterative procedure explained later in Sec. 3.2.5.

Once the ω_{ao} is calculated from Eq. (3.2), it will be converted into a *relative humidity* φ_{ao} using the following relation (ASHRAE, 2001):

$$\varphi_{ao} = 100 \frac{\psi_{ao}}{\psi''_{ao}} \tag{3.13}$$

where the *partial vapour pressure* ψ_{ao} is calculated as follows;

$$\psi_{ao} = \frac{\omega_{ao} \, \mathrm{P}}{0.62198 + \omega_{ao}} \tag{3.14}$$

The *saturation partial vapour pressure* ψ''_{ao} will be calculated using the relation presented by Glanz and Orlob (1973; as cited by Henderson-Sellers, 1984);

$$\psi''_{ao} = 2.1718 \times 10^7 \exp\left(\frac{-4157}{T_{ao} + 239.24} \right) \tag{3.15}$$

After incorporating Eqs. (3.14) and (3.15) in Eq. (3.13), it becomes

$$\varphi_{ao} = 100 \frac{\omega_{ao} \, \mathrm{P}}{2.1718 \times 10^7 \exp\left(\frac{-4157}{T_{ao} + 239.24} \right) (0.62198 + \omega_{ao})} \tag{3.16}$$

3.2.4. Iterative procedure to obtain outlet water temperature

In order to be able to use Eqs. (3.1) and (3.2), the T_{wo} should be known in advance. But because it is not a measured variable in this study, an iterative approach will be followed to estimate it (as understood from, Halasz, 1999). This approach can be conducted manually or via the use of an assisting tool like Solver in MS-Excel, according to the following sequence:

a) Assume an initial T_{wo} value
b) Calculate h_{cv} (Eq. 3.6)
c) Calculate X_o (Eq. 3.5)
d) Calculate b (Eq. 5.10 or 5.11), B (Eq. 3.9) and W (Eq. 3.4), respectively
e) Calculate z (Eq. 5.3)
f) Once X_o and z are obtained, the *water cooling effectiveness* η_w of the humidifier can be estimated using the η_w - X_o diagram (Fig. 3.2)
g) Use the η_w obtained from step (f) to calculate another value for T_{wo} from the following relation of the *water cooling effectiveness*

$$\eta_w = \frac{T_{wi} - T_{wo}}{T_{wi} - T_{wb,ai}} \tag{3.17}$$

h) Put T_{wo} obtained from step (g) in (a) and repeat steps (a) to (h) till a fixed value for T_{wo} is obtained

In this study, this simulation procedure will be conducted in a MS-Excel spreadsheet with the assistance of the Solver tool.

3.2.5. Calculation of wet-bulb temperature

Usually the *wet-bulb temperature* $T_{wb,ai}$ is a measured parameter but in the case of this study, it will be calculated using measured data. The calculation is not a straightforward process but requires an iterative approach (ASHRAE,

2001; and Zhang et al., 1997). It will be calculated using the two formulae presented by ASHRAE (2001) to calculate the *humidity ratio* of the ambient air. The first formula (Eq. 3.18) calculates the ω_{ai} by knowing the T_{ai}, φ_{ai} and *atmospheric pressure* P of the air entering the humidifier. The second formula (Eq. 3.19) calculates the ω_{ai} by considering the $T_{wb,ai}$ as an input variable.

$$\omega_{ai} = 0.62198 \frac{\psi_{ai}}{\mathrm{P} - \psi_{ai}} \tag{3.18}$$

$$\omega_{ai} = \frac{\left(L_{v,wb} - \left(C_{p,w} - C_{p,wv}\right) T_{wb,ai}\right)\omega''_{wb} - C_{p,ai}\left(T_{ai} - T_{wb,ai}\right)}{L_{v,db} + C_{p,wv} T_{ai} - C_{p,w} T_{wb,ai}} \tag{3.19}$$

The ψ_{ai} in Eq. (3.18) can be calculated using the φ_{ai} and T_{ai} as follows:

$$\varphi_{ai} = 100 \frac{\psi_{ai}}{\psi''_{ai}} \Rightarrow \psi_{ai} = \frac{\varphi_{ai}}{100} \psi''_{ai} \tag{3.20}$$

The ψ''_{ai} will be calculated using the Glanz and Orlob's (1973) relation (Eq. 3.15).

Equation (3.18) estimates the ω_{ai} using the observed temperature and humidity data and thus, it provides the real ω_{ai}. The ω_{ai} of Eq. (3.19) will be adjusted to equal the ω_{ai} calculated from Eq. (3.18) in order to obtain the $T_{wb,ai}$. This adjustment will be done by altering the value of the $T_{wb,ai}$ involved in Eq. (3.19). The $T_{wb,ai}$ value that gives a ω_{ai} value equal to the one obtained from Eq. (3.18) is considered the *wet-bulb temperature* of the air entering the humidifier. This calculation can be carried out in MS-Excel using the Solver tool.

3.3. VALIDATION EXPERIMENTS

A set of experiments was carried out in greenhouse #5 of the AES, Sultan Qaboos University, Oman to test the accuracy of the humidifier sub-model.

More details about the AES greenhouse (Fig. 3.3) are provided in Sec. A.1 of Appendix A.

3.3.1. Experimental set-up

The humidifier used in these experiments was a *cross-flow* air washer fabricated from cellulose material (see Fig. 3.4). The AES greenhouse was equipped with a fan-frequency regulator to vary the air flowrate through the greenhouse and hence, through the humidifier. The flowrate of the water used to wet the pads was also alterable. The water flowrate was monitored by a flow meter and because there was always an excess water flowrate, a return valve was used to discard the excess amount.

In the period 17-28 May, 2008, four experiments were conducted. In these experiments, two water flowrates (6.7 x 10^{-4} and 1.0 x 10^{-3} m^3/s) and two air

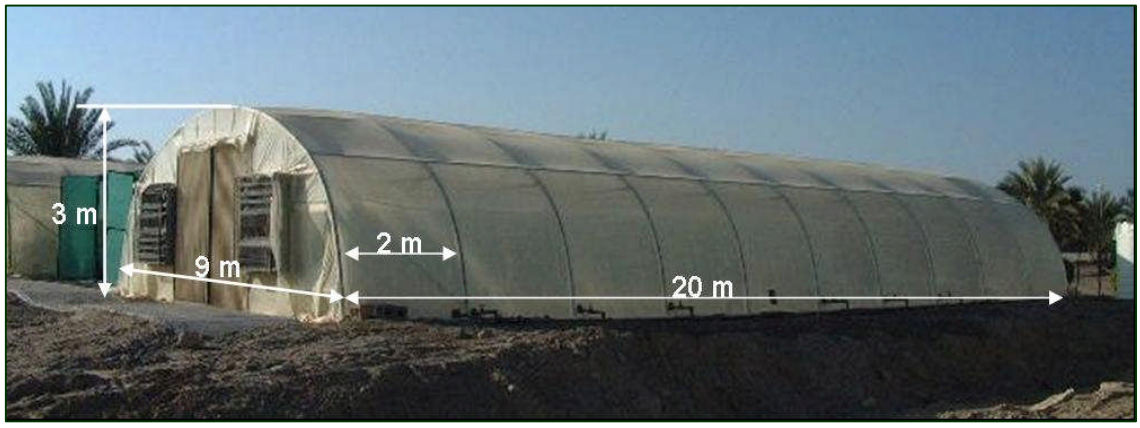

Fig. 3.3: The greenhouse #5 located at AES

Fig. 3.4: The air washer used in the experiments and in this picture, the position of the shielded temperature/relative humidity sensor is enclosed by the circle

flowrates (7.76 and 15.66 m^3/s) were used. Each experiment lasted for almost two days and was running with one combination of those two air-water flowrates. Table 3.1 presents each experiment with the corresponding air-water flowrate combination.

3.3.2. Instrumentation of AES greenhouse

A shielded Delta-T dual temperature/relative humidity sensor was used to measure the T_{ai} and φ_{ai}. This sensor was placed just before the humidifier at the mid-span width and height. A similar sensor was placed at the opposite side of the humidifier to measure the T_{ao} and φ_{ao} (see Fig. 3.4). The T_{wi} and T_{wo} were monitored using two Delta-T sealed temperature probes. A Delta-T photodiode was used to measure the *solar radiation* inside the greenhouse (see Fig. 3.5 [a]). A Delta-T datalogger was programmed to retrieve and record data at ten minute intervals from these sensors (see Fig. 3.5 [b]). *Air velocity* through the humidifier was measured using an Omega digital anemometer. A detailed description of all sensors used in these experiments can be found in Appendix B.

Table 3.1: The air-water flowrate combinations of the four experiments

Experiment	Air flowrate [m^3/s]	Water flowrate [m^3/s]
1st	7.76	1.0×10^{-3}
2nd	15.66	1.0×10^{-3}
3rd	7.76	6.7×10^{-4}
4th	15.66	6.7×10^{-4}

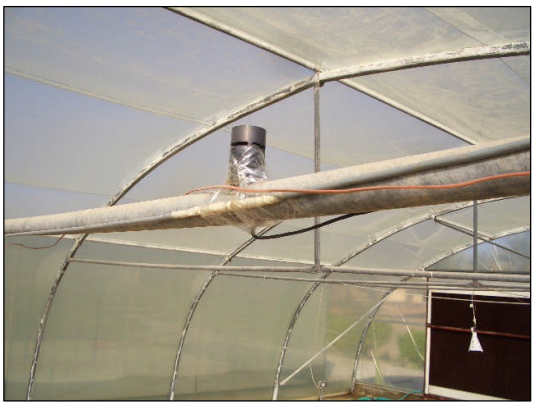

(a)

(b)

Fig. 3.5: The Delta-T (a) photodiode and (b) datalogger used in AES greenhouse

3.3.3. Testing accuracy of simulation sub-model

After running the four experiments, the humidifier simulation sub-model was used to predict outlet conditions of the air and water. The input data used in the simulation included the T_{ai}, φ_{ai}, T_{wi}, *air mass flowrate* $\dot{m}_a$, *water mass flowrate* $\dot{m}_w$ and design parameters of the humidifier. The sub-model was able to predict the T_{ao}, ω_{ao} and T_{wo} using equations and procedures explained in Sections 3.2.3 to 3.2.5. MS-Excel was used to run this simulation.

The observed and predicted values of the T_{ao}, ω_{ao} and T_{wo} were compared to each other for all experiments. This comparison included the calculation of three statistical parameters; the *average predictive error* ($\overline{\text{PE}}$), the *average percentage predictive error* ($\overline{\%\text{PE}}$) and the *root mean square error* (RMSE). It should be noted that the $\overline{\%\text{PE}}$ of T_{ao} and T_{wo} is calculated for degree Celsius. The definition of these expressions can be found in the Glossary. The predicted and observed values were also graphically compared.

3.4. RESULTS

Table 3.2 describes the humidifier operating parameters used in the simulation. There was always a very good conformity between the predicted and observed T_{ao} and T_{wo}. Also, the accuracy of the sub-model to predict the ω_{ao}, from which the φ_{ao} was calculated, was excellent.

3.4.1. Temperature predictions

The humidifier sub-model accurately predicted the T_{ao}. In all experiments, the $\overline{\text{PE}}$ was ranging from 0.32 to 0.72^{o}C (SD≤0.45^{o}C), the $\overline{\%\text{PE}}$ was between 1.16 and 2.86 % (SD≤1.84 %) and the RMSE was between 0.37 and 0.76^{o}C (see Table 3.3 for more details). However, predicted T_{ao} was slightly more than

Table 3.2: Humidifier design and operating parameters used in the simulation

Parameter	Value	Comment
H_{hum} , [m]	1.40	measured
W_{hum} , [m]	5.86	measured
b_{hum} , [m]	0.10	measured
V_{hum} , [m^3]	0.82	calculated
l_{hum} , [m]	2.16×10^{-3}	Rawangkul et al. (2008)
A_{aw} , [m^2]	379.8	calculated
u_a at 25 Hz fan frequency, [m/s]	1.10	measured
u_a at 50 Hz fan frequency, [m/s]	2.26	measured

the observed T_{ao} (i.e. positive PE) (see Fig. 3.6). From Table 3.3, it was also noticed that the $\overline{PE}$ slightly decreased with increasing air flowrate.

The accuracy of the sub-model to predict the T_{wo} was slightly less than its accuracy to predict the T_{ao}. Table 3.4 gives some statistical comparisons between the predicted and observed T_{wo} in all experiments. From this table, the $\overline{PE}$ was between -1.06 and -0.30°C (SD≤0.61°C), the $\overline{\%PE}$ was ranging from -4.91 to -1.30 % (SD≤2.29 %) and the RMSE was between 0.53 and 1.19°C. Figure 3.7 graphically compares the predicted T_{wo} to the observed T_{wo} for all experiments. It can be clearly seen from this figure that the predicted T_{wo} was slightly lower than the observed T_{wo} (i.e. negative PE). It was noticed that the PE was increasing at high *water-cooling ranges* (i.e. $T_{wi} - T_{wo}$). The 1st experiment clearly represents this observation (see Fig. 3.7).

Table 3.3: Accuracy of humidifier sub-model to predict *outlet air temperature* T_{ao}

Experiment	$\overline{PE}$ [°C]		$\overline{\%PE}$ [%]		RMSE [°C]
	Average	SD	Average	SD	
1st	0.72	0.27	2.86	1.01	0.76
2nd	0.32	0.20	1.18	0.68	0.37
3rd	0.57	0.45	2.14	1.84	0.73
4th	0.33	0.22	1.16	0.76	0.39
Maximum	0.72	0.45	2.86	1.84	0.76
Minimum	0.32	0.20	1.16	0.68	0.37

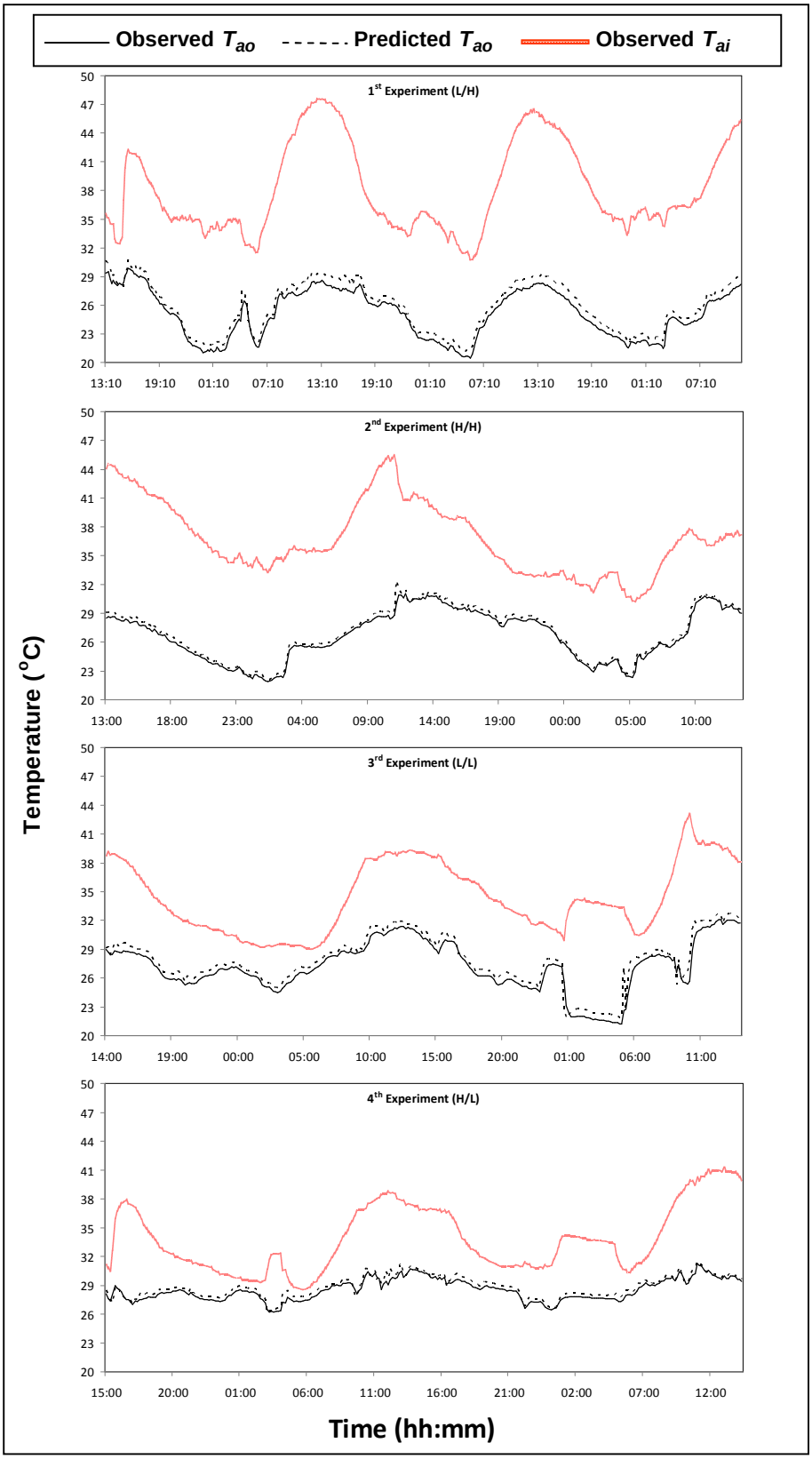

Fig. 3.6: Observed and predicted *outlet air temperature* T_{ao} with observed *inlet air temperature* T_{ai} of all experiments

(L/H, H/H, L/L and H/L: the 1st and 2nd letters of these abbreviations refer to air and water flowrates, respectively; H: indicates high flowrate and L: indicates low flowrate)

Table 3.4: Accuracy of humidifier sub-model to predict *outlet water temperature* T_{wo}

Experiment	$\overline{PE}$ [°C]		$\overline{\%PE}$ [%]		RMSE [°C]
	Average	SD	Average	SD	
1st	-1.06	0.54	-4.91	2.29	1.19
2nd	-0.38	0.36	-1.70	1.51	0.53
3rd	-0.30	0.46	-1.30	2.11	0.55
4th	-0.35	0.61	-1.32	2.29	0.71
Maximum	-0.30	0.61	-1.30	2.29	1.19
Minimum	-1.06	0.36	-4.91	1.51	0.53

3.4.2. Humidity predictions

The accuracy of the sub-model to predict ω_{ao} was excellent. Table 3.5 provides the $\overline{PE}$, $\overline{\%PE}$ and RMSE of the predicted ω_{ao} for all experiments. The $\overline{PE}$ was ranging from -0.00052 to 0.00012 kg (water)/kg (dry air) (SD≤0.00101 kg (water)/kg (dry air)), the $\overline{\%PE}$ was between -2.21 and 0.43 % (SD≤4.82 %) and the RMSE was between 0.00020 and 0.00113 kg (water)/kg (dry air). The results in Table 3.5 are illustrated graphically in Fig. 3.8. The accuracy of the sub-model to predict the ω_{ao} was much better than its accuracy to predict the T_{ao} and T_{wo}. The predicted ω_{ao} was slightly less than the observed ω_{ao}.

When the predicted ω_{ao} was converted into *relative humidity*, the accuracy has slightly deteriorated. It was found that for the φ_{ao} during all experiments, the $\overline{PE}$ was ranging from -6.29 to -2.30 % (SD≤1.68 %), the $\overline{\%PE}$ was ranging from -8.71 to -3.25 % (SD≤2.09 %) and the RMSE was between 2.51 and

Table 3.5: Accuracy of humidifier sub-model to predict *outlet humidity ratio* ω_{ao}

Experiment	$\overline{PE}$ [kg/kg]		$\overline{\%PE}$ [%]		RMSE [kg/kg]
	Average	SD	Average	SD	
1st	-0.00048	0.00029	-3.39	1.77	0.00056
2nd	0.00002	0.00019	0.04	1.27	0.00019
3rd	-0.00003	0.00028	-0.37	1.72	0.00028
4th	-0.00005	0.00026	-0.31	1.29	0.00027
Maximum	0.00002	0.00029	0.04	1.77	0.00056
Minimum	-0.00048	0.00019	-3.39	1.27	0.00019

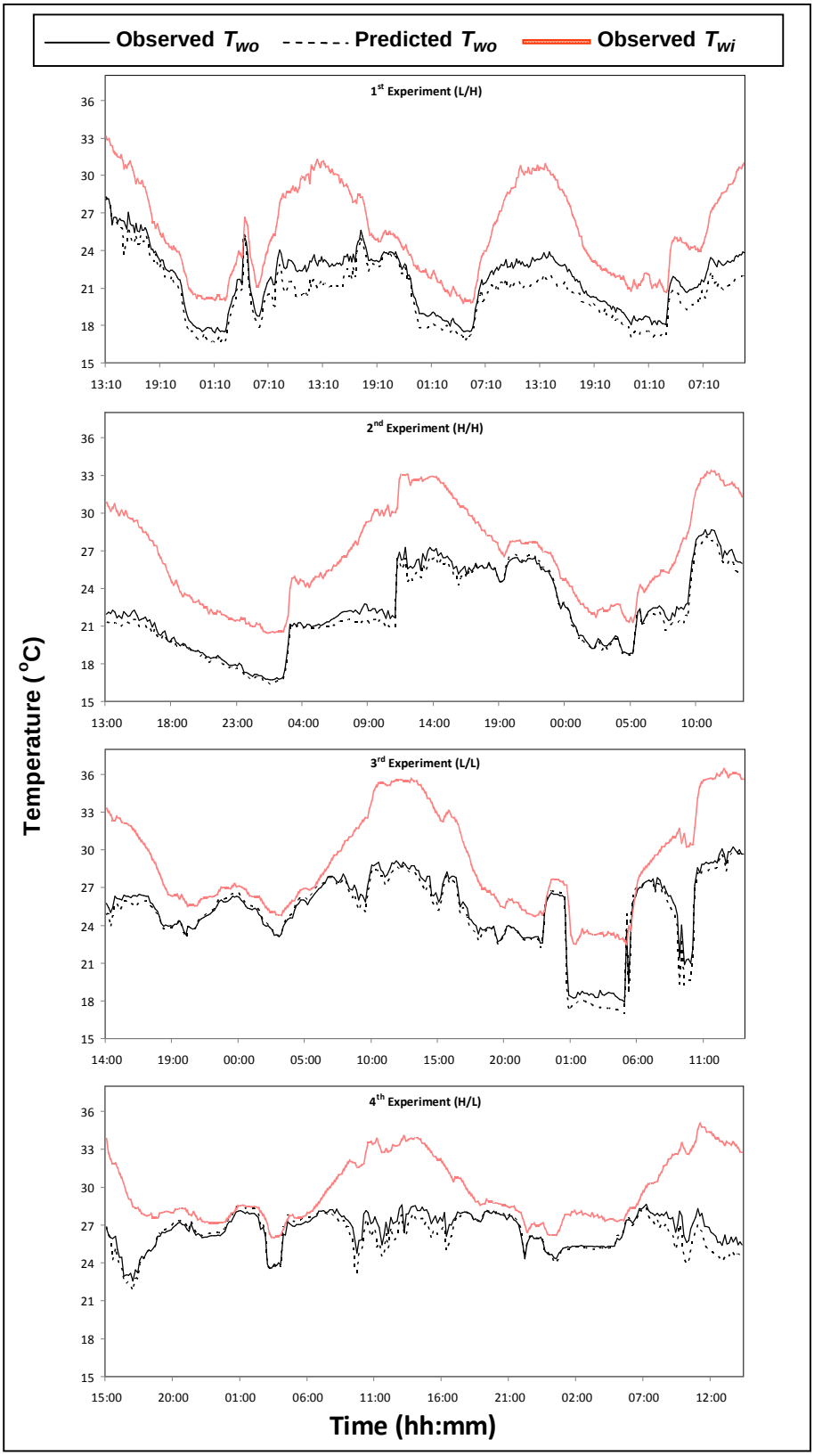

Fig. 3.7: Observed and predicted *outlet water temperature* T_{wo} with observed *inlet water temperature* T_{wi} of all experiments

(L/H, H/H, L/L and H/L: the 1st and 2nd letters of these abbreviations refer to air and water flowrates, respectively; H: indicates high flowrate and L: indicates low flowrate)

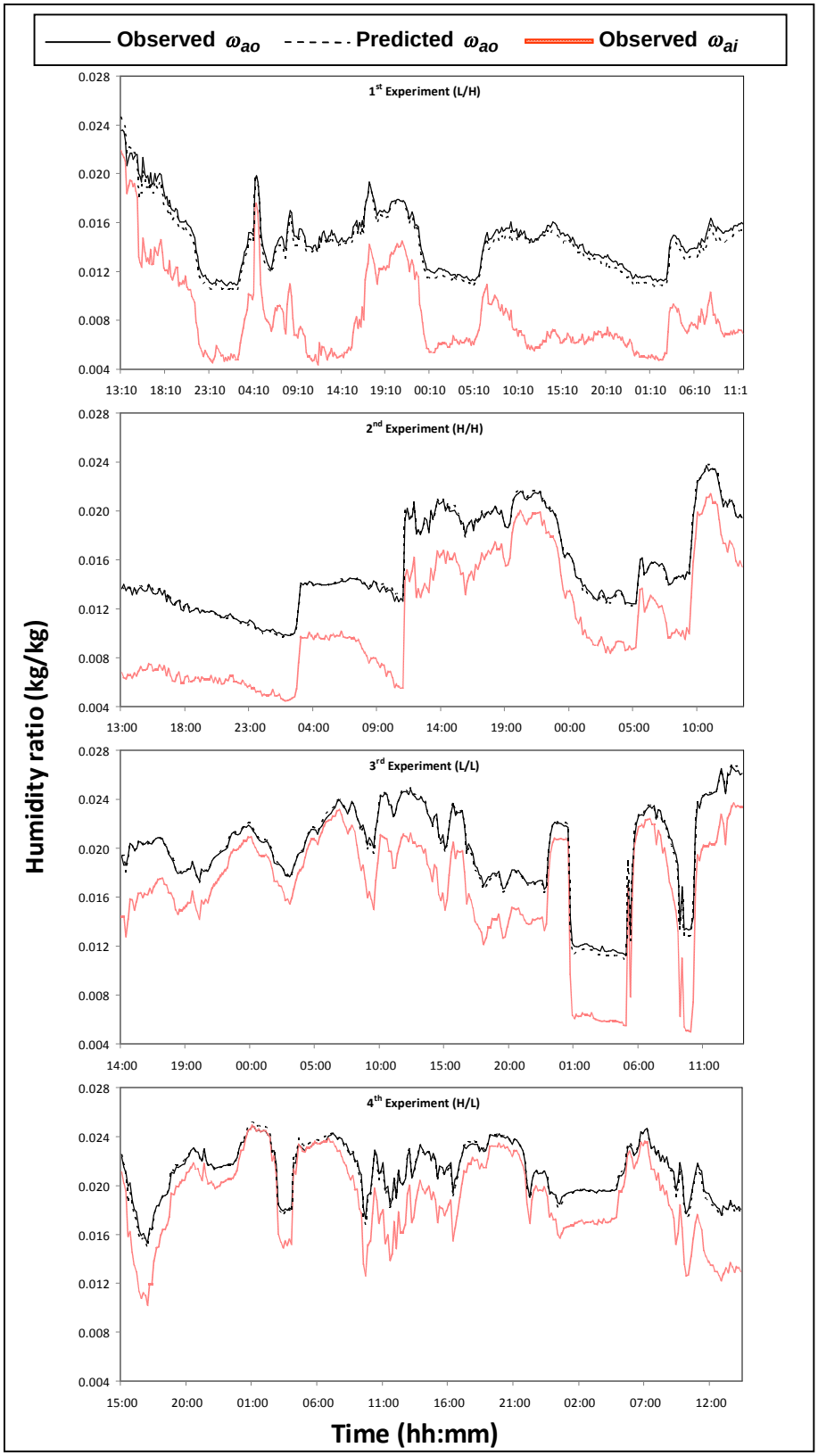

Fig. 3.8: Observed and predicted *outlet humidity ratio* ω_{ao} with the observed *inlet humidity ratio* ω_{ai} of all experiments

(L/H, H/H, L/L and H/L: the 1st and 2nd letters of these abbreviations refer to air and water flowrates, respectively; H: indicates high flowrate and L: indicates low flowrate)

6.39 % (see Table 3.6 for more details). The calculated φ_{ao} was continually lower than the observed φ_{ao} as can be clearly seen from Fig. 3.9. The highest difference between the calculated and observed φ_{ao} took place during the 1st experiment and the lowest difference was observed during the 2nd experiment.

3.4.3. Influence of varying air and water flowrates

Two air flowrates and two water flowrates were investigated in the validation experiments. It was found that the accuracy of the sub-model was not influenced significantly by the changes in the air and water flowrates. However, it was found that varying the flowrates had, to some extent, influenced the humidification process. This influence was observed by comparing the observed *humidity ratios* at the *inlet* ω_{ai} and *outlet* ω_{ao} of the humidifier. The differences between the ω_{ai} and ω_{ao} for all experiments is demonstrated in Fig. 3.8. The humidification increased with increasing air flowrate and increasing water flowrate. For instance, the average *evaporation rate* was 0.060 and 0.093 kg (water)/s during the 1st experiment (low air flowrate) and 2nd experiment (high air flowrate), respectively, at the same water flowrate. Also, the average *evaporation rate* was 0.060 and 0.048 kg (water)/s during the 1st experiment (high water flowrate) and 4th experiment (low water flowrate), respectively, at the same air flowrate.

Table 3.6: Accuracy of humidifier sub-model to predict *outlet relative humidity* φ_{ao}

Experiment	$\overline{PE}$ [%]		$\overline{\%PE}$ [%]		RMSE [%]
	Average	SD	Average	SD	
1st	-6.29	1.11	-8.71	1.59	6.39
2nd	-2.30	1.00	-3.25	1.27	2.51
3rd	-4.89	1.68	-5.68	2.09	5.17
4th	-3.71	0.78	-4.28	0.86	3.79
Maximum	-2.30	1.68	-3.25	2.09	6.39
Minimum	-6.29	0.78	-8.71	0.86	2.51

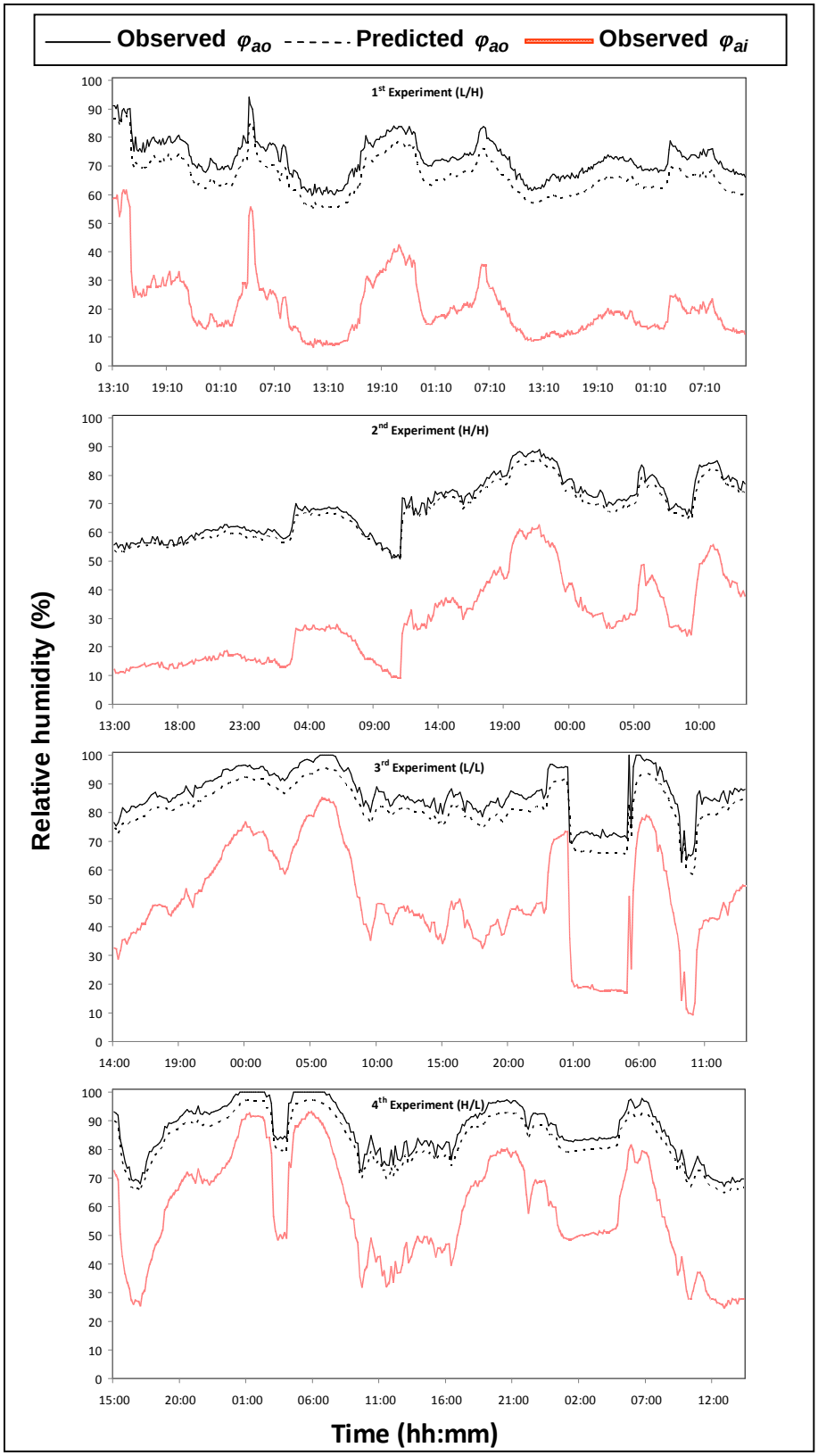

Fig. 3.9: Observed and predicted *outlet relative humidity* φ_{ao} with observed *inlet relative humidity* φ_{ai} of all experiments

(L/H, H/H, L/L and H/L: the 1st and 2nd letters of these abbreviations refer to air and water flowrates, respectively; H: indicates high flowrate and L: indicates low flowrate)

3.5. DISCUSSION

3.5.1. Temperature predictions

Halasz (1999), the model developer, reported that the predicted T_{wo} would be higher than the observed T_{wo} and the predicted T_{ao} would be lower than the observed T_{ao}. This is due to the adoption of assumption (x) which states that "the change in *water mass flowrate* due to evaporation is negligible (i.e. $\dot{m}_w$=constant)". However, Halasz (1999) also reported on some occasions that the predicted T_{ao} was higher than the observed value. Halasz (1999) attributed this to two causes; the large *water-cooling range* (i.e. $T_{wi} - T_{wo}$) and the small *approach* (i.e. $T_{wo} - T_{wb,ai}$) observed during these occasions. Halasz (1999) explained that these two causes could introduce large errors associated with the linearization of the air saturation line (see assumption vii and the Glossary for more details on the air saturation line).

From the results of this study, it was similarly found that the predicted T_{ao} was slightly higher than the observed T_{ao} (i.e. positive PE) and the predicted T_{wo} was slightly lower than the observed T_{wo} (i.e. negative PE) (see Figs. 3.6 and 3.7). The T_{ao} was calculated from Eq. (3.1) in which the T_{wo} is the only unmeasured variable. From this equation, it is very clear that the T_{ao} is influenced inversely by the change in the T_{wo}. Therefore, the positive PE of the T_{ao} can be attributed to the negative PE of the T_{wo}. Furthermore, the negative PE of the T_{wo} can be attributed to the two causes mentioned above; the large *water-cooling range* and the small *approach*. However, during all experiments conducted in this study, it was found that the *water-cooling range* was less than 12.5^{o}C which is well below the problematic values mentioned in Halasz (1999). But, the *approach* was consistently less than 0.5^{o}C. Therefore, the unexpected PE of the T_{wo} can be mainly attributed to the low *approach* (i.e. $T_{wo} - T_{wb,ai}$) experienced during all experiments. The presence of such a discrepancy does

not mean that the accuracy of the sub-model to predict the T_{wo} was poor because it was seen from Table 3.4 and Fig. 3.7 that this PE was very small.

The negative PE of the T_{wo} was slightly increasing as the *water-cooling range* was increasing (see the 1st and 4th experiments in Fig. 3.7). This is because the increase in the *water-cooling range* resulted in an increase in the linearized segment on the real air saturation line (see assumption vii and the Glossary). The increase in the linearized segment would, in turn, have a negative impact on the accuracy of the model.

Although the accuracy to predict the T_{ao} depends on the accuracy of the predicted T_{wo}, it was found that the accuracy of the sub-model to predict the T_{ao} was better than its accuracy to predict the T_{wo}. This can be understood by comparing the flowrates of the air and water. The minimum and maximum ratios of the air-to-water flowrates were almost 10:1 and 31:1, respectively. This implies that the inaccuracy in the predicted T_{wo} observed with relatively small water flowrate was accommodated in a much larger air flowrate which made that inaccuracy less pronounced in the case of the predicted T_{ao}. This can be clearly seen in Fig.3.6 where the PE was lower at high-air-flowrate experiments (i.e. 2nd and 4th experiments) than at low-air-flowrate experiments (i.e. 1st and 3rd experiments).

In the above discussion, the discrepancy in the predicted T_{ao} was considered to be simulation-related. However, it could be measurement-related, too. It was mentioned in Sec. 3.2.2 that Halasz's non-dimensional model (Eqs. 3.1 and 3.2) can be used to simulate *cross-flow* evaporative coolers only when the average outlet air and water conditions are to be obtained. Therefore, the predicted T_{ao} from Eq. (3.1) was representing the average *outlet temperature of the air* leaving the humidifier. The outlet temperature/relative humidity sensor was placed at the mid-span width and height of the humidifier assuming a linear vertical temperature gradient.

However, this gradient was possibly not linear and thus the observed T_{ao} did not represent the average *outlet air temperature*. A further investigation is necessary to determine whether the outlet sensor was observing the average values of the T_{ao} or higher/lower values. This can be done by using several outlet sensors arranged in a vertical profile.

3.5.2. Humidity predictions

The sub-model very accurately predicted the ω_{ao} (see Fig. 3.8). The PE was slightly negative which coincides with that reported by Halasz (1999). When the *outlet relative humidity* φ_{ao} was calculated as a function of the predicted ω_{ao} and T_{ao}, the calculated φ_{ao} was found to be less than the observed φ_{ao} (see Fig. 3.9). Since the ω_{ao} was accurately predicted, this difference between the calculated and observed φ_{ao} was mainly caused by the T_{ao} that had a positive PE. This relation between the predicted T_{ao} and calculated φ_{ao} can be obviously seen from Figs. 3.6 and 3.9. From these figures, it was noticed that the highest difference between the calculated and observed φ_{ao} occurred during the 1st experiment when the highest PE of the T_{ao} was observed. On the other hand, the lowest difference occurred during the 2nd experiment when the lowest PE of the T_{ao} was observed.

3.6. SUMMARY

This chapter, dedicated to discuss the development and validation of the humidifier sub-model, can be summarised in the following points:

- The accuracy of the sub-model to predict the *outlet water temperature* was very good. However, the predicted values were unexpectedly below the observed values. This was attributed to the nearness between the

predicted *water temperature* values and the *wet-bulb temperatures* as well as to the linearization of the air saturation line

- The accuracy of the sub-model to predict the *outlet air temperature* was better than its accuracy to predict the *outlet water temperature*. However, the predicted *outlet air temperature* was slightly higher than the observed value. This was attributed to the involvement of the discrepancy associated with the predicted *outlet water temperature* in the simulation and to the possible inaccuracy in the measured *outlet air temperature*
- The predicted *outlet humidity ratio* was extremely accurate
- The calculated *outlet relative humidity* was slightly below the observed values. This was attributed to the involvement of the *outlet air temperature*, associated with a positive *predictive error*, in the calculation
- Further investigations to study the accuracy of the humidifier sub-model are highly recommended. In these investigations, several outlet sensors arranged in a vertical profile should be used to avoid any possible measurement-related inaccuracy.

CHAPTER FOUR

4. THE MICROCLIMATE SUB-MODEL

This chapter provides a detailed explanation of the mathematical model that will be used in this study to simulate the microclimate of a ventilated Quonset greenhouse. The microclimate considered in the simulation includes only the greenhouse section cultivated with crops. In this chapter, Sec. 4.1 gives a general introduction. The microclimate simulation sub-model that will be used in this study is explained in detail in Sec. 4.2. The validation experiments conducted to test the accuracy of the sub-model are described in Sec. 4.3. Section 4.4 presents the results obtained and Sec. 4.5 gives a critical discussion of these results. Finally, the main conclusions about the microclimate sub-model are given in Sec. 4.6.

4.1. INTRODUCTION

Understanding the relationship between the greenhouse microclimate and its surrounding is an essential requirement for optimal cultivation and for on-line climate control. For the last four decades, quantifying the thermal and moisture parameters that play important roles in the inner environment of greenhouses has been the focus of many researchers (see Sec. 2.2). Consequently, a large number of models simulating different variables of greenhouse microclimate can be found in the literature. The temperature of air, plants, cover and soil, the humidity of the air and the crop yield are examples of the simulated variables. Based on the way those models deal with greenhouse components (e.g. air, plants, cover and soil), they can be classified into two main categories; *steady-state* and *dynamic* models.

Steady-state models (e.g. Walker, 1965; Garzoli and Blackwell, 1973; Price and Peart, 1973; Maher and O'Flaherty, 1973; von Elsner, 1980; Boulard and Baille, 1993; Jolliet, 1994; Seginer, 1994; and Condori and Saravia, 2003)

assume that greenhouse components are time-independent which means that temperature and moisture variations as a function of time are not significant. Despite this assumption, most of these models were able to provide reasonable to good accuracy.

Dynamic models (e.g. Takakura et al., 1971; Kimball, 1973; Froehlich et al., 1979; Kindelan, 1980; Chandra et al., 1981; Duncan et al., 1981; Cooper and Fuller, 1983; Tunç and Venart, 1984; Fuller et al., 1987; and Levit and Gaspar, 1988), on the other hand, do not neglect the time-dependant variations of temperature and humidity of some or all greenhouse components. Although the dynamicity of these models slightly increases their accuracy, Boulard and Baille (1993) and Khalil (1995) reported that complex dynamic models (similar to Takakura et al., 1971) are difficult to be used for online climate control because of their sophistication.

Therefore, in this study, a *steady-state* model will be developed to simulate the microclimate of the HD greenhouse due to the simplicity and acceptable performance of *steady-state* models.

In most of the above mentioned studies, greenhouse components were treated as single homogeneous units for the whole greenhouse and hence, the models generate average values for the simulated variables such as temperature and humidity. For long fan-ventilated greenhouses (see Fig. 4.1), those models should be modified to account for temperature and humidity gradients along the air-flow direction owing to the large differences between the inlet and exit values of temperature and humidity. For instance, the *air*

Fig. 4.1: A Quonset greenhouse used in the experiments

temperature difference can reach between 6 to 14^{o}C (Wiersma and Short, 1983; Bucklin et al., 1993; and Chen, 2003) depending on the air flowrate and *solar radiation input*.

Among the large number of greenhouse simulation models, only a few studies simulate the longitudinal (i.e. air-flow direction) gradient of *air temperature* (Kittas et al., 2001 & 2003) and *humidity* (Chen 2003) of greenhouse inner environment. They achieved that by dividing the greenhouse microclimate into small adjacent sections along the air-flow direction as shown in Fig. (4.2). This type of model enables the prediction of the intermediate and exit conditions of the air when the entrance conditions are known. Also, this type of simulation can be used as a guidance tool for determining the optimal structural (e.g. shading and greenhouse length) and operational (e.g. air flow-rate) variables of tunnel-like greenhouses (i.e. similar to Figs 4.1 & 4.2).

Chen (2003) provided a simple *steady-state* model predicting *air temperature* and *humidity* as a function of distance inside long fan-ventilated greenhouses. However, that model cannot be used for all types of crops cultivated in greenhouses because it uses a transpiration term obtained empirically for tomato plants. The objective of this study is to develop a similar simulation model for a greenhouse cultivated with cucumber, which is the most commonly cultivated crop in greenhouses in Oman. Therefore, Chen's model will be modified to account for a cucumber crop when considering the *evapotranspiration* term in the simulation model. This modified model will, then, be used as a sub-model of the integrated HD greenhouse simulation model.

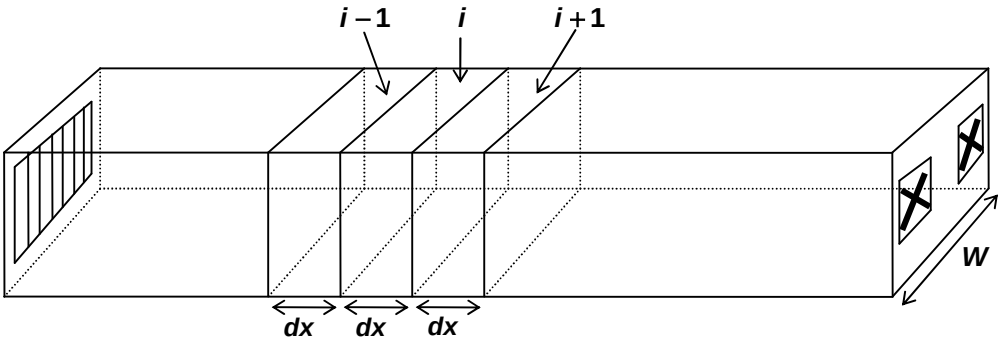

Fig. 4.2: Schematic of three sequential sections along the airflow direction of the greenhouse

4.2. THE MODIFIED CHEN'S MODEL

In order to perform the mathematical simulation that would predict *air temperature* and *humidity* gradients along the greenhouse, the following steps should be followed;

① make reasonable working assumptions
② divide the greenhouse into small sections along the air flow direction
③ determine the important heat and moisture terms and provide methods for estimating them
④ combine all heat and moisture terms together in *heat* and *moisture balance* equations, respectively
⑤ present the balance equations in a final format that enables the calculation of *air temperature* and *humidity* of every section

These steps are described in the following sub-sections in order.

4.2.1. Assumptions

In the development of the simulation sub-model, the following assumptions are considered:

i. Each section within the greenhouse is homogeneous in its temperature and humidity level
ii. Each section has the same temperature for all of its components, namely; air, plants and soil
iii. The greenhouse cover is a translucent surface to the incoming/outgoing *long-wave thermal radiation*
iv. *Soil heat transfer* and *storage* is assumed insignificant which is a practiced assumption with most *steady-state* models to avoid the complication associated with the incorporation of this heat. In addition, the use of forced ventilation in greenhouses alleviates the effect of this heat source/sink

v. All non-reflected *solar radiation* is absorbed by the crop. In reality, a small part of the *solar radiation* finds its way to the soil. Similar to Assumption iv, this assumption was made to avoid the complication associated with the incorporation of the *soil heat transfer* and *storage* which necessitates the use of a *dynamic* model that is not the objective in this study
vi. The canopy presents a full vegetative coverage
vii. Evaporation from the soil is negligible due to the use of a drip irrigation system that localizes water around the plant roots. The soil evaporation plays an important role in the early stages of crop growth and cannot be neglected; however in later stages it is not an important factor (Seginer, 2002)
viii. The water vapour inside plant leaves is at saturation

4.2.2. Greenhouse sections

The development of the model starts by dividing the greenhouse microclimate into adjacent sections (i.e. controlled volumes) along the airflow direction (see Fig. 4.2). The outputs from one section will be the inputs to the subsequent section for the parameters that change with air movement, such as *air temperature* and *moisture content*. By this way, *air temperature* and *humidity* gradients of the greenhouse can be obtained.

4.2.3. Heat and moisture terms

The possible heat sources/losses of any section within the greenhouse are *solar* and *thermal radiation*, ventilation, *convective heat* to/from the cover, soil and plants, and *conductive heat* through the cover (see Fig.4.3). Moisture can be added to the section through *evapotranspiration* and be taken away from it by ventilation. Sub-sections 4.2.3.1 to 4.2.3.6 and 4.2.3.7 to 4.2.3.8 discuss, in more details, these heat and moisture terms, respectively.

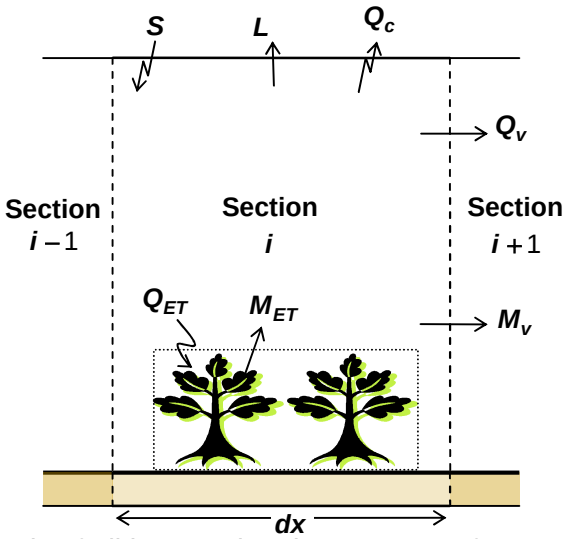

Fig. 4.3: Schematic of all heat and moisture terms of one section within the greenhouse

Heat Terms:

4.2.3.1. Solar radiation

The heating effect of the global solar radiation is the predominant heat source in the daytime for all greenhouse components. The calculation of the *solar heat gain* S to each section of the greenhouse can be estimated once the *ambient solar heat flux* I_{out}, *solar transmittance of the cover* τ_c and *short-wave reflectance of the crop canopy* ϕ_P are known. The formula that can be used to calculate S of section i is

$$S = \tau_c \left(1-\phi_P\right)\left(W\, dx\right) I_{out} \qquad (4.1)$$

Although this expression estimates the amount of *solar heat radiation* received by greenhouse plants, the energy is assumed to be completely transferred to the air (i.e. no heat storage). A similar assumption was made by Walker (1965), Garzoli and Blackwell (1973), Duncan et al. (1981), Kittas et al. (2001 & 2003), Condori and Saravia (2003), Chen (2003) and many others. Equation (4.1) is slightly different from the one used by Chen:

$$S = \left(W\, dx\right) I_{in}$$

which considered the *solar radiation* entering the greenhouse to be fully trapped inside, which is not always the case because part of it is normally reflected away by greenhouse surfaces such as the soil and plants.

4.2.3.2. Thermal radiation

All materials emit radiation in the long wavelength range as their temperatures are not very high. Similarly, all greenhouse elements follow the same behaviour. In order to calculate the *radiative heat transfer rate* L exchanged between any two bodies, the temperature of both bodies should be known as well as their *emissivities* ε_s.

In previous simulation studies, the overall *thermal heat transfer rate* L exchanged between the greenhouse and the atmosphere was sometimes neglected or only considered in the *overall heat transfer coefficient of the cover* U_c (e.g. Ewen et al., 1980; von Elsner, 1980; Duncan et al., 1981; Kittas et al., 2001 & 2003; and Condori and Saravia, 2003). However, it was accounted for in some studies (e.g. Walker, 1965; Garzoli and Blackwell, 1973; Tunç and Venart, 1984; and Chen, 2003). In more detailed studies, even the *thermal exchange* between greenhouse bodies themselves was considered (e.g. Takakura et al., 1971; Kimball, 1973; Maher and O'Flaherty, 1973; Froehlich et al., 1979; Bot, 1980; Kindelan, 1980; Chandra et al., 1981; Avissar and Mahrer, 1982; Cooper and Fuller, 1983; and Levit and Gaspar, 1988).

In this study, the *thermal heat transfer rate* L exchanged between the atmosphere and any section within the greenhouse will be considered. The L of section i will be calculated using Eq. (4.2):

$$L = f_v (W\, dx)\, \sigma \left(\varepsilon_s\, T_{i,K}^4 - T_{sky,K}^4 \right) \tag{4.2}$$

In this equation, the *sky temperature* T_{sky} will be estimated using Swinbank's (1963) suggested relationship,

$$T_{sky,K} = 0.0552 \left(T_{out,K}^{1.5} \right) \tag{4.3}$$

Although Adelard et al. (1998) stated that this formula is problematic due to its correlation nature (i.e. only suitable for certain conditions or sites), it has gained a good acceptance among greenhouse model developers (e.g. Kindelan, 1980; Chandra et al., 1981; Nijskens et al., 1984; and Chen, 2003) who did not report any prediction problems associated with its use.

4.2.3.3. Heat transfer rate by ventilation

Ventilating greenhouses causes *heat* and *moisture transfer.* In this sub-section, only the *sensible heat transfer* is discussed while the *moisture transfer* will be discussed in Sec. 4.2.3.7. In order to perform the calculation of the *sensible heat transfer* Q_v associated with ventilation for any section within the greenhouse, the temperature of the previous section is taken as a boundary condition. In other words, the *outflow temperature* of air leaving section $i-1$ will be taken as the *inflow temperature* of section i. This is illustrated mathematically in the following relation:

$$Q_v = \rho_a C_{p,a} \dot{V}_a (T_i - T_{i-1}) \tag{4.4}$$

4.2.3.4. Convective and conductive heat transfer

Convective heat transfer occurs between moving fluids or between solids and moving fluids whenever a temperature difference exists. In any section within the greenhouse, there is a *convective heat transfer* between the air and the cover. The *convective heat transfer rate* can be calculated once the temperature difference and the *convective heat transfer coefficient* are known. There is also a *conductive heat transfer* that takes place through the greenhouse cover. Calculation of the *conductive heat transfer rate* requires the temperature on both sides of the cover and the *cover thermal conductivity* to be known. The following relation will be used to calculate the *convective and conductive heat transfer rate* through the greenhouse cover:

$$Q_c = (T_{out} - T_i)(P\,dx)U_c \tag{4.5}$$

In this relation, the *overall heat transfer coefficient* U_c of the greenhouse cover is accounting for the *convective heat transfer coefficient* and the *cover thermal conductivity*.

4.2.3.5. Heat loss through evapotranspiration

Evapotranspiration (ET) from greenhouse crops is influenced by several parameters. The first two parameters governing the ET process are the impinging *solar radiation* on plant leaves and the *vapour pressure deficit* ψ''' between the surrounding air and the inside of plant leaves. *Evapotranspiration* is a process that can occur even at nighttime (Yang et al., 1990; and Medrano et al., 2005) because the *solar radiation* and ψ''' can work separately. Different methods to quantify the amount of moisture released from cultivated crops were found in the literature. They ranged from methods accounting for those two parameters together (e.g. Yang et al., 1990; Bakker, 1991; Hatfield and Burke, 1991; Stanghellini and van Meurs, 1992; and Allen et al., 1998) to methods accounting for only one of them (e.g. Kitano and Eguchi, 1989).

In addition to the *solar radiation* and ψ''', there are some other parameters that were considered in the estimation of the amount of moisture released from cultivated crops. These parameters included; the *temperature of plant leaves* T_p (Chamont et al., 1995), *air velocity* u_a (Wolpert, 1962; and Jolliet and Bailey, 1992) and *leaf area index LAI* (Medrano et al., 2005).

In this study, the Penman-Monteith equation will be used due to its wide acceptance and its incorporation of all variables mentioned above. This equation was originally developed for daily measurements of the *evapotranspiration rate* and appeared in the following format:

$$\hat{L}_v \hat{M}_{ET} = \frac{\hat{\Delta}\left(\hat{R}_n - \hat{G}\right) + \dfrac{86400\ \rho_a \hat{C}_{p,a}\ \psi_a'''}{r_a}}{\hat{\Delta} + \gamma\left(1 + \dfrac{r_s}{r_a}\right)} \qquad (4.6)$$

where $\hat{L}_v \hat{M}_{ET}$ is the *latent heat flux of* ET in [MJ/m^2.day]. The techniques of calculating the variables in Eq. (4.6) can be found in Jensen et al. (1990) and Allen et al. (1998).

The Penman-Monteith relation (Eq. 4.6) was used by many researchers to derive simplified mathematical relations to estimate the *latent heat of transpired water* inside greenhouses (e.g. Baille et al., 1994 as cited by Medrano et al., 2005; and Stanghellini, 1987 as cited by Jolliet, 1994). In this study, the Penman-Monteith equation (Eq. 4.6) will be used after modifying it to account for all simplifying assumptions, namely; assumptions (ii), (iv), (vii) and (viii) listed in Sec. 4.2.1. Excluding the *heat transfer rate of the soil* and the evaporation from the soil, Eq. (4.6) can be written as follows:

$$Q_T = (W\,dx)\frac{\hat{\Delta}\left(\dot{S}-\dot{L}\right)+\rho_a\,C_{p,a}\,\frac{\psi'''_a}{r_a}}{\hat{\Delta}+\gamma\left(1+\frac{r_s}{r_a}\right)} \tag{4.7}$$

where Q_T is the *heat transfer rate of transpiration* of any section within the greenhouse. $\dot{S}$ is the non-reflected *solar heat flux* on greenhouse plants which can be estimated using

$$\dot{S} = \tau_c\left(1-\phi_p\right)\mathrm{I}_{out} \tag{4.8}$$

The *long-wave heat flux* $\dot{L}$ exchanged between the greenhouse canopy and the sky can be calculated using

$$\dot{L} = f_v\,\sigma\,\tau_{\lambda,\mathrm{c}}\left(\varepsilon_p\,T_{i,K}^4 - T_{sky,K}^4\right) \tag{4.9}$$

The ψ''' of section i is estimated from

$$\psi'''_i = \psi''_i - \psi_i \tag{4.10}$$

where ψ''_i is the *saturation vapour pressure* at T_i. The ψ''_i will be calculated using Glanz and Orlob's (1973) relation (see Eq. 3.15 of Sec. 3.2.3).

The *surface resistance* r_s will be estimated using the following relation (Allen et al., 2006);

$$r_s = \frac{r_{leaf}}{LAI_{eff}} \tag{4.11}$$

where the *effective leaf area index* LAI_{eff} for semi-dense crops can be calculated using (Ben-Mehrez et al., 1992);

$$LAI_{eff} = \frac{LAI}{0.3\,LAI + 1.2} \tag{4.12}$$

However, because the cucumber crop used in this study is not very dense (i.e. LAI is between 1.2 and 1.4), the whole cucumber crop is considered to be active in the transpiration process. Therefore, LAI will be used in Eq. (4.11) instead of LAI_{eff}. Thus,

$$r_s = \frac{r_{leaf}}{LAI}$$

The *leaf resistance* r_{leaf} will be calculated using the following relation obtained by Bakker (1991) specifically for a cucumber crop cultivated inside a greenhouse;

$$r_{leaf} = \frac{100}{2.081\left[1 - 0.858\exp\left(-0.0098\,PAR\right)\right]\left[\exp\left(-0.5551\psi_i'''\right)\right]} \tag{4.13}$$

The following relations, found in Allen et al. (1998), will be used to compute the rest of the variables of Eq. (4.7);

$$\hat{\Delta} = 4098\frac{\psi_i''}{\left(T_i + 237.3\right)^2} \tag{4.14}$$

$$\gamma = \frac{\mathrm{P}_i\, C_{p,a}}{0.62198\, L_v} \tag{4.15}$$

in which the *latent heat of vaporization* L_v is calculated using the relation developed by Henderson-Sellers (1984);

$$L_v = 1.91846 \times 10^6 \left(\frac{T_i + 273.15}{T_i + 239.24} \right)^2 \tag{4.16}$$

and the *aerodynamic resistance* r_a will be calculated as follows (taking into account approximations given in Allen et al. (1998) provided that the temperature and humidity measurements are taken at a height of 2 m);

$$r_a = \frac{\ln\left(\frac{16.26}{H_p} - 5.423 \right) \ln\left(\frac{162.6}{H_p} - 54.228 \right)}{0.168\, u_2} \tag{4.17}$$

Moisture Terms

4.2.3.6. Moisture addition/removal by ventilation

As air moves from one section to another within the greenhouse, it carries along with it some moisture. The moisture budget of any section may increase or decrease depending on the moisture level of the previous section. Based on that, a comparison of moisture level of both sections will provide the amount removed from any section.

$$M_v = \rho_a \dot{V}_a \left(\varpi_i - \varpi_{i-1} \right) \tag{4.18}$$

4.2.3.7. Moisture addition by plant transpiration

The amount of vapour added from the canopy to the air of any section can be calculated by dividing the *latent heat of transpiration* Q_T (Eq. 4.7) by the *latent heat of vaporization* L_v as follows:

$$M_T = \frac{Q_T}{L_v} \tag{4.19}$$

4.2.4. Heat and moisture balance equations

All significant heat and moisture terms can be collated together to form the following *heat* and *moisture balance* equations, respectively:

$$S - L - Q_v - Q_{cd} - Q_T = 0 \tag{4.20}$$

$$M_T - M_v = 0 \tag{4.21}$$

In Eq. (4.21), the *latent heat of plant transpiration* Q_T (Eq. 4.7) is considered a heat loss since it harnesses part of the impinging *solar radiation* and turns it into moisture.

4.2.5. Final format of the model

Re-arranging Eqs. (4.20) and (4.21) and substituting their primary variables yields Eqs. (4.22) and (4.23), respectively.

$$T_i = \frac{\tau_c (1-\phi_s)(W\,dx)\mathrm{I}_{out} + \dot{V}_a\,\rho_a\,C_{p,a}\,T_{i-1} + T_{out}\,(P\,dx)U_c - f_v\,\sigma\,\tau_{\lambda,c}(W\,dx)\left(\varepsilon_s\,T_{i,K}^4 - T_{sky,K}^4\right) - Q_T}{\dot{V}_a\,\rho_a\,C_{p,a} + (P\,dx)U_c} \tag{4.22}$$

$$\varpi_i = \varpi_{i-1} + \frac{M_T}{\rho_a \dot{V}_a} \tag{4.23}$$

These two relations present the final format of the simulation sub-model that enables the prediction of the temperature and moisture profiles of the air as it streams from one section to another along the air-flow direction of the greenhouse. Equation (4.22) cannot be solved explicitly due to the presence of T_i at both sides of the equation. Therefore, an iterative approach will be followed to solve it implicitly. Solver tool in MS-Excel will be used to carry out the iterations to come up with a final T_i value.

The ϖ_i obtained from Eq. (4.23) will be used to calculate the *relative humidity* φ_i of section *i*. The following relation provided in ASHRAE (2001) will be used to convert the ϖ_i into φ_i:

$$\varphi_i = 100\,\frac{\psi_i}{\psi''} \tag{4.24}$$

where the *partial vapour pressure* ψ_i is calculated using;

$$\psi_i = \frac{\omega_i\,\mathrm{P}_i}{0.62198 + \omega_i} \tag{4.25}$$

in which the *humidity ratio* ω_i can be computed from;

$$\omega_i = \frac{\varpi_i}{1-\varpi_i} \tag{4.26}$$

The saturation vapour pressure ψ'' will be calculated using Glanz and Orlob's (1973) relation (see Eq. 3.15 of Sec. 3.2.3). After substituting Eqs. (4.25), (4.26) and (3.15) in Eq. (4.24), the φ_i will be calculated as follows

$$\varphi_i = 100\,\frac{\mathrm{P}_i\,\dfrac{\varpi_i}{1-\varpi_i}}{2.1718\times10^{7}\,\exp\!\left(\dfrac{-4157}{T_i + 239.24}\right)\left(0.62198 + \dfrac{\varpi_i}{1-\varpi_i}\right)} \tag{4.27}$$

4.3. VALIDATION EXPERIMENTS

The accuracy of analytically developed models cannot be known unless their predicted results are confronted against measured data. For this purpose, the model (Eqs. 4.22 & 4.23) was used to simulate temperature and humidity gradients of a 38 m-long, cucumber-cropped Quonset greenhouse (see Fig. 4.1) located in Nizwa, Oman. More details about this greenhouse are given in Sec. A.2 of Appendix A. This commercial greenhouse was running with two fans drawing air through the greenhouse. The fans were linked to two thermostats that were governing their working schedules. Early morning when the temperature inside the greenhouse was not very high, only one fan was operating. Normally, two fans start working continuously from 10:00 hrs till early evening when the temperature was dropping down. The electricity was

switched off from the greenhouse by the farm owner slightly before sunset for the sake of energy saving.

4.3.1. Experimental setup

In the period 07-15 June, 2008, six experiments were conducted to monitor the *air temperature* and *humidity* variations along the air-flow direction of the greenhouse at two monitoring points. These points were respectively 12 m and 32 m away from the evaporative cooler (Fig.4.4) and at 2 m height from the ground. Although two observation points were used, only the second could be used for the assessment since the data collected from the first was used as input data in the simulation. The number of observation points should ideally have been more than two since the sub-model could simulate the *air temperature* and *humidity* gradients along the greenhouse. Only two observation points could be used due to unavailability of additional accurate sensors to monitor the *air temperature* and *humidity*. However, this drawback was partly mitigated by repeating the experiment six times.

The greenhouse was cultivated with a cucumber crop that was more than 1.8 m high during all experiments (see Fig. 4.5). The greenhouse was ventilated according to the fan working schedule explained above.

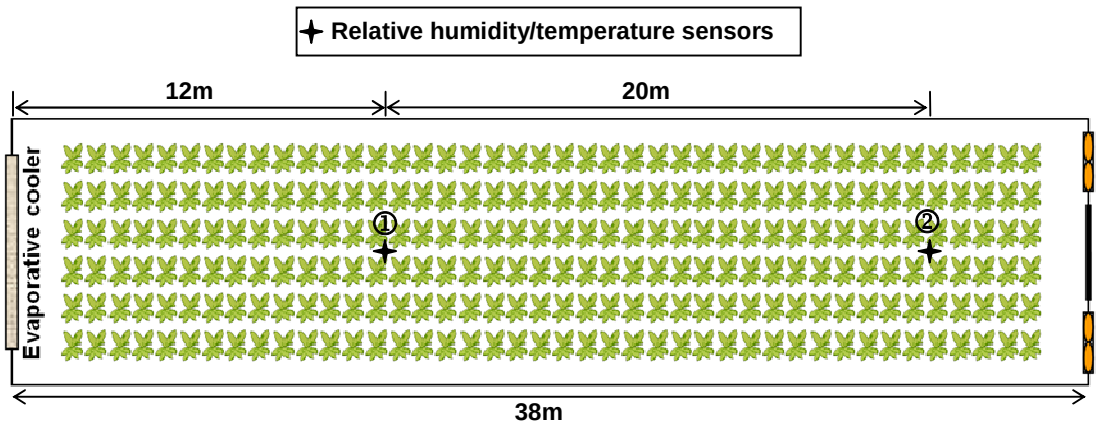

Fig. 4.4: A plan-view of Nizwa greenhouse illustrating the locations of the 1st and 2nd temperature/relative humidity sensors (① and ②, respectively)

(a) (b)

Fig. 4.5: The cucumber crop of Nizwa greenhouse (a) four days before the experiments and (b) at the end of experiments

4.3.2. Instrumentation of Nizwa greenhouse

Two Delta-T dual temperature/relative humidity sensors were used to measure the *air temperature* and *humidity* at the two observation points (see Fig. 4.4). The *solar heat flux* inside and outside of the greenhouse was monitored using two Delta-T photodiodes placed 2 m high from the ground (see Fig. 4.6). The reason for using two photodiodes was to calculate the *transmissivity of the greenhouse cover* τ_c. The τ_c was not known and was varying from one day to another due to the significant dust accumulation on the cover. The τ_c was calculated by dividing the *solar heat flux* measured inside the greenhouse by the *ambient solar heat flux* I_{out}. A Delta-T datalogger was used to retrieve and record data from these sensors at 10 minute intervals. The *ambient temperature* T_{out} was measured using a T-type thermocouple. A Field

(a) (b)

Fig. 4.6: The Delta-T photodiodes placed at 2 m height (a) outside and (b) inside Nizwa greenhouse

Point module was used to read from the thermocouple and an Ethernet interface module was used to transfer the measured temperature data to the PC. The data was acquired from the thermocouple every 10 minutes.

For *leaf area index* (*LAI*) measurements, a high resolution portable CID leaf area meter was used (see Fig. 4.7). *Air velocity* inside the greenhouse was measured using an Omega digital anemometer at three locations; 10, 20 and 32 m from the evaporative cooler at the mid-span width. At each location, the *air velocity* was measured at five heights; 0.5, 1.0, 1.5, 2.0 and 2.5 m (see Fig. 4.8). This anemometer was also used to measure the *air velocity* through the greenhouse fans in order to calculate the air flowrate through the greenhouse. A detailed description of all sensors used in these experiments can be found in Appendix B.

Fig. 4.7: The leaf area meter used to measure the area of cucumber leaves for the leaf area index estimation

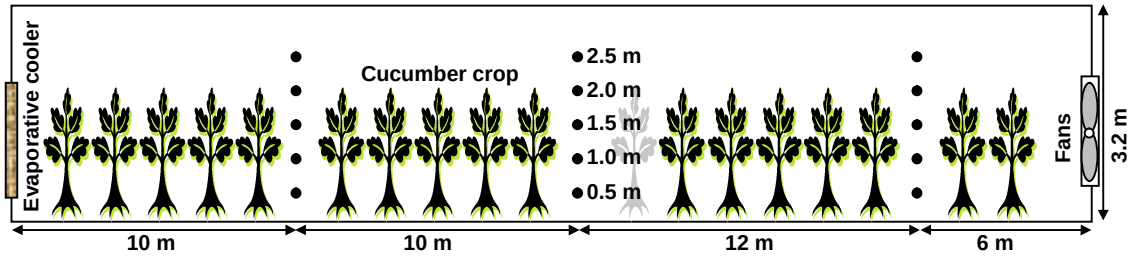

Fig. 4.8: A side-view schematic of Nizwa greenhouse illustrating the locations at which the air velocity measurements were taken (these locations are denoted by ●)

4.3.3. Testing accuracy of microclimate sub-model

The microclimate sub-model was used to simulate the *air temperature* and *humidity* changes along Nizwa greenhouse. The greenhouse configuration parameters as well as the ambient weather data and data collected from the 1st observation points were fed into the sub-model in order to perform the simulation. The sub-model was able to predict the *air temperature* and *humidity* of every section along the airflow direction of the greenhouse. The simulation length of each section (dx) was 1 m (see Fig. 4.2). This length dx can be increased or decreased however, the smaller is the better.

The predicted *air temperature* and *humidity* values of the 20th section (20 m apart from the 1st observation point) were compared to the observed values at that point. This comparison included the calculation of the *average predictive error* ($\overline{PE}$), the *average percentage predictive error* ($\overline{\%PE}$), and the *root mean square error* (RMSE). The predicted and observed *air temperature* and *humidity* were also compared graphically.

4.4. RESULTS

Table 4.1 presents the greenhouse design and operating parameters used in the simulation. The properties of the cucumber crop used in the simulation are provided in Table 4.2.

The overall accuracy of the microclimate sub-model to predict the *air temperature* and *humidity* profiles along the air flow direction of the greenhouse was very good. More details about the predictions of the sub-model are given in the following sub-sections.

Table 4.1: Greenhouse design and operating parameters used in the simulation

Parameter	Value	Comment
τ_c , [dimensionless]	0.82	measured
$\tau_{\lambda,c}$, [dimensionless]	0.698	Walker (1965)
U_c , [W/m^2 ^{o}C]	6.8	Chen (2003)
L_{gh} , [m]	38	measured
H_{gh} , [m]	3.2	measured
W_{gh} , [m]	9.0	measured
P (length of curved arch), [m]	11.78	calculated
V_{gh} , [m^3]	799.48	calculated
dx , [m]	1.0	theoretical
f_v , [dimensionless]	0.81	Chen (2003)
u_2 , (1 fan), [m/s]	0.66	measured
u_2 , (2 fans), [m/s]	0.93	measured
$\dot{V}_a$ (1 fan), [m^3/s]	11.253	measured through fans
$\dot{V}_a$ (2 fans), [m^3/s]	18.987	measured through fans

Table 4.2: Properties of the cucumber crop used in the simulation

Parameter	Value*	Comment
H_p , [m]	1.83 (1st) 1.92 (2nd) 1.94 (3rd) 2.97 (4th) 2.02 (5th) 2.05 (6th)	measured
LAI , [dimensionless]	1.41 (1st) 1.22 (2nd) 1.27 (3rd) 1.31 (4th) 1.41 (5th) 1.45 (6th)	measured
ϕ_p , [dimensionless]	0.25	Levit and Gaspar (1988)
ε_p , [dimensionless]	0.98	Kindelan (1980) and Levit and Gaspar (1988)

* numbers between parentheses indicate the experiment to which the correspondent value belongs

4.4.1. Temperature predictions

Generally, the microclimate sub-model accurately predicted the *air temperature* T_a at the 2nd observation point. Figure 4.9 illustrates the predicted and observed T_a for the 1st, 3rd and 5th experiments (see Fig. C2.1 in Sec. C.2

of Appendix C for the rest of experiments). The predicted T_a was continually greater than the observed T_a when one fan was operating (i.e. low air flowrate). However, when two fans were operating (i.e. high air flowrate), the predicted T_a was slightly lower than the observed values (see Fig. 4.9).

The influence of the *solar radiation* on the accuracy of the sub-model to predict the T_a is given in Fig. 4.10 for the 1st, 3rd and 5th experiments (see Fig. C2.2 in Sec. C.2 of Appendix C for the rest). It was observed from this figure that the curve of the predicted T_a was moving slightly upwards, relative to the curve of the observed T_a, as the *ambient solar radiation* I_{out} was increasing. At the low air flowrate, the $\overline{PE}$ was ranging from 0.04 to 1.03°C, the $\overline{\%PE}$ was between 0.11 and 3.63 % and the RMSE was between 0.27 and 1.07°C (see Table 4.3 for more details). At the high air flowrate, the $\overline{PE}$ was between -1.33 and -0.36°C, the $\overline{\%PE}$ was between -3.95 and -1.12 % and the RMSE was between 0.52 and 1.38°C (see Table 4.4 for more details).

4.4.2. Humidity predictions

In general, the sub-model accurately predicted the ω at the 2nd observation point. However, at the high air flowrate, the predicted ω was slightly less than the observed ω. At the low air flowrate, the predicted ω was slightly higher than the observed ω. The relation between the predicted and observed ω is illustrated in Fig. 4.11 for the 1st, 3rd and 5th experiments (see Fig. C2.3 in Sec. C.2 of Appendix C for the rest). At the low air flowrate, the $\overline{PE}$ was between 0.00005 and 0.00074 kg (water)/kg (dry air), $\overline{\%PE}$ was ranging from 0.28 to 3.84 % and the RMSE was between 0.00038 and 0.00078 kg (water)/kg (dry air) (see Table 4.5 for more details). At the high air flowrate, the $\overline{PE}$ was ranging from -0.0009 to -0.0006 kg (water)/kg (dry air), $\overline{\%PE}$ was ranging from

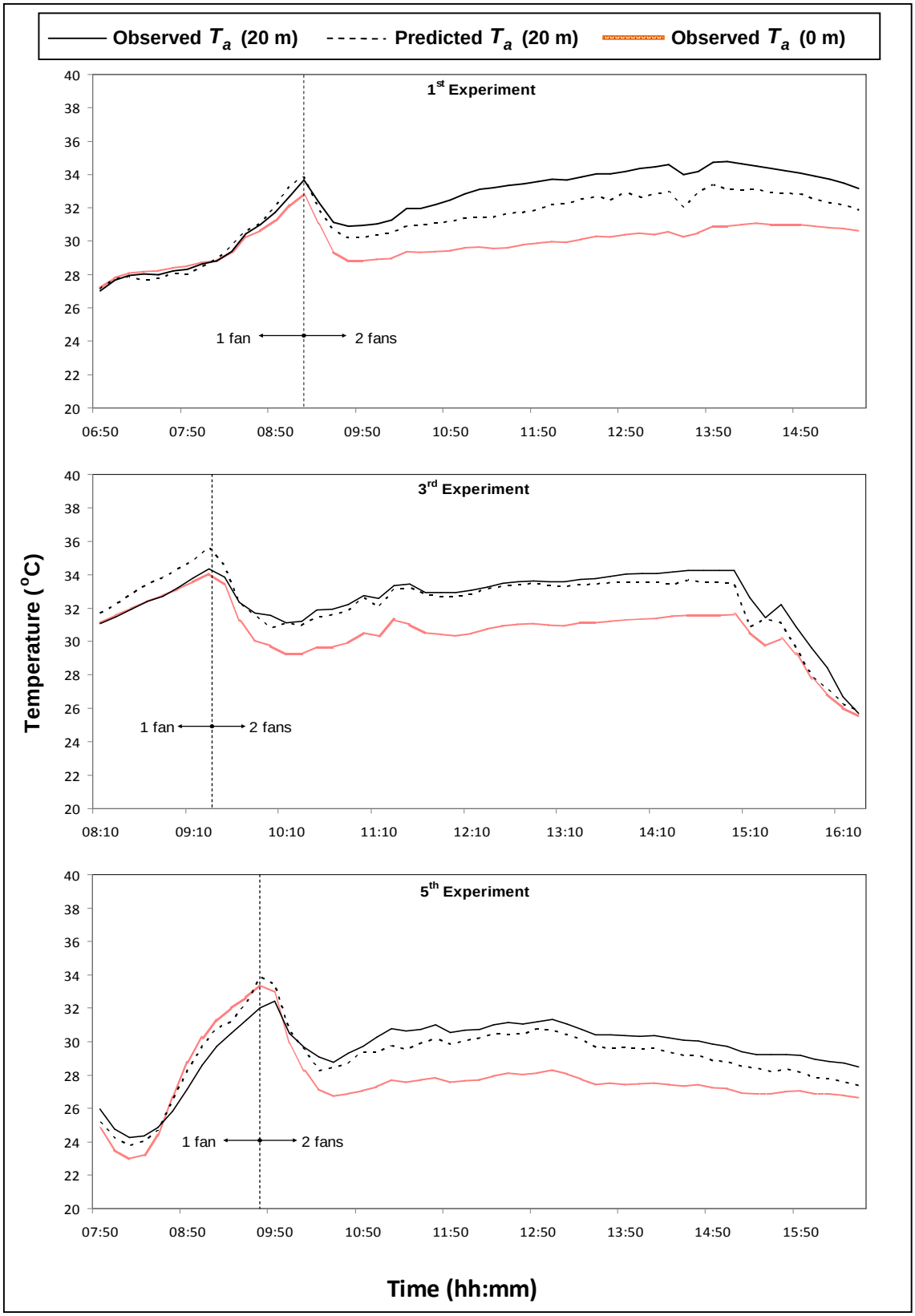

Fig. 4.9: Observed and predicted *air temperature* T_a at 20 m (from the position of the 1st temperature/relative humidity sensor) with the observed *air temperature* T_a at 0 m (by the 1st sensor) of the 1st, 3rd and 5th experiments

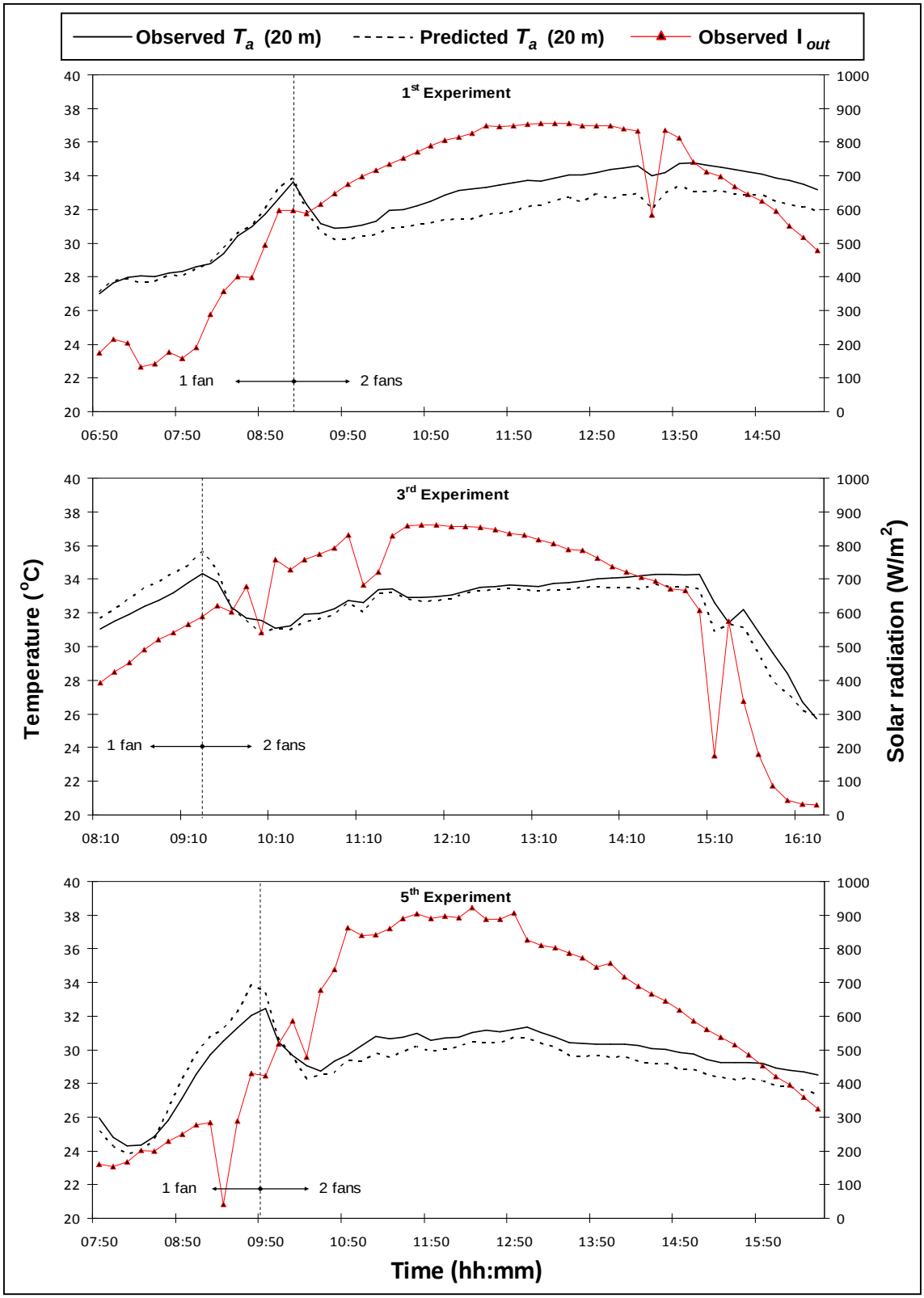

Fig. 4.10: Observed and predicted *air temperature* T_a at 20 m (from the position of the 1st temperature/relative humidity sensor) with the observed *outside solar radiation* I_{out} of the 1st, 3rd and 5th experiments

Table 4.3: Accuracy of microclimate sub-model to predict *air temperature* T_a at 20 m from the position of the 1st temperature/relative humidity sensor at the low air flowrate

Experiment	$\overline{PE}$ [°C]		$\overline{\%PE}$ [%]		RMSE [°C]
	Average	SD	Average	SD	
1st	0.04	0.27	0.11	0.91	0.27
2nd	0.33	0.19	1.03	0.55	0.37
3rd	0.98	0.23	3.00	0.62	1.01
4th	1.03	0.32	3.63	0.85	1.07
5th	0.47	0.83	1.48	2.92	0.93
6th	0.80	0.16	2.52	0.47	0.81
Maximum	1.03	0.83	3.63	2.92	1.07
Minimum	0.04	0.16	0.11	0.47	0.27

Table 4.4: Accuracy of microclimate sub-model to predict *air temperature* T_a at 20 m from the position of the 1st temperature/relative humidity sensor at the high air flwrate

Experiment	$\overline{PE}$ [°C]		$\overline{\%PE}$ [%]		RMSE [°C]
	Average	SD	Average	SD	
1st	-1.33	0.37	-3.95	1.04	1.38
2nd	-0.36	0.45	-1.12	1.45	0.57
3rd	-0.44	0.46	-1.38	1.48	0.63
4th	-0.42	0.30	-1.35	0.99	0.52
5th	-0.75	0.28	-2.50	0.95	0.80
6th	-0.94	0.22	-3.01	0.77	0.96
Maximum	-0.36	0.46	-1.12	1.48	1.38
Minimum	-1.33	0.22	-3.95	0.77	0.52

-5.59 to -2.98 % and the RMSE was between 0.0007 and 0.0010 kg (water)/kg (dry air) (see Table 4.6 for more details). The accuracy of the sub-model to predict the ω at the low air flowrate was slightly better than its accuracy at the high air flowrate. This can be clearly seen from Fig. 4.11

When the predicted T_a and ω were used to estimate the *relative humidity* φ, the accuracy slightly decreased. Figure 4.12 illustrates the predicted and observed φ for the 1st, 3rd and 5th experiments (see Fig. C2.4 in Sec. C.2 of Appendix C for the rest). The predicted φ was overlapping with the observed φ but at some occasions, it was higher than the observed φ. At the low air flowrate, the $\overline{PE}$ was ranging from -4.03 to 2.41 %, the $\overline{\%PE}$ was between

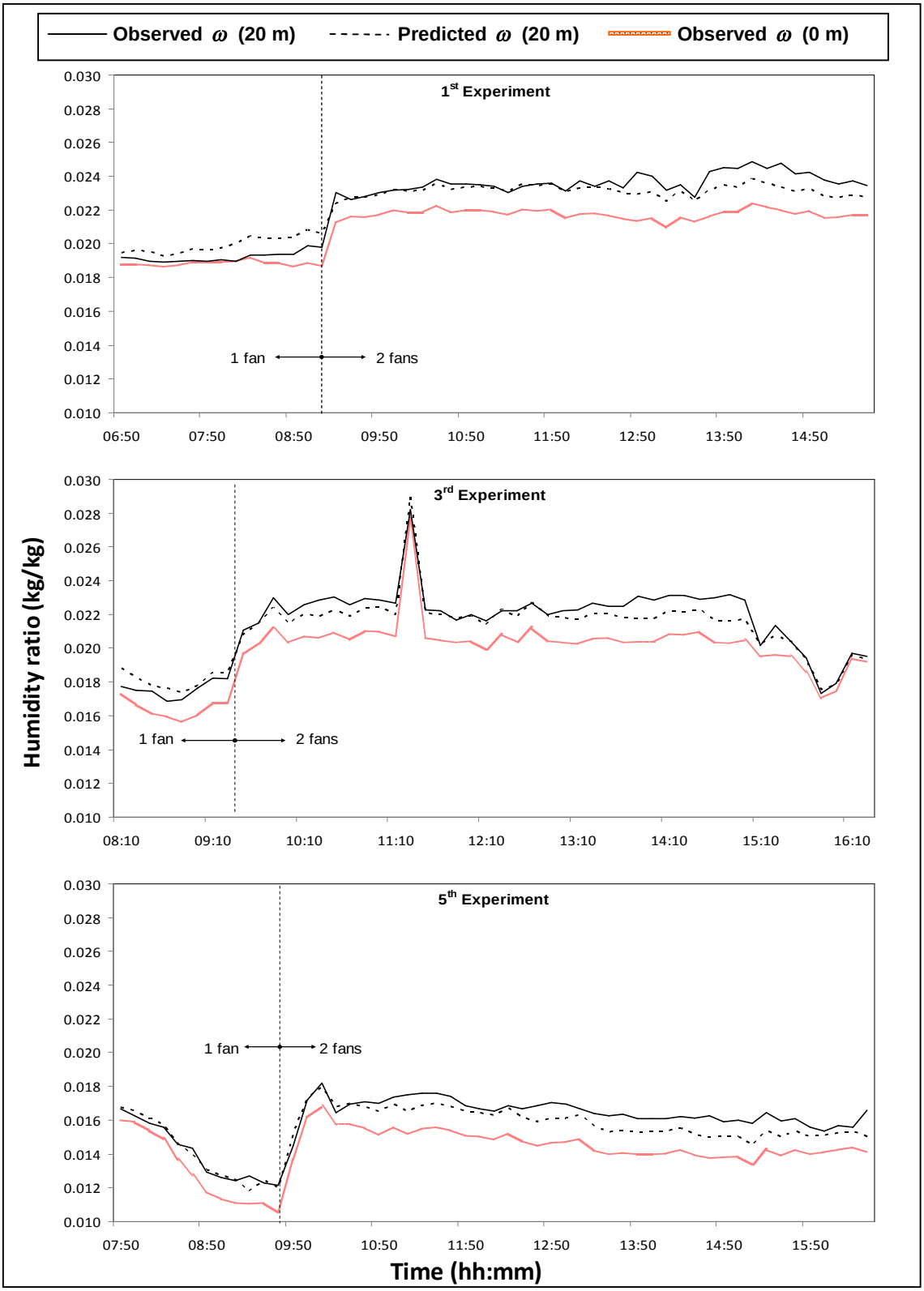

Fig. 4.11: Observed and predicted *humidity ratio* ω at 20 m (from the position of the 1st temperature/relative humidity sensor) with the observed *humidity ratio* ω at 0 m (by the 1st sensor) of the 1st, 3rd and 5th experiments

Table 4.5: Accuracy of microclimate sub-model to predict *humidity ratio* ω at 20 m from the position of the 1st temperature/relative humidity sensor at the low air flowrate

Experiment	$\overline{PE}$ [kg/kg]		$\overline{\%PE}$ [%]		RMSE [kg/kg]
	Average	SD	Average	SD	
1st	0.00074	0.00027	3.84	1.37	0.00078
2nd	0.00028	0.00029	1.53	1.58	0.00039
3rd	0.00052	0.00032	2.99	1.86	0.00061
4th	0.00008	0.00057	0.59	3.20	0.00054
5th	0.00005	0.00040	0.28	2.92	0.00038
6th	0.00044	0.00021	2.89	1.23	0.00048
Maximum	0.00074	0.00057	3.84	3.20	0.00078
Minimum	0.00005	0.00021	0.28	1.23	0.00038

Table 4.6: Accuracy of microclimate sub-model to predict *humidity ratio* ω at 20 m from the position of the 1st temperature/relative humidity sensor at the high air flowrate

Experiment	$\overline{PE}$ [kg/kg]		$\overline{\%PE}$ [%]		RMSE [kg/kg]
	Average	SD	Average	SD	
1st	-0.00048	0.00045	-1.99	1.85	0.00065
2nd	-0.00060	0.00050	-2.76	2.35	0.00078
3rd	-0.00044	0.00048	-1.97	2.07	0.00065
4th	-0.00036	0.00038	-1.71	1.81	0.00051
5th	-0.00062	0.00041	-3.79	2.48	0.00074
6th	-0.00063	0.00037	-3.34	1.99	0.00073
Maximum	-0.00036	0.00050	-1.71	2.48	0.00078
Minimum	-0.00063	0.00037	-3.79	1.81	0.00051

-5.25 and 3.47 % and the RMSE was between 1.00 and 4.27 % (see Table 4.7 for more details). At the high air flowrate, the $\overline{PE}$ was ranging from -0.38 to 3.79 %, the $\overline{\%PE}$ was between -0.63 and 5.68 % and the RMSE was between 1.36 and 4.17 % (see Table 4.8 for more details).

4.4.3. Temperature and humidity profiles

Because the microclimate sub-model can be used to simulate the *air temperature* and *humidity* profiles along the airflow direction inside the greenhouse, the generated profiles for the 1st experiment, as an example, are shown in Figs. 4.13 and 4.14, respectively. These figures present the *air temperature* and *humidity* profiles for a distance of 20 m inside the greenhouse.

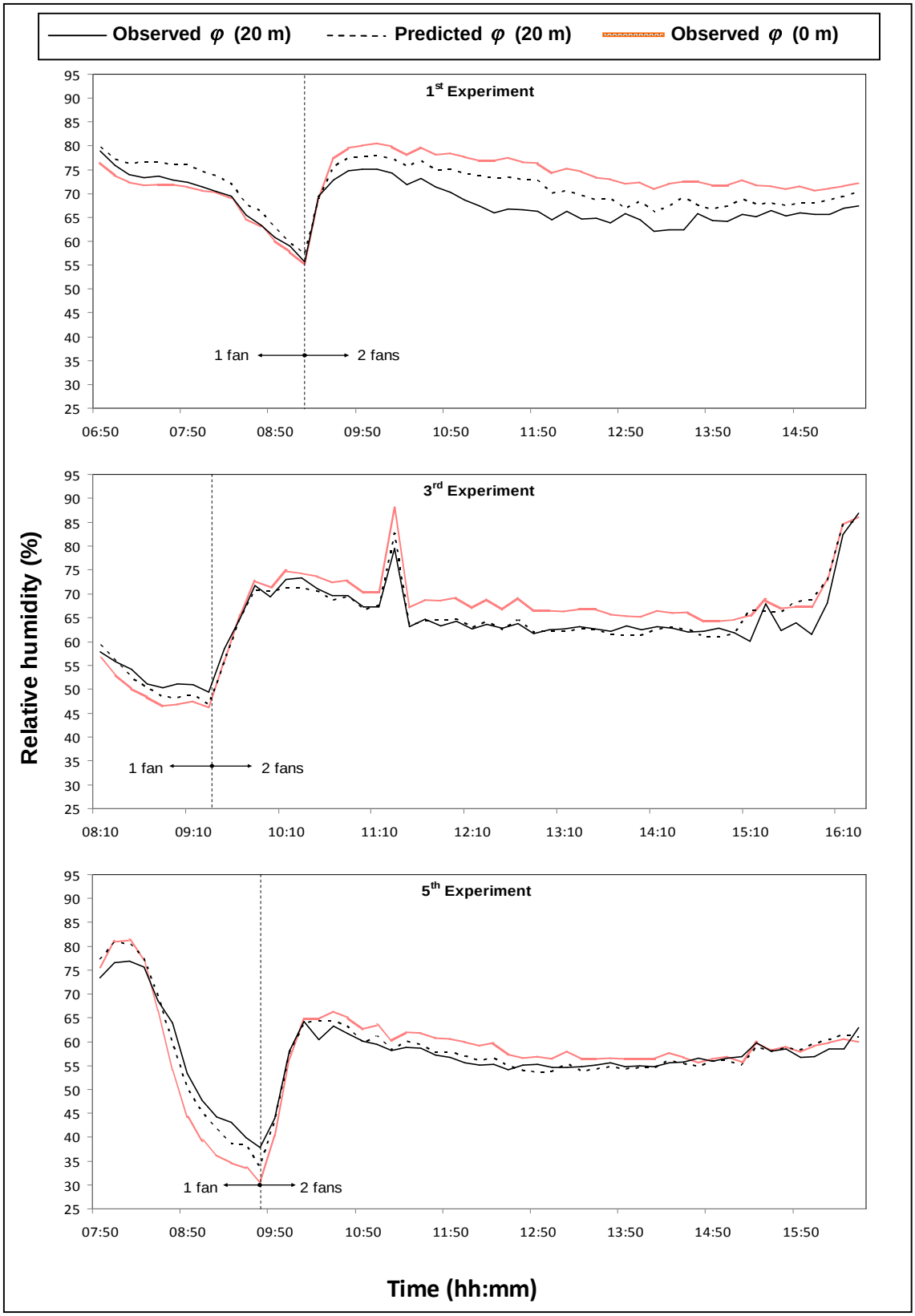

Fig. 4.12: Observed and predicted *relative humidity* φ at 20 m (from the position of the 1st temperature/relative humidity sensor) with the observed *relative humidity* φ at 0 m (by the 1st sensor) of the 1st, 3rd and 5th experiments

Table 4.7: Accuracy of microclimate sub-model to predict *relative humidity* φ at 20 m from the position of the 1st temperature/relative humidity sensor at the low air flowrate

Experiment	$\overline{PE}$ [%]		$\overline{\%PE}$ [%]		RMSE [%]
	Average	SD	Average	SD	
1st	2.41	0.97	3.47	1.32	2.58
2nd	-0.15	1.16	-0.37	2.06	1.13
3rd	-1.30	1.44	-2.59	2.74	1.87
4th	-4.03	1.51	-5.25	1.85	4.27
5th	-0.61	3.25	-2.25	5.81	3.18
6th	-0.80	0.65	-1.71	1.41	1.00
Maximum	2.41	3.25	3.47	5.81	4.27
Minimum	-4.03	0.65	-5.25	1.32	1.00

Table 4.8: Accuracy of microclimate sub-model to predict *relative humidity* φ at 20 m from the position of the 1st temperature/relative humidity sensor at the high air flowrate

Experiment	$\overline{PE}$ [%]		$\overline{\%PE}$ [%]		RMSE [%]
	Average	SD	Average	SD	
1st	3.79	1.77	5.68	2.74	4.17
2nd	-0.38	2.44	-0.63	3.90	2.44
3rd	0.39	2.20	0.62	3.45	2.21
4th	0.41	1.71	0.77	2.82	1.74
5th	0.31	1.34	0.53	2.30	1.36
6th	1.23	1.43	2.07	2.45	1.87
Maximum	3.79	2.44	5.68	3.90	4.17
Minimum	-0.38	1.34	-0.63	2.30	1.36

It can be observed from these figures that the temperature and humidity were changing somewhat linearly. This observation is clearly illustrated in Figs. 4.15 and 4.16 for three times during the high air flowrate. In these figures, the slopes of the linearly increasing lines are slightly different.

4.4.4. Air velocity inside the greenhouse

As expected, the velocity profile of the air was varying along the greenhouse. Table 4.9 presents the results of the *air velocity* measurements. The velocity was highest at 2 m and 2.5 m, above the crop height, but it was also higher at 0.5 m than at 1.0 and 1.5 m. This was because there were fewer leaves at lower heights due to removing of old leaves. From the readings, it appears that the air flow is similar to that shown in Fig. 4.17.

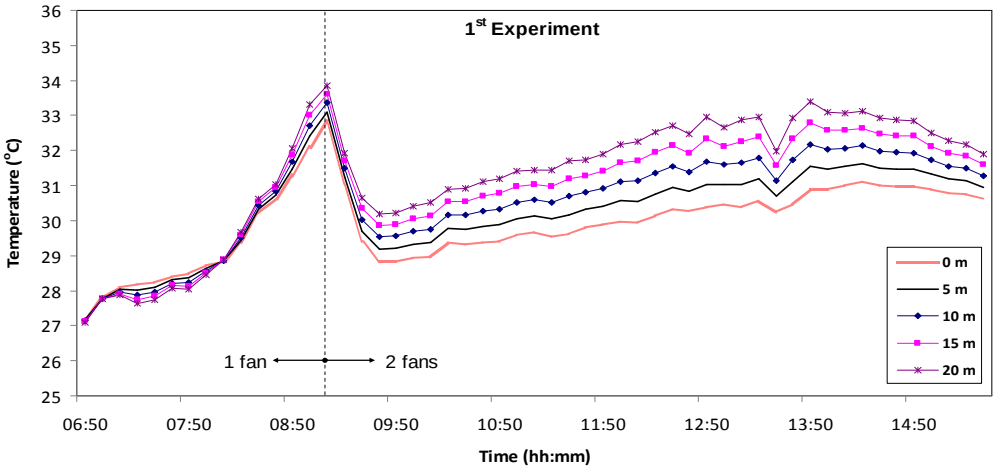

Fig. 4.13: Predicted *air temperature* profile along the airflow direction inside the greenhouse during the 1st experiment

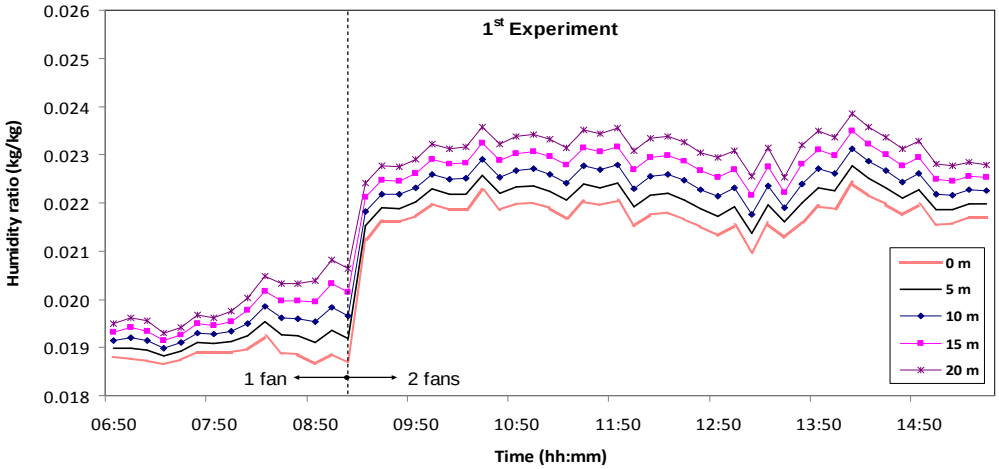

Fig. 4.14: Predicted *air humidity ratio* profile along the airflow direction inside the greenhouse during the 1st experiment

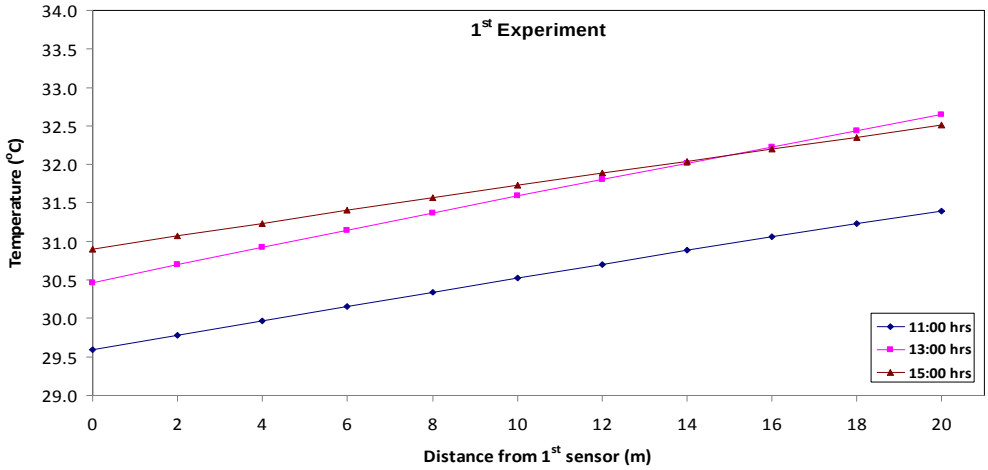

Fig. 4.15: Predicted *air temperature* profile along the airflow direction inside the greenhouse at three instances during the 1st experiment

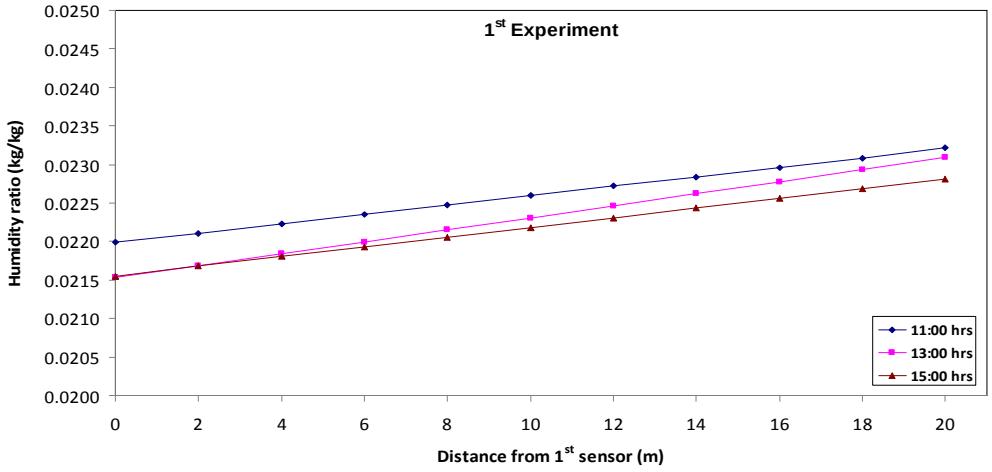

Fig. 4.16: Predicted *air humidity ratio* profile along the airflow direction inside the greenhouse at three instances during the 1st experiment

Table 4.9: Air velocity inside Nizwa greenhouse measured at 3 locations; 10, 20 and 32 m from evaporative cooler at the low and high air flowrates

Height (m)	**Air velocity (m/s) measured with respect to distance from evaporative cooler and number of fans operated**					
	10 m		20 m		32 m	
	1 Fan	2 Fans	1 Fan	2 Fans	1 Fan	2 Fans
2.5	0.55	0.89	0.86	1.10	1.02	1.40
2.0	0.57	0.91	0.72	0.97	0.68	0.91
1.5	<0.30*	0.80	<0.30*	0.60	<0.30*	0.74
1.0	<0.30*	0.49	<0.30*	0.50	<0.30*	0.69
0.5	0.49	0.84	0.31	0.91	<0.30*	0.87

* Below the anemometer's measuring range of 0.30 to 35 m/s

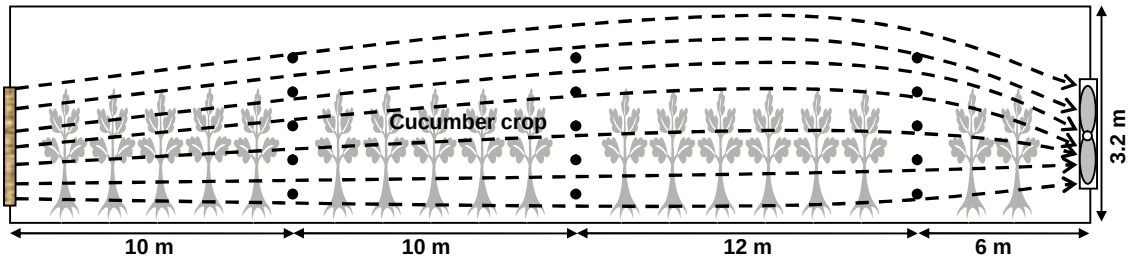

Fig. 4.17: A side-view schematic of Nizwa greenhouse illustrating the expected air flow directions based on the air velocity measurements taken at the 15 locations denoted by •

4.5. DISCUSSION

The microclimate simulation sub-model, in the current format (see Eqs. 4.22 and 4.23), can only be used to simulate ventilated greenhouses. In HD greenhouses, the dehumidification process only takes place when the greenhouse is ventilated.

4.5.1. Temperature predictions

From Fig. 4.9 and Table 4.3, it is very clear that the sub-model was predicting the *air temperature* T_a at the 2nd observation point very accurately during the high air flowrate. The $\overline{\%\mathrm{PE}}$ of the T_a was better than -3.95 %. However, the predicted T_a was slightly less than the observed T_a. During the low air flowrate, the accuracy of the sub-model to predict T_a was also good; the $\overline{\%\mathrm{PE}}$ reached only 3.63 %. The predicted T_a was always more than the observed T_a. Taking the 1st experiment as an example, the largest *predictive error* (PE) and *percentage predictive error* (%PE) were -2.01°C and -5.91 %, respectively. A study of how sensitive the predicted T_a was to some parameters used in the simulation was conducted in order to investigate what probably was the cause for the PE of the T_a. Table 4.10 presents the results of the sensitivity analysis test. An error of $\pm$10 % in any of these parameters could not cause large PE of the T_a.

There was one probable reason for the PE of the T_a that is not simulation-related but measurement related. Figure 4.17 showed that the air layer monitored by the 1st temperature/relative humidity sensor was moving upwards. Bucklin et al. (1993) reported that the air can diverge upward at an angle more than 7° above horizontal. Of course, the movement of air upwards depends on many factors including the density and height of the cultivated crop, configuration of the greenhouse, *solar radiation input* and air flowrate. At low air flowrates, it is expected that the air flow lines to incline upwards sharper than at

Table 4.10: Sensitivity of the predicted *air temperature* T_a to the changes of some parameters used in the simulation

Parameter	±0 %	+10 %		-10 %	
	PE (°C)	PE (°C)	Sensitivity (%)	PE (°C)	Sensitivity (%)
τ_c , 83 [%]	-2.01	-1.87	+6.65	-2.14	-6.62
$\tau_{\lambda,c}$, 69.8 [%]	-2.01	-1.99	+1.02	-2.03	-1.02
U_c , 6.8 [W/m^2 °C]	-2.01	-1.91	+5.07	-2.11	-5.10
ϕ_P , 25 [%]	-2.01	-2.05	-2.21	-1.96	+2.21
f_v , 81 [%]	-2.01	-1.99	+1.02	-2.03	-1.02
$\dot{V}_a$, 18.99 [m^3/s]	-2.01	-2.16	-7.50	-1.83	+9.06

Note: **PE** represents the difference between the predicted and observed T_a under the ±0, +10 and -10 % change in the studied parameters. **Sensitivity** represents the percentage response of the predicted T_a when the studied parameter increases/decreases by 10 %.

high air flowrates due to the tendency of the air to move upwards which, in the case of low air flowrate, is supported by the decrease in the withdrawing force exerted by the fans. Thus, the 2nd temperature/relative humidity sensor placed at the 2nd observation point was observing the temperature of an air mass flowing below the air mass monitored by the 1st sensor. The air flowing at lower heights is normally cooler due to shading by the leaves. This could explain the reason for the positive PE at the low air flowrate during all experiments.

4.5.2. Humidity predictions

The sub-model accurately predicted the *humidity ratio* ω. At the high air flowrate, the predicted ω was slightly lower than the observed ω while at low the air flowrates, the predicted ω was similar to the observed ω with some occasions when it was slightly higher than the observed ω. A sensitivity analysis was conducted for the ω if any of the parameters used in the simulation had an error of ±10 %. The highest PE observed during the 3rd experiment was used to conduct this analysis. During the high air flowrate of this experiment, the highest PE and %PE were -0.00158 kg (water)/kg (dry air) and -6.8 %, respectively. Table 4.11 shows the results of this analysis. From this table, a change of ±10 % of these parameters used in the simulation would have a minute, and sometimes, negligible effect on the predicted ω. Therefore,

Table 4.11: Sensitivity of the predicted *humidity ratio* ω to the changes of some parameters used in the simulation

Parameter	±0 %	+10 %		-10 %	
	PE (kg/kg)	PE (kg/kg)	Sensitivity (%)	PE (kg/kg)	Sensitivity (%)
τ_c , 83 [%]	-0.00158	-0.00151	+4.26	-0.00165	-4.29
$\tau_{\lambda,c}$, 69.8 [%]	-0.00158	-0.00157	+0.52	-0.00159	-0.52
U_c , 6.8 [W/m^2 ^{o}C]	-0.00158	-0.00158	-0.03	-0.00158	+0.03
ϕ_P , 25 [%]	-0.00158	-0.00160	-1.43	-0.00156	+1.42
f_v , 81 [%]	-0.00158	-0.00157	+0.52	-0.00159	-0.52
u_2 , 0.93 [m/s]	-0.00158	-0.00158	-0.33	-0.00157	+0.36
LAI, 1.27	-0.00158	-0.00152	+3.64	-0.00164	-4.11
H_P , 1.94 [m]	-0.00158	-0.00160	-1.45	-0.00156	+1.03
$\dot{V}_a$, 18.99 [m^3/s]	-0.00158	-0.00170	-7.53	-0.00143	+9.19

Note: **PE** represents the difference between the predicted and observed ω under the ±0, +10 and -10 % change in the studied parameters. **Sensitivity** represents the percentage response of the predicted ω when the studied parameter increases/decreases by 10 %.

the negative PE of the ω observed at the high air flowrate was possibly caused by some other reason(s).

Basically, the negative PE of the ω observed at the high air flowrate was caused either by an underestimation of the predicted ω or by an overestimation of the observed ω. The former could have been caused by neglecting the soil water evaporation as explained in assumption (vii). If this amount of moisture was accounted for in the simulation then it would have slightly increased the predicted ω and consequently decreased the PE. At the high air flowrate, the soil water evaporation was expected to be more than at the low air flowrate due to the high I_{out} and *air velocity* at the high air flowrate. On the other hand, the overestimation of the observed ω could have resulted from the non-horizontal air flow directions as illustrated in Fig. 4.17. This flow pattern caused the 2nd temperature/relative humidity sensor (placed at the 2nd observation point) to monitor the moisture level for an air mass different from the air mass monitored by the 1st sensor (placed at the 1st observation point). The influence of the air flow pattern on the predicted ω at the low air flowrate was less pronounced due

to the low soil water evaporation from the soil during this flowrate owing to the low I_{out} and *air velocity*.

From the above discussion, it should be emphasised that a proper validation of the simulation sub-model necessitates having more than one observed value to which the predicted results can be compared. Therefore, it is highly recommended to conduct further investigations using more monitoring points in order to study the accuracy of the microclimate sub-model to predict *air temperature* and *humidity* profiles. Also, due to the type of air flow pattern shown in Fig. 4.17, it should be stressed that placing one sensor at one vertical height might lead to inaccurate measurements representing the temperature/ humidity of that greenhouse section where the sensor is placed. Therefore, more than one sensor should be placed vertically at each observation point and the average of their measurements should then be taken.

4.5.3. Temperature and humidity profiles

It is clearly seen from the results presented in Sec. 4.4.3 that the temperature and moisture of the greenhouse air increased as the air was streaming through the greenhouse. Also, it was found that this increase was linear. However, the slopes of the linear lines representing the increase in the *air temperature* and *humidity* were slightly changing at the three instances shown in Figs. 4.15 and 4.16. This change in the slopes can be attributed to the change in the weather conditions (mainly the *solar radiation*) during these times since all operating and design parameters of the greenhouse as well as the properties of the cucumber crop stayed constant. Having a general linear function representing the temperature and humidity profiles inside the greenhouse is extremely difficult if not impossible owing to the large number of changing variables influencing this function. However, once only one of these variables is changed at a time, a representing linear function can be easily found as was clearly seen from Figs. 4.15 and 4.16.

The advantage of a simulation model capable of predicting the *air temperature* and *humidity* profiles inside the greenhouse is to improve the design and operating conditions of the greenhouse for a better performance. For instance, the microclimate sub-model can be used to determine the proper *ventilation rate* for a given greenhouse design under specific weather conditions only by plotting the temperature profile that would illustrate the temperature increase with distance. A good example of the application of a similar model is given in Kittas et al. (2003). They used their model to study the influence of shading the second half of the greenhouse under different air flowrates once the maximum allowable *air temperature* inside the greenhouse is determined. This allowed them to draw some useful conclusions about the optimal air flowrate with and without shading for their greenhouse.

4.6. SUMMARY

This chapter, dedicated to discuss the development, validation experiments and results of the microclimate simulation sub-model, can be summarized in the following points:

- The accuracy of the sub-model to predict the *air temperature* at the 2nd observation point (20 m away from the 1st observation point where the input data were collected) was very good. Generally, the predicted *air temperatures* were higher than the observed temperatures at the low air flowrate due to the non-horizontal air flow pattern
- The sub-model accurately predicted the *humidity ratio* especially at the low air flowrate. Generally, the predicted *humidity ratio* was lower than the observed value due to the exclusion of the soil water evaporation from the simulation and due to the non-horizontal air flow pattern
- The air was flowing in directions normally upward which had its influence on the measured *air temperature* and *humidity*

- The microclimate sub-model can be used to improve the performance of the greenhouse
- More investigations are highly recommended to further validate the microclimate sub-model. In these investigations, the number of monitoring points should be increased as well as the number of vertical sensors in each monitoring point. The former will extensively clarify the accuracy of the sub-model to predict the *air temperature* and *humidity* profiles and the latter will overcome the vertical *air temperature* and *humidity* gradients by averaging the measurements taken from the vertical sensors in each monitoring point.

CHAPTER FIVE

5. THE DEHUMIDIFIER SUB-MODEL

This chapter focuses on the third sub-model that simulates the changes in temperature and moisture of the air and water as they pass through the dehumidifier of the HD greenhouse. Section 5.1 gives an introduction to the dehumidifier used in the HD greenhouse. Section 5.2 is dedicated to the development of the dehumidifier simulation sub-model. A description of the experiments conducted to test the accuracy of the sub-model is given in Sec. 5.3. Section 5.4 presents the results of the experimental work and Sec. 5.5 provides a critical discussion of these results. Finally, the main conclusions that can be drawn about the dehumidifier sub-model will be found in Sec. 5.6.

5.1. INTRODUCTION

Having a dehumidifier in greenhouses is uncommon (Stanghellini and van Meurs, 1992). However in the HD greenhouses, it is a primary component used to condense the moisture from the greenhouse air, in order to use the water for irrigation. Because these greenhouses typically use saline water as a coolant fluid in the dehumidifier, the tubes of the dehumidifier are made from a salt-resistant material such as *polyvinylchloride* (PVC). This material is not thermally effective due to its relatively low *thermal conductivity*. However, to compensate for the poor *thermal conductivity*, the employed dehumidifier tubes are very thin (i.e. only 240 μm). In the HD greenhouse used in this study, water leaving the 1st humidifier was used as a coolant fluid to lower the temperature of the dehumidifier tubes below the *dew-point temperature* of the air passing through. A detailed description of the dehumidification process and water circulations of the HD greenhouse in Oman can be found in Sec. 2.1.4 (see Sec. A.3 of Appendix A for more details).

A very large dehumidifier (1.8 m high, 15 m wide and 0.8 m thick) is used in the HD greenhouse (see Fig. 5.1). Both fluids (i.e. air and water) flow in a *cross-flow* pattern through the dehumidifier. More precisely, the coolant water flows to the dehumidifier through the last row of tubes, relative to the inflowing air stream. Then, the water flows up and down through the dehumidifier tubes in a direction opposing the flowing air. Eventually, the coolant water leaves the dehumidifier through the 1st row of tubes. Figure 5.2 illustrates the configuration of the dehumidifier and the flow directions of the air and water. The dehumidifier tubes have a *staggered*-type arrangement – see Fig. 5.2 (a) and (c). The dehumidifier comprises 4832 vertical tubes arranged as 302 lines (across) of 16 rows (deep) – see Fig. 5.2 (a). The orientation of the tubes makes the *diagonal pitch* s_D and the *transverse pitch* s_T almost equal – see Fig. 5.2 (c). The dehumidifier is divided into two sides (right and left with respect to the air flow direction) and the condensate from each side is collected using a separate collecting gutter located underneath each side. These two sides are similar in all of their features except that the left side has slightly more tubes which should be accounted for when carrying out any experiment or simulation.

The dimensions and design of this dehumidifier have previously gone through different modifications on a trial-and-error basis which was a time-demanding and costly process. The other alternative to improve the

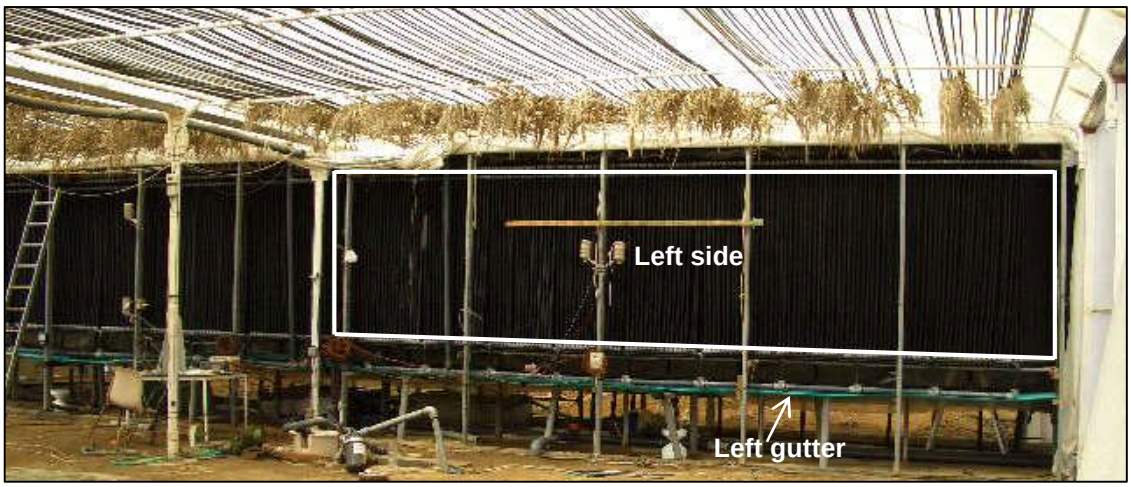

Fig. 5.1: The dehumidifier of the HD greenhouse in Oman (The direction of the air flow is towards the camera)

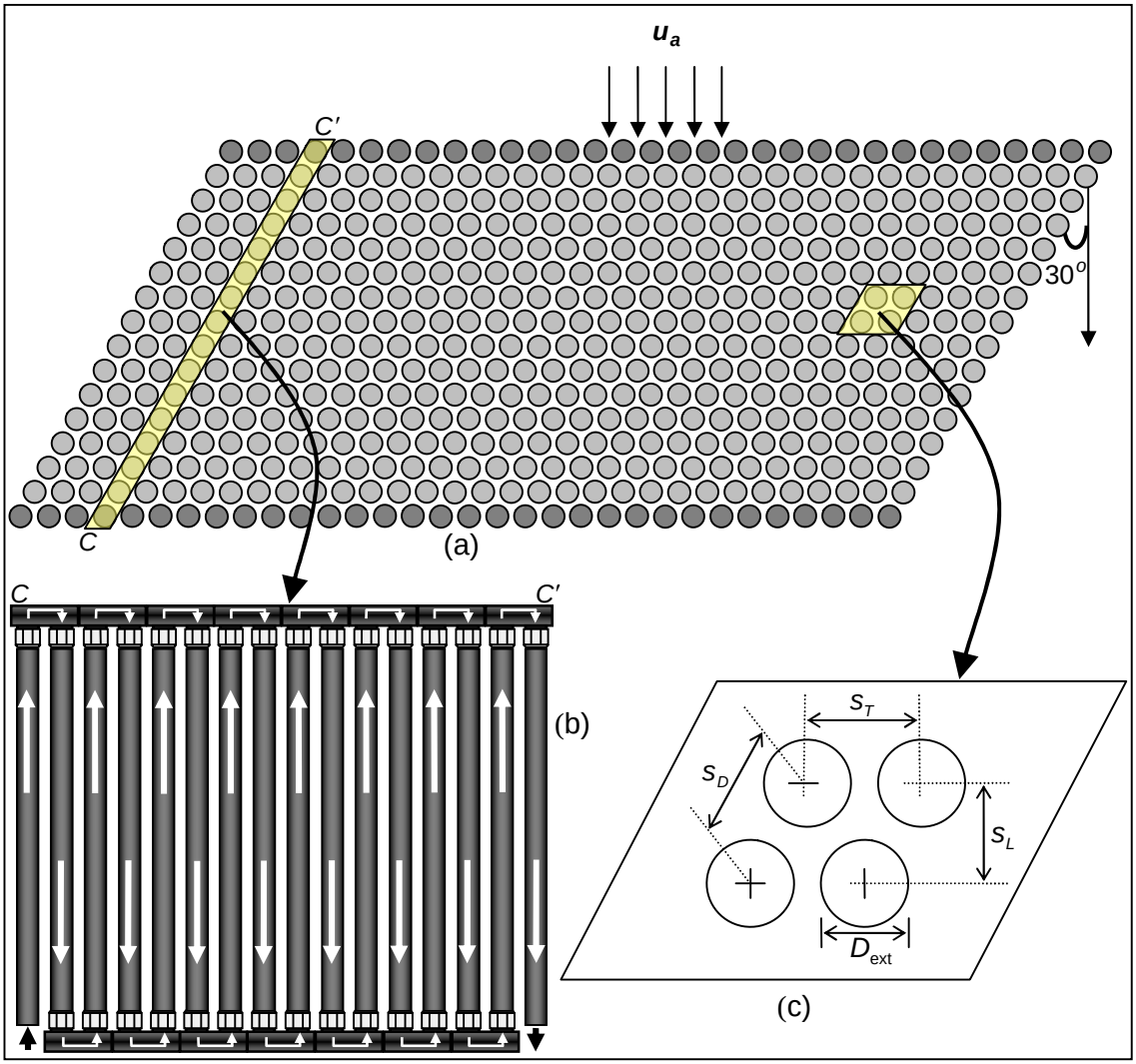

Fig. 5.2: Schematic of (a) a top view of air movement with respect to the *staggered* orientation of the dehumidifier tubes, (b) side view of one line of connected tubes illustrating water movement through the dehumidifier tubes and (c) some terms that are used in the development of the dehumidifier sub-model

performance of the dehumidifier is to use a simulation model that would save both time and money before proceeding with real construction. Such a model, simulating the changes in temperature and moisture content that take place as the air and water pass through the dehumidifier, has been developed in this study.

5.2. MODEL DEVELOPMENT

The developed model aims at predicting the *outlet temperature* and *humidity ratio of the air* passing across the dehumidifier tubes, the *outlet temperature of the water* flowing inside the tubes and the volume of condensate (i.e. *dehumidification rate*) when the known variables are the dehumidifier design parameters and the inlet conditions of the air and water. Because heat transfer mainly occurs between the two fluids involved in the dehumidification process, the dehumidifier is considered as an *adiabatic* system. Therefore, the developed model is based on the *heat balance* of the air and water. The air loses part of its *sensible heat* by *convection* that takes place as a result of the contact with the cold surface of the tubes. This heat, then, transfers by *conduction* through the walls of the dehumidifier tubes, and finally by *convection* between the flowing water and the inner surface of the tubes. During dehumidification periods, there is also a *latent heat* transfer. This heat results from the condensation of some of the moisture carried in the air stream.

The sub-model is composed of three main steps; the calculation of the *convective heat transfer rate* from the air to the external surface of the dehumidifier tubes, the calculation of the *conductive heat transfer rate* through the walls of the tubes and, finally, the calculation of the *convective heat transfer rate* from the internal surface of the tubes to the flowing water.

5.2.1. Assumptions

The working assumptions governing the development of the dehumidifier simulation sub-model are listed below:

i. The air across the dehumidifier is homogeneous in its thermal properties and flows uniformly
ii. The water flow inside the tubes is *hydrodynamically-developed*
iii. Heat transfer in the dehumidifier only occurs between the air and the coolant water (i.e. *adiabatic* process)
iv. The average *internal surface temperature* T_{is} of the tubes is constant

v. In the calculation of the *average external heat transfer coefficient* $\overline{h}_{ext}$, air properties are evaluated as of dry air owing to the small influence of neglecting the *humidity ratio* ω on the evaluation of these properties

5.2.2. Mathematical relations of dehumidifier sub-model

Overall heat transfer rates of air and water:

Figure 5.3 illustrates the dehumidifier inlet and outlet heat terms. The heat comes to the dehumidifier through the inlet air and water and leaves the dehumidifier through the outlet air, water and condensate. The following *heat balance* puts the inlet and outlet heat terms together:

$$\dot{m}_a\, h_{ai} + \dot{m}_w\, h_{wi} = \dot{m}_a\, h_{ao} + \dot{m}_w\, h_{wo} + \dot{m}_a \left(\omega_{ai} - \omega_{ao}\right) C_{P,\,w}\, T_{ao} \qquad (5.1)$$

Rearranging this *heat balance*, yields:

$$\dot{m}_w \left(h_{wo} - h_{wi}\right) = \dot{m}_a \left[\left(h_{ai} - h_{ao}\right) - \left(\omega_{ai} - \omega_{ao}\right) C_{P,\,w}\, T_{ao}\right] \qquad (5.2)$$

where the left hand side of this equation represents the overall *heat transfer rate of the coolant water* Q_w and the right hand side represents the overall *heat*

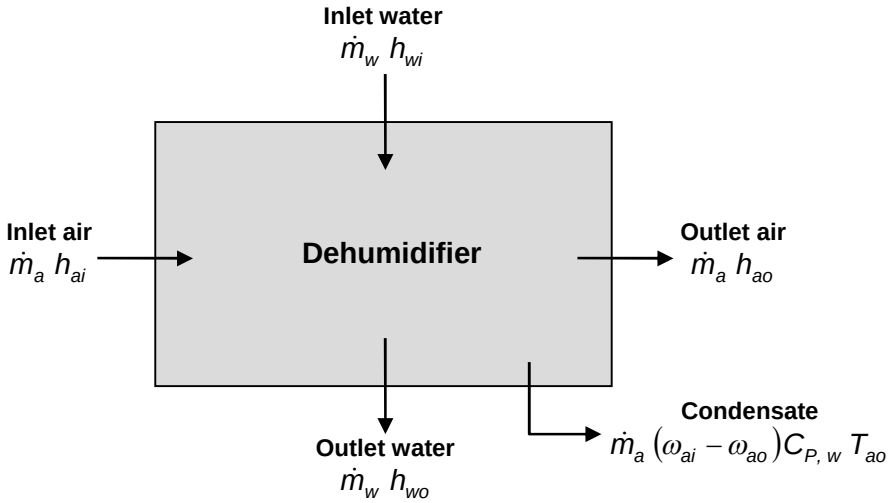

Fig. 5.3: A schematic diagram illustrating the dehumidifier inlet and outlet heat directions

transfer rate of the air Q_a including any condensed water. Thus,

$$Q_w = Q_a \tag{5.3}$$

After substituting the primary variables of the *specific enthalpy of the inlet* and *outlet air* (h_{ai} and h_{ao}, respectively) and the *specific enthalpy of the inlet* and *outlet water* (h_{wi} and h_{wo}, respectively), the Q_a and Q_w can be calculated as follows:

$$Q_a = \dot{m}_a \left[C_{p,da} \left(T_{ai} - T_{ao} \right) + \omega_{ai} \left(L_{v,0} + C_{p,wv}\, T_{ai} \right) - \omega_{ao} \left(L_{v,0} + C_{p,wv}\, T_{ao} \right) - \left(\omega_{ai} - \omega_{ao} \right) C_{P,w}\, T_{ao} \right] \tag{5.4}$$

$$Q_w = \dot{m}_w\, C_{p,\mathrm{w}} \left(T_{wo} - T_{wi} \right) \tag{5.5}$$

The relations used to evaluate the *specific heat capacity of the dry air* $C_{p,da}$, *water vapour* $C_{p,wv}$ and *water* $C_{p,\mathrm{w}}$ are given in Sec. C.1 of Appendix C. The *latent heat of vaporization* $L_{v,0}$ is calculated using the relation developed by Henderson-Sellers (1984) (see Eq. 4.16).

External convective heat transfer rate:

The *convective heat transfer rate* Q_{cv} that occurs between the air and the external surface of the tubes and between the water and the internal surface of the tubes will be calculated using the *Newton's law of cooling*;

$$Q_{cv} = \overline{\mathrm{h}}\, A\, \Delta T \tag{5.6}$$

For the calculation of the *external convective heat transfer rate* (i.e. between the air and the external surface of the tubes), Eq. (5.6) becomes

$$Q_{cv,\mathrm{ext}} = \overline{\mathrm{h}}_{\mathrm{ext}}\, A_{es}\, \Delta T_a \tag{5.7}$$

The *average external heat transfer coefficient* $\overline{\mathrm{h}}_{\mathrm{ext}}$ is evaluated using

$$\overline{h}_{ext} = \overline{Nu}_{ext} \frac{k_a}{D_{ext}} \tag{5.8}$$

where k_a is the *thermal conductivity of the air* and D_{ext} is the *external diameter* of the tubes. The *temperature difference* ΔT_a in Eq. (5.7) is calculated using the *logarithmic-mean temperature difference*;

$$\Delta T_a = \frac{(T_{ai} - T_{es}) - (T_{ao} - T_{es})}{\ln\left(\frac{T_{ai} - T_{es}}{T_{ao} - T_{es}}\right)}$$

but, using its simplified approximation

$$\Delta T_a = \frac{T_{ai} + T_{ao}}{2} - T_{es} \tag{5.9}$$

The *average external Nusselt number* $\overline{Nu}_{ext}$ of Eq. (5.8) is estimated using the relation originally developed by Grimison (1937) for heat exchangers having more than 10 rows when a single fluid is involved. Grimison's relation has the following format:

$$\overline{Nu}_{ext} = q_1 \, Re_{a,max}^{q_2} \, Pr_a^{1/3} \tag{5.10}$$

where the constant q_1 and the exponent q_2 vary with the type of tube arrangement and the spacing between the tubes. Grimison (1937) added a correction factor known as the "*arrangement factor*" f_a to Eq. (5.10) and, therefore, it can be expressed as

$$\overline{Nu}_{ext} = q_1 \, f_a \, Re_{a,max}^{q_2} \, Pr_a^{1/3} \tag{5.11}$$

For a *staggered* arrangement, similar to the arrangement of the dehumidifier used in this study, Hausen (1983) provided the values of the constant q_1 and the exponent q_2 of Eq. (5.11) as well as a slight modification to the exponent of the *Prandlt number* Pr_a

$$\overline{\mathrm{Nu}}_{\mathrm{ext}} = 0.35 f_a \, \mathrm{Re}_{a,\max}^{0.57} \, \mathrm{Pr}_a^{0.31} \tag{5.12}$$

The *Reynolds number* $\mathrm{Re}_{a,\max}$ is calculated using

$$\mathrm{Re}_{a,\max} = \frac{\rho_a \, \mathrm{u}_{a,\max} \, D_{\mathrm{ext}}}{\mu_a} \tag{5.13}$$

where $\mathrm{u}_{\max}$ is the *maximum air velocity* through the dehumidifier tubes. In the case of the dehumidifier used in this study, $\mathrm{u}_{a,\max}$ is calculated from

$$\mathrm{u}_{a,\max} = \frac{s_{\mathrm{T}}}{2\left(s_D - D_{\mathrm{ext}}\right)} \mathrm{u}_{ai} \tag{5.14}$$

Hausen (1983), also, provided the following relation to obtain the *arrangement factor* f_a of Eq. (5.12)

$$f_a = 1 + 0.1 \frac{s_{\mathrm{T}}}{D_{\mathrm{ext}}} + 0.34 \frac{D_{\mathrm{ext}}}{s_L} \tag{5.15}$$

All air properties of Eqs. (5.7) to (5.13) must be evaluated at the *average film temperature* T_{film} (Eq. 5.16) except the *air density* ρ_a that is evaluated at the *mean bulk temperature* T_a (Eq. 5.17).

$$T_{film} = \frac{T_a + T_{es}}{2} \tag{5.16}$$

$$T_a = \frac{T_{ai} + T_{ao}}{2} \tag{5.17}$$

The relations used to evaluate air properties are given in Sec. C.1 of Appendix C. It should be noted that these properties are evaluated assuming a dry-air condition (see Assumption v) owing to the small influence of the *air humidity* on the evaluated air properties. The *external convective heat transfer rate* $Q_{cv,\mathrm{ext}}$ (Eq. 5.7) is equal to the overall *heat transfer rate of the air* Q_a (Eq. 5.4). Therefore,

$$Q_{cv,\text{ext}} = Q_a \tag{5.18}$$

Internal convective heat transfer rate:

For the calculation of the *internal convective heat transfer rate* (i.e. between the coolant water and the internal surface of the tubes), Eq. (5.6) becomes

$$Q_{cv,\text{int}} = \overline{h}_{\text{int}}\, A_{is}\, \Delta T_w \tag{5.19}$$

The *internal convective heat transfer rate* $Q_{cv,\text{int}}$ must be equal to the overall *heat transfer rate of the air* Q_a (Eq. 5.4) in order for the *heat balance* between the air and the coolant water to stay valid (Eq. 5.3). Thus,

$$Q_{cv,\text{int}} = Q_a \tag{5.20}$$

The *average internal heat transfer coefficient* $\overline{h}_{\text{int}}$ in Eq. (5.19) is evaluated using

$$\overline{h}_{\text{int}} = \overline{Nu}_{\text{int}} \frac{k_w}{D_{\text{int}}} \tag{5.21}$$

where k_w is the *thermal conductivity of the water* and D_{int} is the *internal diameter* of the tubes. The *temperature difference* ΔT_w is calculated using

$$\Delta T_w = T_{is} - \frac{T_{wi} + T_{wo}}{2} \tag{5.22}$$

Because the *Reynolds number* Re_w of the water flow inside the dehumidifier tubes, was found to be less than 50, the *average internal Nusselt number* $\overline{Nu}_{\text{int}}$ of Eq. (5.21) is estimated using the following relation originally developed by Hausen (1943) for a constant *wall temperature* T_{is} and a *fully-developed laminar flow condition:*

$$\overline{\mathrm{Nu}}_{\mathrm{int}} = 3.66 + \left(\frac{0.0668 \, \frac{D_{\mathrm{int}}}{\mathrm{L}} \mathrm{Re}_w \, \mathrm{Pr}_w}{1 + 0.045 \left(\frac{D_{\mathrm{int}}}{\mathrm{L}} \mathrm{Re}_w \, \mathrm{Pr}_w \right)^{2/3}} \right) \left(\frac{\mu_w}{\mu_{is}} \right)^{0.14} \tag{5.23}$$

but if

$$\frac{\mu_w}{\mu_{is}} = 1$$

is assumed, which is an assumption normally practiced (Hausen, 1983), then Eq. (5.23) can be written as

$$\overline{\mathrm{Nu}}_{\mathrm{int}} = 3.66 + \left(\frac{0.0668 \, \frac{D_{\mathrm{int}}}{\mathrm{L}} \mathrm{Re}_w \, \mathrm{Pr}_w}{1 + 0.045 \left(\frac{D_{\mathrm{int}}}{\mathrm{L}} \mathrm{Re}_w \, \mathrm{Pr}_w \right)^{2/3}} \right) \tag{5.24}$$

The *Reynolds number* Re_w is calculated using

$$\mathrm{Re}_w = \frac{\rho_w \, \mathrm{u}_w \, D_{\mathrm{int}}}{\mu_w} \tag{5.25}$$

where all water properties are to be evaluated at the *mean bulk temperature* T_w (Eq. 5.26).

$$T_w = \frac{T_{wi} + T_{wo}}{2} \tag{5.26}$$

The relations used to evaluate water properties are given in Sec. C.1 of Appendix C.

Conductive heat transfer through dehumidifier tubes:

For the calculation of the *conductive heat transfer rate* through the tube walls, *Fourier's law of heat conduction* will be used. It can be expressed as

$$Q_{cd} = \frac{2\,\pi\,\mathrm{k}_{tube}\,\mathrm{L}_{tube}\,(T_{es} - T_{is})}{\ln\left(\frac{D_{\mathrm{ext}}}{D_{\mathrm{int}}}\right)} \tag{5.27}$$

The *conductive heat transfer rate* Q_{cd} is equal to the overall *heat transfer rate of the air* Q_a. Thus,

$$Q_{cd} = Q_a \tag{5.28}$$

5.2.3. The procedure for calculating outlet air and water temperatures

In this simulation, the known input parameters are the *air inlet temperature* T_{ai}, *inlet humidity ratio* ω_{ai} and *mass flowrate* $\dot{m}_a$, and the *water inlet temperature* T_{wi} and *mass flowrate* $\dot{m}_w$. The *outlet humidity ratio* ω_{ao} involved in the simulation (Eq. 5.4) is obtained using an empirically developed relation as will be explained in Sec. 5.2.4. Figure 5.4 provides a flow diagram demonstrating the iterative procedure followed to carry out the simulation.

5.2.4. The procedure for calculating outlet humidity ratio

When there is no dehumidification taking place, the *outlet humidity ratio* ω_{ao} is equal to the *inlet humidity ratio* ω_{ai} (i.e. no moisture reduction; $\omega_{ao} = \omega_{ai}$). However, when there is dehumidification, the ω_{ao} will be slightly lower than the ω_{ai}. In this case, the ω_{ao} can be estimated by using a semi-empirical procedure. This procedure depends on finding a *performance factor* F_p for the dehumidifier and then utilizing it to calculate the ω_{ao}. This procedure starts by calculating the F_p from the following relation:

$$F_p = 100\,\frac{\omega_{ai} - \omega_{ao}}{\omega_{ai} - \omega''_{wi}} \tag{5.29}$$

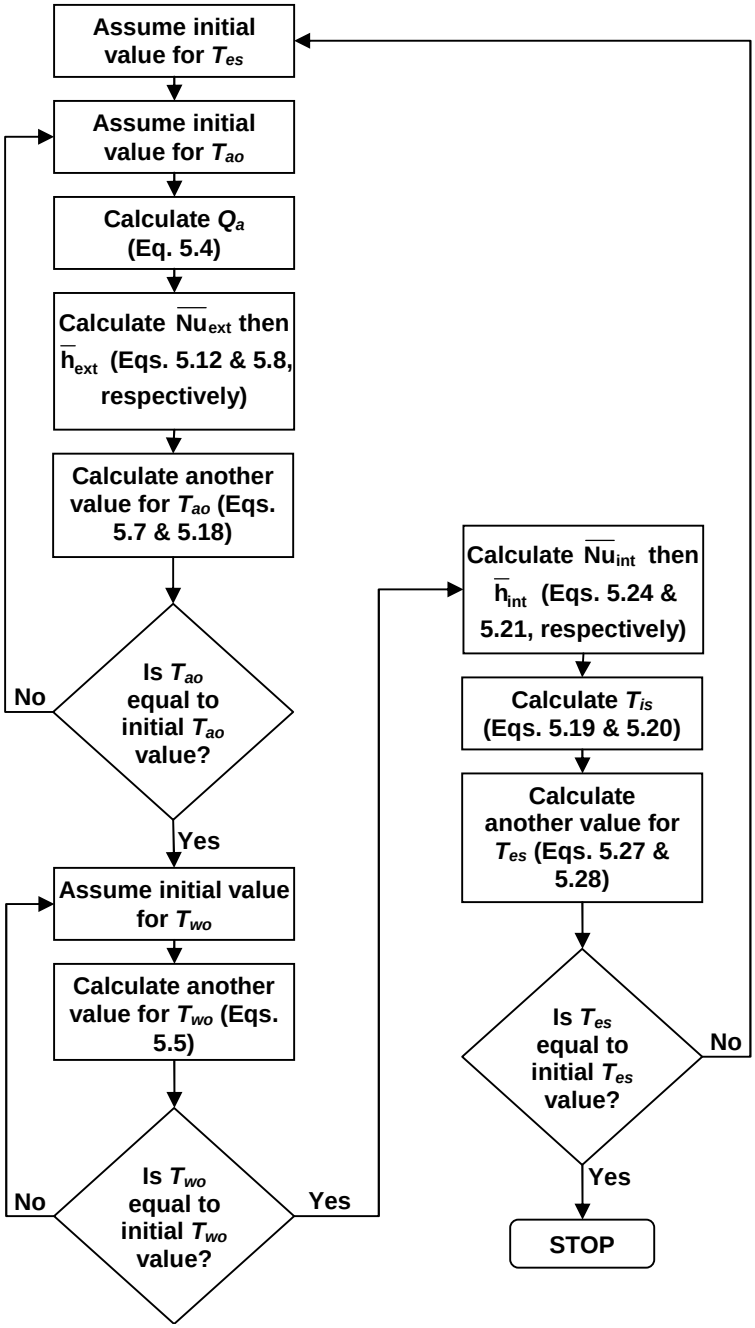

Fig. 5.4: Flow diagram illustrating the iterative procedure followed to predict the *outlet air* and *water temperatures* (T_{ao} and T_{wo}, respectively)

From this equation, the dehumidifier achieves its best performance if it is capable to saturate the air (φ_{ao} =100 %) and reduce the T_{ao} to the T_{wi}. The T_{wi} is used because the coolant water enters the dehumidifier through the last row of tubes at T_{wi} and the flowing air leaves the dehumidifier after coming in contact with this row of tubes (see Fig. 5.2). Therefore, the F_p equals 100 %

when $\omega_{ao} = \omega''_{wi}$. This relation (Eq. 5.29) is only valid when there is dehumidification taking place. The difference between the *inlet air dew-point temperature* $T_{dp,\,ai}$ and the average *external surface temperature* T_{es} of the dehumidifier tubes will be used to predict the dehumidification periods. The dehumidification is thermodynamically possible when the T_{es} is lower than the $T_{dp,\,ai}$ (i.e. $\left(T_{dp,\,ai} - T_{es}\right) > 0$). The $T_{dp,\,ai}$ can be calculated using the following relation (ASHRAE, 2001):

$$T_{dp,ai} = 6.54 + 14.526 \ln\psi_{ai} + 0.7389 \left(\ln\psi_{ai}\right)^2 + 0.09486 \left(\ln\psi_{ai}\right)^3 + 0.4569 \psi_{ai}^{0.1984} \quad (5.30)$$

where the *partial vapour pressure* ψ_{ai} of the coming air can be calculated from Eq. (3.14) of Sec. 3.2.3.

Only half of the data generated from the conducted experiments will be used to calculate the F_p from Eq. (5.29). The same half of the dataset will, then, be used to develop a correlation for the calculated F_p as a function of the influencing input variables such as the T_{ai}, φ_{ai}, $\dot{m}_a$, T_{wi}, $\dot{m}_w$ and *solar heat flux on the dehumidifier* I_{deh}. The I_{deh} is expected to directly influence the *external surface temperature of the tubes* and indirectly influence the *air temperature* (through convection) and *water temperature* (through conduction then convection). The data analysis system known as STATISTICA (StatSoft, Inc., version 8.0) will be used to study the significance of each variable on the F_p. Then, a linear multiple regression will be conducted to the key input variables. Assuming all input variables, mentioned above, are significant, the F_p empirical correlation will appear in the following format:

$$F_p = q_0 + q_1 T_{ai} + q_2 \varphi_{ai} + q_3 \dot{m}_a + q_4 T_{wi} + q_5 \dot{m}_w + q_6 \mathrm{I}_{deh} \quad (5.31)$$

where the constants q_0 to q_6 are to be provided by STATISTICA.

With the 2nd half of the dataset, Eq. (5.31) is used to predict the F_p values that will be used to calculate the ω_{ao} from Eq. (5.29). The ω_{ao} results obtained from this approach will be compared to the observed ω_{ao}.

The *dehumidification rate* Ω will be predicted using two methods to try different ways of predicting its magnitude. The 1st method is semi-empirical and the 2nd method is fully-empirical. The 1st method involves the predicted ω_{ao} to calculate the Ω using the following relation:

$$\Omega = 6.0 \times 10^7 \frac{(\omega_{ai} - \omega_{ao})\dot{m}_a}{\rho_w} \tag{5.32}$$

where the constant 6.0x10^7 is used to give Ω units of ml/min.

The 2nd method used to predict the Ω is performed by developing an empirical correlation for the Ω as a function of the significant input variables. The measured Ω in the 1st half of the dataset is used to develop this correlation using STATISTICA. The developed correlation will have a similar format to Eq. (5.31). This correlation will then be used to predict the Ω with the 2nd half of the dataset. A comparison will then be carried out between the measured Ω and the predicted Ω using the two methods.

5.3. VALIDATION EXPERIMENTS

The dehumidifier located in the HD greenhouse in Oman was used to carry out a number of experiments to test the accuracy of the developed dehumidifier sub-model. A brief description of the HD greenhouse and its dehumidifier component is already given in Sec. 2.1.4 and Sec. 5.1. More details about this greenhouse can also be found in Sec. A.3 of Appendix A.

5.3.1. Experimental setup

Only the left side of the dehumidifier (see Fig. 5.1) was used in the experiments due to the unavailability of accurate humidity sensors required to monitor the humidity variations on both sides of the dehumidifier. Fortunately, each side of the dehumidifier can work independently and thus the left side was considered as a *stand-alone* dehumidifier component.

Eight experiments were conducted in which two operating variables were studied. These variables were the inlet *moisture content* and *mass flowrate of the air* $\dot{m}_a$. Two *moisture content* levels were obtained through turning on/off the 2nd humidifier located at about 1.5 m before the dehumidifier. The $\dot{m}_a$ was altered using a fan-frequency regulator that was controlling the rotation speed of the two fans used to ventilate the HD greenhouse. Two fan-frequencies, 25 and 45 Hz, were used which resulted into two $\dot{m}_a$; "low flowrate" and "high flowrate", respectively. Four treatments thus resulted from turning the humidifier on/off and using the two fan frequencies. The 1st and 2nd treatments, when the humidifier was on, were repeated twice (the 5th and 6th experiments and the 7th and 8th experiments, respectively), to generate more data for the F_p and Ω empirical correlations. Table 5.1 gives the setting of each experiment.

Originally, it was hoped to run each experiment continuously for 48 hrs but due to some limiting constraints, it was decided to run each experiment for at least 24 continuous hours. A problem experienced during the experiments was

Table 5.1: The setting of the dehumidifier experiments

Experiment	Humidifier	Air flowrate	Duration [hrs]
1st	On	High	62.2
2nd	On	Low	96.3
3rd	Off	Low	50.5
4th	Off	High	24.3
5th	On	High	4.2
6th	On	High	4.2
7th	On	Low	22.2
8th	On	Low	21.2

the frequent leakage of the coolant fluid due to the occasional collapse of some tubes of the dehumidifier. This was attributed to a weak mounting of these tubes onto the upper and/or lower connecting pipes – see Fig. 5.2 (b). It was only possible to run the first four experiments for more than 24 hours. The duration of the experiments is also given in Table 5.1.

The time required to prepare the greenhouse for the experiments was circa two months. The overall duration of all experiments was 29 days including the lay out and removal of the necessary instrumentation.

5.3.2. Instrumentation of HD greenhouse

A Delta-T dual temperature/relative humidity sensor located just before the left dehumidifier was used to measure the *inlet air temperature* and *humidity*. A similar sensor was placed on the opposite side just after the dehumidifier to measure the *outlet air temperature* and *humidity* – see Fig. 5.5 (a). *Inlet* and *outlet coolant water temperatures* (T_{wi} and T_{wo}, respectively) were monitored using two Delta-T sealed temperature probes. A Delta-T tipping bucket gauge was used to measure the *dehumidification rate* Ω – see Fig. 5.5 (b). The *solar radiation heat flux* I_{deh}, which was impinging on the outlet side of the dehumidifier, was monitored using a Delta-T photodiode – see Fig 5.5 (c). The inlet side of the dehumidifier was in the shade. Data from all sensors were retrieved and recorded at ten minute intervals using a Delta-T datalogger – see Fig. 5.5 (d).

Two different anemometers were used to measure *air velocity* through the left dehumidifier but they failed to detect any measurement since the HD greenhouse in Oman is operated with two small fans making *air velocities* below the measuring ranges of the anemometers. Therefore, a basic technique of measuring the “distance travelled per unit time” was used to find the *air velocity* through the left dehumidifier. This was done by measuring the time a smoke trace needed to pass through a circular duct of a known length – see Fig. 5.6 (a). This was carried out for the two fan frequencies (i.e. 25 and 45 Hz). For

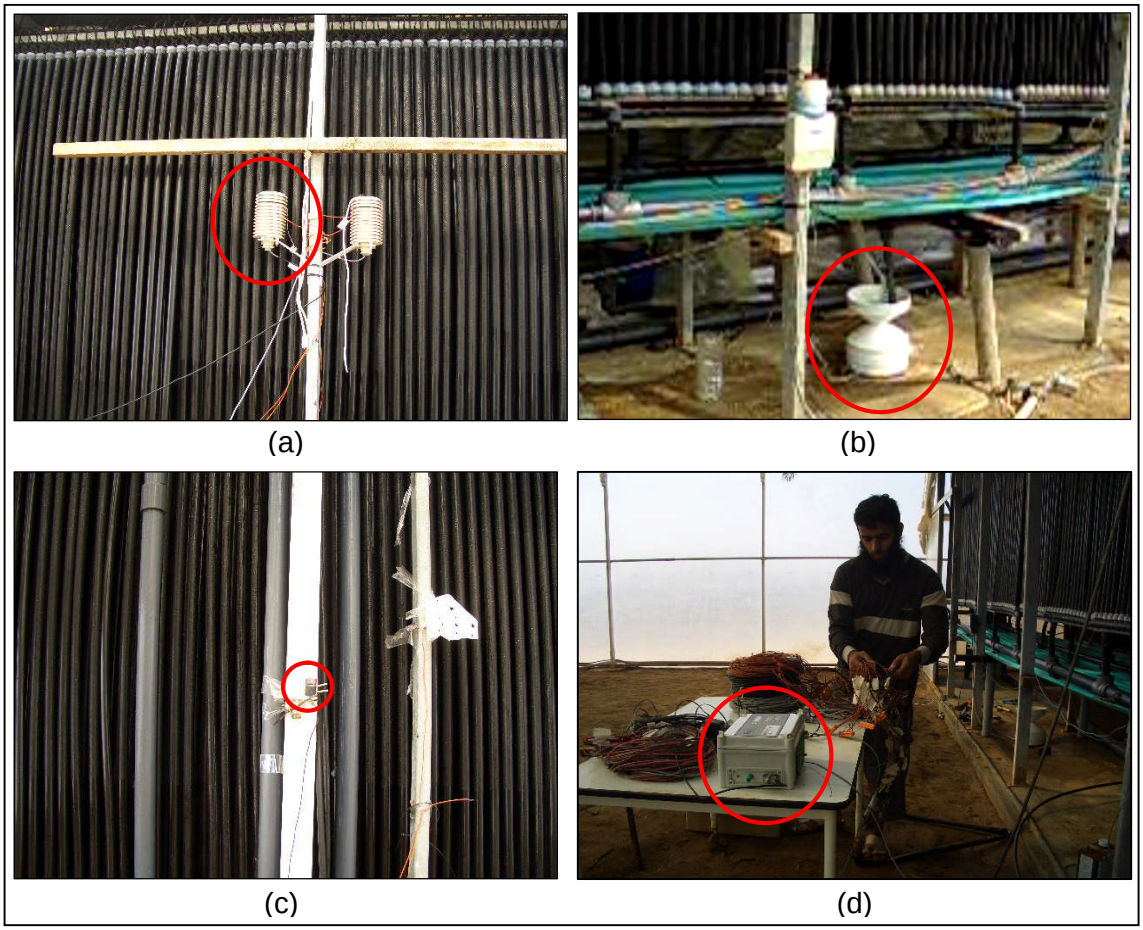

Fig. 5.5: (a) A shielded dual temperature/relative humidity sensor used to measure the T_{ao} and φ_{ao}, (b) a tipping bucket gauge used to measure the amount of condensate, (c) a photodiode placed at the outlet of the dehumidifier and (d) the datalogger used to retrieve and record data from all sensors

each frequency, the measurements were repeated several times at different locations before the dehumidifier and, then, the average value was calculated. The water flowrate through the left dehumidifier was measured from the time needed to fill a container of known volume – see Fig. 5.6 (b).

Air stream directions from the 2nd humidifier towards the dehumidifier were monitored using a smoke trace. The smoke source was placed at five vertical positions on the surface of the 2nd humidifier (see Figs. 5.7 and 5.8). This test was carried out during the 6th experiment when the 2nd humidifier was on and the fan frequency was 45 Hz (u_a=0.27 m/s). From Fig. 5.7, there are a permeable wall and an empty space over and below the dehumidifier, respectively. This was due to an arrangement existed in the HD greenhouse

before the experiments and therefore, it was decided to keep it unaltered. The air leakage through these spaces is not going to influence the validation experiments since the objective of these experiments is to simulate only the air passing through the dehumidifier. A detailed description of all sensors used in these experiments can be found in Appendix B.

(a) (b)

Fig. 5.6: (a) Air velocity measurment using a smoke trace and a circular duct and (b) measuring water flowrate through the left dehumidifier using a big container

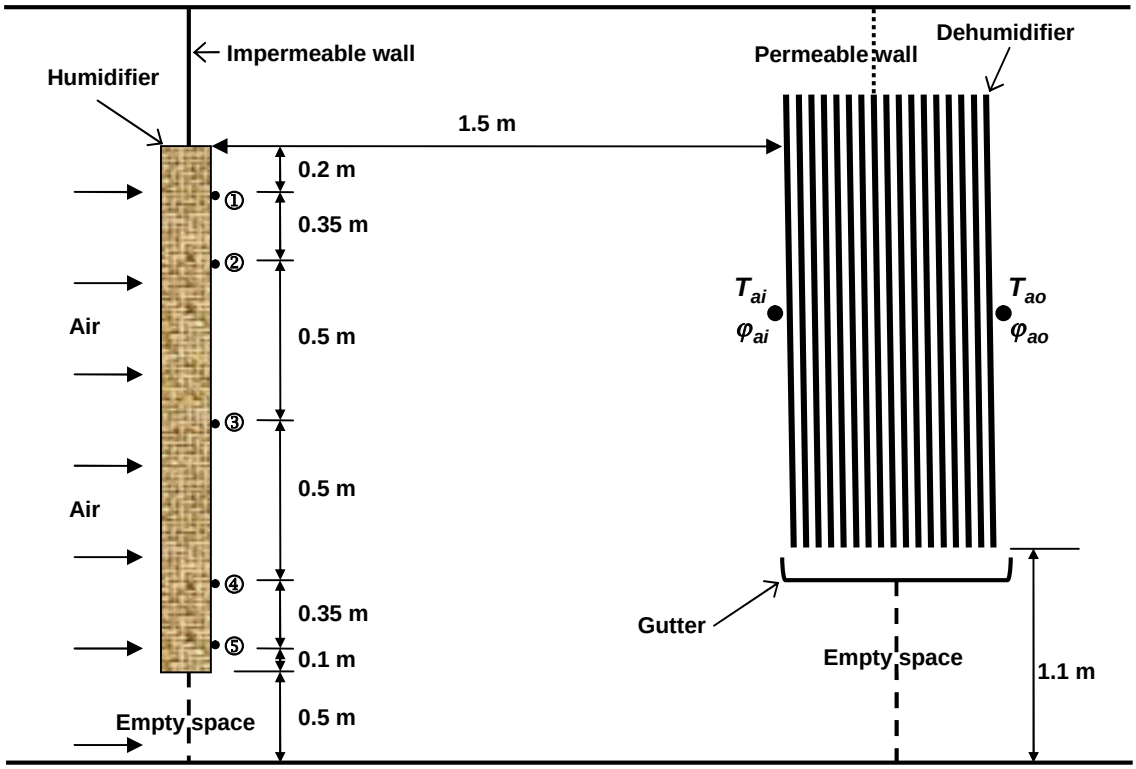

Fig. 5.7: Schematic of the 2nd humidifier and dehumidifier of HD greenhouse (Numbers ① to ⑤: represent the locations where the smoke source was placed)

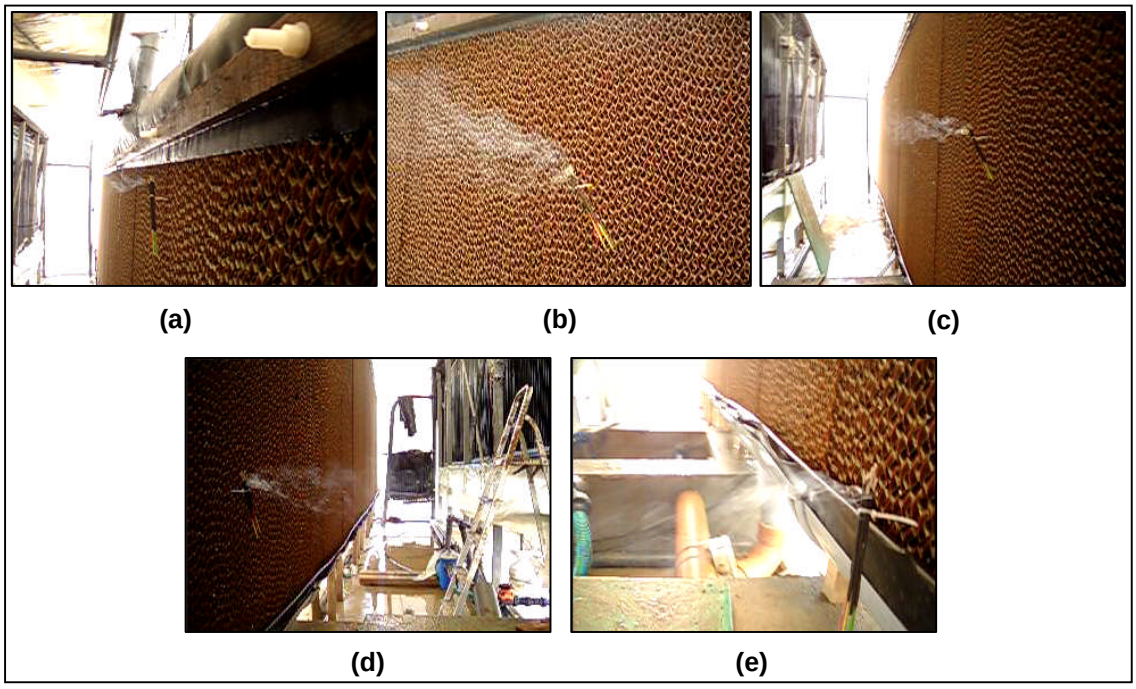

Fig. 5.8: The smoke source placed at positions number (a) ①, (b) ②, (c) ③, (d) ④ and (e) ⑤ of Fig. 5.7

5.3.3. Developing empirical correlations for performance factor and dehumidification rate

The 1st half of data collected from the 1st, 2nd, 3rd and 4th experiments as well as the whole data collected from the 5th and 7th experiments was used to calculate the F_P and develop its empirical correlation as explained in Sec. 5.2.4. The same dataset was also used to develop the Ω correlation. STATISTICA software was used to develop the correlations of the F_P and Ω as a function of the T_{ai}, φ_{ai}, $\dot{m}_a$, T_{wi}, $\dot{m}_w$ and I_{deh}. Then, the accuracy of the developed F_P and Ω correlations to predict the ω_{ao} and Ω, respectively, were tested on the 2nd half of data collected from the 1st, 2nd, 3rd and 4th experiments as well as the whole data collected from the 6th and 8th experiments.

5.3.4. Testing accuracy of simulation sub-model

After running the eight experiments, the results predicted by the dehumidifier sub-model were compared to the observed data. More precisely, the observed and predicted values of the T_{ao}, T_{wo} and ω_{ao} were compared to

each other. This comparison included the calculation of three statistical parameters; the *average predictive error* ($\overline{PE}$), the *average percentage predictive error* ($\overline{\%PE}$) and the *root mean square error* (RMSE). The predicted and observed values were also graphically compared.

5.4. RESULTS

Table 5.2 shows the dehumidifier design and operating parameters used in the dehumidifier simulation sub-model. It should be highlighted that the results presented in the following sub-sections are for the experimental datasets that were not involved in the development of the F_P and Ω correlations. More specifically, these datasets include the 2nd half of data collected from the 1st, 2nd, 3rd and 4th experiments and the whole data collected from the 6th and 8th experiments.

Table 5.2: Dehumidifier design and operating parameters used in the simulation

Parameter	Value*	Comment
D_{ext} , [m]	3.00×10^{-2}	measured
b_{tube} , [m]	2.40×10^{-4}	measured
D_{int} , [m]	2.98×10^{-2}	calculated
H_{tube} , [m]	1.81	measured
s_T , [m]	4.70×10^{-2}	measured
s_D , [m]	4.70×10^{-2}	measured
s_L , [m]	4.07×10^{-2}	calculated
N_R	16	counted
N_C	98 (1st) 103 (2nd, 3rd and 4th) 122 (5th) 131 (6th and 7th) 127 (8th)	counted
u_a , [m/s]	0.27 (1st, 4th, 5th and 6th) 0.14 (2nd, 3rd, 7th, and 8th)	measured
$\dot{V}_w$, [m^3/s]	1.01×10^{-3}	measured
k_{PVC}, [W/m ^oC]	0.19	(The Engineering Toolbox, 2005)

* numbers between parentheses indicate the experiment(s) in which the correspondent value was used

5.4.1. Temperature predictions

The overall accuracy of the sub-model to predict the *outlet air temperature* T_{ao} was very good. In all experiments, the $\overline{PE}$ was between -0.39 and 1.93°C (SD≤1.98°C) and the $\overline{\%PE}$ was ranging from -1.39 to 6.61 % (SD≤6.59 %). The RMSE was between 0.73 and 2.35°C. More details about the $\overline{PE}$, $\overline{\%PE}$ and RMSE for each experiment can be found in Table 5.3. Figure 5.9 provides graphical comparisons between the predicted and observed T_{ao} values of the 1st, 3rd, 4th and 8th experiments (see Fig. C3.1 in Sec. C.3 of Appendix C for the rest of experiments). Figure 5.9 also shows the *solar heat flux* impinging on the outlet side of the dehumidifier (I_{deh}) and the measured *dehumidification rate* Ω. At times when there was no dehumidification, the predicted T_{ao} was slightly fluctuating about the observed T_{ao} (see the 3rd and 4th experiments). At two occasions during the dehumidification periods of the 1st experiment, a sudden increase in the *predictive error* (PE) of the T_{ao} was noticed. At very high Ω during the 8th experiment (as well as the 2nd and 6th experiments), the predicted T_{ao} was higher than the observed T_{ao}. There was no tangible relation noticed between the predicted T_{ao} and the I_{deh}.

Generally, the accuracy of the sub-model to predict the *outlet water temperature* T_{wo} was excellent. In all experiments, the $\overline{PE}$ was between -0.41 and 0.51°C (SD≤0.76°C), the $\overline{\%PE}$ was ranging from -1.46 to 1.73 %

Table 5.3: Accuracy of dehumidifier sub-model to predict *outlet air temperature* T_{ao}

Experiment	$\overline{PE}$ [°C]		$\overline{\%PE}$ [%]		RMSE [°C]
	Average	SD	Average	SD	
1st	0.39	1.16	1.28	3.99	1.22
2nd	0.82	1.71	2.94	6.57	1.89
3rd	-0.39	0.78	-1.39	2.92	0.87
4th	0.44	0.59	1.56	2.29	0.73
6th	1.93	1.00	6.61	3.46	2.17
8th	1.29	1.98	4.27	6.59	2.35
Maximum	1.93	1.98	6.61	6.59	2.35
Minimum	-0.39	0.59	-1.39	2.29	0.73

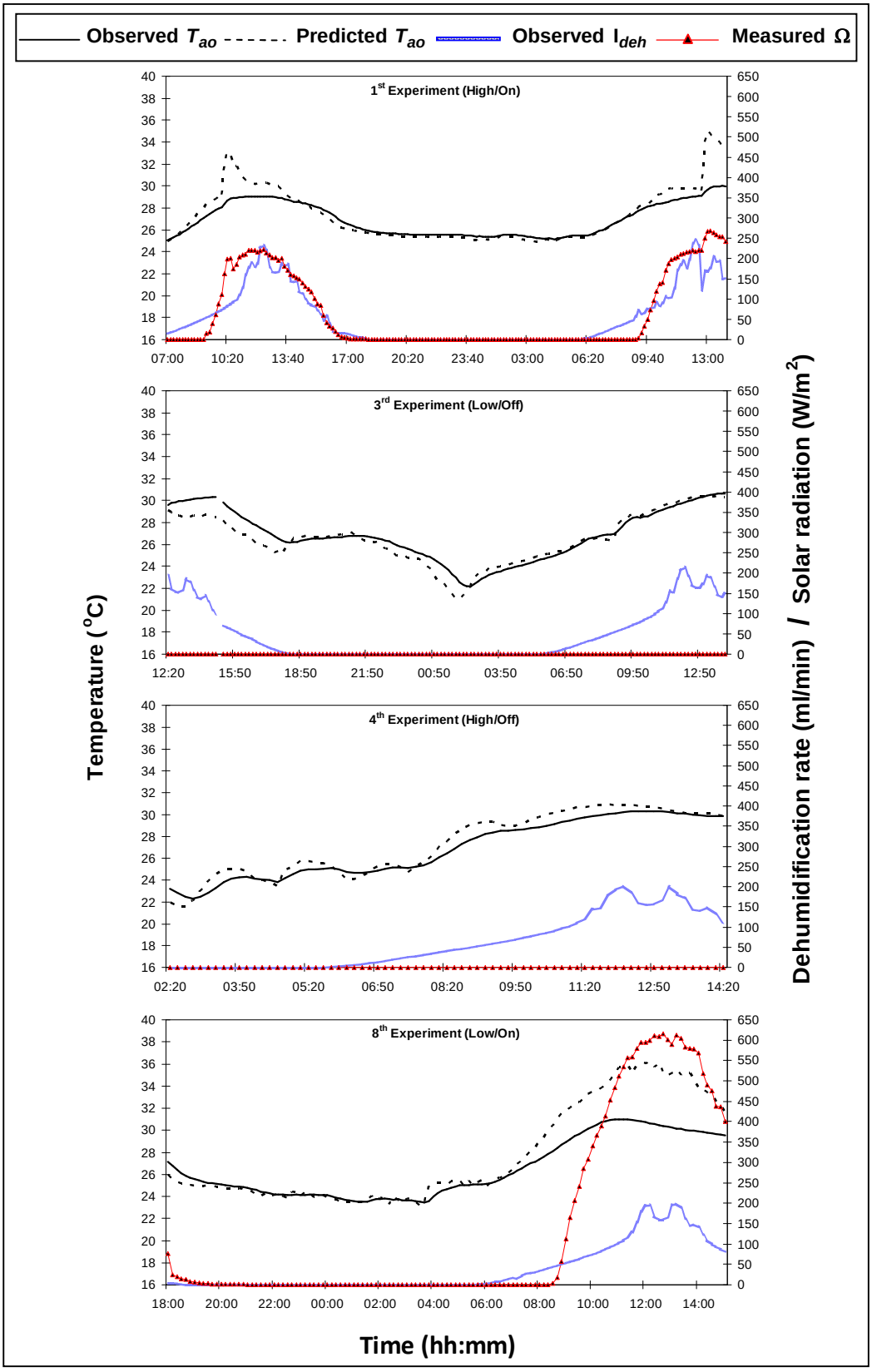

Fig. 5.9: Observed and predicted *outlet air temperature* T_{ao} with the observed *solar heat flux on dehumidifier* I_{deh} and the measured *dehumidification rate* Ω of the 1st, 3rd, 4th and 8th experiments
(High/Low: refers to air flowrate and On/Off: refers to operating status of dehumidifier)

(SD$\leq$3.18 %) and the RMSE was between 0.49 and 0.83^{o}C (see Table 5.4 for more details). Figure 5.10 compares the predicted and observed T_{wo} of the 1st, 3rd, 4th and 8th experiments (see Fig. C3.2 in Sec. C.3 of Appendix C for the rest). It was noticed that the predicted T_{wo} was similar to the observed T_{wo} for most of the time. However, the predicted T_{wo} was slightly lower than the observed T_{wo} at high Ω (see the 1st, 2nd and 8th experiments).

The sub-model was also predicting the average *external surface temperature* T_{es} of the dehumidifier tubes. The predicted T_{es} with the calculated *inlet air dew-point temperature* $T_{dp,ai}$ were used to predict the dehumidification periods. Figure 5.11 presents the predicted dehumidification periods (i.e. $(T_{dp,ai} - T_{es}) > 0$) and the measured *dehumidification rate* Ω of the 1st, 3rd, 4th and 8th experiments (see Fig. C3.3 in Sec. C.3 of Appendix C for the rest). There was a good conformity between the predicted dehumidification periods and the measured Ω. It was noticed that the sub-model was predicting the beginning of the dehumidification event 1 to 2 hrs before any measurement of the Ω was recorded as would be expected. Similarly, the predicted dehumidification event was ending 1.5 to 2.5 hrs before the end of the measured Ω.

Table 5.4: Accuracy of dehumidifier sub-model to predict *outlet water temperature* T_{wo}

Experiment	$\overline{PE}$ [^{o}C]		$\overline{\%PE}$ [%]		RMSE [^{o}C]
	Average	SD	Average	SD	
1st	-0.41	0.41	-1.46	1.39	0.58
2nd	-0.34	0.76	-1.19	3.18	0.83
3rd	-0.03	0.49	-0.13	1.93	0.49
4th	0.22	0.63	0.83	2.56	0.66
6th	0.51	0.18	1.73	0.60	0.53
8th	-0.16	0.63	-0.42	2.21	0.64
Maximum	0.51	0.76	1.73	3.18	0.83
Minimum	-0.41	0.18	-1.46	0.60	0.49

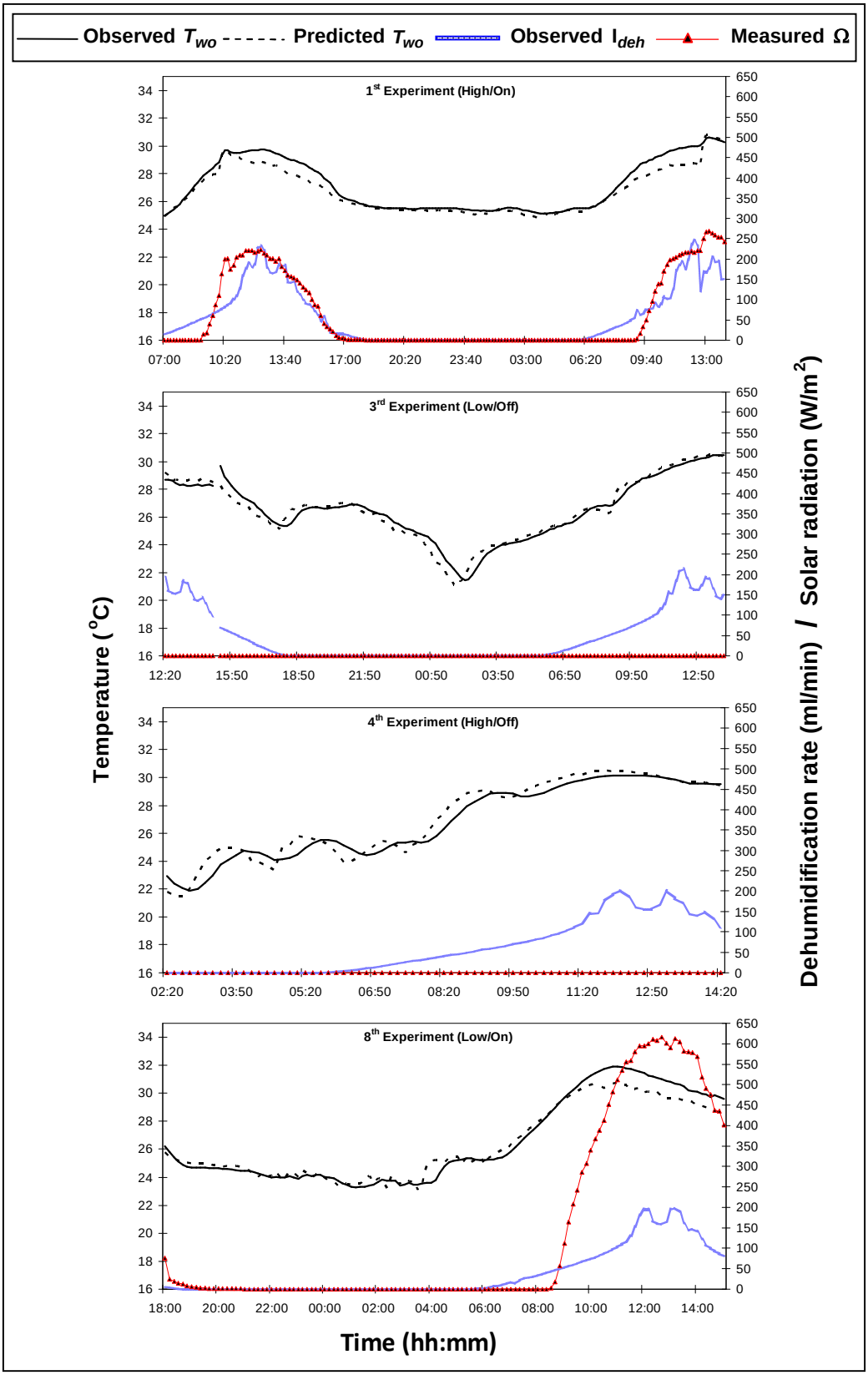

Fig. 5.10: Observed and predicted *outlet water temperature* T_{wo} with the observed *solar heat flux on dehumidifier* I_{deh} and measured *dehumidification rate* Ω of the 1st, 3rd, 4th and 8th experiments
(High/Low: refers to air flowrate and On/Off: refers to operating status of dehumidifier)

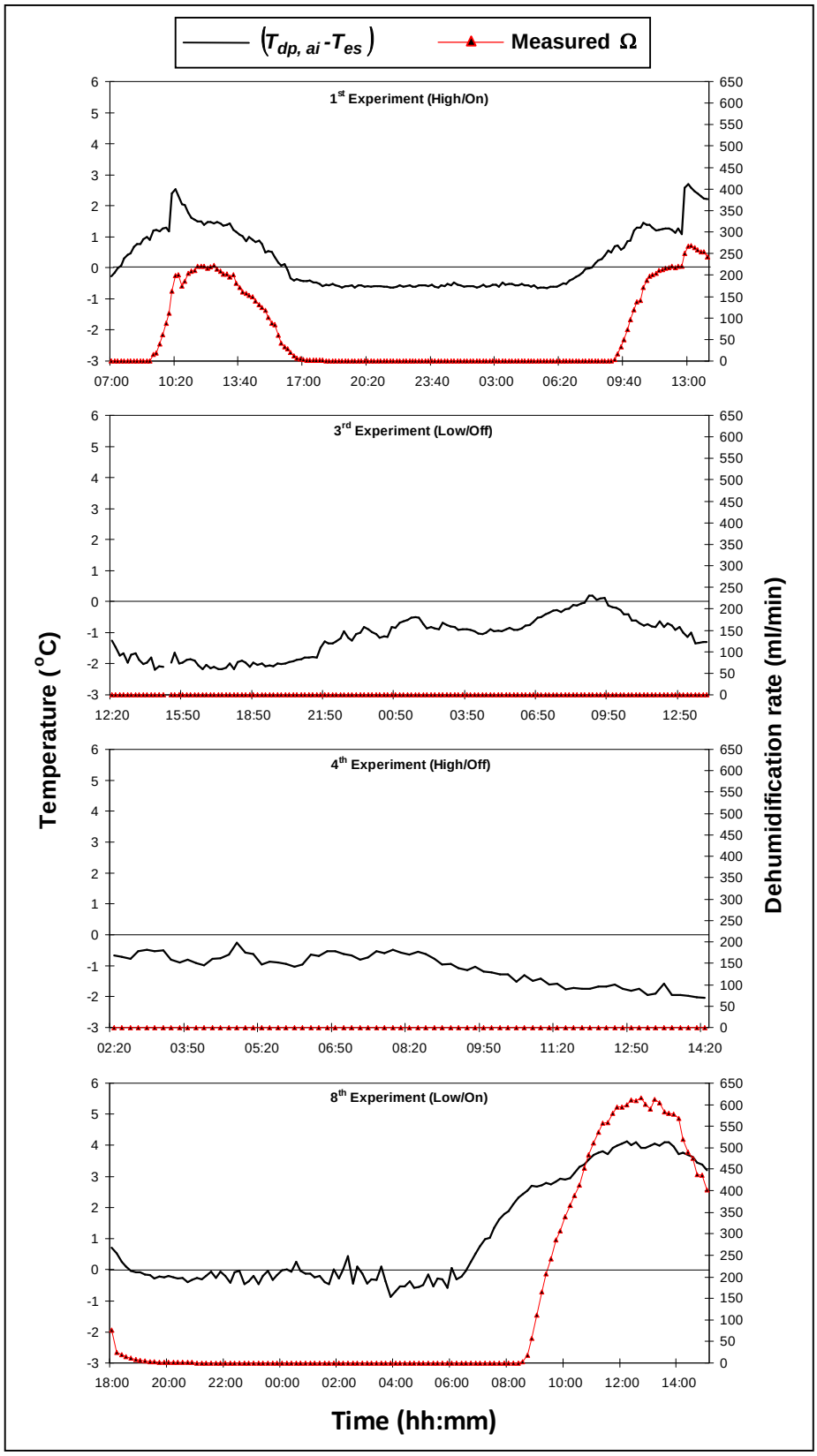

Fig. 5.11: Predicted dehumidification event (i.e. $(T_{dp,ai}-T_{es}) > 0$) and measured *dehumidification rate* Ω of the 1st, 3rd, 4th and 8th experiments
(High/Low: refers to air flowrate and On/Off: refers to operating status of dehumidifier)

5.4.2. Humidity predictions

As explained in Sections 5.2.4 and 5.3.3, the procedure followed to predict the *outlet humidity ratio* ω_{ao} started by developing an empirical relation correlating the *performance factor* F_p of the dehumidifier to the influencing inlet variables. With the aid of STATISTICA, the F_p correlation can be written as

$$F_p = -22920.5 + 5.1T_{ai} + 1.2\,\varphi_{ai} - 2.5\,\dot{m}_a + 22593.7\,\dot{m}_w \qquad (5.33)$$

As provided by STATISTICA, the *coefficient of determination* (R^2) and *standard error* of estimates (SE) of the F_p are approximately 0.34 and 17.45 %, respectively. Some statistical data of the different parameters (i.e. coefficients and variables) of Eq. 5.33 are provided in Table 5.5.

It was found that the *solar heat flux on dehumidifier* I_{deh} and *inlet water temperature* T_{wi} were insignificant in the prediction of the F_p. The I_{deh} became redundant since its indirect influence on the F_p is already accounted for by considering the *inlet air temperature* T_{ai} and *relative humidity* φ_{ai} that are, in turn, affected by the I_{deh}. Also, STATISTICA considered the T_{wi} redundant possibly because it could not find a consistent trend between the F_p and T_{wi} owing to the small fluctuations in the T_{wi} during the experiments that was not sufficient to cause a tangible influence on the F_p. Equation (5.29) was, then, used to predict the ω_{ao}.

Table 5.5: Some statistical data about the parameters (i.e. variables and coefficients) of Eq. 5.33

Parameter	Calibration range of variables	Standard error of coefficients
Intercept	-	2090.4
T_{ai}	19.1 – 34.3°C	0.3
φ_{ai}	62.3 – 100.0 %	0.1
$\dot{m}_a$	2.1 – 4.5 kg/s	2072.3
$\dot{m}_w$	1.00 – 1.01 kg/s	0.7

A comparison between the calculated and predicted F_p for the 1st, 3rd, 4th and 8th experiments is provided in Fig. 5.12 (see Fig. C3.4 in Sec. C.3 of Appendix C for the rest of experiments). From Fig. 5.12, the predicted F_p was somewhat following the general increasing/decreasing trend of the calculated F_p. However, a large discrepancy between the predicted and calculated F_p was observed. Indeed, such a discrepancy is expected to result into some inaccurate predictions of the ω_{ao}.

Generally, the sub-model accurately predicted the ω_{ao}. Figure 5.13 compares the predicted ω_{ao} to the observed ω_{ao} of the 1st, 3rd, 4th and 8th experiments (see Fig. C3.5 in Sec. C.3 of Appendix C for the rest). This figure also includes the observed *inlet humidity ratio* ω_{ai} and the Ω. The predicted ω_{ao} was comparatively equal to the observed ω_{ao}. However, in the 1st experiment there was a sudden increase in the predicted ω_{ao} at two occasions during the periods of high Ω. This could be due to the simultaneous sharp increase in the ω_{ai}. It was also noticed that at very large Ω, the predicted ω_{ao} was lower than the observed ω_{ao} (see the 8th experiment in Fig. 5.13 and the 2nd experiment in Fig. C3.5). Table 5.6 presents the $\overline{\text{PE}}$, $\overline{\%\text{PE}}$ and RMSE of the ω_{ao} for all experiments. From this table, the $\overline{\text{PE}}$ was between -0.00023 and 0.00021 kg (water)/kg (dry air) (SD$\leq$0.00103 kg (water)/kg (dry air)), the $\overline{\%\text{PE}}$ was ranging from -0.77 to 0.87 % (SD$\leq$4.47 %) and the RMSE was between 0.00011 and 0.00105 kg (water)/kg (dry air).

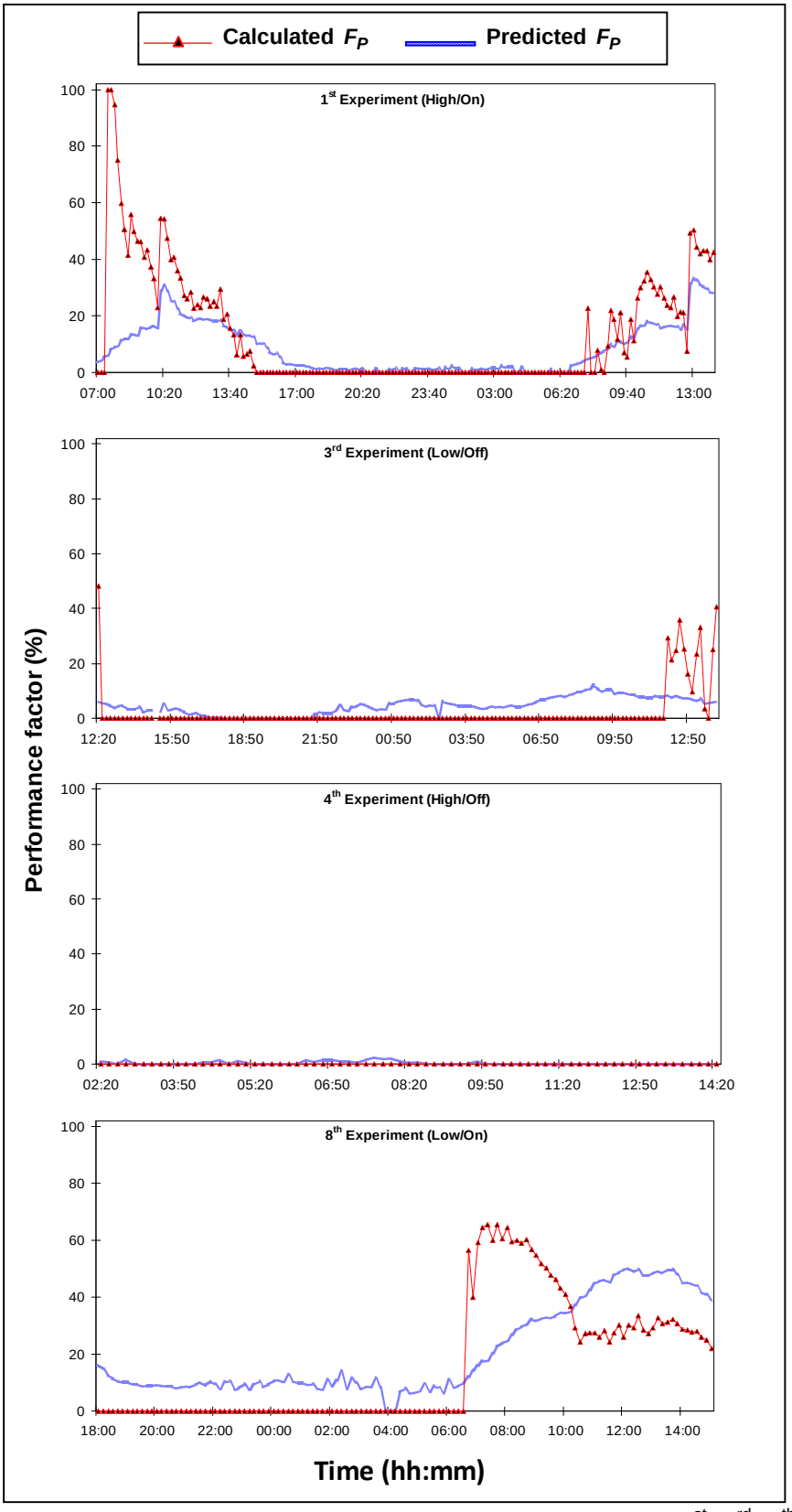

Fig. 5.12: Calculated and predicted *performance factor* F_P of the 1st, 3rd, 4th and 8th experiments
(High/Low: refers to air flowrate and On/Off: refers to operating status of dehumidifier)

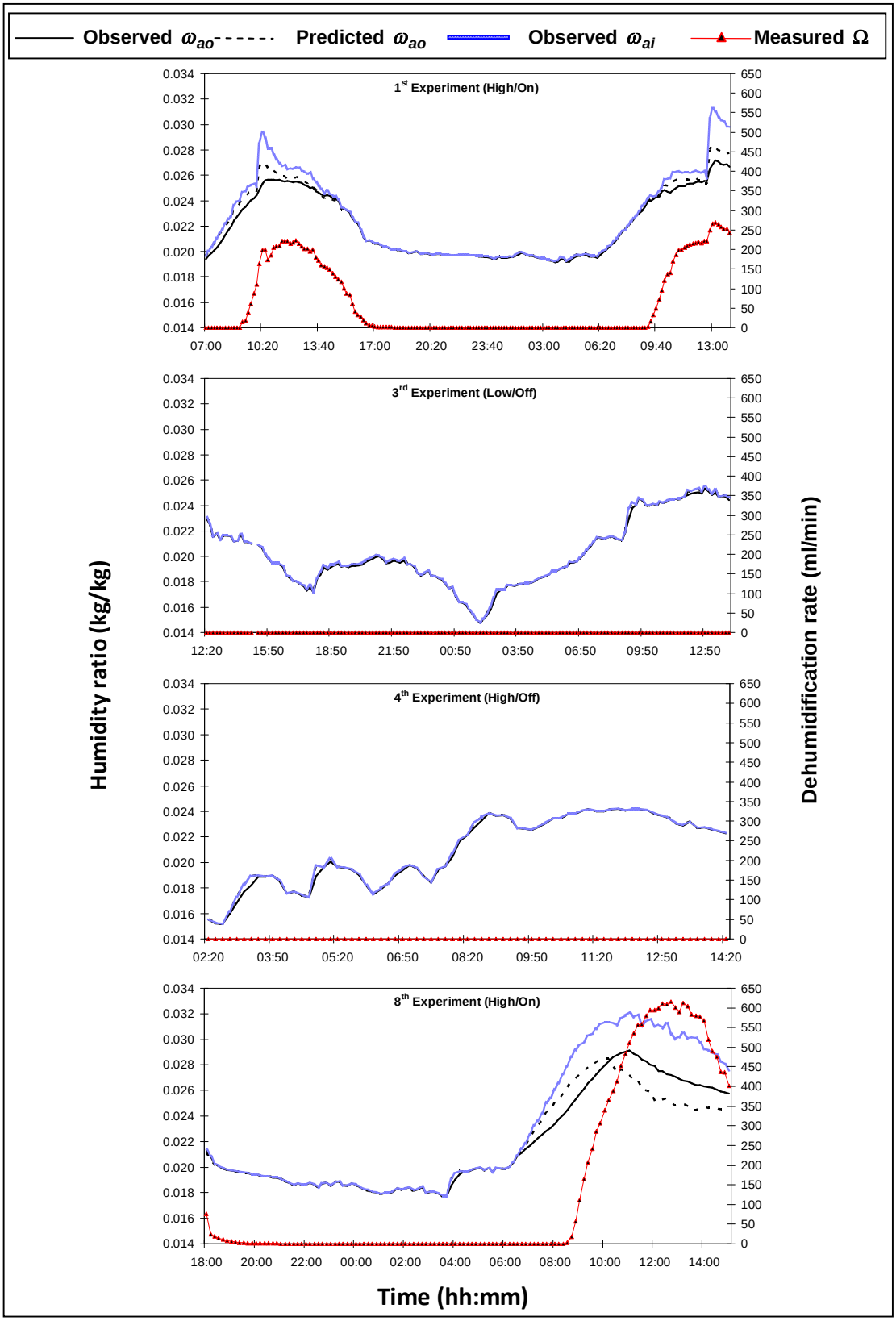

Fig. 5.13: Observed and predicted *outlet humidity ratio* ω_{ao} with the observed *inlet humidity ratio* ω_{ai} and measured *dehumidification rate* Ω of the 1st, 3rd, 4th and 8th experiments
(High/Low: refers to air flowrate and On/Off: refers to operating status of dehumidifier)

Table 5.6: Accuracy of dehumidifier sub-model to predict outlet humidity ratio ω_{ao}

Experiment	$\overline{PE}$ [kg/kg]		$\overline{\%PE}$ [%]		RMSE [kg/kg]
	Average	SD	Average	SD	
1st	0.00021	0.00036	0.87	1.45	0.00042
2nd	0.00002	0.00086	0.51	4.47	0.00086
3rd	0.00004	0.00010	0.18	0.47	0.00011
4th	0.00006	0.00016	0.32	0.84	0.00017
6th	-0.00019	0.00030	-0.72	1.15	0.00035
8th	-0.00023	0.00103	-0.77	3.89	0.00105
Maximum	0.00021	0.00103	0.87	4.47	0.00105
Minimum	-0.00023	0.00010	-0.77	0.47	0.00011

5.4.3. Dehumidification rate predictions

The *dehumidification rate* Ω was predicted using two methods. The 1st method was to use the predicted F_P (Eq. 5.33) to obtain the ω_{ao} (Eq. 5.29), and then, Eq. (5.32) was used to calculate the Ω. The 2nd method was to develop an empirical correlation using STATISTICA for the Ω as a function of all influencing input variables:

$$\Omega = -329610.5 + 46.5\,T_{ai} + 9.0\,\varphi_{ai} + 6.2\,\dot{m}_a + 31.7\,T_{wi} + 325406.7\,\dot{m}_w + 0.3\,I_{deh} \quad (5.34)$$

The *coefficient of determination* (R^2) and *standard error* of estimates (SE) of the Ω in Eq. (5.34) are approximately 0.82 and 53.8 ml/min, respectively. Table 5.7 provides some statistical data of the different variables (i.e. variables and coefficients) of Eq. (5.34).

Table 5.7: Some statistical data about the parameters (i.e. variables and coefficients) of Eq. 5.34

Parameter	Calibration range of variables	Standard error of coefficients
Intercept	-	67063.1
T_{ai}	19.1 – 34.3°C	1.4
φ_{ai}	62.3 – 100.0 %	0.3
$\dot{m}_a$	2.1 – 4.5 kg/s	2.2
T_{wi}	16.9 – 27.7°C	14.7
$\dot{m}_w$	1.00 – 1.01 kg/s	66416.2
I_{deh}	0 – 266.8 W/m^2	0.05

Figure 5.14 illustrates the measured and predicted Ω using the 1st and 2nd methods for the 1st, 3rd, 4th and 8th experiments (see Fig. C3.6 in Sec. C.3 of Appendix C for the rest). The 1st method mostly overestimated the Ω and the 2nd method underestimated it. Nevertheless, the predicted Ω using both methods was most of the times following the general trend of the measured Ω. The predicted Ω was starting slightly before any Ω was measured (see the 1st and 8th experiments).

5.4.4. Influence of changing inlet moisture level and air flowrate

Two moisture levels and two air flowrates were studied in the experiments as explained in Sec. 5.3.1. The moisture levels were obtained through turning on/off the 2nd humidifier located approximately 1.5 m before the dehumidifier. There was always an observed daily dehumidification when the humidifier was operating (see the 1st and 8th experiments in Fig. 5.14). In contrast, there was no dehumidification when it was off (see the 3rd and 4th experiments in Fig. 5.14). Therefore, the 2nd humidifier is an important component of the HD greenhouse since the performance of the dehumidifier depends on its operation.

Regarding the influence of changing the air flowrate on the Ω, it was noticed that the Ω was increasing significantly in the low-air-flowrate experiments when compared to the high-air-flowrate ones. The 1st and 8th experiments are typical examples of high- and low-air-flowrate experiments, respectively (see Fig. 5.14). The former had a maximum observed Ω of 269.1 ml/min and the latter had a maximum of 615.6 ml/min. These two experiments were similar in everything except for the air flowrate. A similar observation was also found with the 2nd and 6th experiments (see Fig. C3.6).

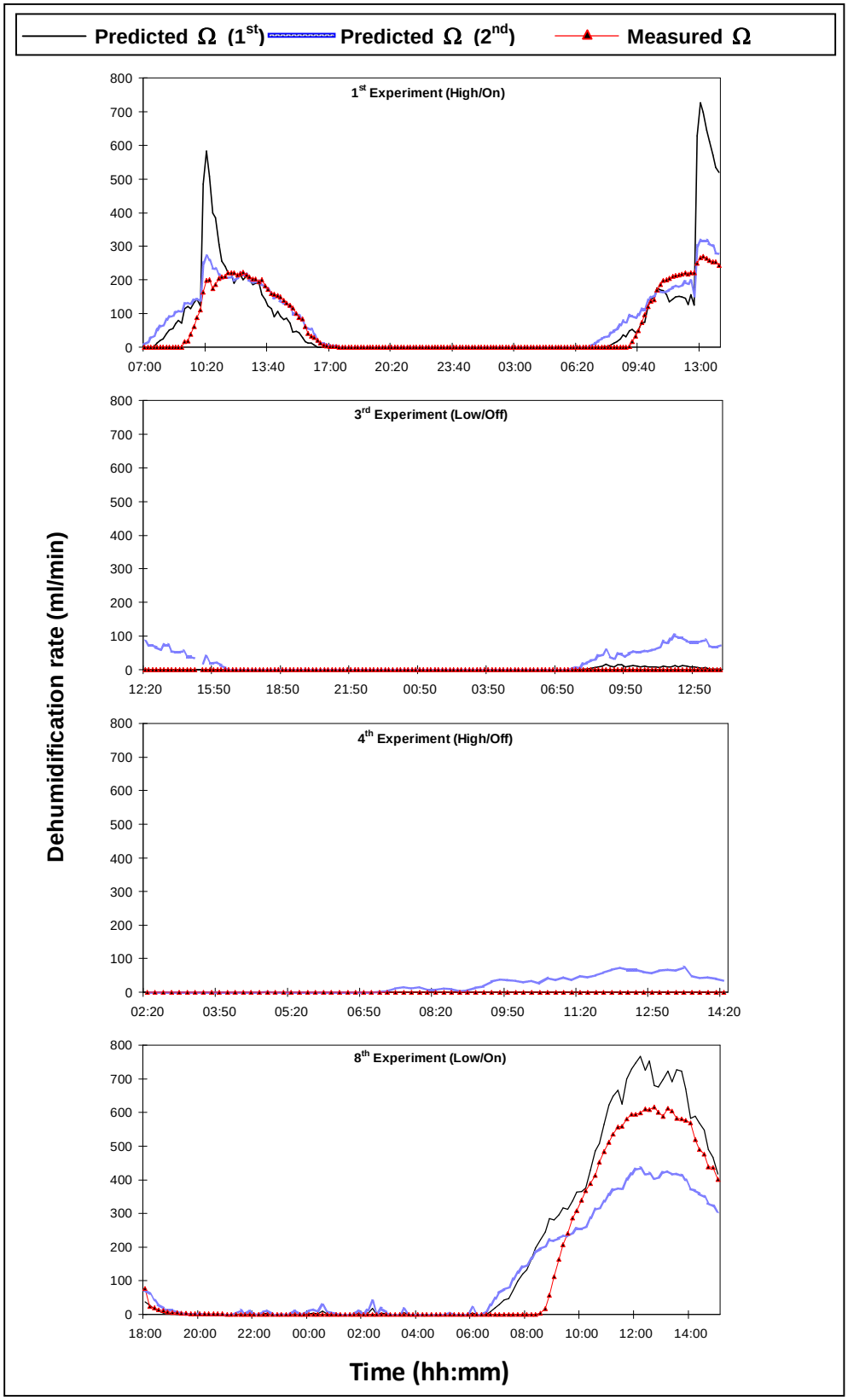

Fig. 5.14: Measured and predicted *dehumidification rate* Ω (using the 1st and 2nd methods) of the 1st, 3rd, 4th and 8th experiments
(High/Low: refers to air flowrate and On/Off: refers to operating status of humidifier)

It was found from the smoke trace used to delineate air movement from the 2nd humidifier to dehumidifier that the air was not moving in horizontal lines (see Fig. 5.15). The relatively hot water used to wet the 2nd humidifier (to increase the *evaporation rate*) was warming the higher air stream, giving it a tendency to move upwards. Furthermore, the evaporation decreases as water flows downwards and the water cools. In other words, the air passing through the 2nd humidifier at position ② will be less humid than the air at position ①; and so on. Hence, the temperature/relative humidity sensor placed at the outlet of the dehumidifier was not observing the same air layer observed by the sensor placed at the inlet; introducing an error into measured change in humidity.

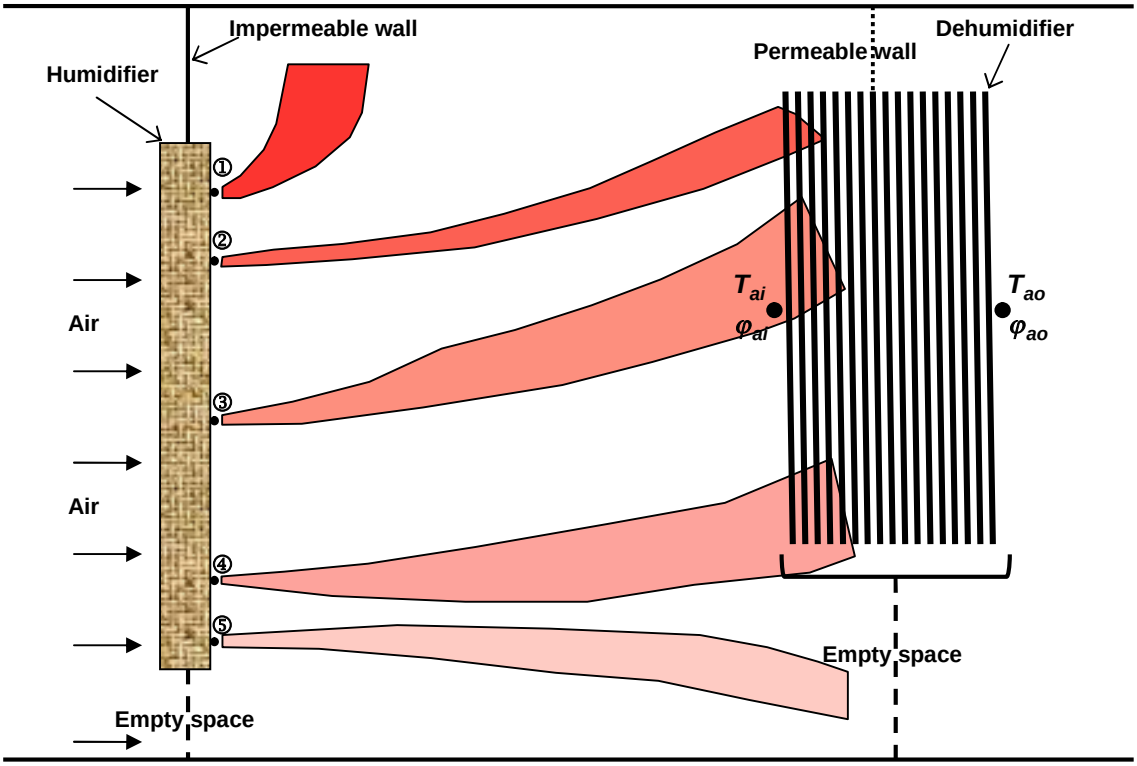

Fig. 5.15: Observed air movement from the humidifier to dehumidifier using a smoke source placed at 5 vertical positions on the surface of the humidifier

5.5. DISCUSSION

This section starts by discussing the sub-model's humidity predictions before the temperature predictions due to the dependency of the latter on the accuracy of the former.

5.5.1. Humidity predictions

It was clearly seen from Table 5.6 and Fig. 5.13 that the accuracy of the sub-model to predict the ω_{ao} was very good. In this discussion, the accuracy of the sub-model will be highlighted for three situations; when there was no dehumidification, at the sudden increase in the *inlet air humidity* at two occasions during the 1st experiment, and at very high *dehumidification rates* Ω of the 2nd and 8th experiments.

The sub-model very accurately predicted the ω_{ao} at times when there was no dehumidification. During the 3rd and 4th experiments, as an example, the predicted ω_{ao} was continually overlapping with the observed ω_{ao} (see Fig. 5.13).

In the 1st experiments, it was noticed that at two occasions when there was dehumidification, the predicted ω_{ao} was slightly higher than the observed ω_{ao}. During these occasions, there was a sharp increase in the *air humidity* that was detected by the inlet sensor but not by the outlet sensor. This implies that the air layer observed by the outlet sensor was less humid than the air layer observed by the inlet sensor. To recall, the ω_{ao} was calculated using Eq. (5.29) that involved the F_p predicted from Eq. (5.33). The F_p was predicted as a function of the significant input variables including the *inlet humidity* of the air. Because the F_p correlation accounted for the increase in the *inlet air humidity* and the outlet sensor did not detect a similar increase, the predicted ω_{ao} was slightly higher than the observed ω_{ao}. Therefore, it can be deduced that the positive PE of the ω_{ao} during the 1st experiment was related more to the

measured values of the ω_{ao} than to the predicted values. Therefore, the air flow pattern illustrated in Fig. (5.15) was attributable to the underestimation of the observed ω_{ao} as explained in Sec. 5.4.4.

At very high Ω of the 2nd and 8th experiments, the predicted ω_{ao} was slightly lower than the observed ω_{ao} (see Figs. 5.13 for the 8th experiment and Fig. C3.5 for the 2nd experiment). In the 8th experiment, it was noticed that there was a relatively large discrepancy in the predicted F_p when compared to the calculated F_p at the high Ω (see Fig. 5.12); the predicted F_p was initially lower than the calculated F_p and eventually *vice versa*. A similar observation was also noticed with the 2nd experiment (see Figs. C3.4 and C3.5). This discrepancy in the predicted F_p can be attributed to two factors; the small dataset used to develop the F_p correlation (Eq. 5.33) and the incorporation of several input variable that may support or abate the influence of each other in predicting the F_p. Improving the accuracy of the F_p correlation would certainly enhance the accuracy of predicting the ω_{ao}.

From the above discussion, the small inaccuracy of the ω_{ao} observed at some occasions during the dehumidification periods was caused by an inaccuracy either related to the predicted or observed ω_{ao}. The source of inaccuracy related to the predicted ω_{ao} can be resolved by increasing the accuracy of the predicted F_p. This can be achieved by using more datasets to develop the F_p empirical correlation (Eq. 5.33). On the other hand, the source of inaccuracy related to the observed ω_{ao} can be overcome by using several input and output sensors arranged in a vertical profile at both sides of the dehumidifier.

5.5.2. Temperature predictions

The accuracy of the dehumidifier sub-model to predict the T_{ao} and T_{wo} was good. In this section, the accuracy of the sub-model will be highlighted according to the three situations used in Sec. 5.5.1.

At times when there was no dehumidification, there was a small fluctuation in the predicted T_{ao} and T_{wo} with respect to the observed values. It was noticed in the 3rd and 4th experiments, for instance, that the predicted T_{ao} and T_{wo} were slightly higher or lower than the observed values at the same operating conditions (see Figs. 5.9 and 5.10). This fluctuation was most probably measurement-related. Because the air was flowing in lines inclined upwards (Fig. 5.15), the sensor used to observe the T_{ao} was somewhat monitoring an air layer lower than the air layer monitored by the inlet sensor. Thus, the observed T_{ao} could be higher or lower than the predicted T_{ao} depending on the temperature of the air layer monitored by the outlet sensor. The T_{wo} was indirectly affected by the fluctuation in the T_{ao} due to the iterative procedure mutually linked the predicted T_{ao} and T_{wo} (see Fig. 5.4).

In the 1st experiment, there was an unexpected sharp increase in the PE of the T_{ao} at two occasions during dehumidification. This increase in the PE resulted from a simultaneous increase in the ω_{ai} owing to the dependency of the predicted T_{ao} on the *inlet humidity ratio* ω_{ai}. Hence, it was found that the curve of the predicted T_{ao} (Fig. 5.9) was following the curve of the ω_{ai} (Fig. 5.13). It was deduced in Sec. 5.5.1 that the PE of the ω_{ao} experienced at these two occasions was due to the non-horizontal air flow pattern (see Fig. 5.15). Analogously, the sharp increase in the PE of the T_{ao} can be attributed to the inaccuracy in measurements caused by the air flow pattern.

At very high Ω of the 2nd and 8th experiments, it was noticed that the predicted T_{ao} was always higher than the observed T_{ao} and the predicted T_{wo}

was mostly lower than the observed T_{wo} (see Figs. 5.9 and 5.10 for the 8th experiment and Figs. C3.1 and C3.2 for the 2nd experiment). This can be attributed to the under-predicted ω_{ao} involved in the calculation of the overall *heat transfer rate of the air* Q_a (Eq. 5.4). Its involvement resulted in a higher Q_a value and consequently, an over-prediction of T_{ao}. In the last five hours of the 8th experiment, it was noticed that the predicted T_{ao} was even more than the T_{ai} which ideally cannot be the case. Having the predicted T_{ao} value greater than the T_{ai} means that the air was getting extra heat from the coolant water since the process was assumed adiabatic between these two fluids. Therefore, during the last few hours of the 8th experiment, the predicted T_{wo} was slightly lower than the observed T_{wo}. Since all of this inaccuracy was caused by using the under-predicted ω_{ao} in the simulation, the accuracy of predicting the T_{ao} and T_{wo} can be increased once the accuracy of predicting the ω_{ao} is improved.

From the above discussion, the sub-model accurately predicted the T_{ao} and T_{wo}. However, there were some occasions when the predicted T_{ao} was higher than the observed T_{ao} and the predicted T_{wo} was lower than the observed T_{wo} due to either the non-horizontal air flow pattern or the under-prediction of the ω_{ao}. The former source of error can be reduced by using several inlet and outlet sensors arranged in the same way explained in Sec. 5.5.1. The latter source of error can be eliminated by improving the accuracy of predicting the ω_{ao} as explained in Sec. 5.5.1.

5.5.3. Dehumidification rate predictions

To recall, two methods were followed to predict the Ω; the 1st method was using the predicted ω_{ao} (Eq. 5.29) to calculate the Ω (Eq. 5.32) and the 2nd method was using the Ω empirical correlation (Eq. 5.34). The overall performance of the sub-model to predict the Ω using the two methods was good. Generally, both methods showed a good agreement between the

predicted and observed Ω. However, the 1st method was mostly overestimating the Ω and the 2nd method was underestimating it (see Fig. 5.14). It is difficult to favourite one method over the other but it was observed that the discrepancy in the predicted Ω using the 1st method was more than that obtained from the 2nd method.

What one can do, although it is not very scientific, is to predict the Ω using both methods. By this way, the real Ω is at most of the times bounded between the predicted Ω from the two methods. It should always be remembered that the prediction of the Ω was based on two empirical correlations. These correlations were developed for a specific type of dehumidifier under specific conditions. Extending the use of these correlations on different type of dehumidifiers or under different conditions might lead to significant inaccurate predictions. The accuracy of predicting the Ω, as well as the F_P, can be improved by increasing the size and calibration range of dataset used to develop their empirical correlations. Also, it can be improved by trying different values for the same influencing variable(s) incorporated in the empirical correlation.

At the end of this discussion, it is recommended to conduct more experiments to further validate the dehumidifier simulation sub-model under different operating and weather conditions. In these experiments, the number of accurate temperature/relative humidity sensors should be increased in order to determine in a definite way the responsible (i.e. the simulation sub-model or the sensor or both) for the PE of the T_{ao} and ω_{ao}. Using the data generated from the proposed experiments in addition to the data collected from the experiments of this study would certainly improve the accuracy of the empirical correlations.

5.6. SUMMARY

This chapter, dedicated to discuss the development and validation of the dehumidifier simulation sub-model, can be summarised in the following points:

- The sub-model accurately predicted the *outlet air* and *water temperatures*. However, at high dehumidification rates, the predicted *outlet air temperatures* were sometimes higher than the observed values and the predicted *outlet water temperatures* were lower than the observed values. This was attributed to the non-horizontal air flow pattern and to the under-predicted values of the *outlet humidity ratio* used in the simulation
- The accuracy of the sub-model to predict the *outlet humidity ratio* was very good. However, there were some occasions when the predicted *outlet humidity ratio* was slightly higher or lower than the observed values. This was attributed to the inaccuracy of the empirical correlation used to predict the *performance factor*
- The sub-model was accurately predicting the periods of dehumidification
- The *dehumidification rate* was predicted using two empirical correlations that were giving good accuracy within the range of conditions used for developing these correlations
- Further investigations on the performance of the sub-model under different operating and climatic conditions will help in studying the accuracy of the sub-model in a broader context. Also, the data generated from these investigations will help to improve the accuracy of the empirical correlations.

CHAPTER SIX

6. THE INTEGRATED HD GREENHOUSE MODEL

The overall aim of this study was to develop a mathematical model simulating the main processes of the HD greenhouse. These processes are the evaporation process taking place in the 1st and 2nd humidifiers, the temperature and moisture changes of the greenhouse microclimate located between the two humidifiers and finally the condensation taking place in the dehumidifier. So far, three sub-models were developed/modified to simulate these processes. The development, validation experiments and experimental results of these sub-models were discussed in details in the previous three chapters.

In this chapter, the three sub-models are compiled together to form an integrated HD greenhouse model simulating the significant temperature and moisture changes taking place as the air streams through the greenhouse. The model is also capable of predicting the amount of condensate whenever there is dehumidification.

Unfortunately, the accuracy of the integrated model could not be tested against experimental data because the HD greenhouse located in Oman was not in good condition to run the validation experiments. However, using some weather data, the model has been used to simulate a standard Quonset-type greenhouse in Oman assuming that a 2nd humidifier and a dehumidifier are integrated inside the greenhouse. Different operating conditions have been studied to foresee their influence on the *dehumidification rate* Ω.

6.1. THE WORKING PROTOCOL OF THE INTEGRATED MODEL

A MS-Excel workbook is used to compile the three sub-models in a way permitting the simulation of the HD greenhouse. This workbook is composed of six spreadsheets where the first and last are for the input data and output

results, respectively. Each of the other spreadsheets is reserved for one sub-model. These spreadsheets are arranged in the same order the air flows through the greenhouse. The ambient air initially passes through the 1st humidifier then through the greenhouse microclimate before it passes through the 2nd humidifier and finally through the dehumidifier. A detailed explanation about the concept and processes of HD greenhouses is already given in Sec. 2.1.4.

The 2nd spreadsheet is used for the simulation of the 1st humidifier. The input data used in the humidifier sub-model are the humidifier design and operating parameters, the *ambient air temperature* and *humidity* and the *inlet water temperature*. In the greenhouse microclimate sub-model (3rd spreadsheet), the greenhouse configuration parameters, *ambient solar radiation*, *ambient air temperature* and the *outlet air temperature* and *humidity* from the 1st humidifier are used as input data. The *outlet air temperature* and *humidity* from the last section of the microclimate are used as input data in the simulation of the 2nd humidifier (4th spreadsheet). The dehumidifier sub-model (5th spreadsheet) uses the *outlet air temperature* and *humidity* from the 2nd humidifier as input data assuming no heat gain/loss taking place to the air as it flows through the short distance between the 2nd humidifier and the dehumidifier. Also, the *outlet water temperature* from the 1st humidifier is used as *inlet water temperature* in the dehumidifier sub-model assuming no heat gain/loss taking place to the water as it flows from the 1st humidifier to the dehumidifier. However, if a significant heat gain/loss exists then it should be accounted for.

6.2. SIMULATION OF A QUONSET HD GREENHOUSE

In this simulation, a Quonset greenhouse with configuration similar to Nizwa greenhouse is considered (see Fig. 4.1, and for more details Sec. A.2 of Appendix A). Two more components are added to Nizwa greenhouse; a 2nd humidifier at a distance 36 m from the 1st humidifier and a dehumidifier

immediately after the 2nd humidifier. The area between the two humidifiers is cultivated with cucumber crop. The greenhouse with this setting is similar to the one illustrated in Fig. 6.1. The greenhouse is ventilated with a flowrate equal to the flowrate obtained when one fan is operated. This is because low air flowrate through the dehumidifier results in more condensate as was seen in Chapter 5. However, even the air flowrate obtained from running only one fan (approximately 13.3 kg/s) is significantly more than the calibration range of the *mass air flowrate* $\dot{m}_a$ (i.e. 2.1 to 4.3 kg/s) used to develop the F_P and Ω correlations (for calibration ranges, see Tables 5.5 and 5.7). This extrapolation on the use of these correlations is expected to lead to some inaccuracy in predictions.

Five-day weather data collected from the weather station located next to the HD greenhouse in Oman are used in this simulation. These data were collected by other researchers in May, 2005. Data used as the *inlet water temperatures* to the 1st and 2nd humidifiers were obtained from the experiment that was running in the HD greenhouse during the collection of the weather data. The main objectives of this simulation are to demonstrate the use of the integrated model, to investigate the *temperature* and *humidity* changes taking place in the HD greenhouse and to predict the amount of condensate the greenhouse can produce with the given design and operating conditions.

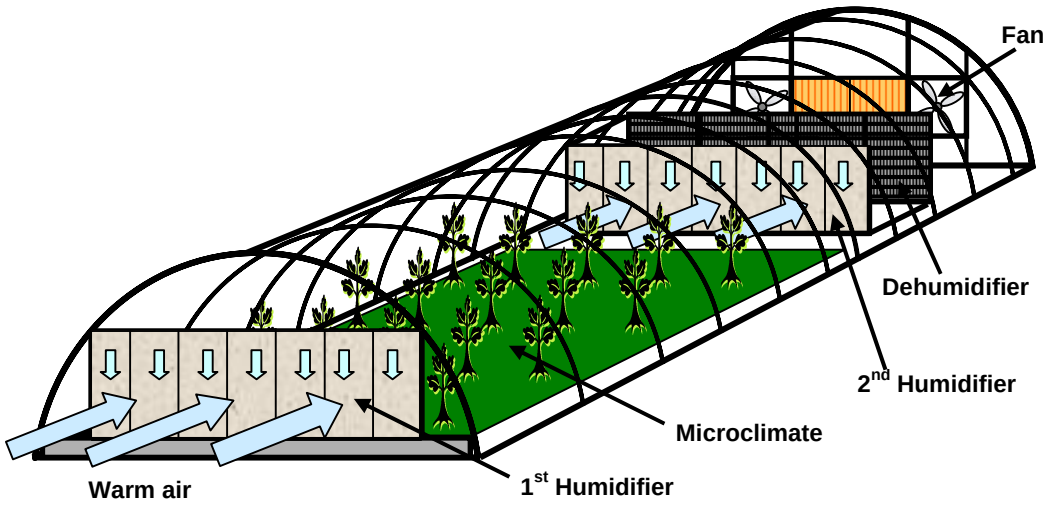

Fig. 6.1: Schematic of the simulated hypothetical HD greenhouse

6.2.1. Simulation results from normal operating conditions of hypothetical Quonset HD greenhouse

The greenhouse, humidifier(s) and dehumidifier design and operating parameters used in the simulation are provided in Tables 6.1, 6.2 and 6.3, respectively. Table 6.4 presents the properties of the cucumber crop used in the simulation.

The *inlet* and *outlet air temperatures* (T_{ai} and T_{ao}, respectively) and the *inlet* and *outlet humidity ratio* (ω_{ai} and ω_{ao}, respectively) obtained from the HD simulation model for the 1st humidifier, greenhouse microclimate, 2nd humidifier

Table 6.1: Greenhouse design and operating parameters used in the simulation

Parameter	Value	Comment
τ_c, [dimensionless]	0.82	measured
$\tau_{\lambda,c}$, [dimensionless]	0.698	Walker (1965)
U_c, [W/m^2 ^{o}C]	6.8	Chen (2003)
L_{gh}, [m]	38	measured
H_{gh}, [m]	3.2	measured
W_{gh}, [m]	9.0	measured
P (length of curved arch), [m]	11.78	calculated
V_{gh}, [m^3]	799.48	calculated
dx, [m]	1.0	theoretical
f_v, [dimensionless]	0.81	Chen (2003)
u_2, [m/s]	0.66	measured
$\dot{V}_a$, [m^3/s]	11.25	measured through fans

Table 6.2: Humidifier design and operating parameters used in the simulation

Parameter	Value	Comment
H_{hum}, [m]	2.0	measured
W_{hum}, [m]	6.0	measured
b_{hum}, [m]	0.1	measured
V_{hum}, [m^3]	1.2	calculated
l_{hum}, [m]	2.16x10^{-3}	Rawangkul et al. (2008)
A_{aw}, [m^2]	555.6	calculated
u_a, [m/s]	0.94	measured
$\dot{V}_w$, [m^3/s]	1.01x10^{-3}	measured

Table 6.3: Dehumidifier design and operating parameters used in the simulation

Parameter	Value	Comment
D_{ext} , [m]	3.00×10^{-2}	measured
b_{tube} , [m]	2.40×10^{-4}	measured
D_{int} , [m]	2.98×10^{-2}	calculated
H_{tube} , [m]	1.81	measured
s_T , [m]	4.70×10^{-2}	measured
s_D , [m]	4.70×10^{-2}	measured
s_L , [m]	4.07×10^{-2}	calculated
N_R	16	counted
N_C	160	counted
u_a , [m/s]	0.83	measured
$\dot{V}_w$, [m^3/s]	1.01×10^{-3}	measured
k_{PVC} , [W/m ^oC]	0.19	(The Engineering Toolbox, 2005)

Table 6.4: Properties of the cucumber crop used in the simulation

Parameter	Value	Comment
H_p , [m]	2.0	measured
LAI , [dimensionless]	1.36	measured
ϕ_p , [dimensionless]	0.25	Levit and Gaspar (1988)
ε_p , [dimensionless]	0.98	Kindelan (1980) and Levit and Gaspar (1988)

and dehumidifier are illustrated in Figs. 6.2, 6.3, 6.4 and 6.5, respectively. From these figures, the changes in *air temperature* and *humidity* taking place as the air flows through the HD greenhouse can be clearly seen. Figure 6.2 shows a significant drop in *air temperature* and increase in moisture as air passes through the 1st humidifier due to evaporation process. Figure 6.3 shows that as the air passes through the microclimate, the *air temperature* and *humidity* significantly increase at the day but there is a small change at night. Figure 6.4 then shows that the air gets more moisture as it passes through the 2nd humidifier. Figure 6.5, showing the dehumidifier stage, shows that the T_{ao} is slightly lower than T_{ai} but the ω_{ao} is equal to the ω_{ai} (i.e. no dehumidification occurs).

The changes in the *temperature of the water* used to wet the 1st humidifier and to cool the dehumidifier are given in Fig. 6.6; as expected, it cools through the 1st humidifier and then warms up in the dehumidifier. Figure 6.7 illustrates the *inlet* and *outlet water temperatures* of the 2nd humidifier.

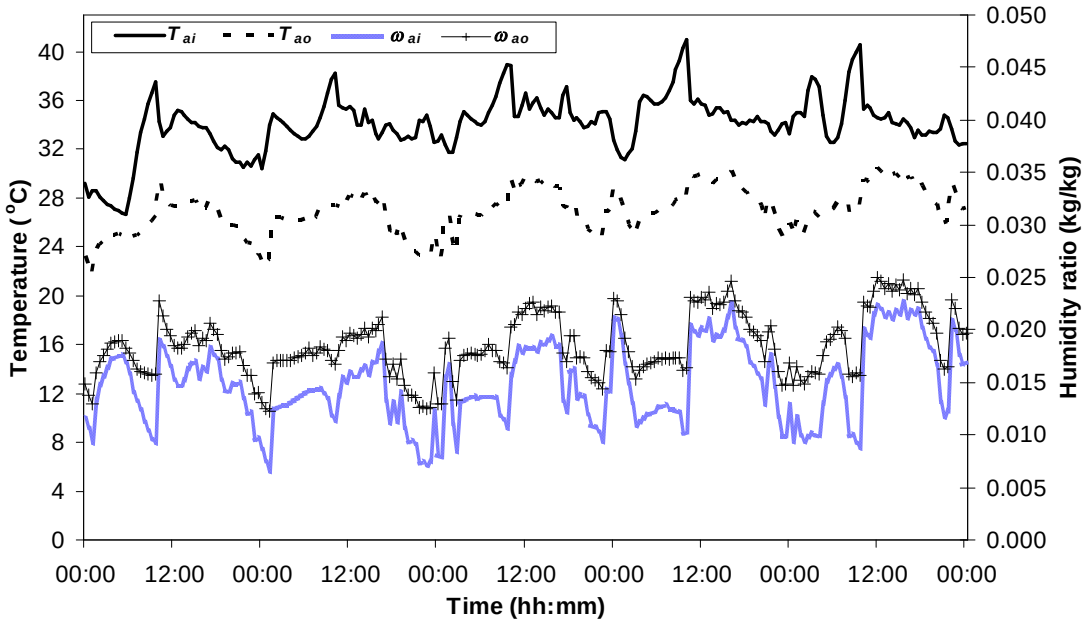

Fig. 6.2: The *inlet* and *outlet air temperatures* (T_{ai} and T_{ao}, respectively) and *inlet* and *outlet humidity ratio* (ω_{ai} and ω_{ao}, respectively) of the 1st humidifier

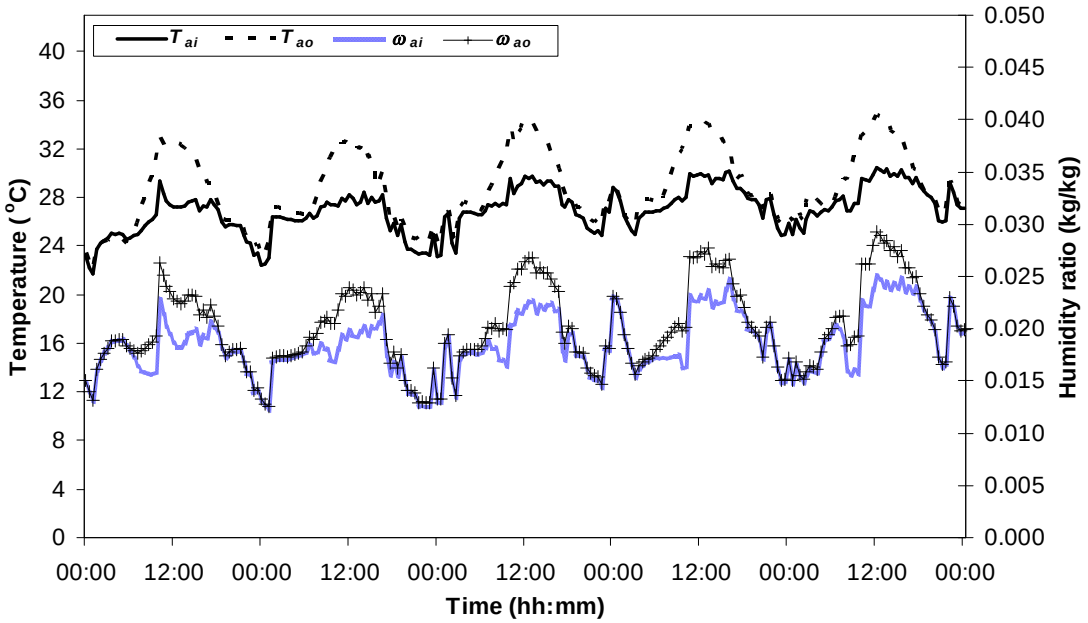

Fig. 6.3: The *inlet* and *outlet air temperatures* (T_{ai} and T_{ao}, respectively) and *inlet* and *outlet humidity ratio* (ω_{ai} and ω_{ao}, respectively) of the greenhouse microclimate

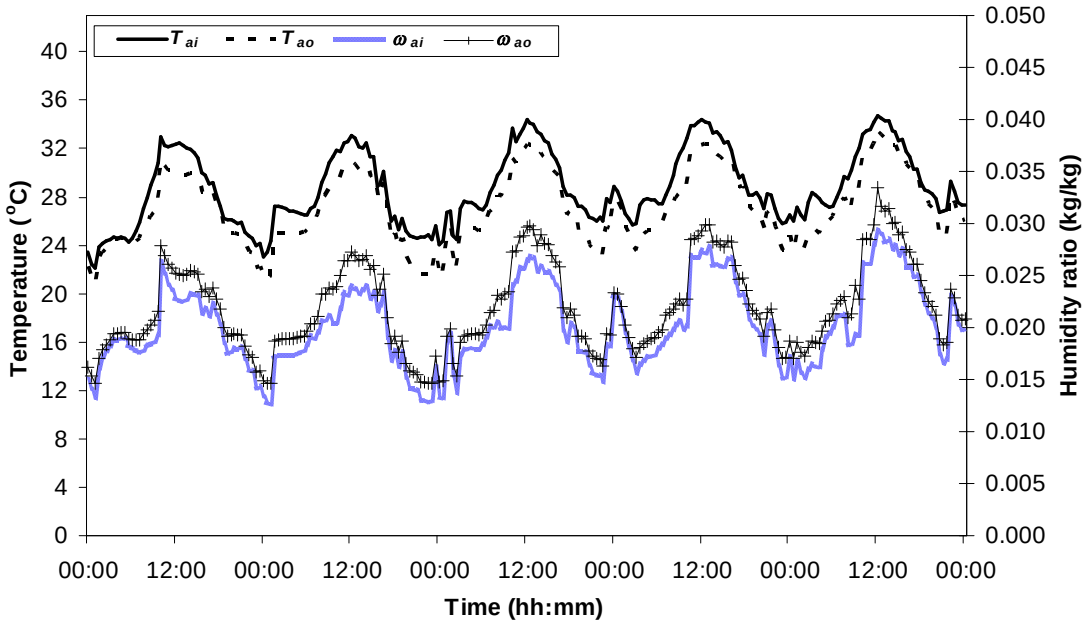

Fig. 6.4: The *inlet* and *outlet air temperatures* (T_{ai} and T_{ao}, respectively) and *inlet* and *outlet humidity ratio* (ω_{ai} and ω_{ao}, respectively) of the 2nd humidifier

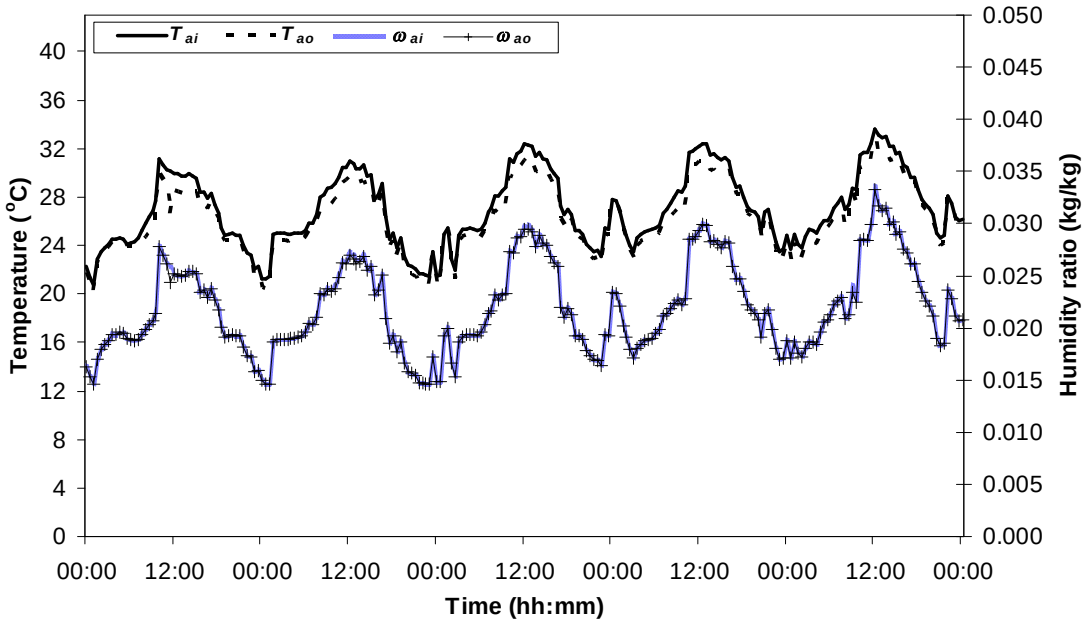

Fig. 6.5: The *inlet* and *outlet air temperatures* (T_{ai} and T_{ao}, respectively) and *inlet* and *outlet humidity ratio* (ω_{ai} and ω_{ao}, respectively) of the dehumidifier

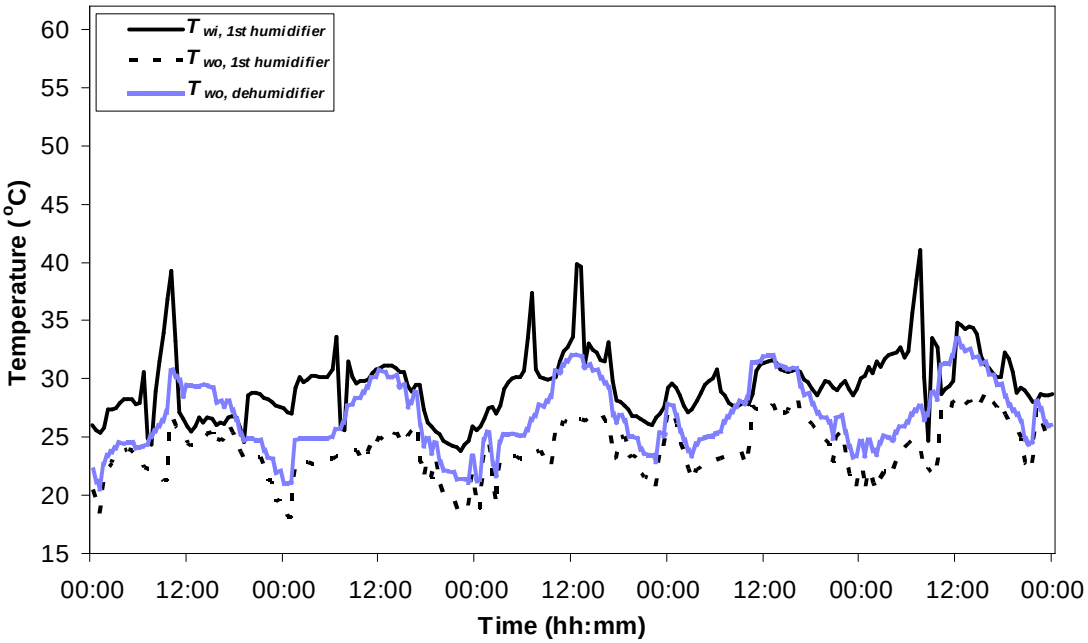

Fig. 6.6: The inlet and outlet water temperatures of the 1st humidifier ($T_{wi,\ 1st\ humidifier}$ and $T_{wo,\ 1st\ humidifier}$, respectively) and the outlet water temperature of the dehumidifier ($T_{wo,\ dehumidifier}$)

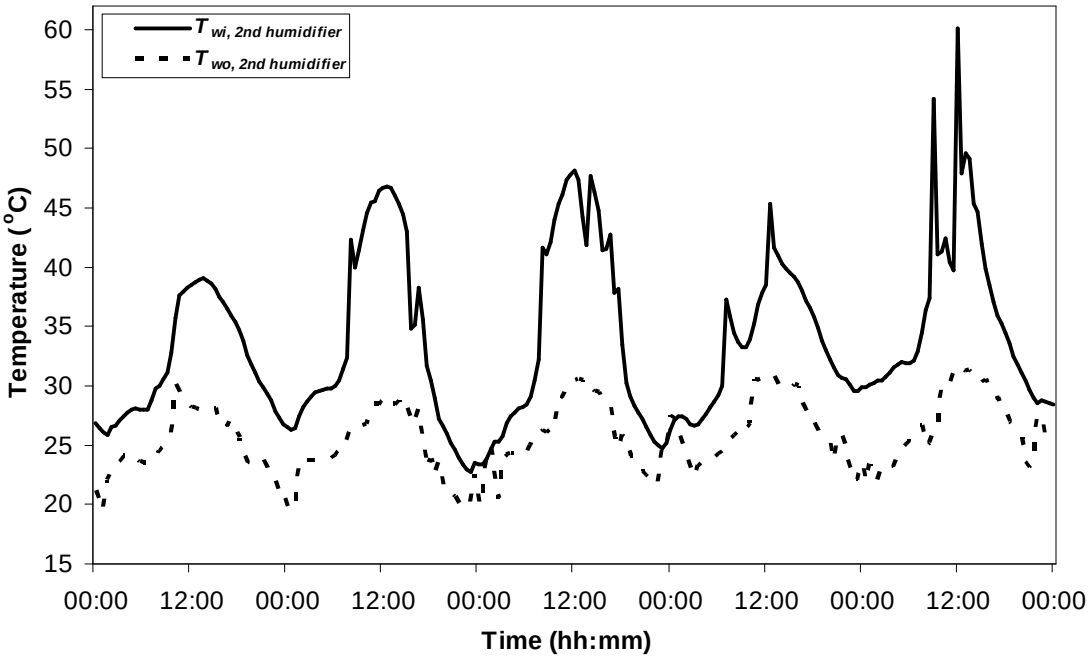

Fig. 6.7: The inlet and outlet water temperatures of the 2nd humidifier ($T_{wi,\ 2nd\ humidifier}$ and $T_{wo,\ 2nd\ humidifier}$, respectively)

The *dehumidification rate* Ω was predicted using two methods as mentioned in Chapter 5; the 1st method calculates Ω using the predicted ω_{ao} (as calculated above and shown in Fig. 6.5) and the 2nd methods predicts Ω from an empirically developed relation correlating the Ω as a function of the significant input variables. The results of the Ω predicted using the two methods are shown in Fig. 6.8. In this figure, the 1st method only predicted the Ω at very few occasions whilst the 2nd method continually predicted the Ω. The predicted Ω values from the 2nd method were ranging from 0 to nearly 300 ml/min. A comparison between the moisture added to the air by crop *evapotranspiration* (ET) (and hence indicating the volume of irrigation water required) and the moisture removed by dehumidification (both methods) is given in Fig. 6.9.

6.2.2. Discussion

Since all predictions of the model were as expected except the *outlet humidity ratio* ω_{ao} of the air leaving the dehumidifier (see Fig. 6.5), the focus in this discussion will be about the accuracy of the HD model to predict the ω_{ao}. The predicted ω_{ao} was equal to the ω_{ai} and therefore, there was mostly no

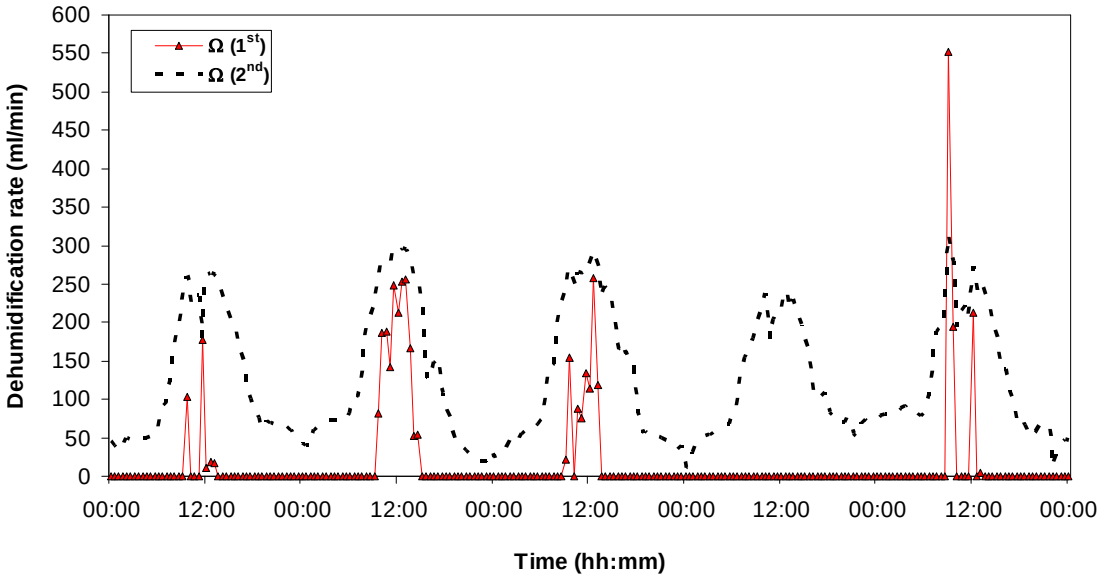

Fig. 6.8: The *dehumidification rate* Ω predicted using the 1st and 2nd methods

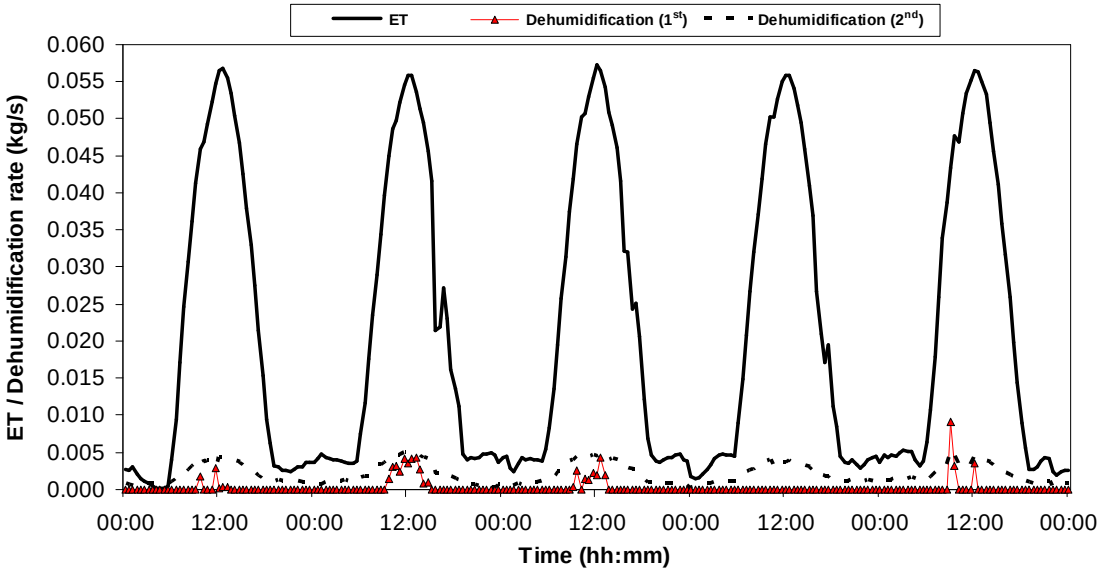

Fig. 6.9: Moisture added through *evapotranspiration* (ET) and removed through dehumidification (predicted using the 1st and 2nd methods)

dehumidification rate Ω predicted by the 1st method (Eq. 5.32). In contrary, the 2nd method predicted a good amount of Ω (see Fig. 6.8).

It should be remembered that for the 1st method, the *performance factor* F_P of the dehumidifier (Eq. 5.33) that was involved in the calculation of the ω_{ao} (Eq. 5.29) was predicted from an empirical correlation. This correlation was developed for a specific dehumidifier under specific conditions. Extending the use of this correlation beyond the calibration range of its variables is expected to lead to significant inaccuracy. The calibration range of the *mass air flowrate* $\dot{m}_a$ used in the simulation (i.e. 13.3 kg/s) was considerably higher than the range of $\dot{m}_a$ used in the development of the F_P correlation (i.e. 2.1 to 4.3 kg/s). This could be one reason to the incapability of the dehumidifier sub-model to predict the ω_{ao} and consequently, the Ω (using the 1st method).

The 2nd method used to predict the Ω is also an empirical correlation (Eq. 5.34). The only difference between this correlation and the F_P correlation is that the Ω correlation was developed using the measured Ω as a function of the significant inlet variables whereas the F_P correlation was developed using

calculated F_P values (5.29) as a function of the significant inlet variables. Equation (5.29) involved some more measured variables than Eq. (5.34) and therefore, its prediction accuracy (R^2=0.34) was less than the accuracy of Eq. (5.34) (R^2=0.82). Although the 2nd method was able to predict the Ω, more caution should be taken when applying the Ω correlation to conditions outside the calibration range of the variables under which it was developed.

6.2.3. Simulation within calibration ranges

In a trial to test whether the high $\dot{m}_a$ was handicapping the 1st method from predicting the Ω or there was some other cause, only 25 % of the $\dot{m}_a$ is assumed to pass through the dehumidifier and the rest bypasses it (or passes through 3 other similar dehumidifiers). This gives $\dot{m}_a$ values within the calibration ranges that were used to develop the F_P correlation. With the new $\dot{m}_a$ (approximately 3.3 kg/s), the dehumidifier managed to predict ω_{ao} (see Fig. 6.10) and also, the Ω. The Ω obtained from the two methods using the new $\dot{m}_a$ is illustrated in Fig. 6.11. The Ω predicted with the 1st method is slightly higher than that predicted with the 2nd method as would be expected from the

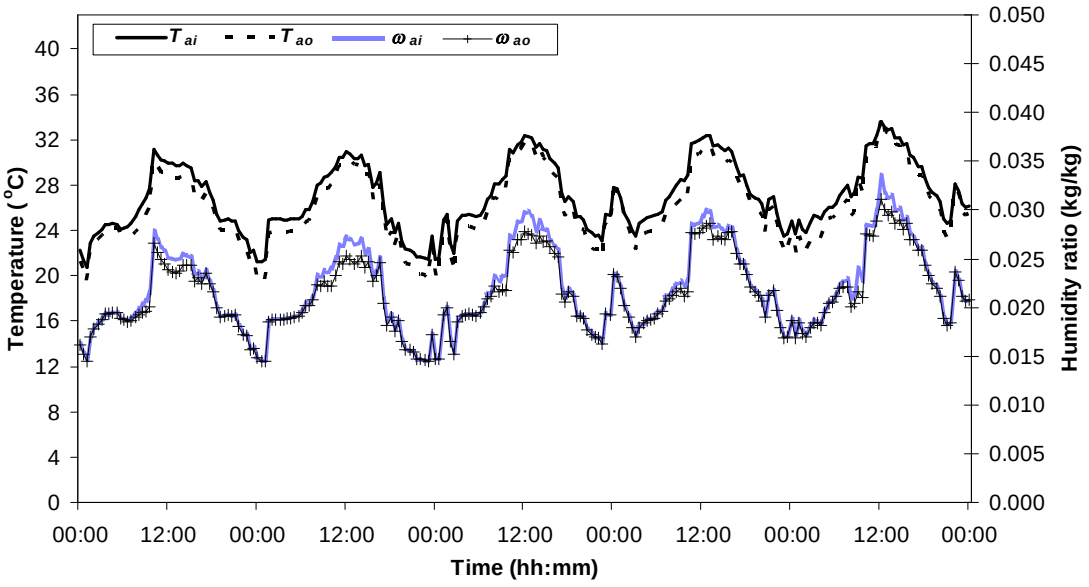

Fig. 6.10: The *inlet* and *outlet air temperatures* (T_{ai} and T_{ao}, respectively) and *inlet* and *outlet humidity ratio* (ω_{ai} and ω_{ao}, respectively) of the dehumidifier using the new *air flowrate*

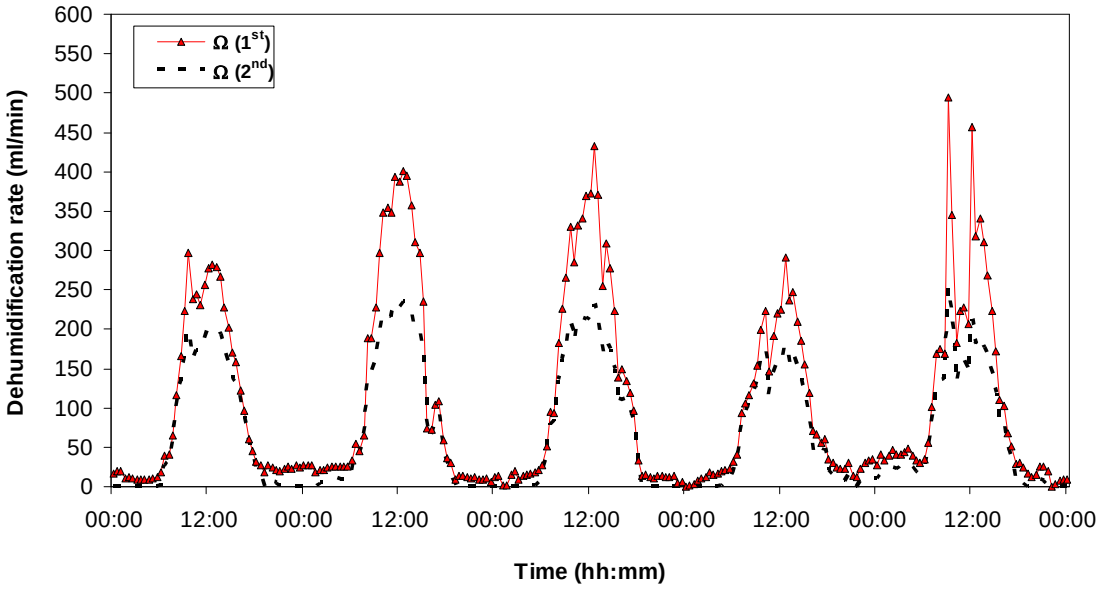

Fig. 6.11: The *dehumidification rate* Ω predicted with the 1st and 2nd methods using the new *air flowrate*

experimental results discussed in Chapter 5 (see Fig. 5.14 and Sec. 5.5.3). The real Ω is expected to be bounded between the Ω predicted with the two methods (see also Sec. 5.5.3). It was noticed from Fig. 6.11 that the Ω predicted with the 2nd method using the new $\dot{m}_a$ is less than that predicted previously (see Fig. 6.8). This is also expected since with the new $\dot{m}_a$, 75 % of the moisture carried in the air is bypassed.

Figure 6.12 compares the moisture added to the air from the greenhouse microclimate (ET) and the moisture removed from the air through dehumidification (both methods) at the new $\dot{m}_a$. From this figure, it is very clear that the *dehumidification rate* is still far below the ET rate. Therefore, more effort needs to be done to improve the performance of the HD greenhouse owing to the fact that the main objective of HD greenhouses is to dehumidify water vapour for the sake of irrigating the cultivated crops.

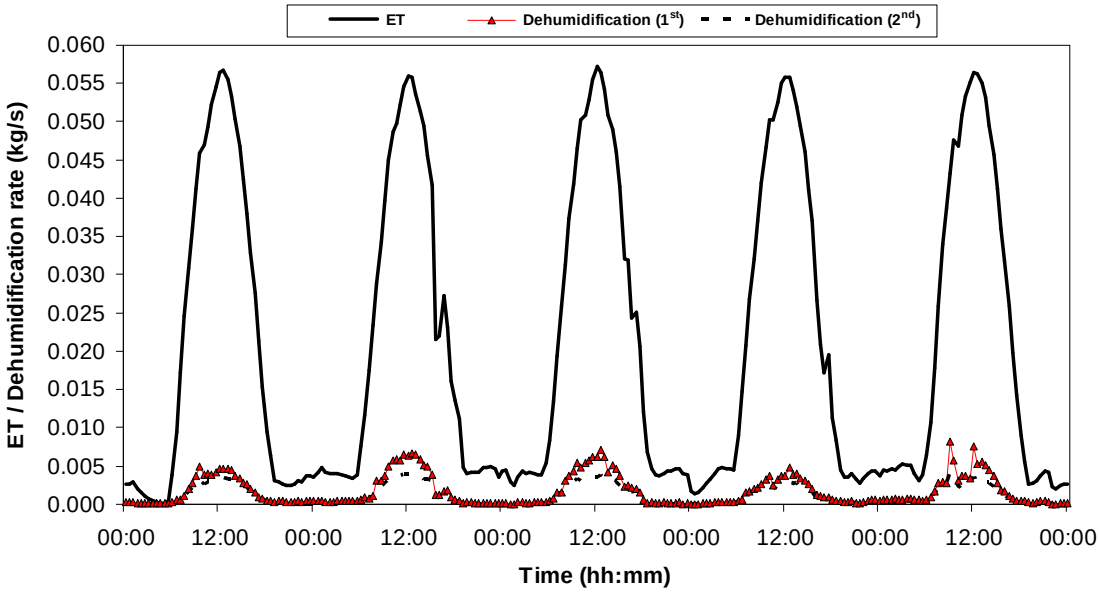

Fig. 6.12: Moisture added through evapotranspiration (ET) and removed through dehumidification (both methods) with the new *air flowrate*

6.3. STUDYING INFLUENCE OF DIFFERENT VARIABLES ON DEHUMIDIFICATION RATE

The HD simulation model in its current format enables studying the influence of different input variable on the main processes of the HD greenhouse. For instance, the influence of changing the design and operating variables of humidifier(s) on the evaporation process can be studied using the model. Also, the model enables investigating the influence of those variables as well as the design and operating variables of the greenhouse microclimate and dehumidifier on the dehumidification process. As an example of the model's simulation capability, the influence of not having the 2nd humidifier before the dehumidifier, the influence of not cultivating the greenhouse and the influence of placing the dehumidifier immediately after the 1st humidifier; the influence of all of these on the *dehumidification rate* Ω is investigated below.

6.3.1. Influence of not having 2nd humidifier on dehumidification rate

A question that is frequently asked, why is there a 2nd humidifier inside the HD greenhouse? In order to answer this question, an HD greenhouse with the

design and operating properties similar to those given in Tables 6.1, 6.2 and 6.3 is considered. However, this greenhouse does not include a 2nd humidifier and the *air temperature* and *humidity* outputs from the last section of the microclimate will be the inputs to the dehumidifier. The *air flowrate* $\dot{m}_a$ through the dehumidifier is 25 % of the total $\dot{m}_a$ through the greenhouse while the rest is bypassed.

The simulation results of the Ω obtained using both methods are illustrated in Fig. 6.13. When the 2nd humidifier is not included in the HD greenhouse, the Ω predicted from the two methods is significantly lower than that predicted with the 2nd humidifier included (see Figs. 6.11 and 6.13). Therefore, this proves the significance of having the 2nd humidifier to increase the Ω.

6.3.2. Influence of no cultivation on dehumidification rate

In the simulation of the HD greenhouse explained in Sec. 6.2, the greenhouse was cultivated with a cucumber crop having the properties provided in Table 6.4. Here, the greenhouse, humidifier(s) and dehumidifier will have the same design and operating properties provided in Tables 6.1, 6.2 and 6.3 however, the greenhouse is not cultivated. Again, the *air flowrate* $\dot{m}_a$ through

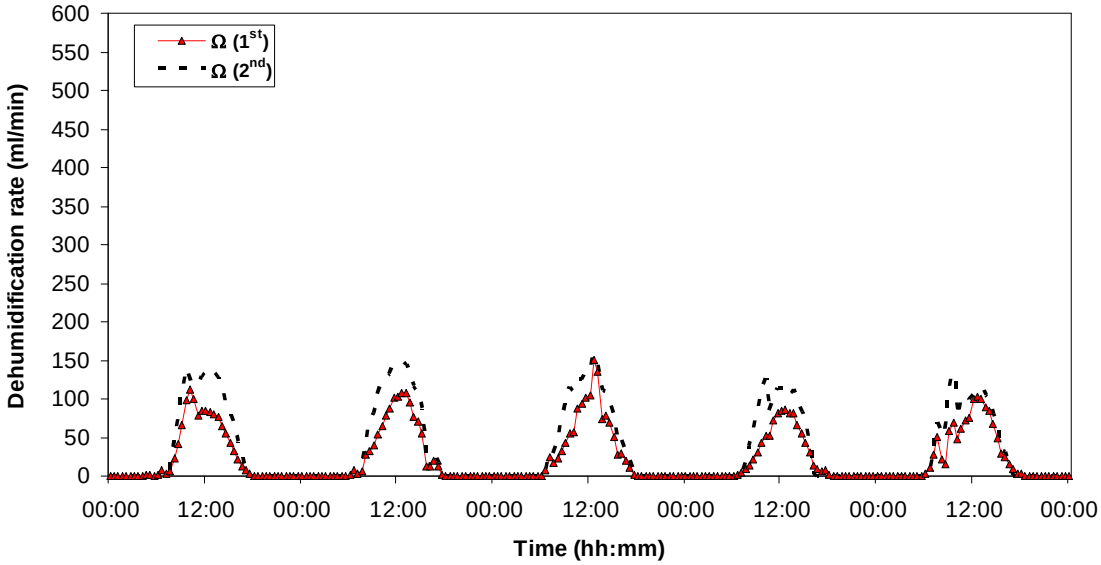

Fig. 6.13: The *dehumidification rate* Ω predicted with the 1st and 2nd methods when there is no 2nd humidifier

the dehumidifier is 25 % of the total $\dot{m}_a$ through the greenhouse. The purpose of conducting this simulation is to foresee the influence of having no cultivation on the Ω.

Figure 6.14 shows the simulation results of the Ω obtained from the two methods. It is clearly seen that the two methods were giving similar predictions. It is noticed that the Ω predicted when the greenhouse was not cultivated is slightly less than that predicted when it was cultivated (see Figs. 6.11 and 6.14). This implies that cultivated HD greenhouses produce slightly more condensate than uncultivated greenhouses owing to the moisture added to the air through plant *evapotranspiration*.

6.3.3. Influence of placing dehumidifier after 1st humidifier on dehumidification rate

What would be the influence on the Ω if the dehumidifier is placed just after the 1st humidifier? To answer this question, the same design and operating conditions for the humidifier and dehumidifier, mentioned in Sec. 6.3.2 are considered here. The *air temperature* and *humidity* and *water temperature* outputs from the 1st humidifier are the inlet values to the dehumidifier. The

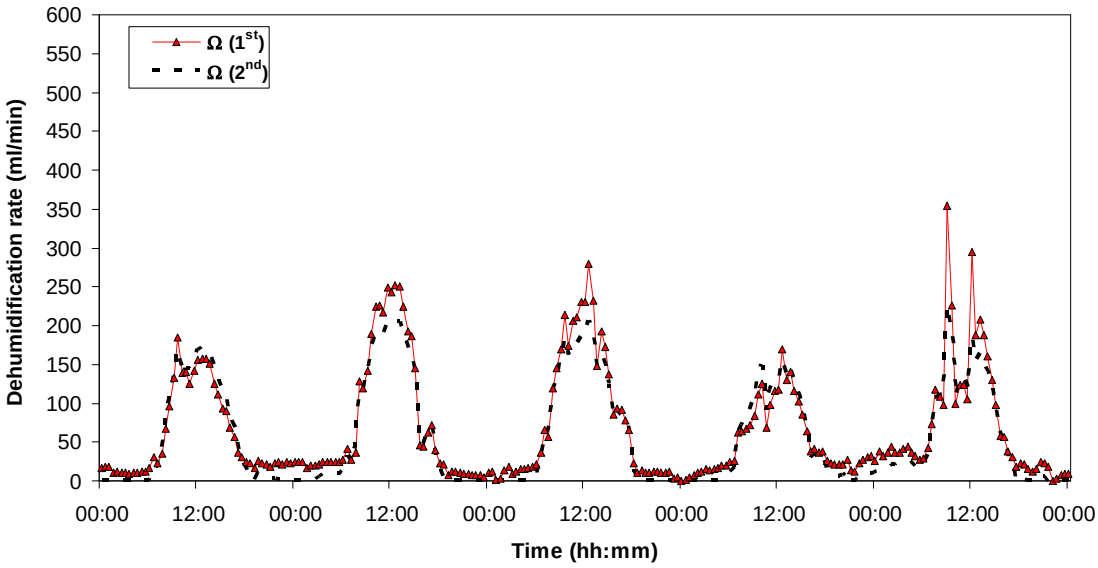

Fig. 6.14: The *dehumidification rate* Ω predicted with the 1st and 2nd methods when the greenhouse is not cultivated

simulation results show that there is no dehumidification taking place with the new setting. This is because the temperature of the air flowing through the dehumidifier and the *coolant temperature* are always higher than the *dew-point temperature of the inlet air* $T_{dp,ai}$ (see Fig. 6.15). Dehumidification is feasible with the ordinary setting of the HD greenhouse (see Sec. 6.2) because the *air temperature* T_a leaving the 1st humidifier is allowed to increase as it flows through the greenhouse microclimate. In addition to the increase in the *dry-bulb temperature of the air* T_a, its $T_{dp,ai}$ also increases. This increase causes the temperature differential necessary for the 2nd humidifier to work and also for dehumidification to take place. Thus, the absence of this temperature differential is the cause for not having dehumidification when the dehumidifier is located just after the 1st humidifier.

At the end of this chapter, it should be remembered that the simulation carried out for the HD greenhouse under different conditions was not validated against experimental results. Therefore, it is highly recommended to conduct validation experiments in order to understand the accuracy of the integrated model.

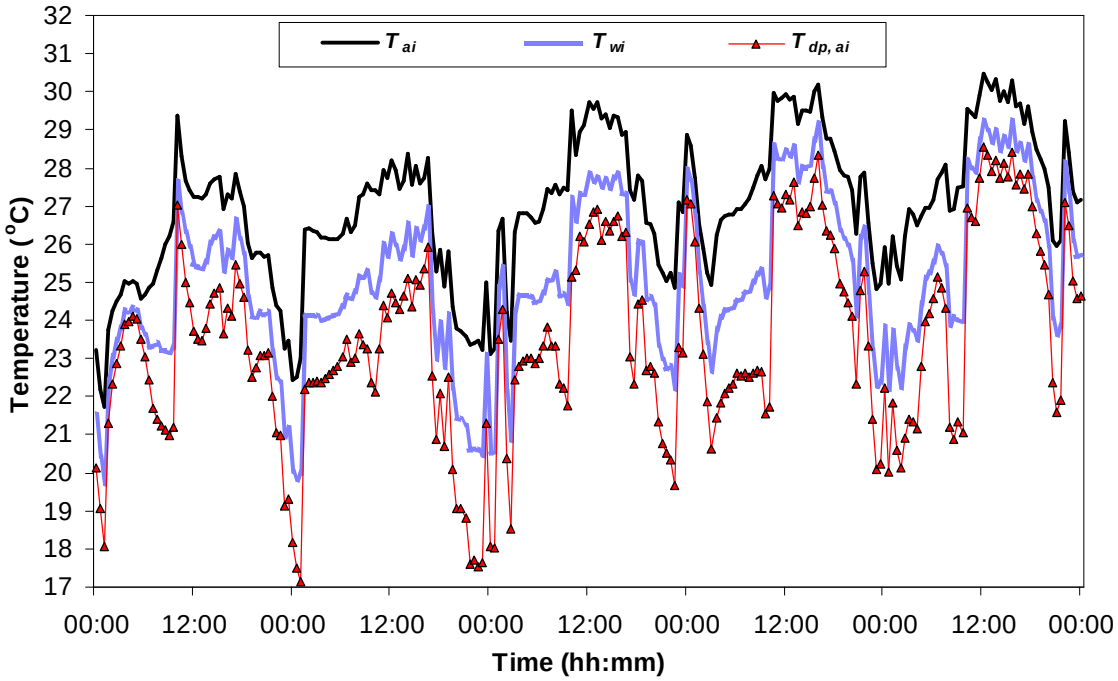

Fig. 6.15: The *inlet air temperature* T_{ai} and *dew-point* $T_{dp,ai}$ with the *inlet water temperature* T_{wi} of the dehumidifier when it is placed just after the 1st humidifier

CHAPTER SEVEN

7. CONCLUSIONS AND RECOMMENDATIONS

This chapter is divided into two sections; main conclusions drawn from this research study (Sec. 7.1) and recommendations for future work (Sec. 7.2).

7.1. MAIN CONCLUSIONS FROM THIS STUDY

This section presents the main conclusions that can be drawn about the HD greenhouse simulation model. These conclusions overview the development of the three sub-models making up the integrated model, their validation experiments, accuracy of each sub-model based on the experimental results and finally a general summary about the integrated model. The three sub-models are the humidifier sub-model, the greenhouse microclimate sub-model and the dehumidifier sub-model.

1. The accuracy of the humidifier sub-model to predict the *outlet air* and *water temperatures* was very good. Its accuracy to predict the *outlet humidity ratio* was extremely good. However, the unexpected small discrepancy of the predicted *outlet water temperature* was attributed to the nearness between the *wet-bulb temperature of the air* and the *water temperatures*. Also, the unexpected positive *predictive error* of the *outlet air temperature* was attributed to two causes; the involvement of the predicted *outlet water temperature* that was associated with small discrepancy and to the way of measuring the *outlet air temperature*
2. The microclimate sub-model accurately predicted the *air temperature* and *humidity ratio* of a point 20 m away from the point where the input data were collected. However, the small difference between the observed and predicted *air temperature* was attributed to the non-horizontal air flow pattern through the greenhouse microclimate; and

the small difference between the observed and predicted *humidity ratio* was due to the air flow pattern and due to the exclusion of the soil-water evaporation from the simulation

3. The dehumidifier sub-model was accurately predicting when dehumidification (condensation) would occur. Also, the two methods used to predict the *dehumidification rate* were showing good accuracy when used within the calibrated range. At times when there was no dehumidification, the accuracy of the dehumidifier sub-model to predict the *outlet air temperature* and *humidity ratio* and the *outlet water temperature* was very good. However, the sub-model was under-predicting the *outlet humidity ratio* at high *dehumidification rates*. The involvement of the under-predicted *humidity ratio* in the simulation equations then caused a small inaccuracy of the *outlet air* and *water temperatures*. The non-horizontal air flow pattern through the dehumidifier was also contributing to the small discrepancy between the predicted and observed values
4. Although the simulation results of the integrated HD greenhouse model could not yet be validated yet, they were in good agreement with the expected results. The integrated model can be used to study the influence of different design and operational input variables on the main processes of the HD greenhouse and to optimise processes such as the evaporation taking place in the humidifiers and dehumidification taking place in the dehumidifier. However, further validation of the individual models and the integrated model is important.

7.2. RECOMMENDATIONS FOR FUTURE WORK

Development of the integrated HD greenhouse model, presented in this study, is an important step forward towards improving the performance of HD greenhouses. But the model still requires further investigations to evaluate and, if necessary, to improve its accuracy.

It is therefore highly recommended to use the HD greenhouse located in Oman to study the accuracy of the HD greenhouse model in its integrated format. In this proposed study, different design (e.g. configuration of the humidifiers and dehumidifier) and operational (e.g. *air* and *water flowrates* through the humidifiers and dehumidifier) parameters should be investigated. For this study, the following recommendations should also be considered:

1. In order to avoid any possible errors in measuring the *outlet temperature of the air* leaving the humidifier(s), more than one sensor should be used to monitor the *outlet air temperature*. They should be arranged in a vertical profile and their measurements should be averaged
2. In order to study the model's capability to predict the *air temperature* and *humidity* gradients through the greenhouse microclimate, the number of monitoring points should be at least two, excluding the point where the input simulation data are collected
3. To avoid the measurement inaccuracy caused by the non-uniform air flow pattern through the greenhouse microclimate, several sensors should be used in a vertical profile at each monitoring point and their measurements should be averaged
4. Similarly, to reduce the measurement inaccuracy resulting from the non-uniform air flow pattern through the dehumidifier, several sensors should be used in a vertical profile at the inlet and outlet of the dehumidifier
5. The accuracy of the empirical correlations used to predict the dehumidifier *performance factor, outlet humidity ratio* and *dehumidification rate* should be enhanced by running experiments to generate additional data and then re-calculating the correlations. In these experiments, the operational input variable (e.g. *air* and *water flowrates*, *inlet air temperature* and *humidity* and *inlet water temperature*) should be varied to enable the revised correlations to cover a broader range of operating conditions.

REFERENCES

Abdellatif, S. M. (1993). Air relative humidity affecting effectiveness of evaporative cooling system under hot and humid conditions. In: *Energy Conversion Engineering Conference*, August 8-13, Atlanta, Georgia: 2.13-2.18.

Abdel-Rahman, H. A. (1996). Traditional systems application of modern irrigation techniques in the Sultanate of Oman. *Agricultural Mechanization in Asia, Africa and Latin America*, 27(1): 41-45.

Adelard, L., Pignolet-Tardan, F., Mara, T., Lauret, P., Garde, F. and Boyer, H. (1998). Sky temperature modelisation and applications in building simulation. *Renewable Energy*, 15(1-4): 418-430.

Al-Ajmi, H. A. and Abdel-Rahman, H. A. (2001). Water management intricacies in the Sultanate of Oman: The augmentation-conservation conundrum. *Water International*, 26(1): 68-79.

Al-Ismaili, A. M. (2003). *Modification of a Quonset greenhouse to a humidification-dehumidification system: Design, construction and pilot testing*. Unpublished MSc. Thesis, Sultan Qaboos University, Muscat, Oman.

Allen, R. G., Pereira, L. S., Raes, D. and Smith, M. (1998). *Crop evapotranspiration: Guidelines for computing crop water requirement*. FAO Irrigation and Drainage Paper 56. Food and Agriculture Organization of the United Nations, Rome.

Allen, R. G., Pruitt, W. O., Wright, J. L., Howell, T. A., Ventura, F., Snyder, R., Itenfisu, D., Steduto, P., Berengena, J., Yrisarry, J. B., Smith, M., Pereira, L. S., Raes, D., Perrier, A., Alves, I., Walter, I. and Elliott, R. (2006). A recommendation on standardized surface resistance for hourly calculation

of reference ET_o by the FAO56 Penman-Monteith method. *Agricultural Water Management*, 81(1-2): 1-22.

ASHRAE (2001). *Fundamentals Handbook (SI)*. American Society of Heating, Refrigerating, and Air-conditioning Engineering, New York.

ASHRAE (2004). *HVAC Systems and Equipment (SI)*. American Society of Heating, Refrigerating, and Air-conditioning Engineering, New York.

Avissar, R. and Mahrer, Y. (1982). Verification study of a numerical greenhouse microclimate model. *Transactions of the ASAE*, 25(6): 1711-1720.

Bailey, B. J. (1990). The environment in evaporatively cooled greenhouses. *Acta Horticulturae*, 287: 59-66.

Bailey, B. J. and Raoueche, A. (1998). Design and performance aspects of a water producing greenhouse cooled by seawater. In: *International symposium on water quality and quantity in greenhouse horticulture,* November 05-08, 1996, Tenerife, Spain: 311-315.

Baille, A. (1989). Greenhouse microclimate and its management in mild winter climates. *Acta Horticulturae*, 246: 23-36.

Bakker, J. C. (1991). Leaf conductance of four glasshouse vegetable crops as affected by air humidity. *Agricultural and Forest Meteorology*, 55: 23-36.

Baroon's Brae, D. W. R. (1991). Development in plastic structures and materials for horticultural crops. URL: http://www.agnet.org/library/eb/331/ [accessed: May 05, 2008].

Bartzanas, T., Boulard, T. and Kittas, C. (2002). Numerical simulation of the airflow and temperature distribution in a tunnel greenhouse equipped with insect-proof screen in the openings. *Computers and Electronics in Agriculture*, 34(1-3): 207-221.

Ben-Mehrez, M., Taconet, O., Vidal-Madjar, D. and Valencogne, C. (1992). Estimation of stomatal resistance and canopy evaporation during the HAPEX-MOBILHY experiment. *Agricultural and Forest Meteorology*, 58(3-4): 285-313.

Bernier, M. A. (1994). Cooling tower performance: Theory and experiments. *ASHRAE Transactions*, 100(2): 114-121.

Beshkani, A. and Hosseini, R. (2006). Numerical modeling of rigid media evaporative cooler. *Applied Thermal Engineering*, 26(5-6): 636-643.

Boodley, J. W. (1981). *The commercial greenhouse*. Delmar Publishers Inc., New York, USA.

Bot, G. P. A. (1980). Validation of a dynamical model of greenhouse climate. *Acta Horticulturae*, 106: 149-158.

Boulard, T. (1987). Preliminary results on the use of absorbent materials for greenhouse air dehumidification. In: *French Israeli symposium on greenhouse technology*, December 7-11, Shefayim and Bet Dagan, Israel: 47-50.

Boulard, T. and Baille, A. (1993). A simple greenhouse climate control model incorporating effects of ventilation and evaporative cooling. *Agricultural and Forest Meteorology*, 65: 145-157.

Boulard, T., Baille, A., Lagier, J. and Mermier, M. (1989). Water vapour transfers and dehumidification in a inflatable plastic greenhouse. *Acta Horticulturae*, 245: 462-469.

Boulard, T. and Wang, S. (2002). Experimental and numerical studies on the heterogeneity of crop transpiration in a plastic tunnel. *Computers and Electronics in Agriculture*, 34(1-3): 173-190.

Brundrett, G. W. (1987). *Handbook of dehumidification technology*. Anchor Brendon Ltd., Essex.

Bucklin, R.A., Leary, J.D., McConnell, D.B. & Wilkerson , E.G. (1993) [last update: 11/2004]. Fan and pad greenhouse evaporative cooling systems (IFAS Extension Circular#1135, UF/IFAS). URL: http://edis.ifas.ufl.edu /ae069 [accessed: August 05, 2008].

Camargo, J. R., Ebinuma, C. D. and Cardoso, S. (2003). A mathematical model for direct evaporative cooling air conditioning system. *Engenharia Termica*, 4: 30-34.

Camargo, J. R., Ebinuma, C. D. and Silveira, J. L. (2005). Experimental performance of a direct evaporative cooler operating during summer in a Brazilian city. *International Journal of Refrigeration*, 28: 1124-1132.

Campen, J. B. and Bot, G. P. A. (2003). Determination of greenhouse-specific aspects of ventilation using three-dimensional computational fluid dynamics. *Biosystems Engineering*, 84(1): 69-77.

Cengel, Y. A. and Boles, M. A. (1988). *Thermodynamics: An engineering approach*, 3rd ed. The McGraw-Hill Companies, Inc., New York, USA.

Chaibi, M. T. (2000). An overview of solar desalination for domestic and agriculture water needs in remote arid areas. *Desalination*, 127(2): 119-133.

Chalabi, Z. S. and Bailey, B. J. (1989). *Simulation of the energy balance in a greenhouse*. Divisional note D. N. 1516, AFRC Silsoe Research Institute, Silsoe, UK.

Chalabi, Z. S. and Bailey, B. J. (1991). Sensitivity analysis of a non-steady state model of the greenhouse microclimate. *Agricultural and Forest Meteorology*, 56(1-2): 111-127.

Chamont, S., Strainchamps, D. and Thunot, S. (1995). Short- and long-term stomatal responses to fluctuations in environment in Southern European greenhouses. *Annals of Botany*, 75: 39-47.

Chandra, P., Albright, L. D. and Scott, N. R. (1981). A time dependent analysis of greenhouse thermal environment. *Transactions of the ASAE*, 24: 442-449.

Chen, C. (2003). Prediction of longitudinal variation in temperature and relative humidity for evaporative cooling greenhouse. *Agricultural Engineering Journal*, 12(3&4): 143-164.

Condori, M. and Saravia, L. (2003). Analytical model for the performance of the tunnel-type greenhouse drier. *Renewable Energy*, 28(3): 467-485.

Cooper, P. I. and Fuller, R. J. (1983). A transient model of the interaction between crop, environment and greenhouse structure for predicting crop yield and energy consumption. *Journal of Agricultural Engineering Research*, 28(5): 401-417.

Czarick, M. and Lacy, M. (1996). How much evaporative cooling pad is needed? *Poultry Digest*, 55(5): 10-12.

Davies, P. A. and Paton, C. (2005). The seawater greenhouse in the United Arab Emirates: Thermal modelling and evaluation of design options. *Desalination*, 173(2): 103-111.

Davies, P., Turner, K. and Paton, C. (2004). Potential of the seawater greenhouse in Middle Eastern climates. In: *Proc. International Engineering Conference Mutah 2004*, April 26-28, Mutah University, Jordan: 523-540.

Delyannis, E. and Belessiotis, V. (2000). Solar desalination for remote arid zones. In: *Water management, purification & conservation in arid climates, Volume 2: Water purification*, edited by Goosen, M. F. A. and Shayya, W. H. Technomic Publishing Company, Inc., Pennsylvania: 297-330.

Dowdy, J. A. and Karabash, N. S. (1987). Experimental determination of heat and mass transfer coefficients in rigid impregnated cellulose evaporative media. *ASHRAE Transactions*, 93(2): 382-395.

Duncan, G. A., Loewer, J., O. J. and Colliver, D. G. (1981). Simulation of energy flows in a greenhouse: Magnitudes and conservation potential. *Transactions of the ASAE*, 24: 1014-1021.

Esmay, M. L. and Dixon, J. E. (1986). *Environmental control for agricultural buildings*. AVI Publishing Company, New York.

Ewen, L. S., Walker, J. N. and Buxton, J. W. (1980). Environment in a greenhouse thermally buffered with ground-conditioned air. *Transactions of the ASAE*, 23: 985-989, 993.

Fang, W. (1995). Greenhouse cooling in subtropical regions. *Acta Horticulturae*, 399: 37-48.

Fatnassi, H., Boulard, T., Poncet, C. and Chave, M. (2006). Optimisation of greenhouse insect screening with computational fluid dynamics. *Biosystems Engineering*, 93(3): 301-312.

Feuilloley, P. and S. Guillaume. 1990. Heat pumps. A method of controlling excessive humidity in greenhouses. *Bulletin Technique du Machinisme et de l'Equipement Agricoles*. 54: 9-18.

Floriculture Factsheet (1994). Understanding humidity control in greenhouses, (File#400-5, Ministry of Agriculture, Fisheries and Food, British Columbia). URL: http://www.agf.gov.bc.ca/ornamentals/floriculture/humidity.pdf [accessed: August 05, 2008].

Froehlich, D. P., Albright, L. D., Scott, N. R. and Chandra, P. (1979). Steady-periodic analysis of greenhouse thermal environment. *Transactions of the ASAE*, 22: 387-399.

Fujii, T. (1991). *Theory of laminar film condensation*. Springer-Verlag New York Inc., New York.

Fuller, R. J., Meyer, C. P. and Sale, P. J. M. (1987). Validation of a dynamic model for predicting energy use in greenhouses. *Journal of Agricultural Engineering Research*, 38: 1-14.

Garzoli, K. and Blackwell, J. (1973). The response of a glasshouse to high solar radiation and ambient temperature. *Journal of Agricultural Engineering Research*, 18: 205-216.

Glanz, D. J. and G. T. Orlob (1973). *Lincolon Lake ecologic study*. Water resources engineering report (DACW27-73-C0064).

Goosen, M. F. A., Al-Hinai, A., H. and Sablani., S. (2000a). Capacity building strategies for desalination: Activities, facilities and educational programs in Oman. In: *Proc. EUROMED 2000: Desalination strategies in South Mediteranean Countries*, September 11-13, Jerba.

Goosen, M. F. A., Sablani, S. S., Shayya, W. H., Paton, C. and Al-Hinai, H. (2000b). Thermodynamic and economic considerations in solar desalination. *Desalination*, 129(1): 63-89.

Goosen, M. F. A., Sablani, S. S., Paton, C., Perret, J., Al-Nuaimi, A., Haffar, I., Al-Hinai, H. and Shayya, W. H. (2003). Solar energy desalination for arid coastal regions: development of a humidification-dehumidification seawater greenhouse. *Solar Energy*, 75(5): 413-419.

Grimson, E. D. (1937). Correlation and utilization of new data on flow resistance and heat transfer for cross flow of gases over tube banks. *Transactions of the ASME*, 59: 583-594.

Haberman, W. L. and John, J. E. A. (1989). *Engineering thermodynamics with heat transfer*, 2nd ed. Allyn and Bacon, Massachusetts.

Halasz, B. (1998). A general mathematical model of evaporative cooling devices. *Revue Generale De Thermique*, 37(4): 245-255.

Halasz, B. (1999). Application of a general non-dimensional mathematical model to cooling towers. *International Journal of Thermal Sciences*, 38(1): 75-88.

Halasz, B. (2000). A single mathematical model for all kinds of heat exchangers. In: *Proc. 3rd European Thermal Sciences Conference*, September 10-13, Heidelberg, Germany: 1089-1094.

Halasz, B. (2007). Air washer as a means of air conditioning. In: *22nd International Congress of Refrigeration, August 21-26,* Beijing, China.

Hatfield, J. L. and Burke, J. J. (1991). Energy exchange and leaf temperature behaviour of three plant species. *Environmental and Experimental Botany*, 31(3): 295-302.

Hausen, H. (1943). Darstellung des warmeuberganges in rohern durch verallgemeinerte potenzbeziehungen. *Z. VDI-Beiheft Verfahrenstechnic*, 4: 91-98.

Hausen, H. (1983). *Heat transfer in counter flow, parallel flow and cross flow*. McGraw-Hill, New York.

Henderson-Sellers, B. (1984). A new formula for latent heat of vaporization of water as a function of temperature. *Quarterly Journal of the Royal Meteorological Society*, 110: 1186-1190.

Huang, F. F. (1988). *Engineering thermodynamics: Fundamentals and applications*, 2nd ed. Macmillan Publishing Company, New York.

Jarvis, W. R. (1992). *Managing diseases in greenhouse crops*. The American Phytopathological Society, St. Paul, Minnesota, USA.

Jensen, M.E., Burman, R.D. and Allen, R.G. (1990). Evaporation and irrigation water requirements. ASCE Manuals and Reports on Engineering Practices No. 70, American Society of Civil Engineers, New York.

Jolliet, O. (1994). HORTITRANS, a model for predicting and optimizing humidity and transpiration in greenhouses. *Journal of Agricultural Engineering Research*, 57(1): 23-37.

Jolliet, O. and Bailey, B. J. (1992). The effect of climate on tomato transpiration in greenhouses: Measurements and models comparison. *Agricultural and Forest Meteorology*, 58(1-2): 43-62.

Jones, J. B. and Hawkins, G. A. (1986). *Engineering thermodynamics: An introductory textbook*. Jones Wiley & Sons, Inc., New York.

Kairouani, L., Hassairi, M. and Tarek, Z. (2004). Performance of cooling tower in south of Tunisia. *Building and Environment*, 39(3): 351-355.

Kakac, S., Bergles, A.E., Mayinger, F. & Yuncu, H. (eds.) (1999). *Heat transfer enhancement of heat exchangers*. Kluwer Academic Publishers, Netherlands.

Kano, A. and Salder, E. J. (1985). Survey of greenhouse models. *Journal of Agricultural Meteorology*, 41(1): 75-81.

Khalil, A. (1995). Optimum utilization of solar energy in greenhouses. *American Society of Mechanical Engineers, Petroleum Division*, 66: 131-135.

Kim, K., Yoon, J., Kwon, H., Han, J., Eek-Son, J., Nam, S., Giacomelli, G. A. and Lee, I. (2008). 3-D CFD analysis of relative humidity distribution in greenhouse with a fog cooling system and refrigerative dehumidifiers. *Biosystems Engineering*, 100(2): 245-255.

Kimball, B. A. (1973). Simulation of the energy balance of a greenhouse. *Agricultural Meteorology*, 11: 243-260.

Kindelan, M. (1980). Dynamic modeling of greenhouse environment. *Transactions of the ASAE*, 23: 1232-1239.

Kitano, M. and Eguchi, H. (1989). Dynamic analysis of stomatal responses by an improved method of leaf heat balance. *Environmental and Experimental Botany*, 29(2): 175-185.

Kittas, C., Bartzanas, T. and Jaffrin, A. (2001). Greenhouse evaporative cooling: Measurement and data analysis. *Transactions of the ASAE*, 44(3): 683-689.

Kittas, C., Bartzanas, T. and Jaffrin, A. (2003). Temperature gradients in a partially shaded large greenhouse equipped with evaporative cooling pads. *Biosystems Engineering*, 85(1): 87-94.

Langhans, R. W. (1990). *Greenhouse management*, 3rd ed. Halcyon Press of Ithaca, Ithaca, New York.

Levit, H. J. and Gaspar, R. (1988). Energy budget for greenhouses in humid-temperate climate. *Agricultural and Forest Meteorology*, 42(2-3): 241-254.

Liao, C. and Chiu, K. (2002). Wind tunnel modeling the system performance of alternative evaporative cooling pads in Taiwan region. *Building and Environment*, 37(2): 177-187.

Liao, C. M., Singh, S. and Wang, T. S. (1998). Characterizing the performance of alternative evaporative cooling pad media in thermal environmental control applications. *Journal of Environmental Science and Health, Part A: Environmental Science and Engineering and Toxic and Hazardous Substance Control*, 33(7): 1391-1417.

Lovichit, W., C. Kubota, C. Y. Choi and J. Schoonderbeek (2007). *Greenhouse water recovery system for crop production in semi-arid climate*. An ASABE meeting presentation (Paper Number: 074012), American Society of Agricultural and Biological Engineers, Michigan.

Luchow, K. and Zabeltitz, C. v. (1992). Investigation of a spray cooling system in a plastic-film greenhouse. *Journal of Agricultural Engineering Research*, 52: 1-10.

Maher, M. J. and O'Flaherty, T. (1973). An analysis of greenhouse climate. *Journal of Agricultural Engineering Research*, 18: 197-203.

Mangold, D. W., Bundy, D. S. and Hellickson, M. A. (1983). Psychrometrics. In: *Ventilation of agricultural structures*, edited by Hellickson, M. A., Walker, J. N. and Mich, S. J. ASAE monograph. No.6. XY/N-1: 9-22.

McClellan, C. H. (1985). Fundamentals and current practice for comfort evaporative cooling. In: *Proc. 1985 international symposium on moisture and humidity*, April 15-18, Instrument Society of America, North Carolina: 173-174.

Medrano, E., Lorenzo, P., Sánchez-Guerrero, M. C. and Montero, J. I. (2005). Evaluation and modelling of greenhouse cucumber-crop transpiration under high and low radiation conditions. *Scientia Horticulturae*, 105(2): 163-175.

Mistriotis, A. and Briassoulis, D. (2002). Numerical estimation of the internal and external aerodynamic coefficients of a tunnel greenhouse structure with openings. *Computers and Electronics in Agriculture*, 34(1-3): 191-205.

Mistriotis, A., Bot, G. P. A., Picuno, P. and Scarascia-Mugnozza, G. (1997a). Analysis of the efficiency of greenhouse ventilation using computational fluid dynamics. *Agricultural and Forest Meteorology*, 85(3-4): 217-228.

Mistriotis, A., Arcidiacono, C., Picuno, P., Bot, G. P. A. and Scarascia-Mugnozza, G. (1997b). Computational analysis of ventilation in greenhouses at zero- and low-wind-speeds. *Agricultural and Forest Meteorology*, 88(1-4): 121-135.

Moran, M. J. and Shapiro, H. N. (1992). *Fundamentals of engineering thermodynamics*, 2nd ed. John Wiley & Sons, Inc., New York.

Nelson, P. A. (1998). *Greenhouse operation and management*, 5th ed. Prentice-Hall, Inc., Upper Saddle River.

Nijskens, J., Deltour, J., Coutisse, S. and Nisen, A. (1984). Heat transfer through covering materials of greenhouses. *Agricultural and Forest Meteorology*, 33(2-3): 193-214.

Norton, T., Sun, D., Grant, J., Fallon, R. and Dodd, V. (2007). Applications of computational fluid dynamics (CFD) in the modelling and design of ventilation systems in the agricultural industry: A review. *Bioresource Technology*, 98(12): 2386-2414.

Ould-Khaoua, S. A., Bournet, P. E., Migeon, C., Boulard, T. and Chassériaux, G. (2006). Analysis of greenhouse ventilation efficiency based on computational fluid dynamics. *Biosystems Engineering*, 95(1): 83-98.

Paton, C. and Davis, P. (1996). The seawater greenhouse for arid lands. In: *Proc. Mediterranean conference on renewable energy sources for water production*, June 10-12, Santorini: 163-166.

Perret, J. S., Al-Ismaili, A. M. and Sablani, S. S. (2005). Development of a humidification-dehumidification system in a Quonset greenhouse for sustainable crop production in arid regions. *Biosystems Engineering*, 91(3): 349-359.

Price, D. R. and Peart, R. M. (1973). Simulation model to study the utilization of waste heat using a combination multiple reservoir and greenhouse complex. *Journal of Environmental Quality*, 2(2): 216-224.

Raoueche, A. (1997). *Seawater greenhouse for arid lands*. unpublished PhD thesis, Cranfield University, Bedford, UK.

Raoueche, A., Bailey, B. and Stenning, B. (1996). Sensitivity analysis of the seawater greenhouse. In: *22nd WEDC Conference on reaching the*

unreached - Challenges for the 21st-Century, September 09-13, New Delhi, India, pp. 291-294.

Rawangkul, R., Khedari, J., Hirunlabh, J. and Zeghmati, B. (2008). Performance analysis of a new sustainable evaporative cooling pad made from coconut coir. *International Journal of Sustainable Engineering*, 1(2): 117-131.

Raznjevic, K. (1976). *Handbook of thermodynamic tables and charts*. Hemisphere Publishing Corporation, USA.

Reichrath, S. and Davies, T. W. (2002). Computational fluid dynamics simulations and validation of the pressure distribution on the roof of a commercial multi-span Venlo-type glasshouse. *Journal of Wind Engineering and Industrial Aerodynamics*, 90(3): 139-149.

Sablani, S. S., Goosen, M. F. A., Paton, C., Shayya, W. H. and Al-Hinai, H. (2003). Simulation of fresh water production using a humidification-dehumidification seawater greenhouse. *Desalination*, 159(3): 283-288.

Sauer, H. J. and Howell, R. H. (1983). *Heat pump systems*. John Wiley & Sons, Inc., New York.

Seginer, I. (2002). The Penman-Monteith evapotranspiration equation as an element in greenhouse ventilation design. *Biosystems Engineering*, 82(4): 423-439.

Seginer, I. (1994). Transpirational cooling of a greenhouse crop with partial ground cover. *Agricultural and Forest Meteorology*, 71(3-4): 265-281.

Selcuk, M. K. and Tran, V. V. (1975). Solar stills for agricultural purposes. *Solar Energy*, 17(2): 103-109.

Shklyar, A. and Arbel, A. (2004). Numerical model of the three-dimensional isothermal flow patterns and mass fluxes in a pitched-roof greenhouse.

Journal of Wind Engineering and Industrial Aerodynamics, 92(12): 1039-1059.

Stanger, G. (1985). Coastal salinization: A case history from Oman. *Agricultural Water Management*, 9: 269-286.

Stanghellini, C. (1987) *Transpiration of greenhouse crops: An aid to climate management*. Published PhD Thesis, Wageningen Agricultural University.

Stanghellini, C. and van Meurs, W. T. (1992). Environmental control of greenhouse crop transpiration. *Journal of Agricultural Engineering Research*, 51: 297-311.

Strobel, B. R., Stowell, R. R. and Short, T. H. (1999). Evaporative cooling Pads: Use in lowering indoor air temperature, (Ohio State University Fact Sheet No. AEX-127-99). URL: http://ohioline.osu.edu/aex-fact/0127.html [accessed: May 04, 2009].

Swinbank, W. F. (1963). Long-wave radiation from clear skies. *Quarterly Journal of the Royal Meteorological Society*, 89(381): 339-348.

Takakura, T., Jordan, K. A. and Boyd, L. L. (1971). Dynamic simulation of plant growth and environment in the greenhouse. *Transactions of the ASAE*, 14: 964-971.

The Engineering Toolbox (2005). URL: http://www.engineeringtoolbox.com [accessed: May 03, 2009].

Trigui, M., Barrington, S. F. and Gauthier, L. (1999). Effects of humidity on tomato (Lycopersicon esculentum cv. Truss) water uptake, yield, and dehumidification cost. *Canadian Agricultural Engineering*, 41(3): 135-140.

Tunç, M. and Venart, J. E. S. (1984). Unsteady thermal behaviour on the greenhouse environment. *International Communications in Heat and Mass Transfer*, 11(3): 251-266.

USGR (2007) [last update: February 08, 2007]. Cooling pads, (U.S. Global Resources). URL: http://cooling-pads.usgr.com/cooling-pads.html [accessed: July 12, 2007].

von Elsner, B. (1980). Significant parameters for characterization of the ventilation and cooling of glasshouses. *Acta Horticulturae*, 107: 91-97.

von Elsner, B., Briassoulis, D., Waaijenberg, D., Mistriotis, A., von Zabeltitz, C., Gratraud, J., Russo, G. and Sauy-Cortes, R. (2000). Review of structural and functional characteristics of greenhouses in European Union countries, Part II: Typical designs. *Journal of Agricultural Engineering Research*, 75: 111-126.

Walker, J. N. (1965). Predicting temperatures in ventilated greenhouses. *Transactions of the ASAE*, 8: 445-448.

Weirsma, F. and Short, T. H. (1983). Evaporative cooling. In: *Ventilation of agricultural structures*, edited by Hellickson, M. A., Walker, J. N. and Mich, S. J. ASAE monograph. No.6. XY/N-1: 103-118.

Wolpert, A. (1962). Heat transfer analysis of factors affecting plant leaf temperature. Significance of leaf hair. *Plant Physiology*, 37(2): 113-120.

Yang, X., Short, T. H., Fox, R. D. and Bauerle, W. L. (1990). Transpiration, leaf temperature and stomatal resistance of a greenhouse cucumber crop. *Agricultural and Forest Meteorology*, 51: 197-209.

Zhang, H., Gates, R. S. and Colliver, D. G. (1997). Turing machine approach to solve psychrometric attributes. *Transactions of the ASAE*, 40(3): 823-831.

APPENDIX A: GREENHOUSES USED IN EXPERIMENTS

Section A.1: AES Greenhouse

The Quonset greenhouse (Fig. A1.1) located at the Agricultural Experimental Station (AES) of the Sultan Qaboos University, Oman (N 23^{o}38', E 58^{o}20', altitude 35 m) was used to run a set of experiments to test the accuracy of the non-dimensional model. This greenhouse is 20 m long, 9 m wide and 3 m high. It is covered by a 200 μm thick *polyethylene* sheet that makes an airtight structure. The greenhouse is evaporatively cooled using a pad-and-fan cooling system. A set of cooling pads are placed at one end of the greenhouse and the fans at the opposite end (see Fig. A1.2). The pads are wetted by spraying water on top of them. The water flows downward by gravity

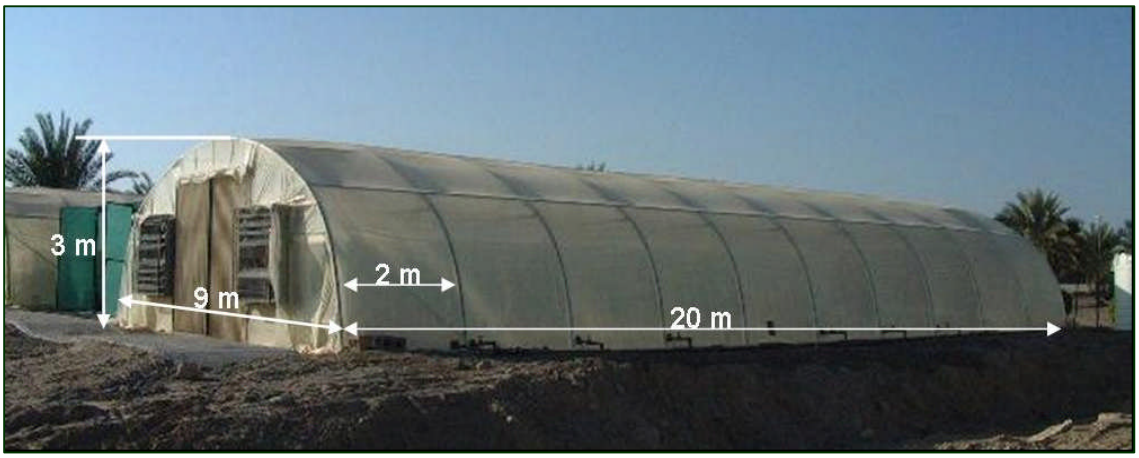

Fig. A1.1: The Quenset-type greenhouse located at AES

(a) (b)

Fig. A1.2: (a) The set of evaporative cooling pads at one side of the greenhouse and (b) the fans at the opposite side

and is then collected in a sump tank. This water is then circulated again to the top of the pads. The greenhouse is ventilated by the two fans which withdraw air through the wet pads. This results in an “evaporative cooling” of the air flowing to the greenhouse microclimate. Detailed description about this process is given in Sec. 2.1.2

The AES greenhouse is equipped with a fan-frequency regulator that enables the alteration of the air flowrate through the greenhouse. It is also equipped with a water flow meter and a return valve combination which makes varying the water flowrate to the evaporative cooling pads possible. In 2003, this greenhouse was used by an MSc student (Al-Ismaili, 2003) who designed and manufactured a metallic frame that can carry another set of evaporating pads (see Fig. A1.3). For the presence of all of these facilities, this greenhouse was chosen to run the experiments for testing the accuracy of the humidifier sub-model.

Fig. A1.3: The metallic frame carrying the 2nd set of evaporative cooling pads

Section A.2: Nizwa Greenhouse

Figure A2.1 shows the Quonset greenhouse (38 m long, 9.0 m wide and 3.2 m high) in which the experiments to test the accuracy of the microclimate sub-model were carried out. This greenhouse is owned by a farmer called Mr. Musappah Jumay'a whose farm has six more greenhouses. This farm is located in Nizwa, Oman (N 22^{o}59', E 57^{o}33', altitude 542 m). The common crop cultivated in the greenhouses is cucumber (see Fig. A2.2). Similar to most greenhouses in Oman, the Nizwa greenhouse is pad-and-fan evaporatively cooled. The microclimate sub-model incorporates an empirical relation to estimate the leaf resistance of cucumber as part of the calculation of the *latent heat of evapotraspiration* inside the greenhouse. Therefore, the reason for choosing the Nizwa greenhouse to run the experiments was the type of crop cultivated inside it as well as the type of greenhouse structure "Quonset".

Fig. A2.1: The Nizwa Quonset greenhouse

Fig. A2.2: Cucumber crop cultivated in the Nizwa greenhouse

Section A.3: HD Greenhouse

The humidification-dehumidification (HD) greenhouse (see Fig. A3.1) was built in 2004 in Al-Hail research site, Seeb, Oman (N 23°38', E 58°14', altitude 1 m). This greenhouse is well known as the "seawater" greenhouse (SWGH). It was built in a collaboration project between the idea inventor, Seawater Greenhouse Ltd., UK, and the Sultan Qaboos University, Oman. The HD greenhouse is only a few meters from the sea. The main purpose of this greenhouse is to desalinate seawater in an agricultural structure cultivated with a certain type of crop. The freshwater produced is to be used for irrigating the

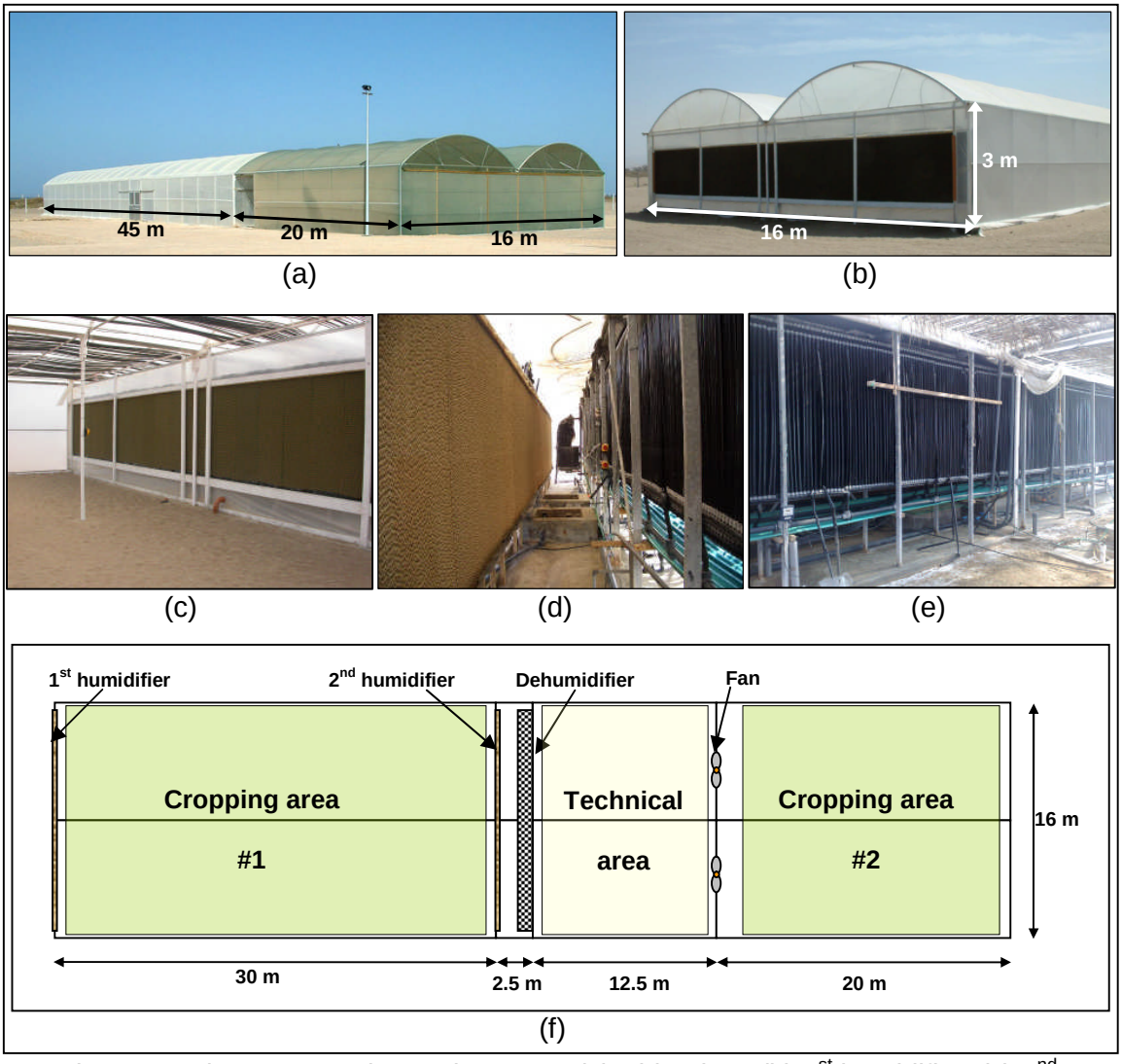

Fig. A3.1: The HD greenhouse in Oman; (a) Side-view, (b) 1st humidifier, (c) 2nd humidifier, (d) gap between 2nd humidifier and dehumidifier, (e) dehumidifier and (e) plan-illustration

cultivated crop. The greenhouse is divided into two cropping areas (see Fig. A3.1). The Cropping area #1 is evaporatively cooled by the 1st humidifier and the cropping area #2 is a shade area benefiting from the cool air leaving the cropping area #1 and the technical area. More details about the configuration, HD processes and water circulations of the HD greenhouse can be found in Sec. 2.1.

APPENDIX B: SENSING AND DATALOGGING EQUIPMENT

Table B.1 provides a detailed description of all instruments used in the experimental part of this study. The last column of this table indicates the experiments in which the correspondent instrument was used.

Table B.1: The instruments used in the experiments

Instrument Type	Model Number	Manufacturer	Description	Experiments*
Anemometer	HHF300A	Omega Engineering Inc., US	This is a handheld vane-type anemometer. Measuring range: 0.3 to 35 m/s (±0.25 % of reading)	A and B
Datalogger	DL2e	Delta-T Devices Ltd., UK	This datalogger can read from all sensors listed above. It is easily program and operated. It can accommodate up to 60 differential analogue or counter channels.	A, B and C
Ethernet interface module	FP-1601	National Instruments, US	It is used to connect the Field Point module reading data from the connected sensors to the PC.	B
Field point module	FP-TC-120 8-Ch	National Instruments, US	It is used to read from thermocouples. It can accommodate up to 8 thermocouples.	B
Leaf area meter	CI-202	CID Inc., US	It is used to measure the surface area of plant leaves. Resolution: 0.1 mm^2 Accuracy: ±1 % for samples >10 cm^2	B
Photodiode	ES2	Delta-T Devices Ltd., UK	It is used to measure the solar radiation heat flux. Measuring range: 0 to 2 kW/m^2 (±15 %)	A, B and C

* Letters A, B and C indicate the set of experiments conducted to test the accuracy of A: the humidifier sub-model, B: the microclimate sub-model and C: the dehumidifier sub-model

Table B.1: (cont.)

Instrument Type	Model Number	Manufacturer	Description	Experiments*
Temperature/Relative humidity sensor	RHT2nl	Delta-T Devices Ltd., UK	This is a dual sensor measuring the dry-bulb temperature of the air and the relative humidity. Two sensing elements are used to measure these two parameters and are working independently. Measuring range: $0 \leq T \leq 70^{o}$C ($\pm 0.1^{o}$C) $5\ \% \leq \varphi \leq 95\ \%$ ($\pm 2\ \%$ at 23^{o}C) $5\ \% > \varphi$ and $\varphi > 95\ \%$ ($\pm 2.5\ \%$ at 23^{o}C)	A, B and C
Thermistor probe	BT1	Delta-T Devices Ltd., UK	This probe can be used to measure the temperature of freshwater or even saline water since it is salt-resistant. Measuring range: -20 to 80^{o}C ($\pm 0.1^{o}$C)	A and C
Tipping bucket gauge	RG1	Delta-T Devices Ltd., UK	It can be used to measure the rainfall depth or the number of tips its bucket makes in a certain period of time. The datalogger to which the gauge is connected can be programmed to give one of these output types. In this study, the latter was used. Each tip is equivalent to 0.2 mm. Measuring range: 0.2 to 500 mm/hr.	C
Type-T Thermocouple	TT-T-22S-SLE	Omega Engineering Inc., US	This type of thermocouples is made up of a copper wire and a constantan wire. Maximum temperature: 260^{o}C (deviation of less than 0.16^{o}C at 100^{o}C)	B

* Letters A, B and C indicate the set of experiments conducted to test the accuracy of A: the humidifier sub-model, B: the microclimate sub-model and C: the dehumidifier sub-model

APPENDIX C: ADDITIONAL INFORMATION AND RESULTS

Section C.1: Air and Water Properties

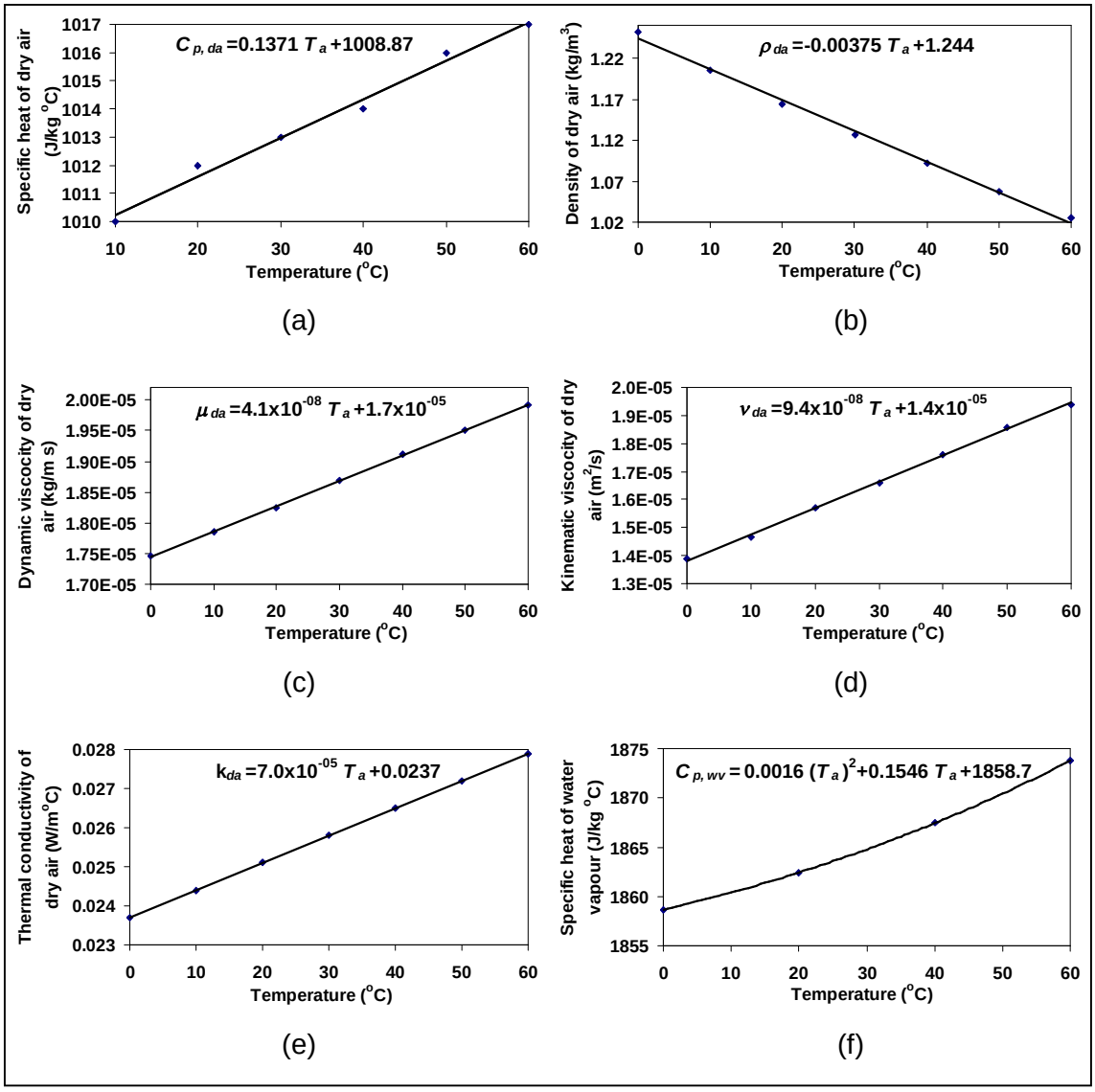

Fig. C1.1: Mathematical relations of (a) *specific heat* $C_{p,da}$, (b) *density* ρ_{da}, (c) *dynamic viscosity* μ_{da}, (d) *kinematic viscosity* ν_{da}, (e) *thermal conductivity* k_{da} *of dry air* as a function of *air temperature* T_a (plotted from data obtained from; Razenjevic, 1976) and (f) *specific heat of water vapour* $C_{p,wv}$ as a function of *air temperature* T_a (plotted from data obtained from; The Engineering Toolbox, 2005)

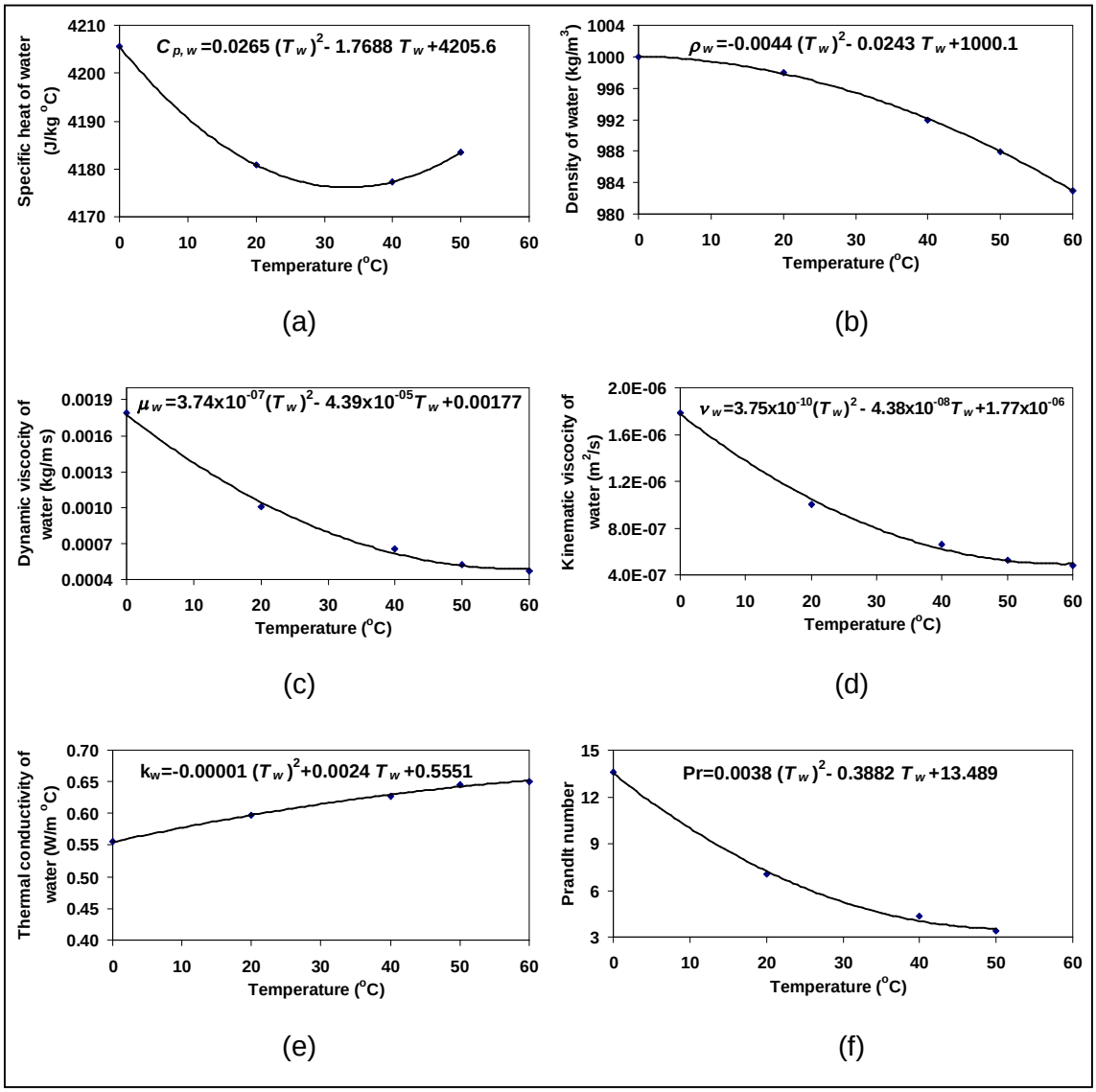

Fig. C1.2: Mathematical relations of (a) *specific heat* $C_{p,w}$, (b) *density* ρ_w, (c) *dynamic viscosity* μ_w, (d) *kinematic viscosity* ν_w, (e) *thermal conductivity* k_w and (f) Prandlt number Pr of water as a function of *water temperature* T_w (plotted from data obtained from; Razenjevic, 1976)

Section C.2: Microclimate Simulation Sub-model

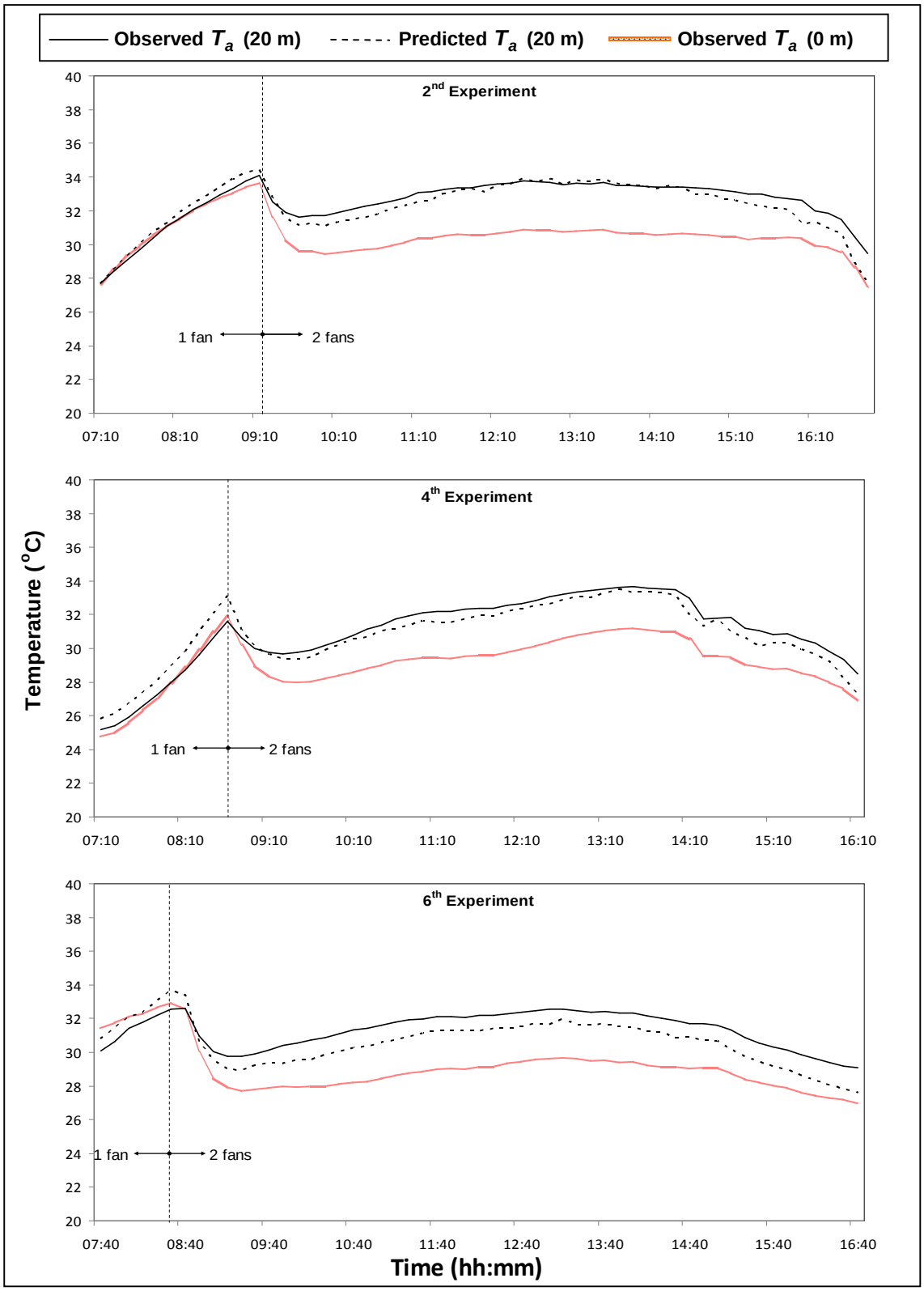

Fig. C2.1: Observed and predicted *air temperature* T_a at 20 m (from the position of the 1st temperature/relative humidty sensor) with the observed *air temperature* T_a at 0 m (by the 1st sensor) of the 2nd, 4th and 6th experiments

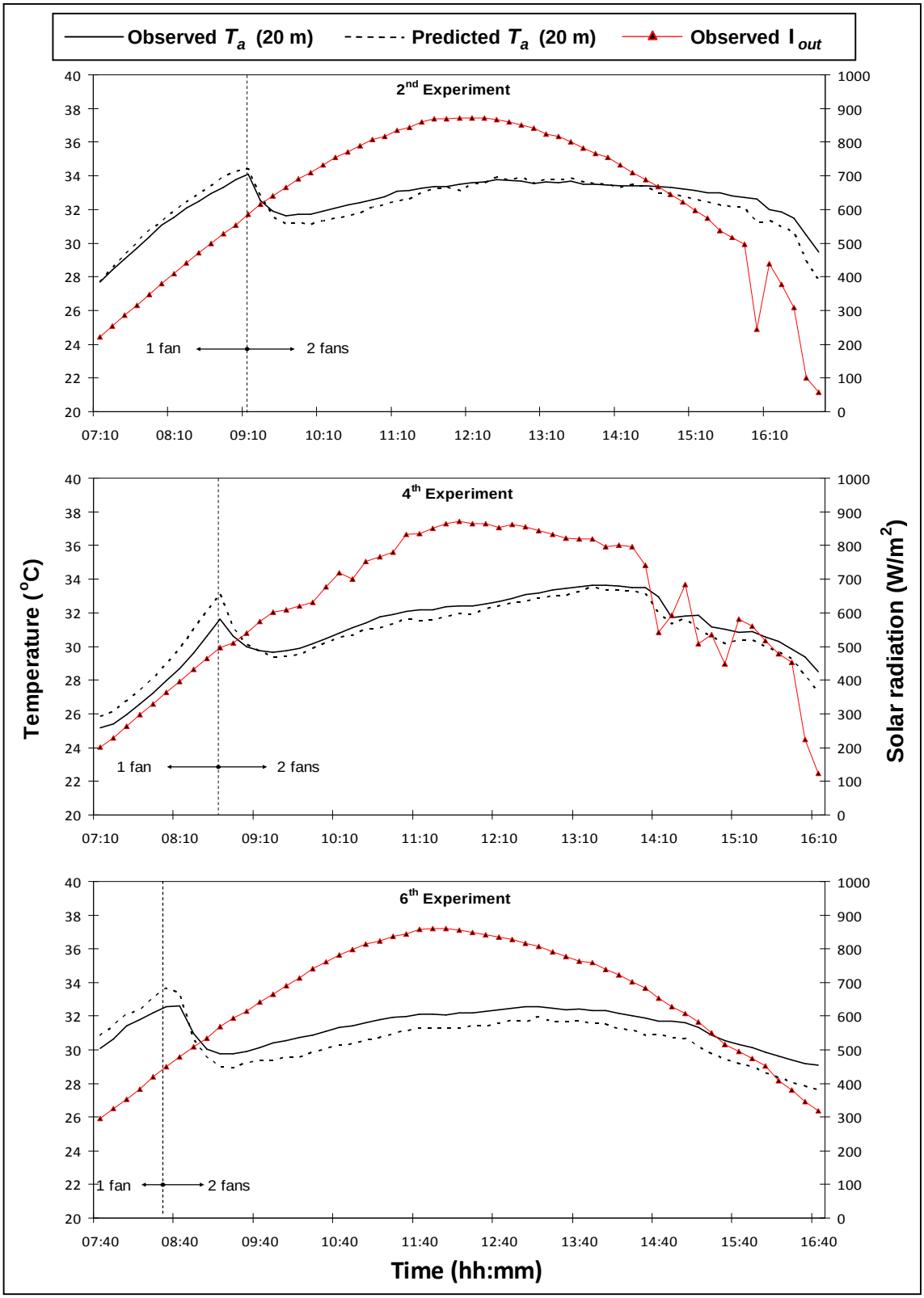

Fig. C2.2: Observed and predicted *air temperature* T_a at 20 m (from the position of the 1st temperature/relative humidity sensor) with the observed *outside solar radiation* I_{out} of the 2nd, 4th and 6th experiments

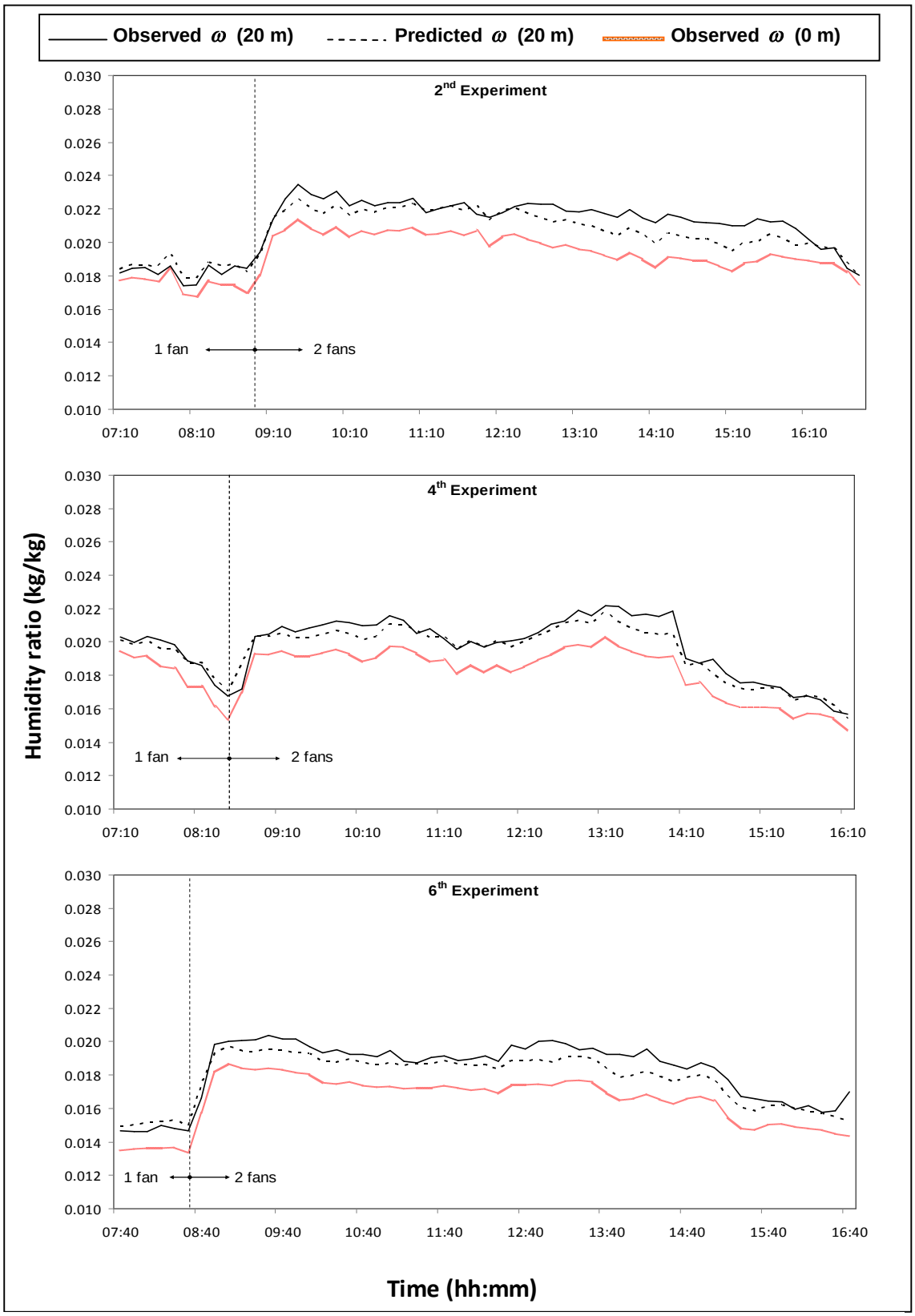

Fig. C2.3: Observed and predicted *humidity ratio* ω at 20 m (from the position of the 1st temperature/relative humidity sensor) with the observed *outside solar radiation* I_{out} of the 2nd, 4th and 6th experiments

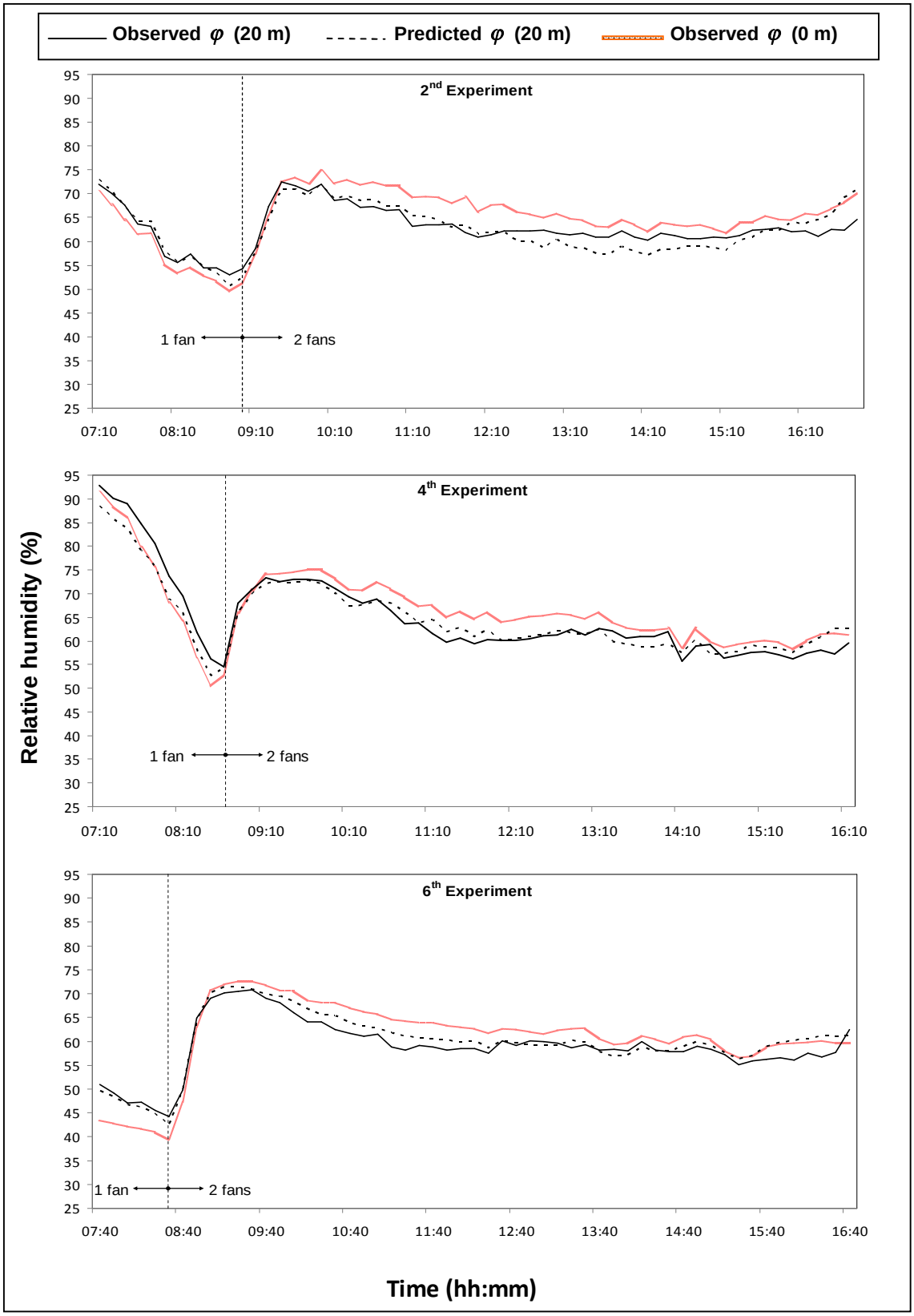

Fig. C2.4: Observed and predicted *relative humidity* φ at 20 m (from the position of the 1st temperature/relative humidity sensor) with the observed *relative humidity* φ at 0 m (by the 1st sensor) of the 2nd, 4th and 6th experiments

Section C.3: Dehumidifier Simulation Sub-model

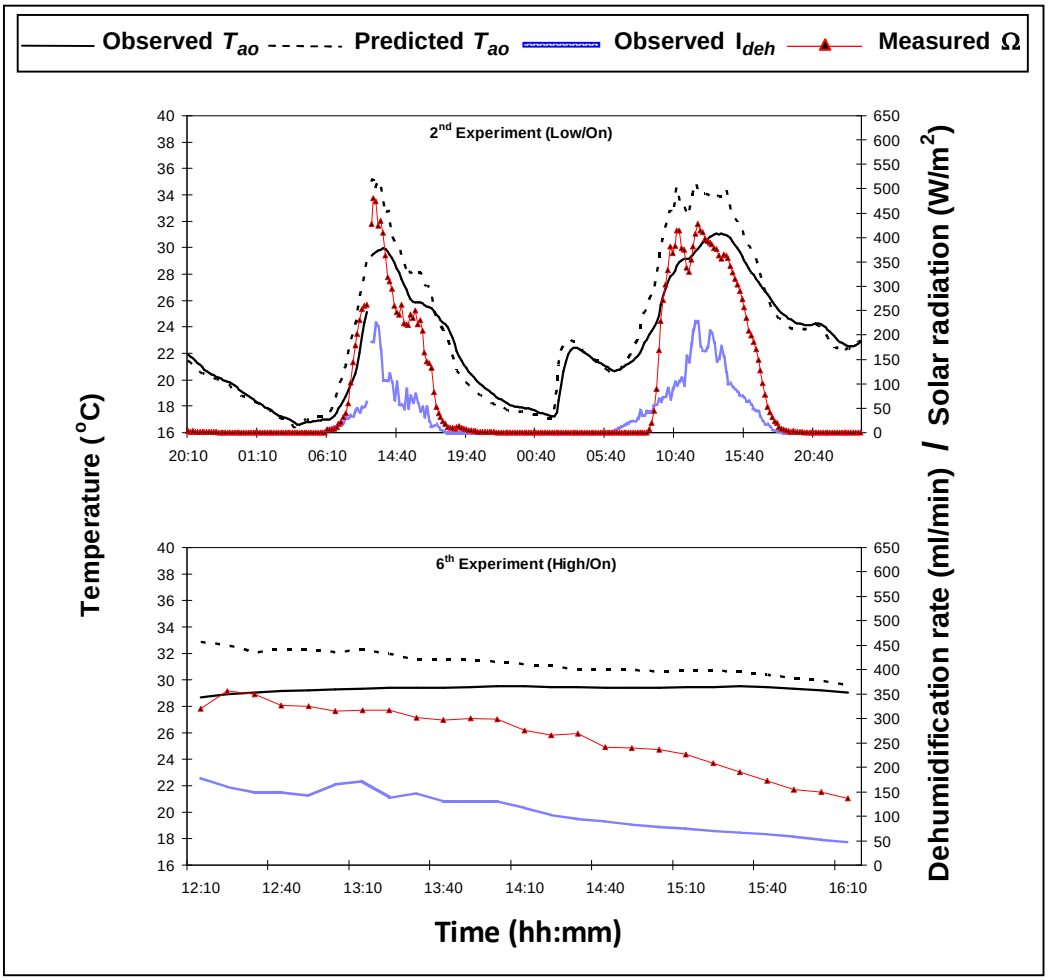

Fig. C3.1: Observed and predicted *outlet air temperature* T_{ao} with the observed *solar heat flux on dehumidifier* I_{deh} and the measured *dehumidification rate* Ω of the 2nd and 6th experiments

(High/Low: refers to air flowrate and On/Off: refers to operating status of humidifier)

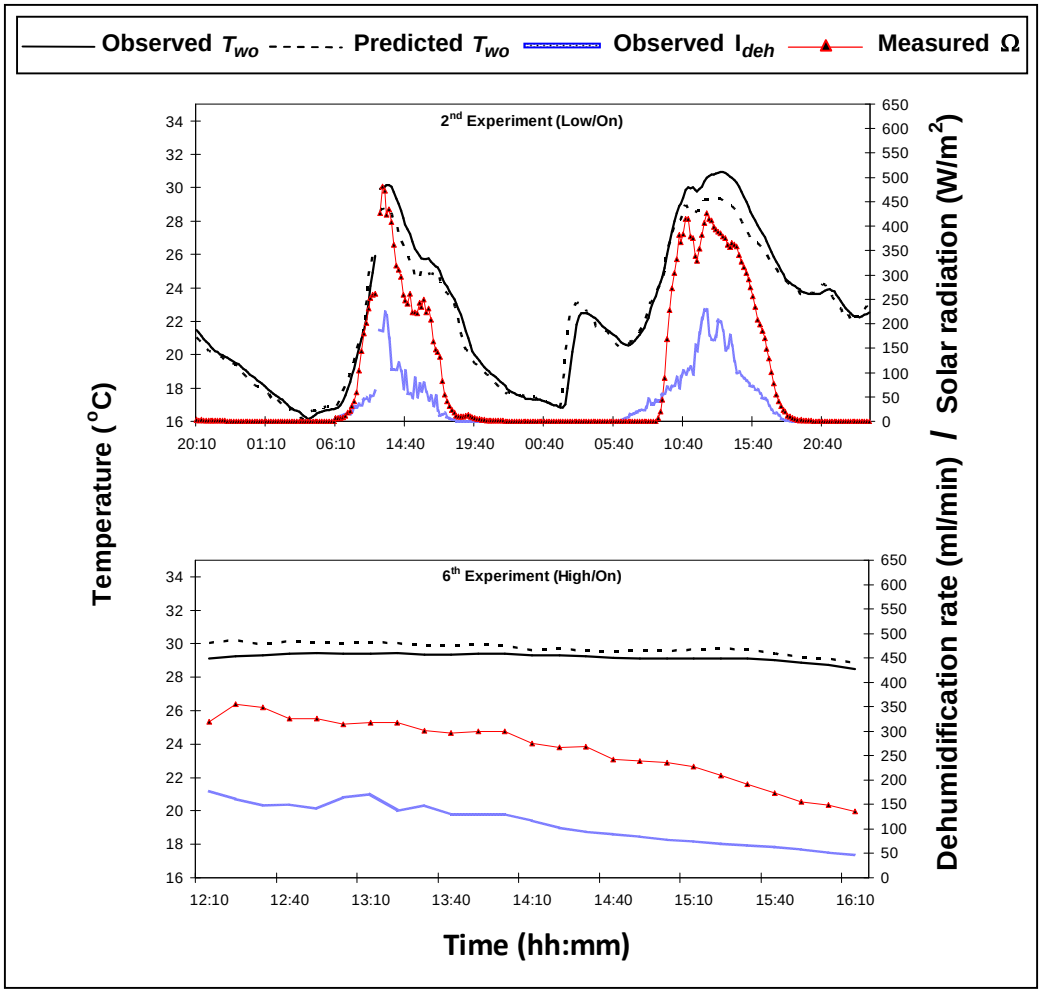

Fig. C3.2: Observed and predicted *outlet water temperature* T_{wo} with the observed *solar heat flux on dehumidifier* I_{deh} and the measured *dehumidification rate* Ω of the 2nd and 6th experiments

(High/Low: refers to air flowrate and On/Off: refers to operating status of humidifier)

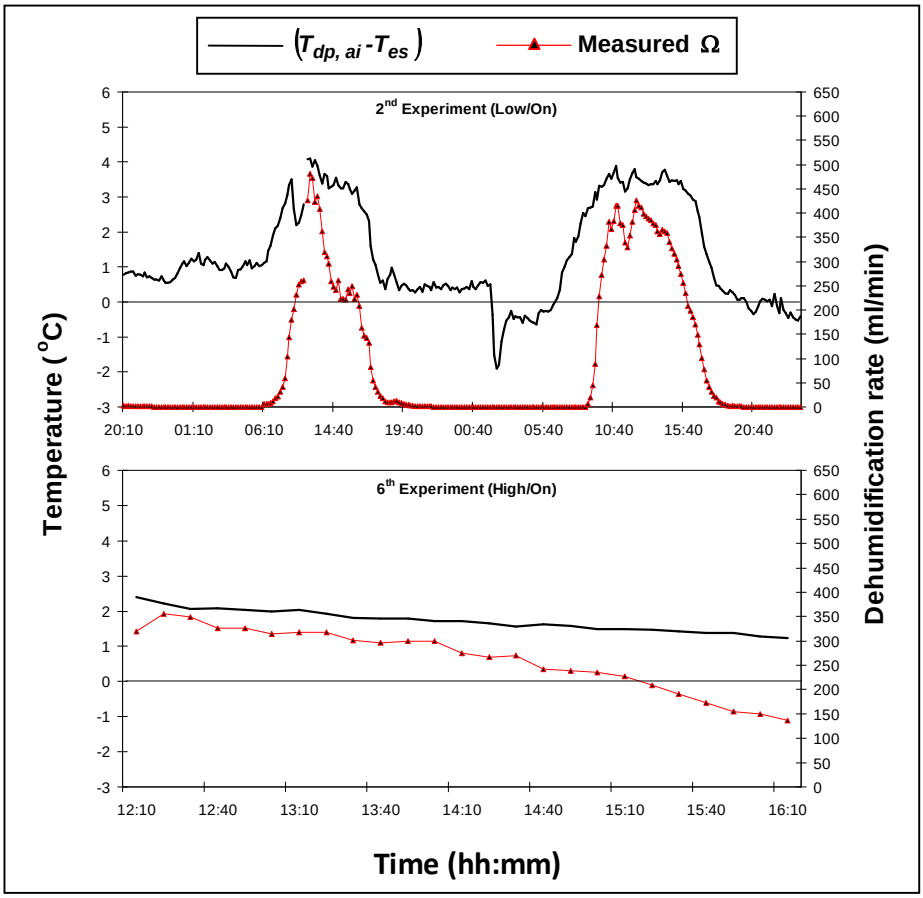

Fig. C3.3: Predicted dehumidification event (i.e. $(T_{dp,ai}-T_{es}) > 0$) and observed *dehumidification rate* Ω of the 2nd and 6th experiments
(High/Low: refers to air flowrate and On/Off: refers to operating status of dehumidifier)

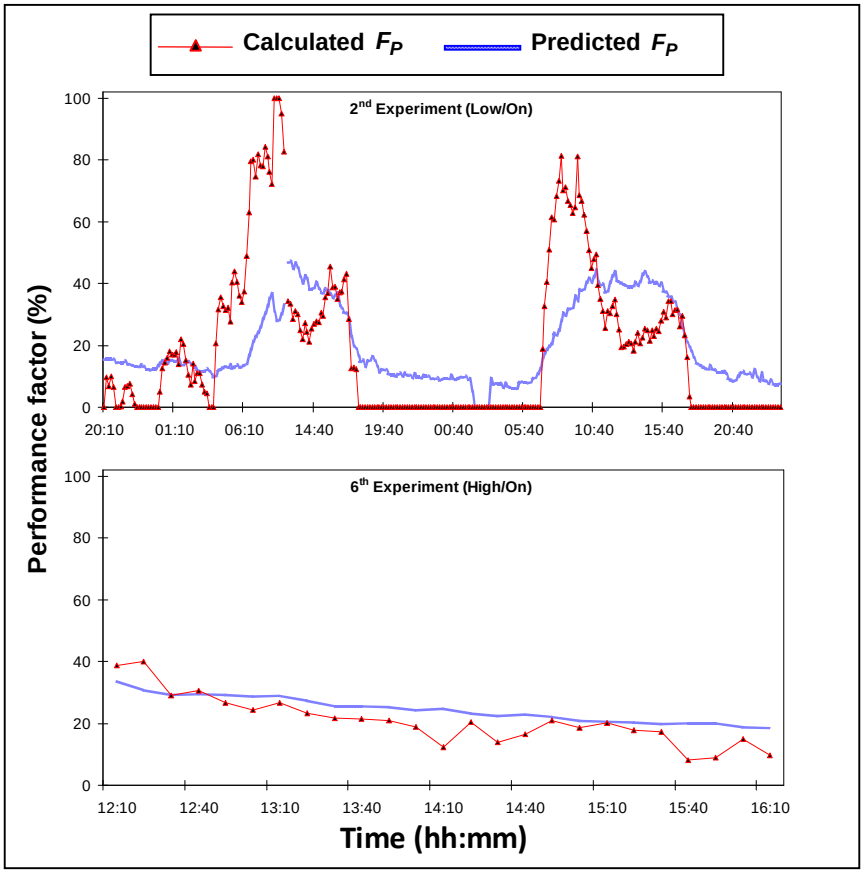

Fig. C3.4: Calculated and predicted *performance factor* F_P of the 2nd and 6th experiments
(High/Low: refers to air flowrate and On/Off: refers to operating status of humidifier)

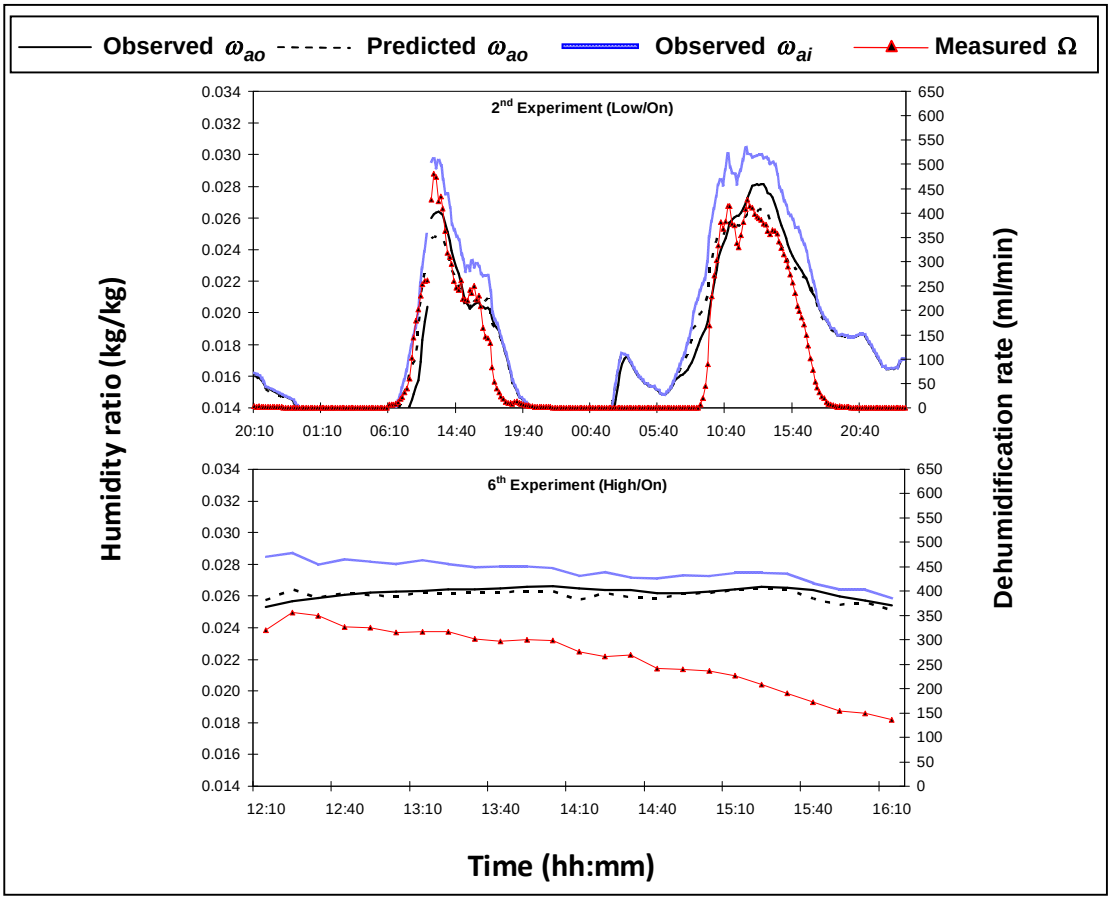

Fig. C3.5: Observed and predicted *outlet humidity ratio* ω_{ao} with the observed *inlet humidity ratio* ω_{ai} and measured *dehumidification rate* Ω of the 2nd and 6th experiments

(High/Low: refers to air flowrate and On/Off: refers to operating status of dehumidifier)

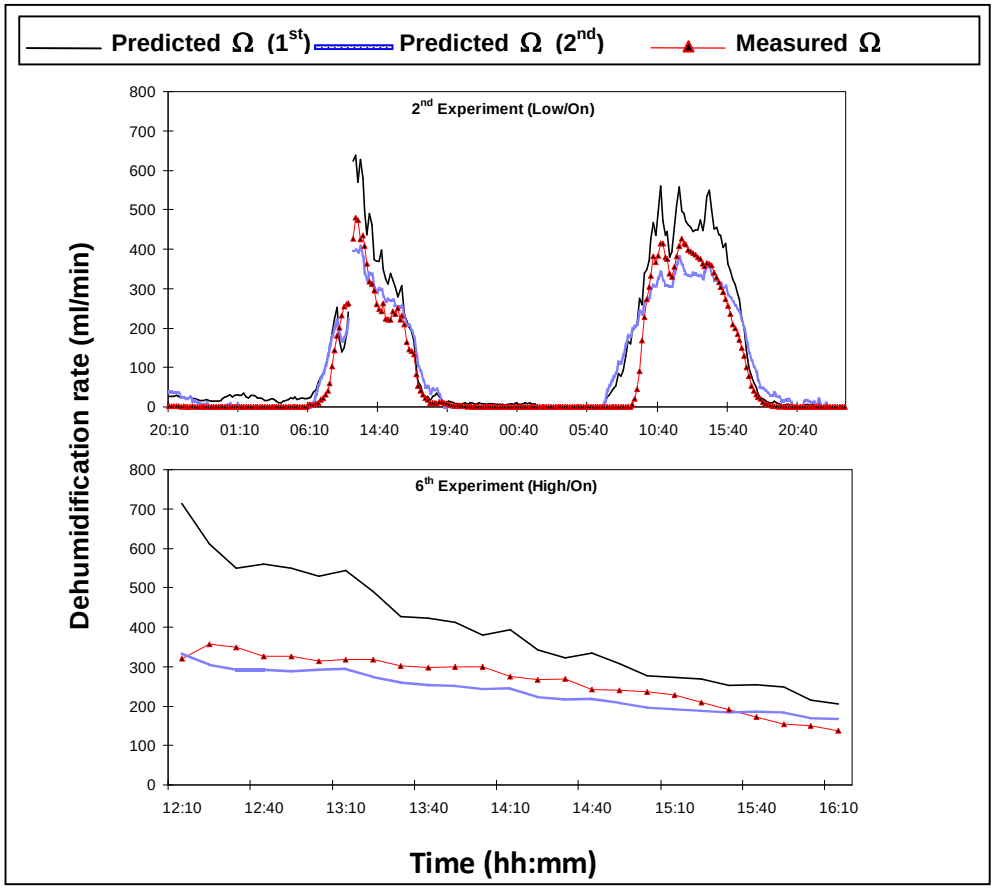

Fig. C3.6: Measured and predicted *dehumidification rate* Ω (using the 1st and 2nd methods) of the 2nd and 6th experiments
(High/Low: refers to air flowrate and On/Off: refers to operating status of humidifier)